2013

Fabrication of surface amine gradients by controlled-rate infusion for chromatographic applications

Balamurali Kannan
Virginia Commonwealth University

Fabrication of surface amine gradients by controlled-rate infusion for chromatographic applications

A dissertation submitted in partial fulfillment of the requirements for the degree of Doctor of Philosophy at Virginia Commonwealth University.

by

Balamurali Kannan

Master of Science, University of Madras, India, 2003

Bachelor of Science, University of Madras, India, 2001

Director: Maryanne M. Collinson

Professor, Department of Chemistry

Virginia Commonwealth University

Richmond, Virginia

August 2013

Acknowledgement

I am extremely thankful to my advisor Professor Maryanne M. Collinson for the opportunity to work under her supervision and also for her inestimable guidance and support throughout my graduate research at VCU. I would like to thank her especially for the critical analysis of my work and her receptiveness on various occasions. I would like to thank Professor Daniel Higgins (Kansas State University) for his valuable suggestions for all the projects I was involved with. Also, I am thankful to him for the opportunity he has provided to work in his lab and for teaching the single molecule fluorescence spectroscopic technique. I would like to thank my committee members especially Prof. Sarah Rutan for her help and support on the gradient stationary phase project. I would also like to thank Kenji Nokura and Professor Julio Alvarez for their help on streaming potential measurements for allowing me to use their equipments. I sincerely appreciate the guidance and instructions of Dr. Dmitry Pestov with X-ray photoelectron spectroscopic analysis.

I would like to thank my friends Daniel Gerard and Suresh Kumar for their invaluable support and help, especially during my hard times. Finally, I am thankful to my parents and loving wife Malavika Srinivasan for their moral and emotional support throughout these years. Lastly, I would like to humbly dedicate this work to the supreme master “Sai” as a gratitude for guiding me through this journey of life.

Table of contents

Page

Acknowledgement ……..….ii

List of figures …… .ix

List of tables ……..…..xviii

List of scheme ……....xix

List of abbreviations ……..…..xx

Abstract ……xxiii

Chapter 1 : Introduction ……...1

1.1 Abstract ……...1

1.2 Gradient material ……..2

1.2.1 Surface chemical gradients ……..……2

1.3 Gradient preparation methods ……3

1.3.1 Gradient preparation methods based on constructive modification. ……..4

1.3.1 A Alkanethiol based SAM approaches. ……..……4

1.3.1 B Silane based SAM approaches. ……..…….5

1.3.1 C Polymer based constructive methods. ……7

1.3.2 Gradient preparation methods based on destructive modification. …….9

1.4 Organoalkoxysilanes ……..12

1.5 Reactivity of aminosilane. ……16

1.6 Controlled-rate infusion (CRI) ……17

1.6.1 Substrate for gradient preparation. ……19

1.6.2 Attributes of CRI method. ……21

1.6.3 CRI for gradient stationary phases ……21

1.7 Stationary phase (SP) gradients in chromatography …….. 22

1.8 Evaluation of aminoalkoxysilane reactivity by gradient profiles ……..25

1.9 Metal chelation gradients ……...26

1.10 Scope of the dissertation …….27.

Chapter 2 : Characterization Techniques . ..……29

2.1 Introduction ……...29

2.2 X-ray photoelectron spectroscopy (XPS) ……..29

2.2.1 Area normalization and peak fit. …….32.

A. N 1s peak fit ……...32

B. Area normalization to determine nitrogen to metal ratio ……33

2.3 Contact angle measurements ……34

2.4 Visualization TLC plates-ninhydrin test …….36

2.4.1 Digitally enhanced TLC analyzer (DE-TLC analyzer) ……..38

2.4.2 Detection for analyte separation …….39

2.5 Streaming potential measurement ……40

Chapter 3: Profile Control in Surface Amine Gradients Prepared by Controlled-Rate Infusion ……45

3.1 Abstract ……...45

3.2 Introduction ……46

3.3 Experimental section ……..48

3.3.1 Sample preparation. ……48

3.3.2 Characterization ……49

3.4 Results and Discussion ……49

3.4.1 Preparation. ……..49

3.4.2 XPS analysis. ……...51

3.4.3 Gradient profile control. ……..59

3.4.4 Contact angle analysis. ……..……..……..63

3.5 Summary ……65

Chapter 4: Aminoalkoxysilane Reactivity in Surface Amine Gradients Prepared by Controlled-Rate Infusion ……66

4.1 Abstract ……..66

4.2 Introduction ……67

4.3 Experimental section ……69

4.3.1 Sample preparation ……69

4.3.2 XPS characterization ……70

4.4 Results and Discussion ……70

4.4.1 Gradient formation. ……70

4.4.2 Gradient profile. ……75

4.4.3 Reactivity of aminosilanes and profile control. ……77

4.4.4 Gradient amine basicity. ……81

4.5 Summary ……85

Chapter 5 : Fabrication and Investigation of Surface Metal Chelation Density Gradients prepared by Controlled Rate Infusion ……..87

5.1 Abstract ……..87

5.2 Introduction ……88

5.3 Experimental section ……89

5.3.1 Sample preparation ……...89

5.3.2 XPS measurements ……91

5.4 Results and discussion ……...91

5.4.1 Cu^{2+} amine complex gradients ……..91

5.4.2 Controls ……96

5.4.3 Metal-amine coordination number along the gradients ……99

5.4.4 Zn^{2+} amine gradients ……101

5.5 Summary ……108

Chapter 6. Continuous Stationary Phase Gradients for Planar Chromatographic Media……110

6.1 Abstract ……...110

6.2 Introduction ……...111

6.3. Experimental section ……113

6.3.1. Reagents ……113

6.3.2 Stationary phase preparation ……114

6.3.3. Stationary phase characterization ……115

6.3.4. Separation ……116

6.4. Results and Discussion ……116

6.4.1. Characterization of gradient ……....116

6.4.2 Separation of weak acids and bases ……..121

6.4.3. Separation of over-the-counter drugs ……130

6.4.4. Preparation of other bonded-phase gradients ……134

6.5 Summary ……136

Chapter 7. Fabrication of surface charge density gradients on open-tubular capillary and its characterization by streaming/zeta potential measurements. .....……137

7.1. Abstract ……137

7.2. Introduction. ……..138

7.2.1 Types of capillary column ……138

7.2.2 Surface coating on open-tubular capillary column ……138

7.2.3 Gradients on capillary column ……139

7.2.4. Open tubular capillary electochromatography (OT-CEC) ……142

7.2.5. Gradient characterization on capillary column ……143

7.3 Experimental section: ……...144

7.3.1 Gradient preparation : ……144

7.3.2. Measurement of Streaming Potential. ……146

7.4 Results and discussion ……....149

7.5 Summary ……..158

Chapter 8. Conclusion and Future Work……..…….159

8.1 Conclusion ….……..159

8.2 Future work …….161

8.2.1 Dual bonded phase gradient stationary phase …….161

8.2.2 Gradient on high pressure packed column …….162

References ……163

List of figures

Chapter 1

Figure 1.1 constructive and destructive modification for gradient preparation …….3

Figure 1.2.Cross - diffusion of two different alkanethiols from two ends of polysaccharide-coated gold surface a) top view and b) side view. ……5

Figure 1.3 Silane based gradient preparation methods. a) Elwing's et al liquid-liquid diffusion method b) Chaudhary's vapor diffusion method ……..6

Figure 1.4. Infusion-withdrawal dip coating for the preparation of polarity gradient. (Reprinted from Ref 40 with permission from American Chemical Society, Copyright ……..7

Figure 1.5. Genzer and coworker's set up for the preparation of polymer gradients. The initiator coated substrate is soaked gradually into the polymerization reaction mixture. Inset : Polymerization at solution-solid interface to form polymer brush gradients ……8

Figure 1.6. Set-up for the preparation of protein density gradient by infusing nanoparticle-tagged protein in to a beaker containing substrate coated with a reactive ……9

Figure 1.7. Gradient preparation set-up for a) Corona-discharge on polyethylene surface with movable sample stage and b) Solution etching of polyvinylcarbonate in a time-based contact method. ……10

Figure 1.8. Schematic of controlled-rate infusion (CRI). (Reprinted from Ref 51 with permission from American Chemical Society, Copyright 2011.) ……18

Figure 1.9. Plot represents the effect of infusion rate on steepness of the gradient in CRI A) Gradients prepared with different infusion rates B) Programmed gradients where infusion rates are programmed within the gradient formation. ……19

Figure 1.10. Base-layer formation by spin coating of TEOS and DMDEOS sol ……..20

Figure 1.11. Amine gradient formation by controlled-rate infusion from dimethyl base-layer (For clarity, only terminal groups are shown) ……..20

Figure 1.12. Continuous and discontinuous gradients ……24

Figure 1.13 : Metal chelation gradient on di/tri amine gradient ……27

Chapter 2

Figure 2.1. Removal of a carbon 1s electron by photoelectric effect. ……30

Figure 2.2. Schematic sketch of an X-ray Photoelectron Spectrometer ……31

Figure 2.3. Schematic sketch of a droplet on a surface for contact angle measurement …..34

Figure 2.4. Schematic sketch of a droplet on a hydrophobic and hydrophilic surfaces …..35

Figure 2.5. Spotting ninhyhdrin on gradient TLC plate ……..38

Figure 2.6. DETLC analyzer- Snapshot of uploaded TLC picture and corresponding spectra (red, green , blue & black/white) for the scan across the sample spot. ……39

Figure 2.7. Schematic sketch of double-layer. ……41

Figure 2.8. Schematic sketch of streaming potential measurement ……42

Chapter 3

Figure 3.1. Simplified schematics of of deposition of a second one-dimensional gradient orthogonal to the first. ……..50

Figure 3.2. N1s and Si2p XPS spectra acquired along the length of the gradient from top to bottom at ~ 1 mm intervals for the negative control (NC), positive control (PC), and gradient films (G). The black line corresponds to the spectrum acquired at the very top of the gradient. ……52

Figure 3.3. N1s and Si2p XPS areas as a function of distance along the length of the gradient from top to bottom for the gradient (G) film. For the positive control (PC) sample, the peak area

ratio of N1s/Si2p as a function of distance is shown. In this case, both the N1s and Si2p peak areas are relatively invariant with distance. ……54

Figure 3.4. N1s and Si2p XPS peak areas as a function of distance along the length of the gradient in two orthogonal directions. The arrows indicate the direction of the gradient from top → bottom. For the positive control (PC) sample, the N1s/Si2p peak area ratio as a function of distance is shown. In this case, both the N1s and Si2p peak areas are relatively invariant with distance. ……56

Figure 3.5. Schematic sketch that shows the set-up for vapor-phase reactivity experiments. Inset shows N1s spectra of vapor exposed part and solution exposed part of the sample. ……58

Figure 3.6. Area under the N1s XPS peak (squares) as a function of distance along the length of the substrate for gradients prepared at infusion rates (dashed line) of (A) 5.4 mL/h and (B) 81 mL/h, using identical sols. The solid lines depict first order kinetic models (Eqn. 4) for the XPS data using $kC_{sol} = 11.8\ h^{-1}$. These results demonstrate that the gradient profile (e.g. steepness) can be controlled by simply changing the infusion rate. ……61

Figure 3.7. Area under the N1s XPS peak (squares) as a function of distance along the length of the substrate for programmed gradients prepared using varied infusion rates. Shown are data from gradients prepared using (A) six-step, (B) six-step (two-fold diluted solution), (C) three-step and (D) two-step programmed infusion rates (dashed lines). The solid lines depict first order kinetic models for the XPS data using $kC_{sol} = 11.8\ h^{-1}$ for A, C, and D and $kC_{sol} = 5.9\ h^{-1}$ for B. ……63

Figure 3.8. Top: Experimental scheme to enhance the difference in hydrophobicity in amine gradient. Bottom: Water droplets along a 1D surface amine gradient. ……64

Chapter 4

Figure 4.1 N1s spectra acquired along the length of the gradient from top to bottom at ~ 1.5 mm intervals for six amine gradients prepared from Triamine, Diamine, N-Butyl, N,N-Diethyl, APTEOS[14] and APTMOS. Infusion solution: ethanol:silane:water volume ratio: 5:0.25:0.05).

Infusion time was ~30 min. The black line corresponds to the spectrum acquired at the very top of the gradient. ……72

Figure 4.2. N1s XPS area as a function of distance along the length of the gradient from top (distance = 0 mm) to bottom for gradient films prepared from Diamine (diamonds), Triamine (triangles), N-Butyl (circles), N,N-Diethyl (inverted triangles), and APTMOS (squares). The data for Diamine and Triamine were divided by 2 and 3, respectively. Infusion solution: ethanol:silane:water (5:0.25:0.05) by volume. The solid lines represent fits to the kinetic model described below. ……..73

Figure 4.3 N1s XPS area as a function of distance along the length of the gradient from top to bottom for gradient films prepared from N,N-Diethyl and N-Butyl. Infusion solution: ethanol:silane:water (5:0.25:0.05 by volume). The infusion time was ~30 min. The solid lines represent fits to the kinetic model described below. ……..75

Figure 4.4. N1s high resolution XPS spectra curve fitted to obtain two peaks. Spectra were collected near the bottom of the gradient. ……82

Figure 4.5. Area ratio of the N1s high energy peak (protonated amine) to low energy peak (free amine) for the different aminosilane precursors. Inset: Trend in the area ratio vs distance along the length of the film from top (1 mm) to bottom (16 mm) for four line scans acquired on the gradient film prepared from the N,N-Diethyl precursor. ……83

Figure 4.6. Trend in the area ratio vs distance along the length of the film from top (1 mm) to bottom (16 mm) for three line scans acquired on the gradient film prepared from the N-Butyl gradient. ……84

Chapter 5

Figure 5.1. N1s and Cu2p spectra of Cu2+-diamine complex at three different gradient profiles. Cu-Di-L, Cu-Di-M and Cu-Di-H. The arrow indicates the direction from low amine end to the high amine end. ……92

Figure 5.2. Peak area profile of N1s (A) and Cu2p (B) peaks along the Cu^{2+}-diamine complex gradients at three different gradient profiles (Cu-Di-L, Cu-Di-M and Cu-Di-H). ……..93

Figure 5.3. N1s and Cu2p spectra of Cu2+-triamine complex at three different gradient profiles. Cu-Tri-L, Cu-Tri-M and Cu-Tri-H. The arrow indicates the direction of the gradient from the low amine end to high amine end. …….95

Figure 5.4. Peak area profile of N1s (A) and Cu2p (B) peaks along the Cu^{2+}-triamine complex gradients at three different gradient profiles (Cu-Tri-L, Cu-Tri-M and Cu-Tri-H).…….96

Figure 5.5. N1s and Cu2p spectra and corresponding area under the N1s and Cu ($2p_{3/2}$) peak acquired along the length of the substrate at ~ 1.5 mm intervals for a negative control (NC) sample prepared from EDAPTMOS but not exposed to Cu solution and a positive control (PC) sample exposed to Cu^{2+} solution. ……97

Figure 5.6. N1s (a) and Cu2p (b) spectra along APTMOS gradient soaked in Cu^{2+}; (c) and (d) are the profile plots of N1s area and $Cu2p_{3/2}$ area. Arrow indicates the direction from low amine end to high amine …….98

Figure 5.7. Normalized peak area ratio (N1s to $Cu2p_{3/2}$) of Cu^{2+}-diamine gradients (A) and Cu^{2+}-triamine gradients (B) The profiles of the three gradients prepared with different concentrations of amine are indicated in black, blue and red (low, medium and high, respectively). ……100

Figure 5.8. Structural (A) and Schematic (B) representation of Cu^{2+} diamine complex on gradient surface (C) Effect of free amine groups on N/Cu ratio. ……101

Figure 5.9. N1s and Zn 2p spectra of Zn^{2+}-triamine complex at two different gradient profiles. Zn-Tri-L and Zn-Tri-M. Arrow indicates the direction from low amine end to high amine end. ……102

Figure 5.10. Peak area profile of N1s (A) and Zn $2p_{3/2}$ (B) peaks along the Zn^{2+}-triamine complex gradients at two different gradient profiles (Zn-Tri-L and Zn-Tri-M) ……103

Figure 5.11. Normalized peak area ratio (N1s to Zn $2p_{3/2}$) of Zn^{2+}-triamine gradients. Two gradients in this case are formed with different profiles and are showed in black and red (low and medium). ……104

Figure 5.12. N1s and Zn 2p spectra of Zn^{2+}-diamine complex at two different gradient profiles. Zn-Di-L and Zn-Di-M. ……105

Figure 5.13. Peak area profile of N1s (A) and Zn $2p_{3/2}$ (B) peaks along the Zn^{2+}-diamine complex gradients at two different gradient profiles (Zn-Di-L and Zn-Di-M). ……106

Figure 5.14. Normalized peak area ratio (N1s to Zn $2p_{3/2}$) of Zn^{2+}- diamine gradients . Black symbols correspond to the Zn – Di – L profile and the red is for the Zn-Di-M gradient profile ……107

Figure 5.15. Structural representation of Zn^{2+}-dimaine complex on the top and bottom of the gradient based on N/Cu ratio……..108

Chapter 6

Figure 6.1 A) Plot of spot intensity after exposure to ninhydrin vs distance along the length of the plate for PC (red), gradient (blue, infusion rate = 80 mL/hr), and NC (black). The error bars signify ±1σ. N=3. Inset: A digital photograph of the gradient TLC plate from which the intensity data were extracted. Chromatographic data on these TLC plates are shown in Figures 6.4 and 6.5. **B)** Screenshot picture of DETLC analyzer. Picture from figure 6a is uploaded and ninhydrin spots across the gradient plate were scanned. Below are the four spectra (red, green, blue and b/w). ……119

Figure 6.2 Plot of spot intensity after exposure to ninhydrin as a function of distance along the TLC plate for PC (red), NC (black), and gradient TLC plates. Gradient formation was accomplished using an infusion rate of 400 mL/hr (green), 700 mL/hr (blue), and 1000 mL/hr (pink). The error bars signify ±1σ. N = 3. ……..120

Figure 6.3 Spotting location on gradient and control plates. G_a is gradient where analyte mixture was spotted on low amine end and G_b is gradient in which analyte mixture was spotted on the high amine end. ……..122

Figure 6.4 A) Image of four TLC plates (NC, PC, G_b and G_a) where the separation of two basic (lane 1), two acidic (lane 2) and all 4 component (lane 3) separation was performed under acidic mobile phase condition. Blue lines in NC plates is to indicate the three lanes The picture was taken under UV light (254 nm). **B)** Screenshot from DETLC analyzer. The top of the figure is the image of TLC plates (NC, PC, G_b and G_a). Below are the red, blue, green, b/w spectra for the corresponding line scan in the Gradient (G_a) image where the separation of four compounds occurred. ……124

Figure 6.5 TLC chromatograms for the negative control (NC), positive control (PC), and the gradient TLC plates (Ga, Gb) where the mixture (Benzoic acid (BA), 3-Aminobenzoic acid (ABA), 2-Aminopyridine (APy) and 4-Aminophenol (APh)) was spotted on the high amine end (Gb) and the low amine end (Ga). Circular dots in each plot represent the point where the analyte mixture was spotted. Rectangular bars at the top of each plot represent the amine density (dark brown for high amine) along the length of the gradient. Mobile phase: methylene chloride:methanol:acetic acid (90:10:0.5). ……125

Figure 6.6. TLC chromatograms for the negative control (NC), positive control (PC), and gradient TLC plates (Ga, Gb) where the mixture (Benzoic acid (BA), 3-Aminobenzoic acid (ABA), 2-Aminopyridine (APy) and 4-Aminophenol (APh)) was spotted on the high amine end (Gb) and low amine end (Ga). Circular dots in each plot represent the point where the analyte mixture was spotted. Rectangular bars at the top of each plot represent the amine density (dark brown for high amine) along the length of the gradient. Mobile phase: Methylene chloride:methanol:triethylamine (90:10:0.5). ……..127

Figure 6.7. TLC chromatograms for the separation of doxylamine succinate (Dx), diphenhydramine hydrochloride (Dp) and acetaminophen (Ac) on a negative control (NC), a positive control (PC) and three gradient TLC plates formed using infusion rates of 1000 mL/hr, 700 mL/hr, and 400 mL/hr. The samples were spotted on the high amine end (at 0). Mobile phase: Ethyl acetate: methanol:water (7:7:1.5). ……..131

Figure 6.8. Image of gradient-TLC plates under UV light after the separation. Each plate has three lanes in which two bottom lanes showing separation of individual components. Only the top lane on each plate shows the separation of all three drug mixture. ……..132

Figure 6.9. Phenyltrimethoxysilane (PTMOS) structure and TLC plates modified with PTMOS. Gradient (G) prepared by CRI using a solution containing PTMOS to form gradient and visualized under UV light (254 nm). Control plates are also shown for comparison (NC & PC). The red arrow on the gradient shows the direction of increasing intensity of quenching due to phenyl gradient. ……...134

Figure 6.10. Representative FT-IR spectra CNTEOS modified TLC plates ……..135

Figure 6.11. FT-IR spectra of gradient (G) and uniformly modified (PC) cyano plates. Gradient prepared by CRI using a solution of CNTEOS to form the gradient in cyano groups. The arrow in the gradient spectra indicates the direction of the gradient from low to high cyano end. ……136

Chapter 7

Figure 7.1:A) EOF & **B)** Pressure driven flow profiles ……142

Figure 7.2 : Infusion set-up for the gradient preparation on silica capillary by CRI method. After gradient preparation, the capillary was cut into 1.2 cm segments and characterized via streaming potential measurements ……147

Figure 7.3 : Schematic shows the micro-chip made of 1.2 cm modified silica capillary ……147

Figure 7.4 A). Schematic for streaming potential measurements on surface amine gradient on capillary. Inset: Photograph of acapillary sealed to a micropipette tip with glue. **B)** Photograph of streaming potential measurements set-up ……..……148

Figure 7.5: Representative streaming potential plot of a single run (five cycles) of a 1.2 cm amine modified capillary. ……151

Figure 7.6: Streaming potential plots (five cycles per run) along the control capillaries (A) and surface charge density gradient capillary (B) ……152

Figure 7.7. (A) Zeta potential profile plot on the negative (NC) and positive (PC) control capillaries and a gradient capillary & **(B).** Error bar at each position is ±1 standard deviation of three measurements (n=3).……153

Figure 7.8. (A) Zeta potential profile plot of surface charge density gradients (Gradient 2) prepared on two different days. (B) Zeta potential profile plot of surface charge density gradients prepared under three different conditions (Gradient 1, Gradient 2 and Gradient 3) as described in the text……155

Figure 7.9. Optical image of a capillary segment which is opened to expose the inner wall of the capillary to the X-ray beam in XPS spectrometer. ……156

Figure 7.10. N 1s spectra obtained at the top and bottom of the gradient capillary and on a negative control. ……157

Chapter 8

Figure 8.1. Versatility of controlled-rate infusion (CRI) approach ……..161

List of tables

Table 4.1. Average N1s area for samples prepared by soaking a base-layer coated substrate in the aminosilane solution (same ethanol, silane & water ratio used for gradients in Figure 4.1) for 4 h. The diamine and triamine areas have been divided by 2 and 3, respectively. …….77

Table 4.2: Results from fit to a single-step kinetic model ……..78

Table 5.1. N1s area of diamine (Cu-Di-M) and trimaine (Cu-Tri-M)gradients after normalization for the number of amine groups…….95

Table 15.2. N/Cu ratio (normalized area) of Cu2+ and Zn2+ gradients…….108

Table 6.1 Chromatographic parameters (retention factor (Rf) and resolution (Rs)) obtained for the TLC plates in Figure 5.4 (Acidic mobile phase). Benzoic acid (BA), 3-aminobenzoic acid (ABA), 2-aminopyridine (APy) and 4-aminophenol (APh) are the analytes. ……126

Table 6.2 Chromatographic parameters (retention factor (Rf) and resolution (Rs)) obtained for the TLC plates in Figure 5.5 (Basic mobile phase). benzoic acid (BA), 3-aminobenzoic acid (ABA), 2-aminopyridine (APy) and 4-aminophenol (APh) are the analytes. …….128

Table 6.3 Chromatographic parameters (retention factor (Rf) and resolution (Rs)) obtained for the TLC plates in Figure 5.6 (drug mixture). doxylaminesuccinate (Dx), diphenhydramine (Dp), acetaminophen (Ac) are the analytes. ….. …….133

List of schemes

Scheme 1.1. Hydrolysis and condensation reactions of organoalkoxysilane. ……...……..12

Scheme 1.2. Structures of organoalkoxysilanes (with reactive and non-reactive 'R' groups). ……..13

Scheme 1.3. Hydrolysis and condensation reactions of alkoxysilane with the substrate containing silanol groups. ……14

Scheme 1.4. Schematic represents vertical condensation with neighboring silane on the surface. ……15

Scheme 1.5. 3-Aminopropyltriethoxysilane hydrolyzes and form cyclic structure through hydrogen bonding ……..16

Scheme 2.1.Ninhydrin reaction with primary amines. ……37

Scheme 4.1. Aminoalkoxysilanes used in the study ……..68

Scheme 6.1 Structures of acidic and basic compounds separated. ……121

Scheme 6.2. Structures of over-the-counter drugs separated. ……130

List of abbreviation

ABA	3-Aminobenzoic acid
Ac	Acetaminophen
APh	4-Aminophenol
APy	2-Aminopyridine
APTEOS	3-aminopropyltriethoxysilane
APTMOS	3-Aminopropyltrimethoxysilane
BA	Benzoic acid
CIEF	Capillary iso-electric focusing
CNTEOS	Cyanoethyltriethoxysilane
COC	Cyclic olefin copolymer
CP MAS	Cross-polarization and magic-angle spinning
CRI	Controlled-Rate Infusion
Cu	Copper
DE-TLC	Digitally enhanced TLC
DMDEOS	Dimethyldiethoxysilane
Dp	Diphenhydramine hydrochloride
DRIFT	Diffuse reflectance infrared Fourier transform
Dx	Doxylamine succinate
EDL	Electrical double layer
EOF	Electro-osmotic flow
FTIR	Fourier transform infra-red
FWHM	Full width at half maximum

G	Gradient
HILIC	Hydrophilic interaction chromatography
HPLC	High performance liquid chromatography
HPTLC	High perfomance thin layer chromatography
IEF	Isoelectric focusing
MIP	Molecular imprinted polymer
MTMOS	Methyltrimethoxysilane
NC	Negative control
ODS	Octadecylsilica
OTCEC	Open tube capillary electrochromatography
PC	Positive control
PDMS	Poly di-methyl siloxane
pI	Isoelectric point
pKa	Acid dissociation constant
pK_b	Base dissociation constant
PMMA	Polymethylmethacrylate
PTMOS	Phenyltrimethoxysilane
R_f	Retention factor
RID	Refractive index detector
RP	Ruhemann's purple
SAM	Self –assembled monolayer
SOSLC	Stationary phase optimized selectivity liquid chromatography
TEOS	Tetraethoxysilane
TMOS	Tetramethoxysilane

XPS	Xray photoelectron spectroscopy
Zn	Zinc

Fabrication of surface amine gradients by controlled-rate infusion for chromatographic applications

Abstract

Surface gradients are materials that exhibit a variation in properties such as chemical composition, topography etc., in a continuous and/or discrete fashion. They are broadly classified as chemical and physical gradients depending upon the properties that gradient exhibits. Among those, chemical gradients on various surfaces have been a great interest in materials research for the last two decades. This is due to the applications of gradients in various fields such as biological sciences, separation science, etc. There have been several different approaches developed for the preparation of chemical gradients. Silane-based approaches are among those that are widely used because of the straightforwardness of the chemistry involved and also the availability of silanes with various chemical functionalities. A few of these silane based approaches such as the vapor-diffusion method and liquid diffusion method have been used for various applications so far. Most of these methods were only able to prepare surface chemical gradients for a specific application mainly because of their limitations in terms of gradient-length scale and chemistry involved. Hence, there is a need to develop additional procedures for the preparation of chemical gradients that can be adaptable to different substrates and use them to form gradients at various length-scales such as few hundred microns to tens of centimeters. Using 3-aminopropyltriethoxysilane (APTEOS) as the precursor, a simple method was developed to prepare surface amine gradients termed ‘controlled-rate infusion (CRI).

The CRI method involves the infusion of an organoalkoxysilane solution into a container with a substrate mounted vertically so that time-based exposure along the substrate forms a

gradient in chemical functionality. The most important attribute of this method is that the local steepness of the gradient can be systematically controlled by simply changing the rate of infusion. The steepness of the gradient can also be changed at predefined positions along its length by programming the rate of infusion. The ability to manipulate the gradient profile is particularly important for applications that rely on mass transport and/or those that require spatial control of gradient properties. CRI can also be used to study the reactivity of aminoalkoxysilanes that contain mono, di and tri amino groups and also amines with various substitutions (secondary and tertiary amines). The gradient profiles in each case were different and correlated to their reactivity with surface silanols. Among those aminoalkoxysilanes, ethylenediamine and diethlenetriamine were found to be very good chelating agents to bind with metal ions. Thus, gradients prepared with diamine and triamine were used as ligand density gradients for the investigation of metal-amine complex formation using two different metal ions (Cu^{2+} and Zn^{2+}). The above mentioned work formed the first part of this dissertation (up to Chapter 5). The latter part concentrates on fabrication and application of surface gradients for stationary phases for chromatographic separation.

For the demonstration of proof-of-principle of the application of gradient stationary phases, the CRI approach was employed to prepare continuous stationary phase gradients on HP-TLC plates for planar chromatography. The SiOH groups on the activated HP-TLC plates were reacted with 3-aminopropyltriethoxysilane (APTEOS) in a time dependent fashion by using a programmable syringe pump to control the rate of APTEOS infusion into the deposition reservoir. The shape (profile) of the gradient was controlled by the rate of infusion and the gradients were visualized by utilizing a concentration-dependent color formation reaction between amine groups and ninhydrin. The advantages of such gradients in optimizing the

retention and separation of various components in different mixtures was illustrated using mixtures of (i) four weak acids and bases and (ii) three widely-used over-the-counter drugs. Thus, the gradient stationary phase was successfully fabricated and applied as a planar chromatographic support. The next step of this research was to prepare continuous amine gradients on silica capillaries as these would be useful in open-tubular capillary electrochromatography for separation of complex mixtures and also to study the retention behavior of various components. This was achieved by carefully infusing micro-volumes of APTEOS solution into the activated silica capillaries. To characterize these gradients, a unique set-up was developed to measure streaming potential and zeta potential along the gradient capillary. Since surface amine groups exist as positively charged groups at acidic and neutral pHs, the measured zeta potential increased from the low amine end to the high amine end of the capillary.

In summary, this dissertation work focuses mainly on the development of a simple, rapid and cost-effective method for the preparation of surface chemical gradients. CRI has incredible flexibility and adaptability, which was confirmed by extending it to different substrates such as silica TLC plates and capillary tubes for various applications. The CRI approach is not just helpful in preparing gradients for chromatographic separations; it can be a stable platform to study the reactivity of various precursors which could be a useful tool to develop high-throughput surface modification procedures.

Chapter 1: Introduction

1.1 Abstract

The primary objective of this research work is to develop a simple, straightforward and rapid method to prepare surface chemical gradients that can be extended to applications in various fields including biomaterials, chromatographic separations, micro separation devices etc. In this work, the application of a new technique for stationary phase gradient preparation is the main focus. Numerous techniques have evolved over the past 25 years for the fabrication of gradients on chromatographic stationary phases. Such methods have generally involved complex experimental procedures such as connecting different stationary phases in series or filling the column with different monomer solutions followed by polymerization. Clearly, there is a need to experimentally develop straightforward techniques to form gradients on various platforms like planar supports, open tubular capillaries, and micro-channels etc. In this work, we developed a new approach called 'controlled-rate infusion (CRI)' that is primarily based on the time dependent reactivity of organoalkoxysilanes with surface silanol groups on various substrates. This chapter mainly discusses the classification and significance of surface chemical gradients. It is followed by a discussion of various methods of gradient preparation, especially time-controlled gradient methods using organosilanes. It is continued with a brief description of CRI and its uniqueness relative to other methods for gradient preparation. An introduction to stationary phase gradients for chromatographic separation and the CRI approach to prepare stationary phase gradients on planar and open tubular capillary is then discussed including the potential application of such gradients to electrochromatography. Finally, aminosilane reactivity

and metal chelation gradients are also discussed before summarizing the scope of this dissertation work.

1.2 Gradient materials

Gradient materials are materials that exhibit a variation in properties such as chemical composition, topography etc., in a continuous or discrete fashion. There are mainly two types of gradients according to Genzer in his detailed reviews on gradient materials: physical gradients and chemical gradients.[1, 2] Gradual variations in physical properties such as surface roughness and/or porosity are called physical gradients. Such gradients have found various applications in biological sciences such as cell adhesion, etc.[3-5] Even though physical gradients have found wide range of applications, the main focus of this dissertation work is on chemical gradients..

1.2.1 Surface chemical gradients

A gradual variation of one or more chemistries along the distance of a surface is called a "surface chemical gradient"[6] These gradients can vary along the substrate in one, two or three dimensions.[1, 2] In materials research, one of the key roles of these gradients is high throughput analysis with minimum amount of cost and time. For example, cell and protein adhesion studies are generally performed by screening numerous samples with varying surface properties such as wettability, and these require considerable preparation and analysis time.[6] This could be avoided by preparing surface gradients with varying surface properties on a single platform. Apart from the above mentioned application, gradient materials have been applied in various areas such as chemical separations, controlled transport,[7-12] polymer-templating,[13] chromatographic separation[14] and also as biosensors.[15-18]

Surface chemical gradients are formed mainly in two different ways. Constructive modification is a method in which one or more chemical functionality is gradually added by varying the exposure time or concentration of precursor.[6] On the other hand, in destructive modification the surface layer is removed gradually to obtain the gradient (Figure 1.1). [6]

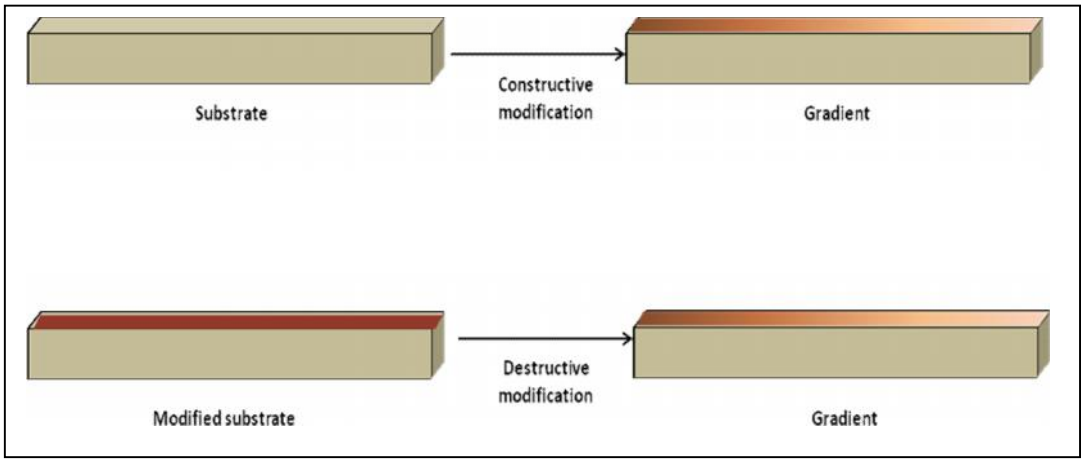

Figure 1.1 : Constructive & destructive modification for gradient preparation.

1.3 Gradient preparation methods

As described in the previous section, gradient preparation methods can broadly classified into two categories which are constructive and destructive modification of the surface.[1, 2] Numerous methods in both the categories have been reported for the past two decades. Silane, alkanethiol and polymer coatings are the three main types of approaches that fall under constructive methods.[1, 2, 6] The first two approaches are self-assembled monolayer (SAM) based approaches. In the following section, gradient preparation methods based on constructive modification will be discussed in detail along with subsections describing SAM based alkanethiol methods, SAM based silane methods and polymer based approaches.[6] Also, some notable methods on destruction modification for gradient preparation will also be discussed.

1.3.1 Gradient preparation methods based on constructive modification

Organosilane and alkanethiols are the two major class of precursors used for the preparation of chemical gradients in SAM-based approaches.

1.3.1A Alkanethiol based SAM approaches

Alkanethiols are the most common molecules that have been used to prepare self-assembled monolayers.[19] The strength of binding of thiol groups to gold is very large and, the lateral van der Waals interaction between the alkyl groups also plays a major role in forming ordered layers.[20] Alkanethiols have been used as precursors in gradient preparation for almost two decades when Leidberg and co-workers first created a gradient by allowing two different alkanethiols to cross-diffuse from two ends of a polysaccharide-coated gold surface (Figure 1.2). The two alkanethiol differed in their alkyl chain lengths and they were placed at two glass filters separated by a distance of 40 mm.[21] Morgenthaler et al published work on chemical gradients using alkanethiols with various substitutions such as hydroxyl and long-chain alkyl groups on gold substrates.[22, 23] In this study, the gold substrate was immersed in the alkanethiol containing solution in a gradual fashion to form gradient in alkyl and hydoxy terminated groups. XPS, contact angle measurements and Infrared spectroscopy were used for gradient characterization. Another method involves electrochemical deposition of alkanethiol by applying an electrode potential.[24, 25] The magnitude of applied potential and the distance between the electrodes determined the width and steepness of the gradient.

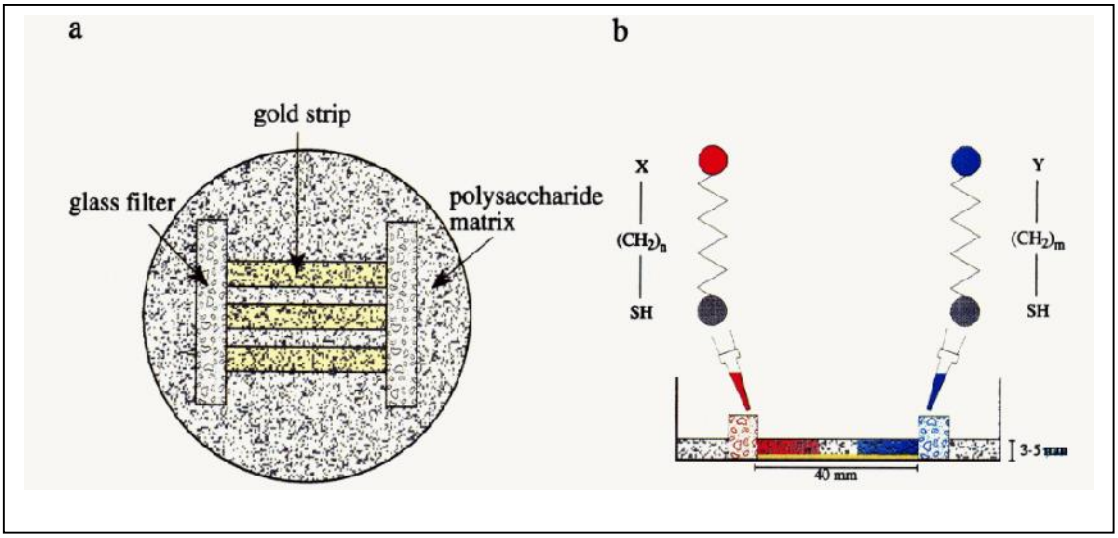

Figure 1.2. Cross-diffusion of two different alkanethiols from two ends of polysaccharide-coated gold surface a) top view and b) side view. (Reprinted from Ref 21 with kind permission, Copyright. 1997). [21]

Other than diffusion and deposition, contact printing and ink-jet printing are other mechanisms by which alkanethiol functional gradients have been prepared. A wedge-shaped PDMS stamp with a uniform hexadecanethiol concentration was applied to the gold substrate and the variation in thickness of the stamp determined the alkanethiol density gradients. Surface chemical gradients prepared from alkanethiol precursors have found applications in protein and cell adsorption,[26, 27] nanoparticle attachment[25], etc. The main advantages of these approaches are their stability due to the strong interaction between thiol groups and the substrate and also their experimental simplicity. However these methods suffer mainly because they are limited to a few metals such as gold, silver, and copper.

1.3.1B Silane based SAM approaches

Silane-based SAM approaches became an important tool for gradient preparation when Elwing[28-30] et al and Chaoudhary[7] et al, developed solvent-diffusion and vapor-diffusion techniques, respectively (Figure 1.3 a and b). In Elwing's approach, a chlorosilane is dissolved in a solvent and allowed to diffuse through another solvent of a different density to create a wettability gradient on the surface. The latter allowed the silane vapors to slowly diffuse along the length of the substrate when the chlorosilane in paraffin slowly evaporated. Based on these two approaches, numerous gradients, particularly in wettability, have been reported for various applications such as droplet movement,[7, 9] and protein and polymer adsorption.[31, 32],

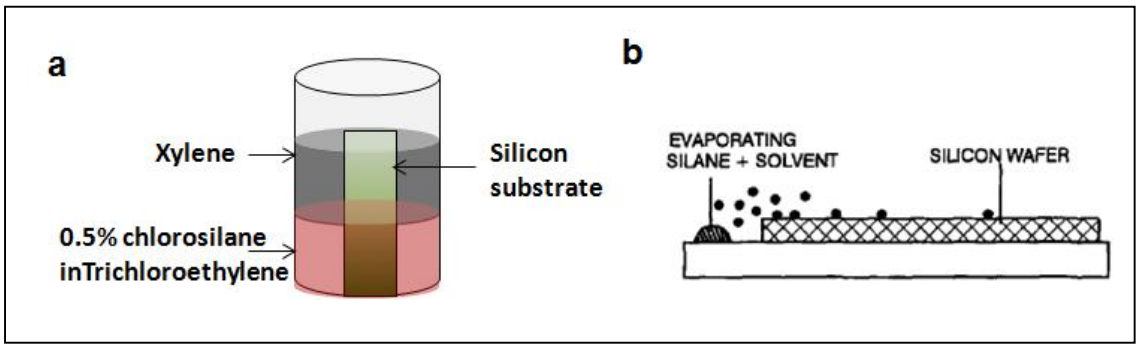

Figure 1.3 Silane based gradient preparation methods. a) Elwing et al liquid-liquid diffusion method b) Chaudhary's vapor diffusion method. (Reprinted from Ref 28 and 7 with kind permission, Copyright. 1992) [28, 7]

A few other notable silane based approaches are micro-scaled contact printing[33] and controlled irradiation through density filters for applications such as enzyme activity. Recently, our collaborators developed a new method for preparing chemical gradients termed 'infusion-withdrawal dip-coating,'[34, 35] where the composition of sol is varied with time in addition to substrate exposure time variation. In this work, the substrate is first immersed totally into a cell containing a tetramethoxysilane (TMOS) sol and withdrawn at a controlled rate using computer-

operated device. Meanwhile, methyltrimethoxysilane (MTMOS) sol, which contains a methyl group, is infused in to the cell at the same rate the mixture is withdrawn simultaneously from the cell. The solution level in the cell remains constant throughout the dip-coating, so that bottom of the substrate is exposed to the MTMOS solution for a longer time than the top. By this procedure, a polarity gradient was formed with the high MTMOS end more hydrophobic (Figure 1.4). Gradients prepared by this method are few tens of nanometers thick.

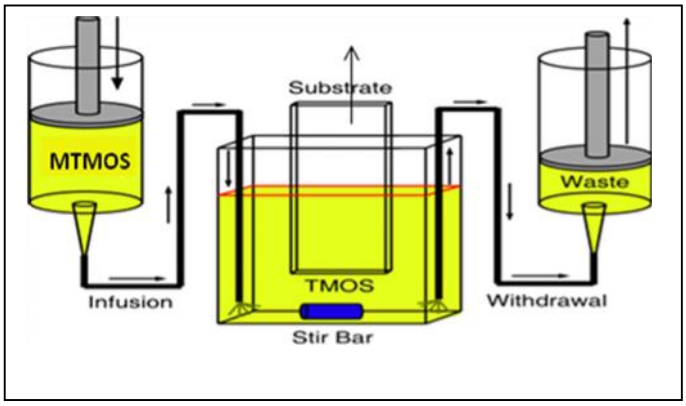

Figure 1.4. Infusion-withdrawal dip coating for the preparation of polarity gradients. (Reprinted from Ref 34 with kind permission from American Chemical Society, Copyright.2010). [34]

This procedure is capable of preparing chemical gradients of various functionalities such as thiol, nitrile, isobutyl etc., by just varying the organosilane.

1.3.1C Polymer based constructive methods

There are numerous polymer-based approaches for the preparation of chemical gradients, especially brush-like polymer gradients.[36, 37] Corona treatment for the preparation of such polymer brush gradients by varying the power of corona discharge is one among the common techniques.[20, 38, 39] Genzer and coworkers formed polymer gradients that exhibit a variation of molecular weight and grafting density by simply controlling the time of radical polymerization

reaction at the solution/solid interface. It was accomplished by a simple set-up in which an initiator-coated substrate is soaked in polymerization-reaction mixture and then the solution is removed by a pump at a controlled rate (Figure 1.5).[39-41] Gradients prepared by this approach were used as biomaterials for cell adhesion and protein adsorption studies.[39-41]

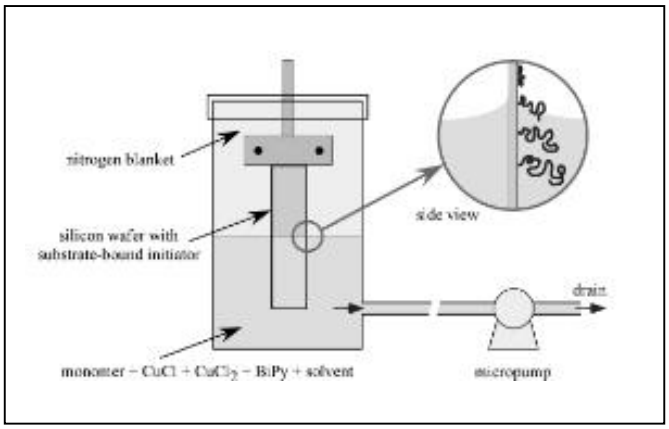

Figure 1.5. Genzer and coworker's set up for the preparation of polymer gradients. The initiator coated substrate is soaked gradually into the polymerization reaction mixture. Inset : Polymerization at solution-solid interface to form polymer brush gradients. (Reprinted from Ref 39 with kind permission, Copyright, 2005).[39]

Ionov et al have reported polymer gradients on surfaces prepared by controlling the temperature.[42-44] Gradients in protein assemblies and pH responsive polymer gradients were prepared by this method.[43, 44] Polymethylmethacrylate (PMMA) gradient surfaces were prepared by Harris and coworkers by gradually moving the position of a photomask during the surface photopolymerization reaction.[45] In another approach, the irradiation time of photopolymerization was varied to form biomolecules to study cellular responses.[46, 47] Another constructive modification to form polymer gradients was reported by Mei and co-workers. In this work, a polymerization-initiator gradient was made by gradually infusing the initiator solution to the substrate.[48] Here, the substrate used was a SAM of octadecyl groups and the defects in the

monolayer on a Silicon wafer were allowed to react with the polymer initiator in a time-based fashion The grafting density was measured by determining the film thickness, and it varied from 20 Å to 80 Å along the gradient. Cell adhesion and protein adsorption were studied on such gradients. In a similar fashion, i.e., by controlling the contact time of the substrate with the monomer solution to prepare polymer brush gradients, surface density gradients in poly (2-hydroxyethyl methacrylate) and poly (L-lysine) were prepared to study cell adhesion and protein adsorption.[48, 49] Kramer and co-workers have also used this approach to create protein density gradients to study protein-cell interaction by controlling the reaction time of protein-nanoparticle conjugates with the modified-substrate (Figure 1.6).[50]

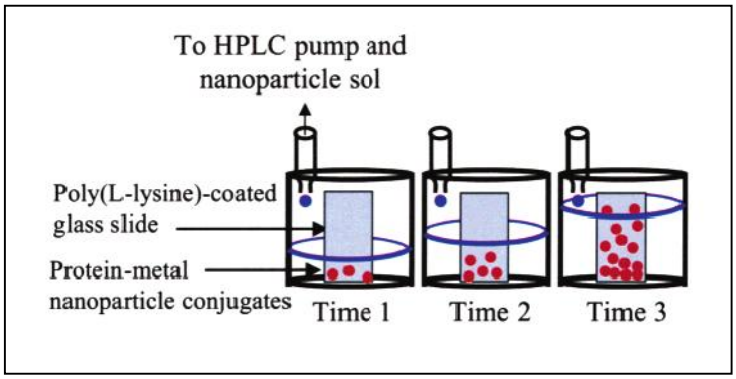

Figure 1.6. Set-up for the preparation of protein density gradient by infusing nanoparticle-tagged protein in to a beaker containing substrate coated with a reactive functional group. (Reprinted from Ref 50 with kind permission, Copyright. 2004).[50]

1.3.2 Gradient preparation methods based on destructive modification

As discussed earlier, gradient methods based on destructive modification involve removal of a surface layer from the substrate. Ruardy et al, discussed a few methods based on destructive modification in his review.[51] Most of these methods utilizes either photochemical or electrochemical desorption of self-assembled monolayer on a polymer surface to form a surface

chemical gradient. Since these methods encounter disadvantages such as limited control on surface chemistry and roughness, these methods are relatively less common compared to constructive modification. However, there are notable methods, such as those based on alkanethiols, polymer coatings, etc. Electrochemical desorption of thiols on Au surface were reported by Bohn et al, to form a gradient in surface composition. Thiol groups in a SAM were stripped from the gold surface by applying a particular potential.[24, 25, 52] These methods were used to prepare one- and two-component gradients and found applications in cell adhesion studies[25] and in the evaluation of a new mass spectroscopic technique.[52]. Alkanethiol desorption was also accomplished using a X-ray beam by controlling the exposure time of irradiation.[53]

Polymer-based destructive methods for gradient preparation generally allow the polymer substrate to be exposed to radiation or an etching solution.[54-57] For example, a wettability gradient was prepared by treating a polyethylene surface with corona discharge and the radiation power was gradually varied along the substrate (Figure 1.7a).[54] In another case, radiofrequency discharge was used at different gas atmospheres on polymer substrates to form a wettability gradient.[55] In another example, polyvinylenecarbonate was exposed to sodium hydroxide solution at a controlled rate. The end that was exposed for a longer time was more hydrophilic than the other end since it had more hydroxyl groups (Figure 1.7b). The other end is rich in carbonate groups, which is relatively more hydrophobic. Gradients prepared by these approaches have been used to study protein adsorption and cellular responses.[57]

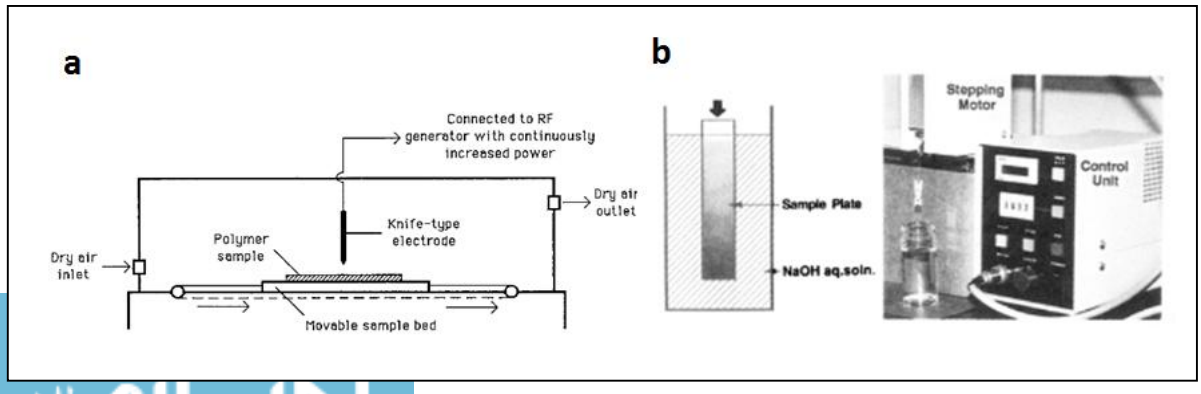

Figure 1.7. Gradient preparation set-up for a) Corona-discharge on polyethylene surface with movable sample stage and b) Solution etching of polyvinylcarbonate in a time-based contact method. (Reprinted from Ref 54 and 55 with kind permission).[54,55]

1.3.3 Section Summary

Although the techniques discussed above based on constructive and destructive modification have various advantages and have also found applications in various areas including biosensors, biomimetic materials etc., none of these single methods have been reported to show all the advantages listed below

a) Simple & straight-forward chemistry and experimental procedure.

b) Ability to control gradient profile.

c) Adaptable to prepare gradients on various substrates for applications in different fields.

d) Rapid and cost-effective.

We wanted to develop a method with all the above attributes using organoalkoxysilanes, as some of these precursors have already been used in our research group, mainly in sol-gel processes. As previously seen, these compounds were widely used for surface modification and, in most cases, the hydrolysis and condensation reactions are well-known. Also, there are numerous organoalkoxysilanes containing different chemical functionalities that are commercially available. This will allow us to use our gradient preparation method for various chemical functionalities, which is not as common in any of the previous methods. Since the chemical properties and reactivities of organoalkoxysilanes form the basis of the new technique termed ‘controlled-rate infusion’ (CRI), the chemistry and reactivity of organoalkoxysilanes will be first discussed in the following sections to better understand this method.

1.4 Organoalkoxysilanes

Organoalkoxysilanes are a unique class of organic-silicon compounds that contain hydrolytically active silicon-containing functional groups.[58, 59]

$$R\text{-}Si\text{-}(OR')_3$$

R is non-hydrolysable moiety which can be alkyl, aryl, organo-functional or a combination of any of these groups. R' represents the substitution on the alkoxy groups, which are hydrolysable and typically a methoxy or ethoxy group (OCH_3 or OCH_2CH_3). Organoalkoxysilanes can react with organic compounds such as epoxy resin through R groups and inorganic substrates such as modified silica, alumina, glass, etc., through the alkoxy groups by a series of hydrolysis and condensation reactions. Organoalkoxysilanes can act as mediators for the coupling of organic polymers, such as epoxy resin to inorganic materials and hence they are called as 'silane couple agents'. They can also react with themselves and with other silanes by similar reactions.[59, 60] The hydrolysis and condensation of organoalkoxysilanes is represented in Scheme 1.1.

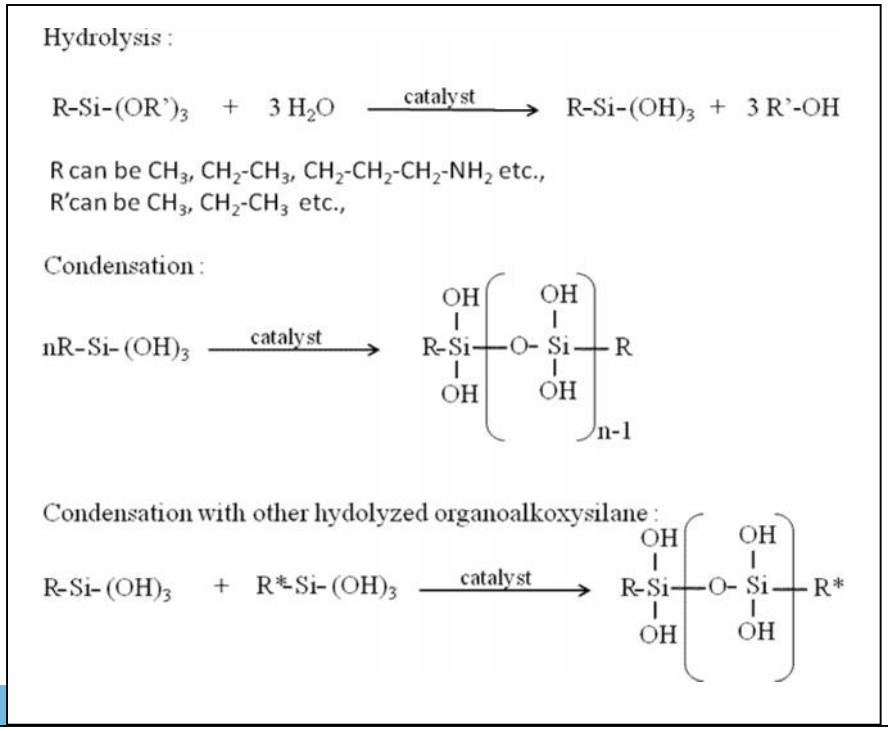

Scheme 1.1. Hydrolysis and condensation reactions of organoalkoxysilane.

The R groups in organoalkoxysilanes are often used to change the physico-chemical properties of a surface, such as wettability[61] and pKa.[62] Also, R can be a reactive group that can further undergo chemical reactions such as amidation,[63] polymerization,[64] etc. Examples of such reactive groups include amino, thiol, cyano, phenyl and azide. The structures of alkoxysilanes with a few reactive and non-reactive R groups are given in Scheme 1.2.

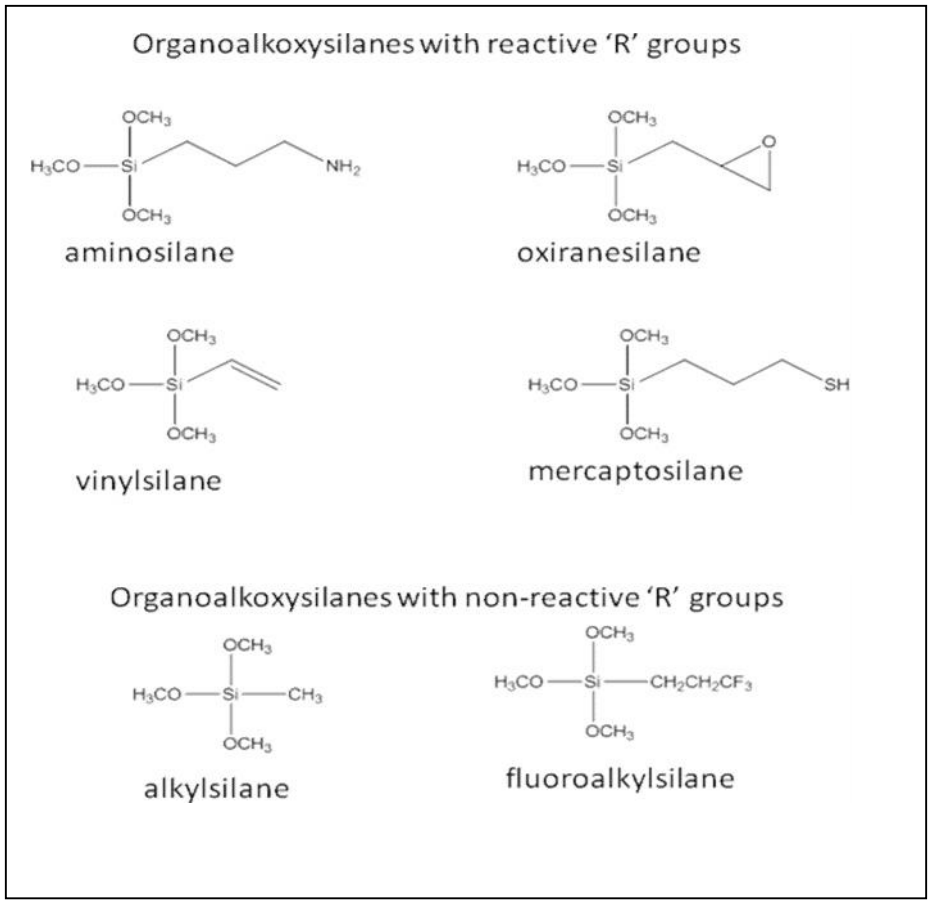

Scheme 1.2. Structures of organoalkoxysilanes (with reactive and non-reactive 'R' groups).

Scheme 1.3 shows a generalized reaction of a trialkoxysilane precursor with a substrate having silanol groups. The alkoxy groups of trialkoxysilanes are hydrolysed to form Si-OH containing compounds. This hydrolysis may occur during the preparation of aqueous solutions of

the silane or in the presence of trace moisture in the atmosphere or adsorbed on the substrates. The rate of hydrolysis of alkoxysilanes depends on steric and inductive effects, and thus the size of the alkoxy group (OCH_3 > OCH_2CH_3 > $OCH_2CH_2CH_3$), replacement of an alkoxy group with an alkyl group and the presence and concentration of catalysts such as a mineral acid or base, and temperature.

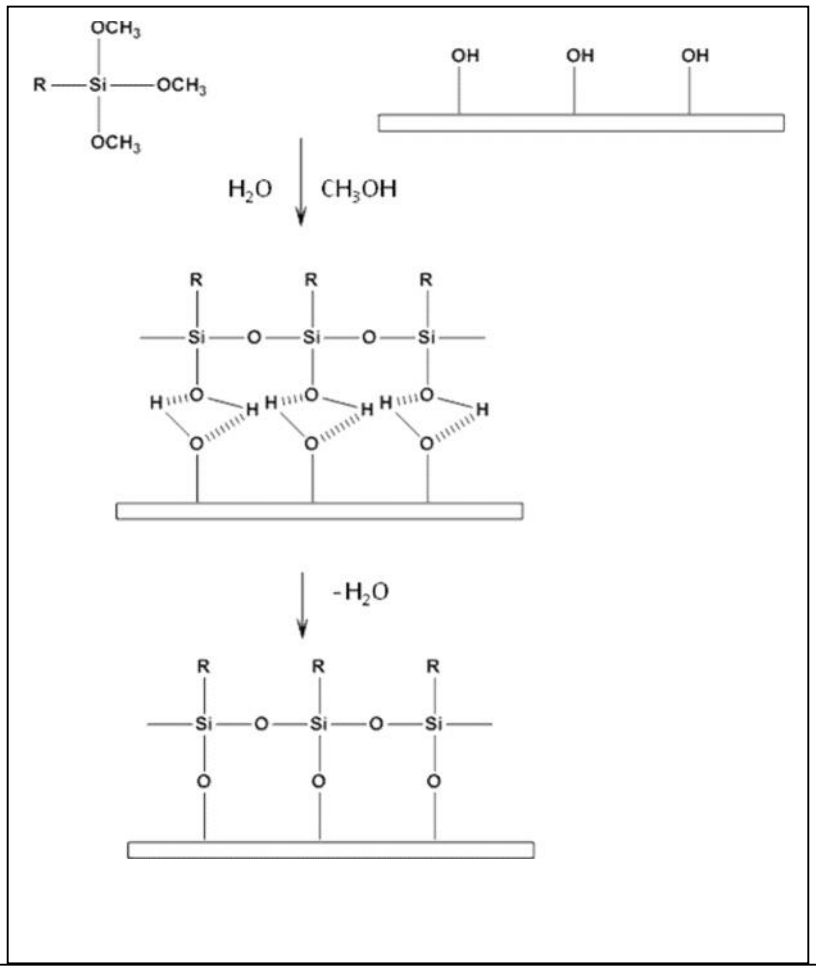

Scheme 1.3. Hydrolysis and condensation reactions of alkoxysilane with the substrate containing silanol groups.

Condensation takes place concurrently with hydrolysis. In this step, a reaction takes place between the hydrolyzed precursor and the substrate silonol groups resulting in covalent Si-O-Si bond formation. But before condensation, an adsorption of hydrolyzed alkoxysilanes resulting

from hydrogen bonding interaction occurs between a hydroxyl group of the silane and a surface-silanols.[65] The condensation reaction occurs horizontally, as wel,l in most cases to form polymeric siloxane structures and this can occur anytime during the process, either before or after adsorption (Scheme 1.4).

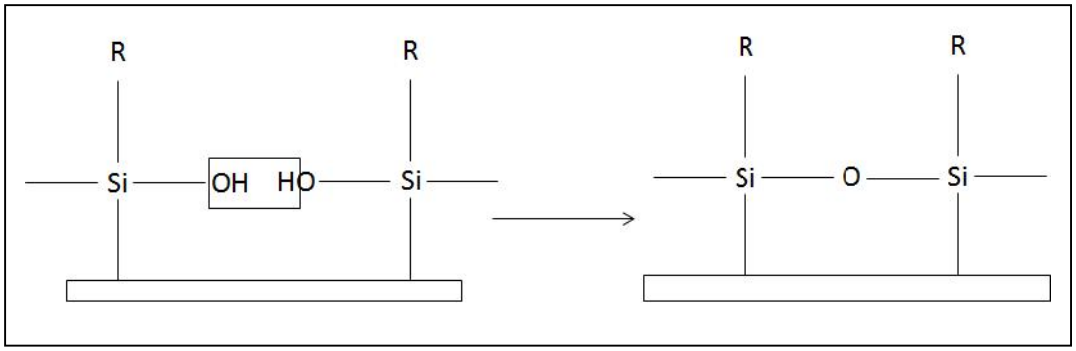

Scheme 1.4. Schematic represents horizontal condensation with neighboring silane on the surface.

The above factors that affect the hydrolysis rate also affect the rate of condensation. Moreover, as the hydrolysis proceeds, the self condensation of silanetriol to form polymeric compounds (Scheme 1.3) will also occur. The organic substituent (R) on the alkoxysilane can also influence the rate of hydrolysis and condensation.[65] For example, the amine group in 3-aminopropyltriethoxysilane (APTEOS) can self-catalyze the rate of hydrolysis and condensation and increase the rate of hydrolysis and condensation.[66] The condensation of an aminosilane with substrates containing silanol groups will be discussed in more detail in the following section as these reactions play a key role in this research study.

1.5 Reactivity of aminosilane

The hydrolysis and condensation reactions of aminoalkoxysilanes with various substrates such as glass, silicon and silica gels have been studied using different techniques like X-ray photoelectron spectroscopy,[67] Fourier transfer-infrared spectroscopy,[68, 69] and Nuclear Magnetic Resonance Spectroscopy.[66] Most of the earlier studies on the reactivity of aminosilanes have been conducted using APTEOS.[70] A general formula for the aminosilanes used in this work is NH_2-R-Si-(OR')$_3$ where R is a propyl in APTEOS. R' can be either a methoxy or ethoxy group. It contains an amino group (-NH_2) that is responsible for the high reactivity of aminosilanes. The N atom in NH_2 group is also involved in hydrogen bonding with neighboring OH groups either from surface silanol groups or from the hydrolyzed silane itself. Fourier transform infrared spectroscopic studies suggested that once the APTEOS starts hydrolyzing, it can form a cyclic structure by hydrogen bonding interactions.[68] The reaction for this is given below in Scheme 1.5.

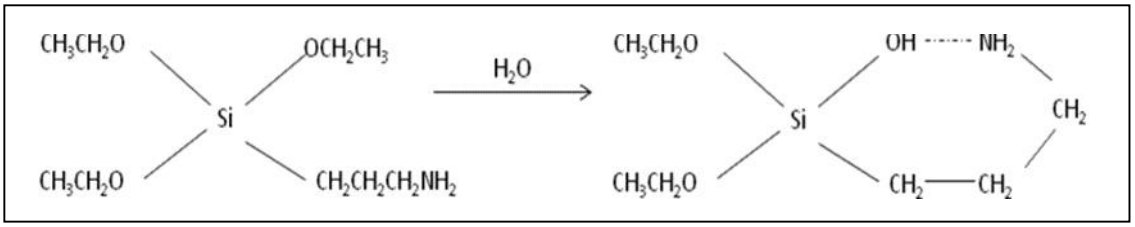

Scheme 1.5. 3-aminopropyltriethoxysilane hydrolyzes and forms a cyclic structure through hydrogen bonding.

The amine groups in aminosilane precursors are involved in hydrogen bonding interactions with surface silanol groups initially and then catalyze condensation to form Si-O-Si bonds.[69, 71] In the case of aminosilanes containing di and triamines, the rate of the reaction is further

increased and the condensation is expected to occur faster. However, alkyl substitution on the amine nitrogen such as secondary and tertiary amines increases the steric effect on the transition state which reduces the condensation rate relative to the primary amines.[72] Since the aminosilane reaction with substrates containing silanol groups is very rapid and straightforward, surface modification using APTEOS has been reported on various substrates for a wide range of applications.[69, 71, 73]

1.6 Controlled-rate infusion (CRI)

As discussed in the previous section, alkoxysilanes will react with surfaces containing silanol groups. The reaction rate depends on various factors such as temperature, water-to-silane ratio, the presence and concentration of a catalyst, etc. For alkoxysilanes that contain an amine group(s) this reaction is very fast because the amine self-catalyzes the reaction. This is one of the primary reasons to start with aminosilane as a precursor to form surface amine gradients using CRI. The other major reason is that the surface amine groups can be further functionalized to form gradients in proteins, nanoparticles, etc, Aminosilane can be used as ligands to prepare gradients in metal-complexes on a surface.

In CRI, gradient formation is done by gradually infusing the silane solution using a syringe pump into a vial containing the substrate.[74] A simple depiction of the process is shown in figure 1.8 for the preparation of surface gradient on a planar surface. For substrates other than planar surfaces (such as for capillary tubes), the infusion procedure is modified accordingly.

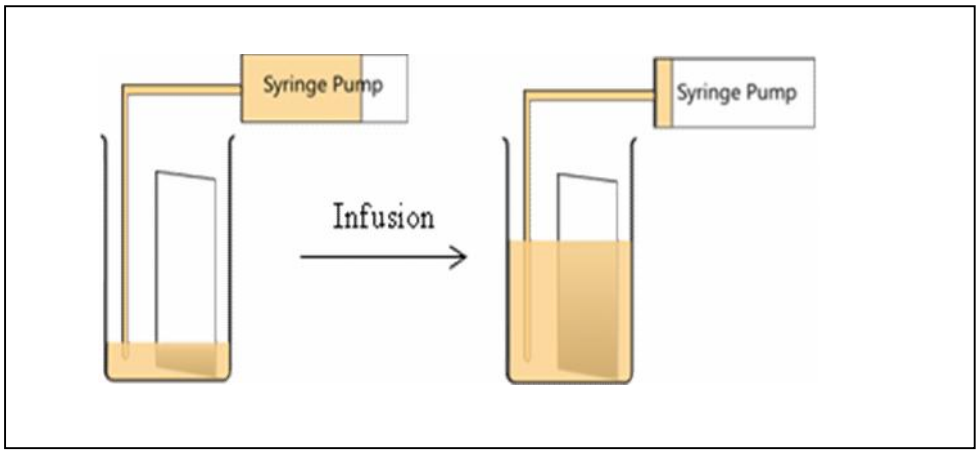

Figure 1.8. Schematic of Controlled-Rate Infusion (CRI). (Reprinted from Ref 74 with permission from American Chemical Society, Copyright 2011).[74]

The experimental procedure for the CRI might sound very simple and rapid. However the key criterion for the CRI to work successfully for the gradient formation is to match the reactivity of silane with the infusion timescale. One of the key attributes of this method compared to other time-dependent gradient methods is the control over the gradient steepness. This can be achieved by simply varying the infusion rates and/or the concentration of the silane. It is expected that slower infusion rates will form shallow gradients and relatively faster rates will form steeper gradients (Figure 1.9A). It is also possible to vary the steepness within a gradient by programming the infusion rates (Figure 1.9B). Chapter 3 discusses the ability of CRI to control the gradient profile by preparing gradients with various slopes. A simple kinetic model was also described which is helpful in predicting the experimental conditions for the desired gradient steepness.

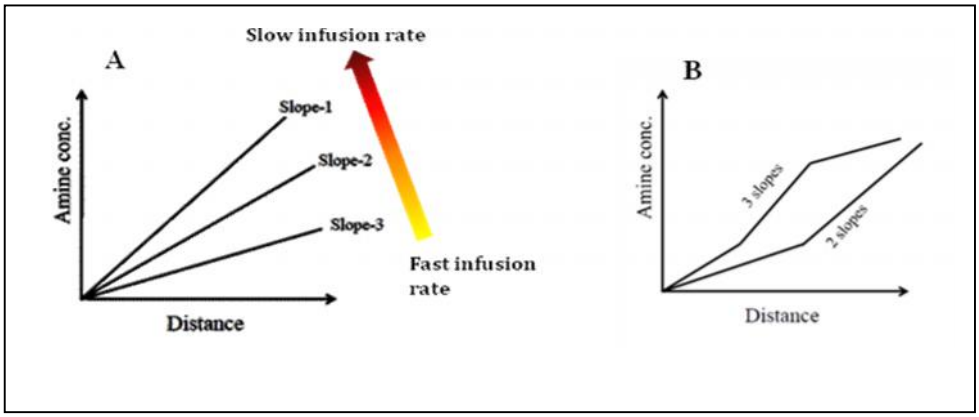

Figure 1.9. Plot represents the effect of infusion rate on steepness of the gradient in CRI: A) Gradients prepared with different infusion rates; B) Programmed gradients where infusion rates are programmed within the gradient formation.

1.6.1 Substrate for gradient preparation

CRI for gradient preparation works on the principle of kinetically controlled Si-O-Si bond formation on surfaces. So, the main criterion for the substrate in the CRI method is the presence of reactive silanol groups. The concentration of silanol groups found on commonly used substrates such as silicon wafer and glass cover slips, will vary depending on the material, its cleanliness, consistency in cleaning procedure and also the age of the reagents used to clean the surface (such as con. H_2SO_4, hydrogen peroxide, etc.,). Hence, prior to gradient deposition, a homogenous film is first formed to provide a consistent and uniform number of reactive silanol groups; it is named 'base-layer' since it forms the base for further gradient formation. The base-layer ensures consistency when the gradient is formed on different substrates like glass coverslips, silicon wafers, gold slides, etc. In this work, the film was made from a sol prepared by co-hydrolyzing and co-condensing tetraethoxysilane (TEOS) and dimethyldiethoxysilane

(DMDEOS) followed by spin coating on the relevant substrate. The base-layer formation is represented structurally in Figure 1.10.

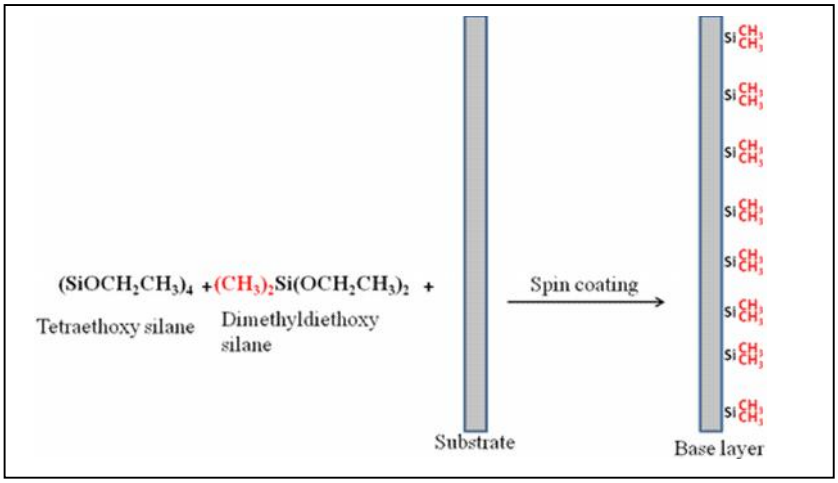

Figure 1.10. Base-layer formation by spin coating of a TEOS and DMDEOS sol on a suitable substrate.

The base-layer also serves as an additional tool to manipulate the surface properties of a substrate via the appropriate selection of other organosilanes. For example an amine gradient on a base-layer containing negatively charged sulfonate groups will provide a charge density gradient from both the ends.

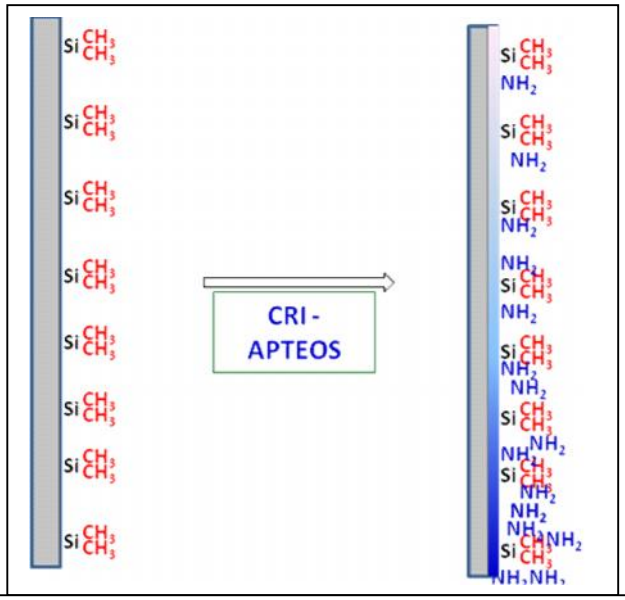

Figure 1.11. Amine gradient formation by controlled-rate infusion from dimethyl base-layer (For clarity, only terminal groups are shown).

Gradient formation using aminopropyltriethoxysilane on a TMOS/DMDEOS base-layer is represented in Figure 1.11. Once the surface amine gradient was prepared on a dimethyl base-layer, it was characterized by X-ray Photoelectron Spectroscopy (XPS) by determining N 1s peak area along the gradient length. Also, gradient steepness was controlled by varying/programming the infusion rates. Chapter 3.3 and 3.4 cover gradient preparation and characterization by XPS, gradient profile control and a simple kinetic model based on APTEOS reaction with surface silanols.

1.6.2 Attributes of CRI method

The attributes of CRI are:

i) Prepare surface chemical gradients in a rapid, simple and inexpensive method. The main equipment used for the preparation is just a syringe pump capable of infusion. It takes about 10 – 30 minutes to fabricate the surface amine gradients.

ii) There is an incredible control over the gradient profile which can be useful to prepare gradient surfaces with multiple profiles.

iii) The main disadvantage of CRI is optimizing conditions for each functional organoalkoxysilane because of the difference in reactivity in each case.

1.6.3 CRI for gradient stationary phases

With the success of amine gradient preparation on a homogenous base-layer, it was decided to prepare such gradients on a longer scale for chromatographic applications, mainly because

i) Continuous silane-based gradients have not been studied to any extent as chromatographic stationary phases.

ii) A wide range of alkoxysilanes with functional groups that are used as bonded

phases in chromatography such as –CN, phenyl, amine, etc. exist.

iii) The CRI method is not only capable of preparing gradients on planar stationary phases, it can also form gradients on open tubular surfaces and microchannels.

Since the main focus of this work is the application of CRI to form gradient stationary phases, a brief introduction on gradients in chromatography and the significance of gradient stationary phases are given in the next section.

1.7 Stationary phase (SP) gradients in chromatography

Separation of complex mixtures by liquid chromatography has always been a challenging area for separation science researchers. This is mainly due to large differences in polarity and pK_a of various components present in a complex mixture. The challenge of separating such complex mixtures into individual components has been overcome mainly by gradient elution (e.g., a mobile phase gradient) where the eluent strength is varied during separation.[75] This is in contrast to isocratic elution where the composition of mobile phase is same throughout the separation. There are numerous applications of gradient elution in liquid chromatography (LC) for the separation and quantitation of a wide range of analytes from simple compounds to complex biological mixtures and metabolites.[76-79] In spite of its ability to separate the various components in a complex analyte mixture, there are limitations that restrict the use of gradient elution.

Even though gradient elution has been widely used by chromatographic researchers in various fields, liquid chromatographic (LC) method development involving gradient elution is relatively more complex than isocratic elution, because the selectivity depends on too many variables.[80-82] In gradient elution, certain experimental parameters are very critical such as

equilibration time[83, 84] and solvent degassing, which can affect the reproducibility of retention times. Also, gradient elution sometimes suffers from baseline shifts due to incompatibility with bulk property detectors (e.g., refractive index detector (RID)) when the mobile phase composition is changed.[85-88] An alternate concept to changing the chemical properties of the mobile phase is to change the chemical properties of the stationary phase along its length.[89] The variations in stationary phase gradients can be i) adsorbents such as silica, alumina etc. ii) stationary phase bonded phase material such as butyl (C_4), octadecyl (C_{18}), amine (NH_2) etc., and iii) concentration of the bonded phase along the stationary phase.

Stationary phase gradients have been prepared on various chromatographic platforms such as thin layer chromatography, high-performance liquid chromatography and capillary chromatography.[14] Though they are not as widely used as gradient elution, stationary phase gradients have been studied since 1965 until very recently for various applications.[90] In 1963, Berger et al, used different adsorbents to demonstrate the first stepwise gradients in TLC stationary phase,[89] and later this approach was developed extensively by Stahl and Warren with various improvements in preparation methods.[91-93] The first continuous gradient stationary phase in TLC was developed by Stahl and co-workers,[93] in which they used a divider box with compartments, a mixing vessel and an applicator to continuously apply various adsorbents on TLC plates. Some other devices were also reported to reduce the complexity of the spreading procedure.[94, 95] The main disadvantage of these methods was their lack of reproducibility to give a uniform gradient layer since the approach needs mechanical skills like spreading, mixing, etc.

Similar to those in TLC, various stationary phases have been used as a means to improve separations in HPLC.[96-98] In HPLC, gradient stationary phase gradients have been made by

serially connecting various columns for selectivity optimization. This approach is called 'stationary phase optimized selectivity liquid chromatography' (SOSLC). The most important application of this technique is liquid chromatographic (LC) method development by optimizing the selectivity of chromatographic separation. The chromatographic parameters such as retention factors (k) determined by SOSLC are used for the selection and optimization of chromatographic conditions for a given mixture of analytes.[98] Until now, the majority of the stationary phase gradients reported were prepared by coupling two or more columns or packing various stationary phases in a discrete fashion. These are discrete gradients wherein each variation along the stationary phase has a specific boundary. The reproducibility of such a method has always been in question and it requires skillful hands to prepare in a reproducible manner. Even though some methods such as connecting various columns in series seem easy, when the analyte travels through these phases it also has to encounter connections (such as tubings) between each of the phases, leading to band broadening. In such cases, the reproducibility of certain parameters such as retention times and peak efficiencies will be affected. Serial gradients differ from continuous gradients where the composition varies gradually without any specific boundary (Figure 1.12).

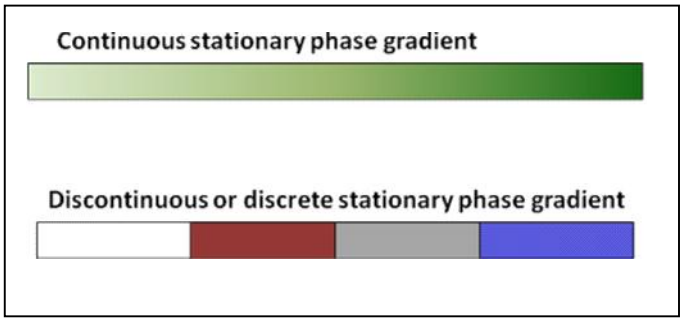

Figure 1.12. Continuous and discontinuous gradients.

Currivan et al. reported continuous stationary phase gradients in capillary polymeric monoliths prepared by photografting and copolymerization,[99] which is laborious. In contrast, CRI more straightforward than photografting and should have better control over the chemistry.

Aminopropyl bonded silica stationary phase has been used extensively for the separation of wide variety of compounds such as sugars, pharmaceutical samples and other acidic & basic compounds.[100-105] Since amine groups are basic in nature, it is expected that aminopropyl gradient prepared by CRI will be highly useful for the separation of analyte mixture with a wide range of pKa values. In Chapter 6, this phenomenon is demonstrated with four compounds whose pKa ranges from ~4.2 to 9.5. In Chapter 7, CRI was used to fabricate surface charge density gradients on fused silica capillaries which can be used for capillary electrochormatography.

1.8 Evaluation of aminoalkoxysilane reactivity by gradient profiles

So far, applications of gradient materials were seen in various fields such as biological sciences, chromatography, controlled transport, etc. Here is a unique application of amine gradients prepared by controlled rate infusion method. Apart from APTEOS, there are a number of commercially available silanes which are widely used for surface modifications for various purposes. It was decided to prepare surface gradients using various aminoalkoxysilanes to study the reactivity of those silanes by using the gradient profiles. The aminoalkoxysilanes chosen for this work are the primary amines that contain 1 (mono), 2 (di) and 3 (tri) amine groups and also monoamines with secondary and tertiary substitutions. Gradient application of this kind (to study the reactivity of various precursors itself) requires the technique to have certain advantages. These are i) the chemistry involved in such reactions should be simple and straightforward so

that the results can be directly interpreted. ii) It should not involve any complex experimental step in the gradient formation procedure so that the interpretations are unambiguous and iii) Lastly, there should not be any undesired reactions which might not be controlled during the course of gradient formation. For example, if the aminosilane vapor phase co-reacts with the substrate along with solution phase, it is difficult to control the reaction during infusion.

The controlled-rate infusion (CRI) technique obeys all the above criteria, and this study was successfully accomplished. Gradient preparation and characterization of these gradients covered in chapter 4. Also, the kinetic model which gives us the quantitative comparison of silane reactivity by evaluation of rate constant values is also discussed there. Information on surface basicity of these amine groups is an additional piece of information derived from XPS data. Two of aminosilane (di and triamine) used in the above study can act as chelating ligands for metal binding. Cu^{2+} and Zn^{2+} amine complex formation on di- and triamine gradients was studied extensively and is described in Chapter 5.

1.9 Metal chelation gradients

Once the surface gradients with ethylenediamine and diethylenetriamine were successfully prepared, it was decided to utilize the chelating property of these multidentate ligands. These ethylenediamine and dithylenetriamine groups grafted on a stable support like silica can act as effective chelating agents for metal complexation. Apart from direct applications of metal complex gradients, it is considered to be an interesting phenomenon to see the different metals binding on a gradually varying ligand concentration. A metal-amine complex gradient is schematically represented in Figure 1.13.

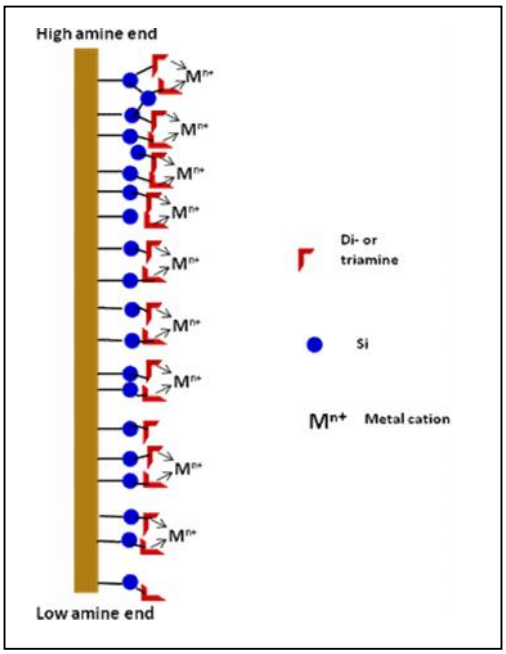

Figure 1.13. Metal chelation gradient on di/tri amine gradient.

In this work, Cu^{2+} and Zn^{2+} complex formation was studied on continuous gradients of di and triamine ligands with different gradient profiles.

1.10 Scope of the dissertation

Though there were many successful gradient preparation methods reported in the past two decades, these methods were developed to target applications in a specific fields such as biomaterials, separation science, etc. There are very few methods that can be extended on various platforms for entirely different applications. To develop such methods, the chemical properties of the precursor and substrate should be well-established. Also, the method should be flexible in order to modify it for other applications. The goal of this dissertation work is to

develop a simple method for gradient preparation by coupling time-based methods and capitalizing on the reactivity differences of organoalkoxysilanes. Obtaining quantitative information on the reactivity and also to have control over the gradient profile are also key attributes of this work.

Once the gradient preparation method was proved to be successful, the method was extended to prepare gradients on thin layer chromatography plates and inside a fused silica capillary tube for applications in chromatography. The method was adopted almost without any change to prepare stationary phase gradients for planar chromatography. The fabrication and characterization of gradients inside capillaries proved challenging. This was mainly because the total infusion volume was small: from sub µL to 2 uL. A small leak in the connections would cause a huge error in the experiment. A novel streaming potential method was developed to visualize the amine gradient inside the capillary. The CRI method is not just helpful in preparing gradients for chromatographic separations; it can also serve as an important tool to study the reactivity of various precursors which could be a useful tool to develop high-throughput surface modification procedures.

2. Characterization Techniques

2.1 Introduction

Numerous techniques have been reported for the characterization of surface chemical gradients. In this chapter, the basic principles and experimental conditions are discussed for all the characterization techniques involved in this dissertation work. X-ray photoelectron spectroscopy (XPS) was used to measure the density of amine groups along the gradient surface on Si wafers. Contact angle measurements were used to study the variation in wettability across the surface of the gradient on a base-layer coated silicon wafer. A simple ninhydrin test was used to visualize amine gradients on TLC plates. Streaming potential measurements and XPS were employed to evaluate gradients on capillary tubes.

2.2 X-ray Photoelectron Spectroscopy (XPS)

XPS is a surface characterization technique that can measure elemental composition and the chemical and electronic state of elements on the surface (typically the top 5-10 nm). X-rays are emitted usually from a Mg or Al anode material. When a surface is irradiated by X-rays of sufficient energy, electrons are removed from the surface atoms due to the photoelectric effect. In Figure 2.1, a schematic of an electron is being removed from the carbon 1s orbital by X-ray photon is depicted. When the electron is removed by an X-ray, the kinetic energy of the ejected electron is measured and it depends on the binding energy (BE) of the electron, the energy of the X-ray irradiation beam (hν) and the work function (ϕ) of the instrument.[106] The binding energy of the electron can therefore be calculated using the equation below, if the work function of the instrument and the energy of the X-ray are known.[106]

$$BE = h\nu - KE - \phi$$

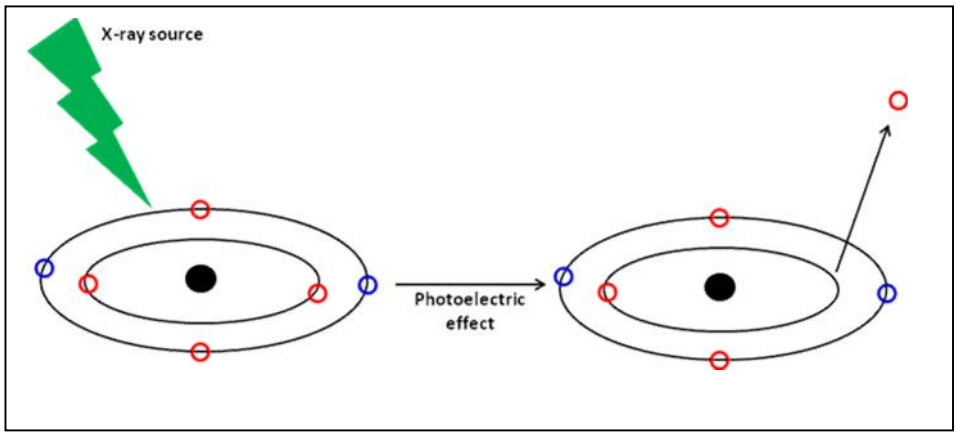

Figure 2.1. Removal of a carbon 1s electron by photoelectric effect.

The binding energies of the electrons are characteristic of the elements and their orbitals. Hence, it is possible to identify the various chemical components present on a surface from XPS spectra by comparing the measured binding energy with reference values. The intensity of the signals is proportional to the amount of a particular group or element present on the surface. This proportionality depends on various factors such as ionization cross-section (sensitivity factor σ_A), transmission function (T_A) of the instrument, the inelastic mean free path (λ_A) and the sine of the take-off angle (θ).[106]

$$N_A = \frac{I_A}{(\sigma_A T_A \lambda_A \sin\theta)}$$

The sensitivity factor and mean free path are characteristic of each element. Therefore it is necessary to correct for these values during quantification or when determining atomic ratios of different elements. Also, depending on the chemical environment of an atom, the binding energy

of the electrons vary slightly, which will result in a characteristic shift of the XPS signal. This can provide additional information about the surface composition, provided the spectrum is acquired with high-resolution.

XPS analysis is generally performed under ultra-high vacuum to avoid collision of the emitted electrons with the gaseous atoms and to reduce contamination of the surface from the atmosphere. An XPS instrument consists of an X-ray source, an analyzer where the electrons are separated based on their kinetic energy, and a detector (as shown in Figure 2.2).

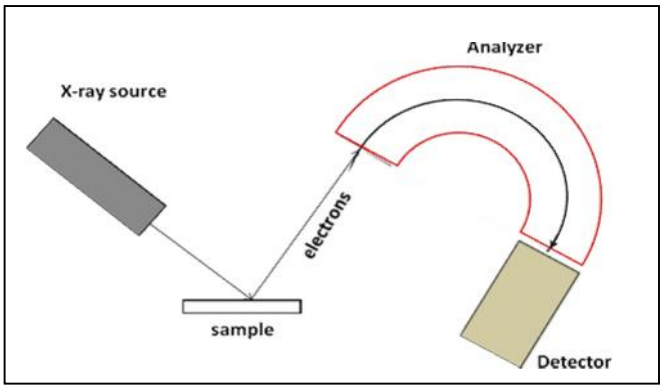

Figure 2.2. Schematic sketch of an X-ray Photoelectron Spectrometer.

The X-ray source is often an Al Kα or a Mg Kα source as they have narrow natural bandwidths, which leads to well resolved XPS signals. Sometimes a quartz crystal is used as monochromator to narrow the line-width before it is focused on the sample. The lens set-up is used to focus the electrons before they reach the analyzer, where the electrons are segregated based on their kinetic energy. The detector carries out electron counting at a particular binding energy and results in a plot of intensity versus binding energy.

By varying the angle between the sample and analyzer (varying the take-off angle), the sampling depth can be varied between 1 - 10 nm.[107] The disadvantages of XPS are the requirement for ultra-high vacuum, the long acquisition times and the possibility of sample

degradation. Apart from that, XPS has a great advantage of providing a wide range of information regarding the surface composition of materials. Almost all the elements can be detected and it is possible to carry out quantitative analysis. The chemical shift in XPS provides valuable information on chemical bonds, substitutions, chemical state, etc.[108] The uniformity of one of more elements at different heights/layers is called "depth profiling" and can be done by XPS using ion-gun etching of the surface.[109, 110]

The X-ray photoelectron spectra in this work were acquired with a ThermoFisher ESCAlab 250 equipped with a radian lens, a concentric hemi-spherical analyzer and a two-dimensional channel-plate detector. A monochromatic Al Kα source with a spot size of 500 μm was used. The instrument was operated with 50 eV pass energy and 0.1 eV step size. To analyze the data, the Thermo Avantage program (Version 4.33) was used. 'Smart' background correction was used for the integration of all peaks. This is the type of background correction is preferred by the Avantage software itself. It gives a 'S-shaped' background similar to Shirley background but it will adjust the background positions so that they will not go above the data-curve..

2.2.1 Area normalization and peak fit.

A. N 1s peak fit

Chapter 4 discusses the application of gradient formation to study the reactivity of various substituted aminoalkoxysilanes and evaluate the surface basicity. This was accomplished by deducing the ratio of protonated and free amine peak in XPS using curve fitting. To perform curve fitting using Avantage software, the N1s spectrum was loaded and the area under the peak from ~ 306-404 eV with 'smart' background correction determined. Then it was curve-fitted using Gaussian-Lorentzian (70:30) function in such a way to give a normalized chi-square value

that was close to 1 (0.7-0.95) and the Abbe criterion was close to 0 (0.1-0.3) in order to qualify as a good fit. The peak fitting function used for the Gaussian-Lorentian product function is

$$f(x) = \frac{\text{peak height}}{[1+ M(x-x_0)^2/\beta^2 \exp\{ (1-M) [\ln 2 (x-x_0)^2]/ \beta^2\}}$$

where x_0 is the peak centre, β is a parameter which is 0.5 (FWHM) and M is the mixing ratio. The value of M is 1 for a pure Lorentzian peak and 0 for Gaussian peak.

Once the N1s curve was successfully fit into two N1s peaks, the ratio of N1s peaks of protonated and free amine was determined and plotted vs distance along the gradient to obtain information on how the surface basicity changed along the length of the gradient.

B. Area normalization to determine the nitrogen to metal ratio

Chapter 5 describes metal-amine complex formation on ligand density gradients through chelation. Also, the variation in metal-amine coordination number along the gradient was investigated by determining the ratio of amine to metal surface concentration. This was achieved by calculating the normalized area ratio of N1s to metal (Cu and Zn) 2p peak along the gradient taking into account the sensitivity ratios as described below. In the case of Cu^{2+} and Zn^{2+} amine gradients, the normalized areas of N1s and metal 2p peaks were obtained using the Wagner library in the software. There are two peak libraries, Wagner and Scofield, but in both the cases the normalized area is determined by

Normalized area = Peak area / (SF * TF * ECF)

SF is sensitivity factor determined from the library. The Wagner and Scofield methods use different sensitivity factors. Wagner library is considered to be more accurate and used in this work.[111] TF is transmission function and it is a correction (for instrumental parameters) to ensure better quantification results. ECF is energy compensation factor and is calculated for Wagner library as Wagner – $KE^{1.0}$ and for Scofield – $KE^{0.6}$ where KE is kinetic energy of the electron. The ratio of the normalized area was plotted along the distance to obtain the profile plot.

2.3 Contact angle measurements

Contact angle measurement is a fast and simple method to evaluate surface wettability. The angle between the solid-liquid interface and the liquid-vapor interface is referred as the contact angle. It is represented in Figure 2.3.

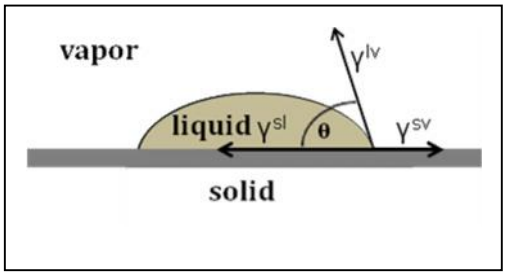

Figure 2.3. Schematic sketch of a droplet on a surface for contact angle measurement.

A drop with a contact angle above 90° on a surface is considered to be hydrophobic and below 90° is considered to be hydrophilic (Figure 2.4). The standard liquid used in this measurement is water. However, other liquids such as hexadecane have been used for evaluating oleophobicity.

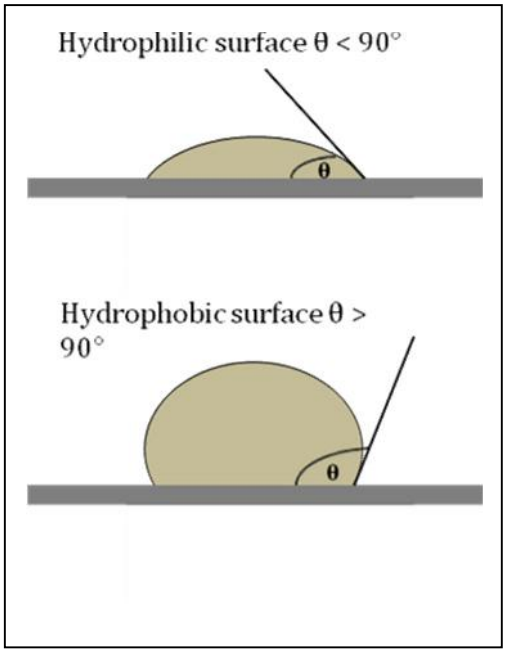

Figure 2.4. Schematic sketch of a water droplet on a hydrophobic and hydrophilic surfaces.

The way in which the contacting liquid is wetting the surface depends on the interfacial surface tension (γ) between surface (s), liquid (l) and gas (g). It is correlated to a contact angle on a flat surface by Young's equation.[112]

$$\gamma^{sv} = \gamma^{sl} + \gamma^{lv}\cos\theta$$

θ is the contact angle
γ^{sv} is solid/vapor Interfacial tension
γ^{lv} is liquid/vapor Interfacial tension
γ^{sl} is solid/liquid Interfacial tension

The easiest of all the reported methods for measuring the contact angle is the 'static sessile drop method'. We have followed this method as one of the characterization methods for surface amine gradients on a dimethyl base-layer coated silicon wafer. Contact angles were measured by

a contact-angle goniometer, which contains the optical unit for capturing the liquid-drop profile on a flat solid surface. In this work, a RameHart goniometer equipped with a high resolution camera was used to capture the water droplet and the software called 'DROPimage CA' was used to analyze the contact angle. Contact angle values in the sessile drop method can be affected by surface roughness and drop size. But in this work, the drop size was kept constant (~0.5 μL) throughout the measurements to avoid any such errors. Static contact angles determined by the above mentioned method can only determine the wettability of the surface. Roughness and other surface inhomogeneities can be determined by the 'dynamic contact angle' which requires a relatively sophisticated set-up compared to the static contact angle measurements.

2.4 Visualization TLC plates-ninhydrin test

Chapter 4 describes the ability of CRI to fabricate surface amine gradients on silica TLC plates for chromatographic separation. XPS analysis cannot be used to visualize amine groups on TLC plates because of amount of moisture present in the porous silica particles, which is harmful to the XPS instrument. Also, the length of the TLC plates is too long for a XPS sample holder. So, a simple visualization method was developed using a widely used amine specific chromogenic reagent, ninhydrin. It is considered as a universal reagent for the detection of amino acids and primary amines especially in forensic science.[113] Ninhydrin reacts with primary amino groups to form the purple dye (Scheme 2.1) called Ruhemann's purple (RP), which was discovered by Siegfried Ruhemann in 1910.[113] This reaction is peculiar among all chromogenic reactions in that it results in the formation of the same soluble chromophore by all primary amines whether they are amine, amino acid, protein etc. The intensity of color formation depends

on the concentration of amine groups on the surface. Ninhydrin is used commonly as a spray reagent for detection and analysis of amino acids, peptides and compounds containing amine groups in a wide range of samples such as food, pesticides, plant extracts, etc.[113]

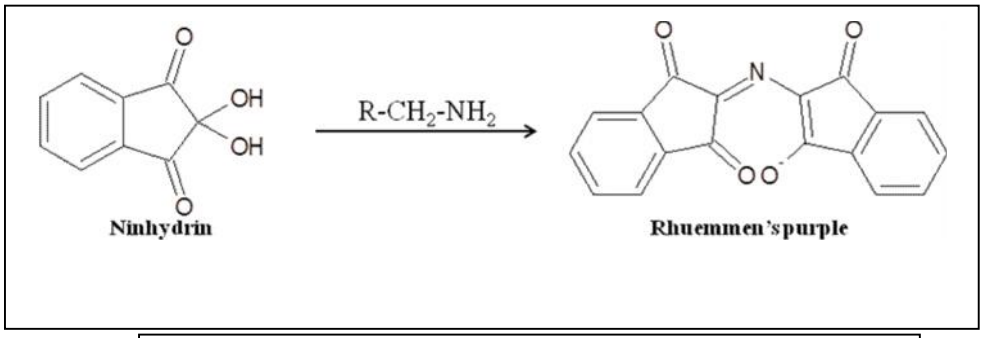

Scheme 2.1. Ninhydrin reaction with primary amines.

Since the silica TLC plate has aminopropyl groups, it was decided to utilize this simple reaction to visualize the variation in surface amine density along the plate. Visualization was accomplished simply by spotting ninhydrin every ~1 cm (figure 2.5) on the gradient and control plates and its image was captured under white light using a digital camera. The time scale between spotting and taking the photograph was kept constant for gradient and control plates. Later the photographs were analyzed by digitally enhanced TLC analyzer, a free software to extract the intensity of colors (black, red, green & blue). The intensities of color formed due to the product formation (Ruhemann's purple) were plotted as a function of distance along the TLC plates to define the profile of the gradient. Another way of treating the plate with ninhydrin was by soaking the whole plate in ninhydrin solution so that the intensity of color formation along the gradient plate could be the measure of amine gradient. However, the spotting method is considered better than soaking because of the way in which ninhydrin reacts with the amine on the plate. It reacts with the alkyl amine, cleaves the NH_2 group to form the free dye, Ruhemann's

purple. Because some of the dye can be lost in solution as the plate is dipped into the reagent solution, its best to spot rather than soak the TLC plates with ninhydrin.

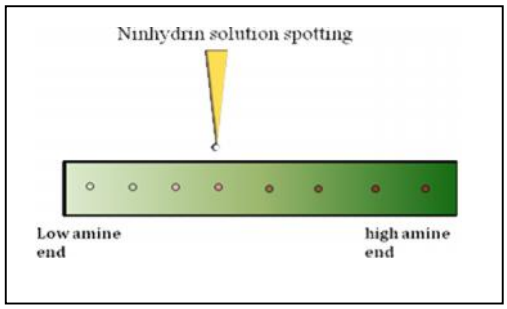

Figure 2.5. Spotting ninhydrin on a gradient TLC plate.

2.4.1 Digitally enhanced TLC analyzer (DE-TLC analyzer)

DE-TLC analyzer is free software mainly developed as an inexpensive tool for qualitative and quantitative detection in TLC analysis.[114, 115] With the aid of a digital camera and this software, it is possible to extract red, blue and green spectrum (RGB) from the TLC plate. It works in such a way that when the picture is uploaded in the software, it allows the user to draw a line across the plate where the analysis needs to be done. It gives four spectra i.e., red, green, blue and black/white (b/w) spectrum along the line (Figure 2.5).

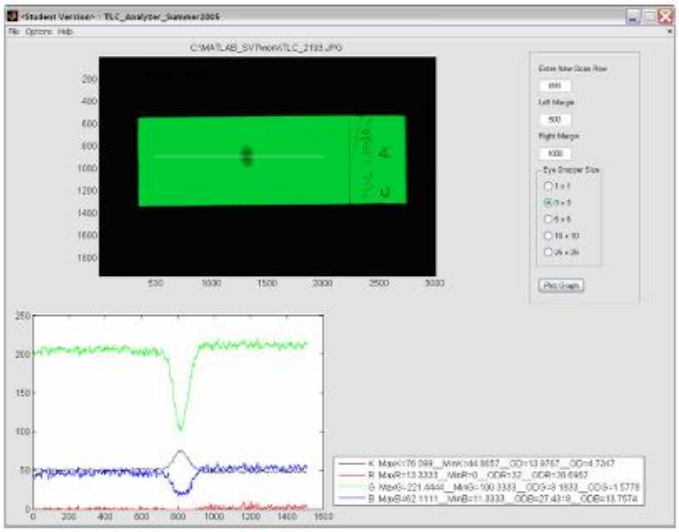

Figure 2.6. DETLC analyzer- Snapshot of uploaded TLC picture and corresponding spectra (red, green , blue & black/white) obtained across the white line drawn across the sample spots..

Because the TLC plate contains a fluorescent indicator, the TLC plate appears green under 254 nm radiation. In Figure 2.5, a test spot in the middle of the plate can be seen. Using the software, a line was drawn across the test spot. Since the spot quenches the green fluorescence, a negative peak is observed in the green spectrum. In the case of separation on TLC plates, the photographs were taken under UV chamber with a 254 nm lamp. The analyte components are present as dark spots because they quench the fluorescence. In the ninhydrin spotted TLC plates, the line was drawn over the dark spots and peaks were obtained. The intensity of the black-white spectrum peaks was plotted vs. distance.

2.4.2 Detection for analyte separation

As mentioned above, the analyte compounds appear as dark spots under UV light because of fluorescence quenching. Hence, the components in the TLC chromatogram will appear as negative peaks similar to the green spectrum in F**igure 2.5.** The distance between analyte spot before elution and the peak apex for each peak was considered as distance travelled by the compound to calculate the retention factor (R_f) factor in each case. R_f is the measure of the retention of a compound in a planar chromatographic system.[116]

$$R_f = \frac{\text{Distance travelled by the compound}}{\text{Distance travelled by the solvent}}$$

Also, resolution between the neighboring peaks was calculated for each component using the equation below[116]

$$R_s = \frac{D}{(W_1 + W_2)/2}$$

where D is the peak-to-peak distance of the two peaks and W_1 and W_2 are base width of the peaks.

Since the sample was spotted on the TLC plate manually, the spot size varied. This could affect the measurement of peak width to compute the number of theoretical plates (N and H). Hence, theses parameters (N and H) were not determined in this study.

2.5 Streaming potential measurement

Characterization of surface amine gradients is a challenging task when they are chemically bound on the inside walls of a capillary. This is mainly because the surface amine groups are not exposed on the outside, which limits the use of common surface characterization techniques such as XPS and contact angle measurements. Streaming potential measurements have long been used for the characterization of surface modification especially surface charge densities on capillary.[117] It is one of the several electrokinetic effects that is influenced by the surface charge. On a charged surface such as a microchannel or colloidal particles, an electrical double layer (EDL) is formed at the interface by the surface charge and the surrounding counter ions in solution. This layer has two distinct parts, a Stern layer where the counter ions are strongly attached to the surface and 'diffuse layer' where the ions are less strongly bound.[118] The ions that exist at the Stern layer and the diffuse layer close to it can move when the charged solution moves. The rest of the counter ions remain static in bulk. The plane that separates the moving and stationary layer of ions is called 'Shear plane'. The potential that exists at this plane is called 'Zeta potential'[119] (Figure 2.6).

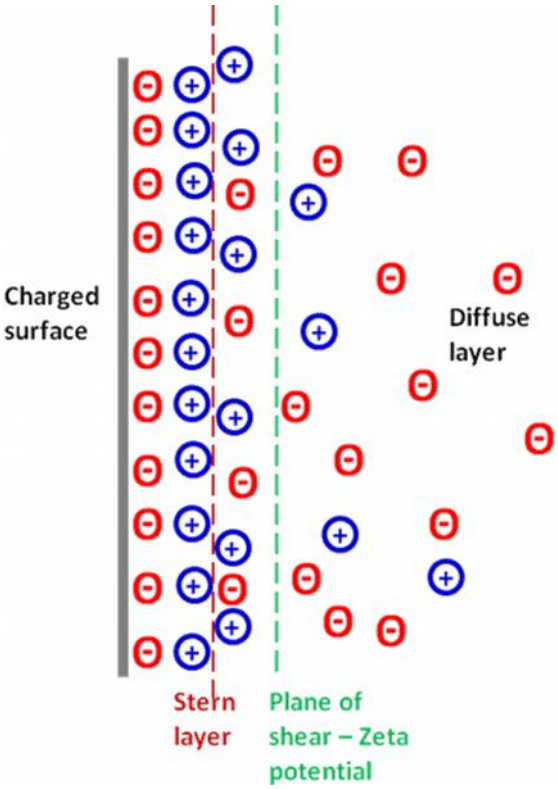

Figure 2.7. Schematic sketch of the double-layer.

Streaming potential measurements are one the methods used to determine the zeta potential at the surface, other than electroosmotic mobility.[120] When an ionic solution is allowed to flow across a charged surface, such as silica capillary, there will be a double layer formed with the counter ions and the ions at the surface. When an external pressure is applied to the capillary solution, the liquid is externally forced to move through it from one end to the other. This will create the counter-ion displacement on the EDL and produces an excess of ions at one end and

depletion at the other end (Figure 2.7). This generates a potential between the two ends of the capillary tube called the 'streaming potential'.[121]

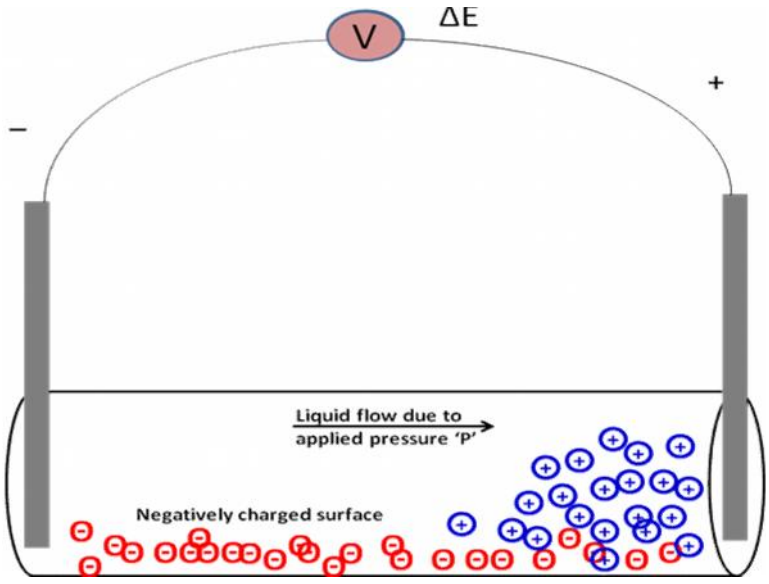

Figure 2.7. Schematic diagram of the streaming potential measurement.

The streaming potential thus generated is measured as a potential drop across two platinum electrodes, the magnitude of which is related to the zeta potential using the Smoluchowsky equation'[122]

$$\Delta E = P\, \zeta\, \varepsilon_r\, \varepsilon_0 / \eta\, \lambda$$

In this equation, ζ is the zeta potential in volts, η is the viscosity of the solution in Pascals-second (Pa-s), λ is the conductivity of the solution in Siemens per meter (S/m), **ε** is the dielectric constant of water, $\boldsymbol{\varepsilon_0}$ is dielectric permittivity of vacuum, ΔE is streaming potential in volts, and P is pressure in Pa. If the applied pressure, dielectric permittivity, viscosity, and conductivity of

the solution are kept constant, the streaming potential depends solely on zeta potential. Streaming potentials measured with pulsed flow allow for accurate and precise values to be obtained quickly using non-reference platinum electrodes.[2, 123] Zeta potential is calculated by rearranging the above equation

$$\zeta = (\eta \lambda/\varepsilon_r \varepsilon_0) \times \Delta E/ P$$

where $\eta = 0.936 \times 10^{-3}$ Pa.s

$\varepsilon_r = 79$

$\varepsilon_0 = 8.85 \times 10^{-12}$ F/m

$\lambda = 0.024 \pm 0.001$ S/m (exact value was measured by conductivity meter each time)

$P = 65 \times (1.333 \times 10^3)$ Pascal

ΔE = Streaming potential in V

Because zeta and streaming potentials are very sensitive to the surface charge density, they can provide a valuable means to characterize the profile of a surface chemical gradient of amine groups in a narrow diameter capillary. However, zeta potential calculated by the Labview software (using the above equation) was used for gradient profile plots since zeta potential is considered as a direct function of surface charge density. Under near neutral pH conditions, the amine groups will be protonated giving rise to a positive zeta potential; an unmodified capillary will give rise to a negative zeta potential because of surface silanol groups. It is understood that zeta potential depends on solution pH as well, because of protonation and deprotonation on the surface.

In our case, the amine groups are protonated at (pH < 7), which gives rise to a positive zeta potential. As the surface amine density changes along the length of the capillary, the zeta

potential will change. Hence, at a given pH, the plot of zeta potential versus distance should exhibit a gradient trend providing there is a gradient of amine groups on the surface. The experimental set-up designed for the streaming and zeta potentials on the amine modified gradient capillaries will be discussed in detail in Chapter 7.

Chapter 3- Profile Control in Surface Amine Gradients Prepared by Controlled-Rate Infusion

Adapted from Kannan, B.; Dong, D.; Higgins, D. A.; Collinson, M. M., *Langmuir* **2011,** *27* (5), 1867-1873

3.1 Abstract

Surface amine gradients that exhibit a wide variety of profiles, including those that incorporate spatially distinct regions having steep and gradual variations in chemical functionality, have been prepared by the sol-gel process using a controlled-rate infusion method. In this work, a substrate that incorporates dimethyl and Si-OH groups is temporally modified with an aminoalkoxysilane ($NH_2(CH_2)_3Si(OC_2H_5)_3$) to build a gradient film for which the amine content changes over a 10-20 mm distance. Both x-ray photoelectron spectroscopy (XPS) and contact angle measurements confirm the presence of a chemical gradient across the surface of the film. As expected, a greater density of amine functionalities and lower contact angle were found at the bottom of the gradient relative to the top. The local steepness of the gradient was systematically controlled by changing the rate of infusion. Fast rates of infusion created gradient surfaces where the amine content changed slowly along the surface and never reached saturation, whereas slow rates of infusion formed a surface exhibiting a steep rise in amine content followed by saturation. The steepness of the gradient was also changed at predefined positions along its length by programming the rate of infusion. Gradients prepared using six-step, three-step, and two-step programmed infusion rates are shown. The data fit nicely to a kinetic model that assumes first-order kinetics. The ability to manipulate the gradient profile is particularly vital for applications that rely on mass transport and/or those that require spatial control of gradient properties.

3.2 Introduction

The ability to spatially organize functional groups on surfaces in a controlled fashion is needed for diverse applications including those that involve directed/controlled transport and the growth and adhesion of proteins and cells on surfaces.[2, 6, 124-126] In particular, for applications related to directed/controlled transport, gradients of precisely controlled steepness along the gradient dimension is necessary. Various methods have been developed over the past two decades for the preparation of chemical gradients. A few of these methods especially the ones that are based on diffusion of silane molecules have been widely used for various applications. An inherent limitation of all methods that rely on diffusion, however, is that the gradient profile (steepness) cannot be easily controlled. Genzer and coworkers circumvented this limitation by forming gradients on stretched PDMS films.[28] When the strain in the PDMS films was released, the steepness of the gradient increased relative to that obtained on an unstretched film. By changing the degree at which the PDMS films were stretched, the slope of the gradient was changed.[28] However, in all cases the shape of the gradient corresponded to "Fickian-type diffusion profiles".[28] Although clever, this method is limited to flexible surfaces.

Another study where the gradient steepness was varied was discussed in Chapter 1. It was used to form metal nanoparticle and nanoparticle-protein gradients of varying slope.[29] In the present study, a sol-gel based immersion method was used to create functionally graded thin films whose steepness was changed at predefined positions along its length. This approach takes advantage of the versatility provided by silane chemistry and, most importantly, affords explicit control over the gradient profile (i.e., the local steepness of the gradient surface). The process begins with the formation of a universal base-layer that contains reactive silanol functionalities on a suitable substrate (glass slide, electrode, silicon wafer, etc.) followed by time-dependent

exposure of the base-layer to a reactive organoalkoxysilane ($R_xSi(OR')_{4-x}$) via controlled-rate infusion. The presence of the base-layer ensures consistency and uniformity when functionally graded thin films need to be produced on different surfaces, such as those needed for chromatographic or biological applications. In addition, it affords a surface of the desired functionality before gradient formation begins. Controlled-rate infusion enables the steepness of the gradient surface to be varied systematically at different points along the gradient surface, providing a high degree of control over local gradient properties.

In this work, this approach is demonstrated by modifying a substrate that contains dimethyl ($(CH_3)_2Si(OCH_3)_2$ and silanol (SiOH) groups with an aminoalkoxysilane ($NH_2(CH_2)_3Si(OC_2H_5)_3$) to build a gradient film for which the amine content changes in a programmed fashion over a 10 to 20 mm distance. Surface amine gradients are particularly advantageous to construct since amine functional groups provide a means to link more complex structures (i.e., peptides, proteins) to the surface via relatively simple chemical reactions. Such gradients have been previously prepared from organic monomers such as allylamine,[7, 30] from aminopropyltriethoxysilane using the vapor diffusion method[127, 128] and a liquid immersion method,[129] electrochemically using 2-aminoethanethiol,[130] from isocyanopropyldimethylsilane gradients,[131] and from amine functionalized alkanethiols using a cross-diffusion method.[132] They have been used as scaffolds to make gradients in nanoparticle density,[128] surface charge density,[133] and fluorescent spheres[130] and to study protein and carbon nanotube adsorption.[129, 132] In contrast to these methods, the approach reported herein is relatively simple and universal, provides control over gradient steepness, and allows surface amine gradients to be formed in both one- and two-dimensions on non-standard surfaces.

3.3 Experimental section

3.3.1 Sample preparation.

Tetraethoxysilane (TEOS, 98%), dimethyldiethoxysilane (DMDEOS, 97%) and 3-aminopropyltriethoxysilane (APTEOS, 99%) were purchased from Acros Organics and used as received. The silica sol for the base-layer was prepared by mixing ethanol, TEOS, DMDEOS, 0.1 M HCl and water in a 1:0.5:0.15:0.15:0.15 volume ratio. The sol was allowed to age for 24 to 36 h prior to use. Silicon wafers (University Wafer, B-doped, <111>) were cut to the appropriate size (1 x 1.3 cm for the one-dimensional (1D), 1.3 x 1.3 cm for two-dimensional (2D)) gradients, and 1 x 2 cm for the programmed gradients) and then cleaned with fresh conc. H_2SO_4:H_2O_2 (70:30) for 15 minutes at 80º C in a water bath (CAUTION: Piranha solutions are extremely dangerous and react violently with organic materials). After cleaning, the silica sol was spin coated on the wafers at 4000 rpm for 30 seconds and then dried in a desiccator overnight. The base-layer coated wafer was subsequently soaked in ethanol for 10 to 12 hours for stabilization.

To prepare the 1D gradient, the base-layer coated wafer was removed from the ethanol bath and mounted vertically in a 5-mL glass shell vial. Using a syringe pump (New Era, NE-1000), an APTEOS sol (prepared by mixing ethanol, APTEOS and water in a 1:0.05:0.01 volume ratio unless otherwise noted) in a 3-mL syringe (8-mm ID) was infused into the vial at a pre-programmed rate. The sol reached the top of the substrate in 2-60 min, depending on the rate of infusion. The substrate was subsequently removed from the sol, rinsed thoroughly with ethanol and dried with nitrogen. The 2D gradient was prepared in a similar fashion. After formation of a 1D gradient, the substrate was rinsed with ethanol, rotated 90º and placed in a new vial. A fresh APTEOS sol was infused into the vial as described above. The substrate was again rinsed with ethanol and dried. Positive control samples were prepared by soaking base-layer coated wafers

in the APTEOS sol for a 30 min time period, removing them and rinsing them with ethanol. This process was repeated a second time during preparation of the positive control for the orthogonal gradient. Negative controls simply consisted of the wafer with the TEOS:DMDEOS base-layer.

3.3.2 Characterization

X-ray photoelectron spectroscopy (XPS) analysis was performed with a ThermoFisher ESCAlab 250 imaging X-ray photoelectron spectrometer (Al Kα (1486.68 eV), 500 μm spot size, 50 eV pass energy, 0.1 eV step size). XPS spectra were acquired in regular fashion (typically every 1-2 mm) across the wafer starting about ~ 1 mm from the edge. Spectra were calibrated by taking the C1s peak as occurring at 284.6 eV. Contact angle measurements were made with a Rame-Hart contact angle Goniometer by the sessile drop method. The volume of the drop of water was 3 μL. To enhance the differences in the contact angle across the gradient, the samples were exposed to HCl vapors to protonate the amine groups. For the negative and positive control samples, two measurements were made at two different positions. For the 1D gradient, four measurements were made from top to bottom. Film thicknesses were measured via spectroscopic ellipsometry (R-SE, J.A. Woollam). In these experiments, the ellipsometric data were acquired at ~ 2 mm intervals along the length of the film. Data were acquired from approximately the same locations (i.e., within 0.5 mm) both before (TEOS-DMDEOS base-layer alone) and after gradient deposition.

3.4 Results and Discussion

3.4.1 Preparation

In this work, a controlled-rate infusion method was used to create a surface chemical gradient with spatially controlled chemical composition on a relatively hydrophobic surface.

This method relies on the presence of a reactive, homogenous (on the macroscopic scale) base-layer and a reactive organosilane that can condense with surface silanol groups on the time scale of infusion. The extent of the gradient thus formed depends on the reactivity of the organoalkoxysilane in the sol and the rate at which the sol is infused into the reaction vial. The experimental set-up consists of a glass vial that contains a suitably modified substrate and a programmable syringe pump that is used to infuse the reactive silane into the vial. In this case, the base-layer was formed from a sol that contained TEOS and DMDEOS (3:1 mole ratio). The organosilane that was infused into the vial was APTEOS. After gradient deposition, the top of the film, which was in the sol for the shortest period of time, has a lower density of NH_2 sites while the bottom has the greatest density of NH_2 sites. Gradients in two orthogonal directions can also be easily formed by rotating the as-prepared 1D gradient 90 degrees and repeating the APTEOS deposition, as depicted in the cartoon shown in Figure 3.1. In this case, the lower left corner of the substrate should contain a high density of NH_2 groups and the upper right corner a low density of NH_2 groups. By controlling the rate of infusion, the steepness of the gradient can be controlled and strategically modified along its length.

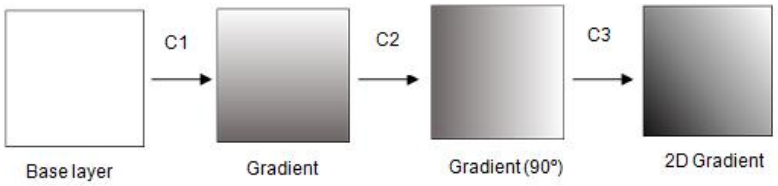

Figure 3.1. Simplified schematics of of deposition of a second one-dimensional gradient orthogonal to the first.

The base-layer serves many purposes; most importantly it ensures a consistent, uniform source of surface silanol groups regardless of the type of substrate used, whether it is a silicon

wafer, glass, conductor, etc., and it provides a means to add additional functionalities to the surface. The use of a base-layer is particularly valuable when functionally graded thin films need to be formed on non-traditional substrates such as those that may be needed in biochemical research. The only requirements are for the base-layer to be stable during gradient deposition and that it has reactive Si-OH groups. In this work, the base-layer also contained an organic modifier (dimethyldialkoxysilane). The presence of the dimethyl groups will impart some hydrophobicity to the surface so that during infusion the surface changes from one that is relatively hydrophobic to one that is more hydrophilic. The reactivity of the organoalkoxysilane in the infusion sol also is important. An added benefit of using an aminoalkoxysilane is that the amine groups act to catalyze (self catalysis) the sol-gel reaction, thus increasing the rate at which the silane hydrolyzes and condenses to the surface.[134] The gradient surfaces thus formed were characterized with XPS, contact angle measurements, and profilometry.

3.4.2 XPS Analysis.

Figure 3.2 shows N1s (399.2 eV) and Si2p (102.9) overlay spectra acquired at defined intervals along the length of 1D gradient films and controls. The negative control (**NC**) shows a total of 10 spectra acquired every 1.2 mm along the length of the film; the positive control (**PC**) shows 9 spectra acquired every 1.4 mm; the gradient (**G**) shows 9 spectra acquired every 1.4 mm. As expected, the negative control (base-layer coating only) shows a small N1s peak and a large Si2p peak of nearly constant intensity across the length of the film. Shifts in the baseline and measurement noise across the 10 spectra shown for the negative control in Figure 3.2 (**NC-N**) mask the true height of the N1s peak. Careful integration of these data yields a mean peak area of 3100 cps eV. The presence of the small N1s peak in the negative control is due to minor contamination of the surface. The positive control shows strong N1s and Si2p signals that

remain relatively constant across the length of the film. This is expected as a relatively homogeneous distribution of NH_2 and Si should be found when the surface of the substrate is modified using a self-assembly like procedure. In contrast, in the gradient film (**G-N**), the N1s peak clearly increases from top to bottom along the film, consistent with the presence of a gradient in amine functionality. The shoulder observed at 401.6 eV in the N1s peak is due to the presence of ammonium species.[33] The protonated form of the amine group has been shown to result from hydrogen bonding interactions with surface silanol groups, as elucidated by XPS and FTIR measurements.[135, 136] We noticed that as the films aged for days/weeks, this shoulder increased in intensity. XPS spectra acquired from a self-assembled NH_2-terminated film treated with 5% methyl iodide (v/v in ethanol) to convert the NH_2 groups to quaternary amine groups ($N(CH_3)_3^+$) showed a large peak at 401.7 eV and a small shoulder at 399.3 eV.

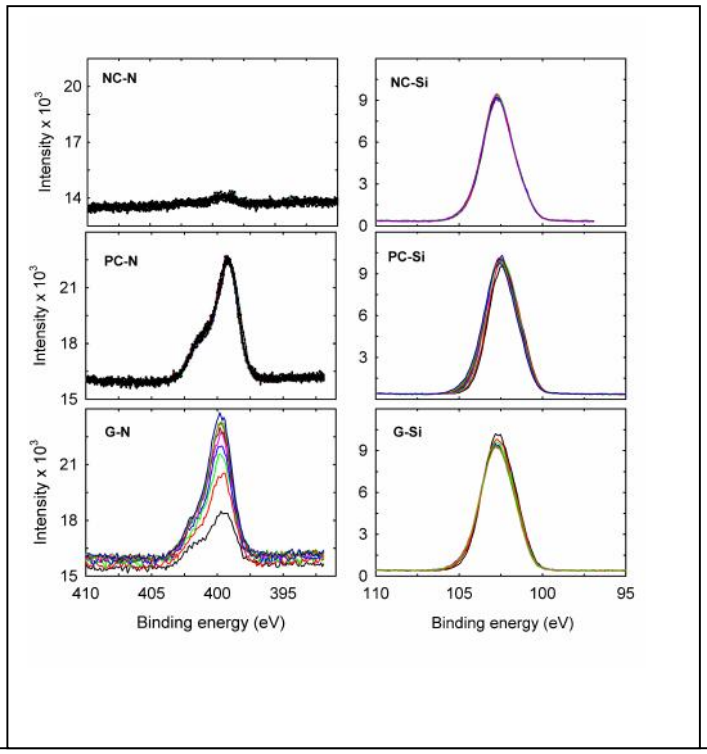

Figure 3.2. N1s and Si2p XPS spectra acquired along the length of the gradient from top to bottom at ~ 1 mm intervals for the negative control (**NC**), positive control (**PC**), and gradient films (**G**). The black line corresponds to the spectrum acquired at the very top of the gradient.

Figure 3.3 more clearly shows how the area under the N1s and Si2p peaks change along the length of the gradient (**G**) and positive control (**PC**) films. For the gradient, the area under the N1s peak initially increases from top to bottom, consistent with the formation of a gradient in amine groups. For the positive control, the area of the N1s peak is relatively invariant with distance. As can be seen in Figure 3.3, the N1s signal begins to level off in the middle of the gradient. This leveling off is attributed to a saturation of surface reactive sites (Si-OH groups) and/or the reduced accessibility of such sites as the 3-aminopropyl groups populate the surface. The relative standard deviation of the areas measured under the XPS spectra acquired within a single gradient film ranges from ca. 1-3% indicating the films are continuous. Significantly more variability is observed in samples prepared weeks/months apart. While the shape of the gradient is the same, the magnitude of the area under the N1s peak (or the N1s/Si2p peak ratio) at saturation varies ~ 10 to 30%. Such sample-to-sample differences likely result from variations in relative humidity and temperature, both of which influence the rates of hydrolysis/condensation and the extent of cross-linking in the base-layer. Small changes in the surface concentration of reactive Si-OH groups will influence the amount of APTEOS that condenses to the surface and thus the N1s XPS signal.

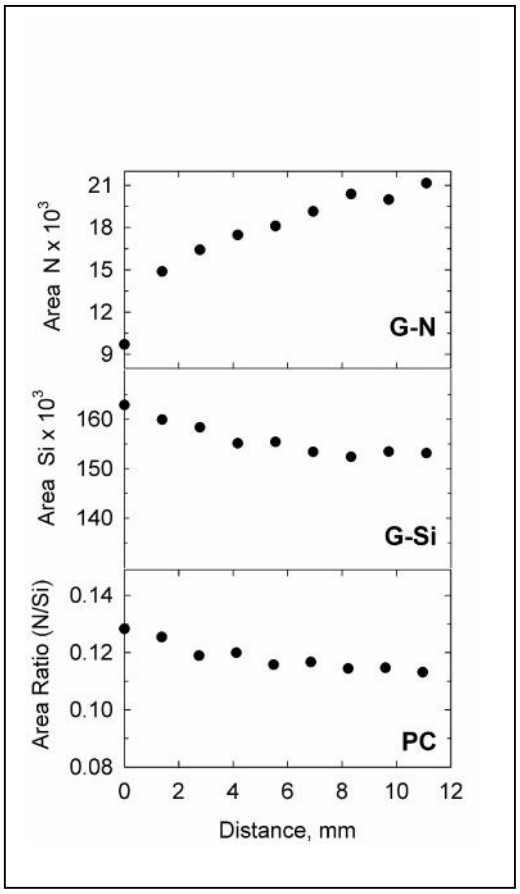

Figure 3.3. N1s and Si2p XPS areas as a function of distance along the length of the gradient from top to bottom for the gradient (**G**) film. For the positive control (**PC**) sample, the peak area ratio of N1s/Si2p as a function of distance is shown. In this case, both the N1s and Si2p peak areas are relatively invariant with distance.

In contrast to what is observed for the N1s peak, the area under the Si2p peak decreases slightly (~ 10%) along the gradient, indicative of less Si present near the bottom of the film relative to the top. Such results are not observed for the positive control (PC), where the area under the Si peak is relatively invariant with distance. Because XPS is inherently a surface sensitive technique, only the top few nanometers of the gradient film are interrogated. At the top of the film, more of the base-layer will be probed, whereas at the bottom of the film the aminosilane layer will make a relatively greater contribution to the observed signal. The area

under the Si2p peak likely decreases from top to bottom because the density of the Si atoms in the spin coated base-layer is greater than the density of Si atoms in the aminosilane layer.

The thickness of the aminosilane layer as a function of position along the gradient was evaluated using ellipsometry. Ellipsometric data were first collected on the base-layer at 2 mm intervals. Data were then acquired from approximately the same locations after gradient deposition. Ellipsometric measurements show no measurable difference in the film thickness before and after gradient formation, indicating that the thickness of the amine gradient is < 5 nm (i.e., within the error of these measurements). This result indicates that the amine layer is very thin (i.e., from sub-monolayer to a few monolayers at most).

Orthogonal 2D gradients in amine groups can also be formed in a similar fashion by rotating a previously formed 1D gradient 90^0, and then repeating the procedure. Figure 3.4 shows XPS results for a 2D gradient along with its positive control. For the 2D gradient, the area under the N1s peak increases from top to bottom in each orthogonal direction as indicated by the arrows; there is also a monotonic increase along the diagonal (bottom left to top right) of the substrate, consistent with the formation of a bidirectional gradient in amine groups. The area under the Si2p peak for the gradient film also changes slightly in a similar but somewhat more complex manner than in the unidirectional (1D) gradient. The slight changes in the Si2p peak area likely reflect slight differences in the density of the aminosilane layer relative to the base-layer as described earlier. For the positive control (see Figure 3.4), the area ratio of N1s/Si2p as a function of distance is shown. The Si2p and N1s peak areas are both relatively invariant with distance and thus the N1s/Si2p area ratio is roughly constant in all directions.

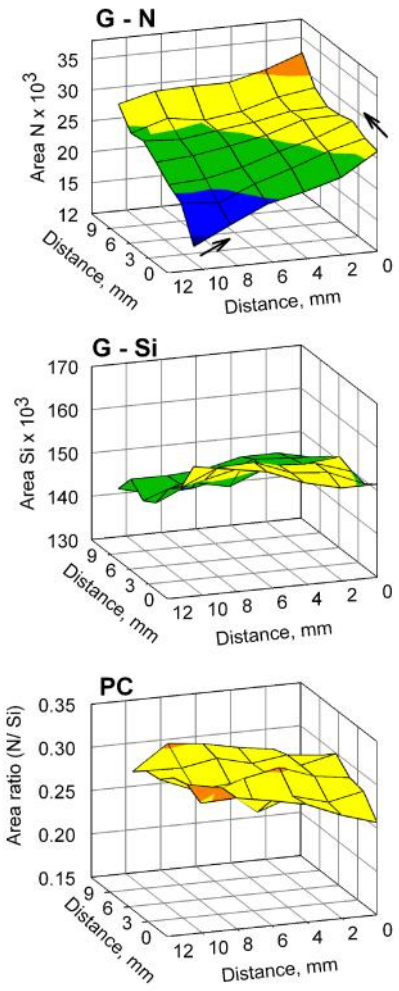

Figure 3.4. N1s and Si2p XPS peak areas as a function of distance along the length of the gradient in two orthogonal directions. The arrows indicate the direction of the gradient from top → bottom. For the positive control (**PC**) sample, the N1s/Si2p peak area ratio as a function of distance is shown. In this case, both the N1s and Si2p peak areas are relatively invariant with distance.

It is also apparent in Figures 3.3 and 3.4 that at distance, d = 0, the area under the N1s peak is not zero. The origin of this nonzero intercept arises in part because the XPS data acquired in this region (~ 1 mm from the edge of the silicon wafer) does not exactly correspond to the start of the gradient. It also includes contributions from contamination by adventitious nitrogen species, some vapor phase reactivity, and contributions from an initial fast reaction[66] of the aminosilane with surface silanol groups. An estimate of the contributions to the peak area from adventitious nitrogen, obtained from the negative control samples, is 3200 (± 350) CPS eV. Thus, a significant portion of the observed offset results from surface contamination, with the remainder arising from the initial fast reaction and/or vapor phase reactivity of the aminosilane. Additional experiments were undertaken to evaluate these two possibilities.

To evaluate whether or not the condensation reaction also takes place in the vapor phase above the solution-air interface, an additional control experiment was done (Figure 3.5). In this experiment, the infusion process was stopped before the sol reached the top of the wafer. The bottom (exposed to APTEOS in solution for 15 min) and top (only exposed to APTEOS that may reside in the vapor phase) regions of the substrate were examined via N1s XPS and the results compared to that observed for a negative control. The N1s signals were nearly identical in the negative control in the region of the film exposed only to APTEOS vapor (within experimental error). In contrast, the N1s signal was substantially higher in the region of the film exposed to APTEOS in solution. This result is in contrast to a recent report where the presence of amine moieties in regions not directly exposed to APTEOS was believed to result from vapor phase reactions.[130] The concentration of aminosilane in solution was significantly higher (by a factor 5 to 500) in that study. A high concentration of APTEOS in paraffin oil (1:1 w/w) was also used to form amine gradients via the vapor diffusion method.[127] Neat APTEOS has a fairly high

boiling point (~220 ^{0}C) and thus a relatively low vapor pressure at room temperature (~ 2 Pa). By keeping the concentration low (<< 1mM), the concentration of APTEOS in the vapor phase is expected to be small.

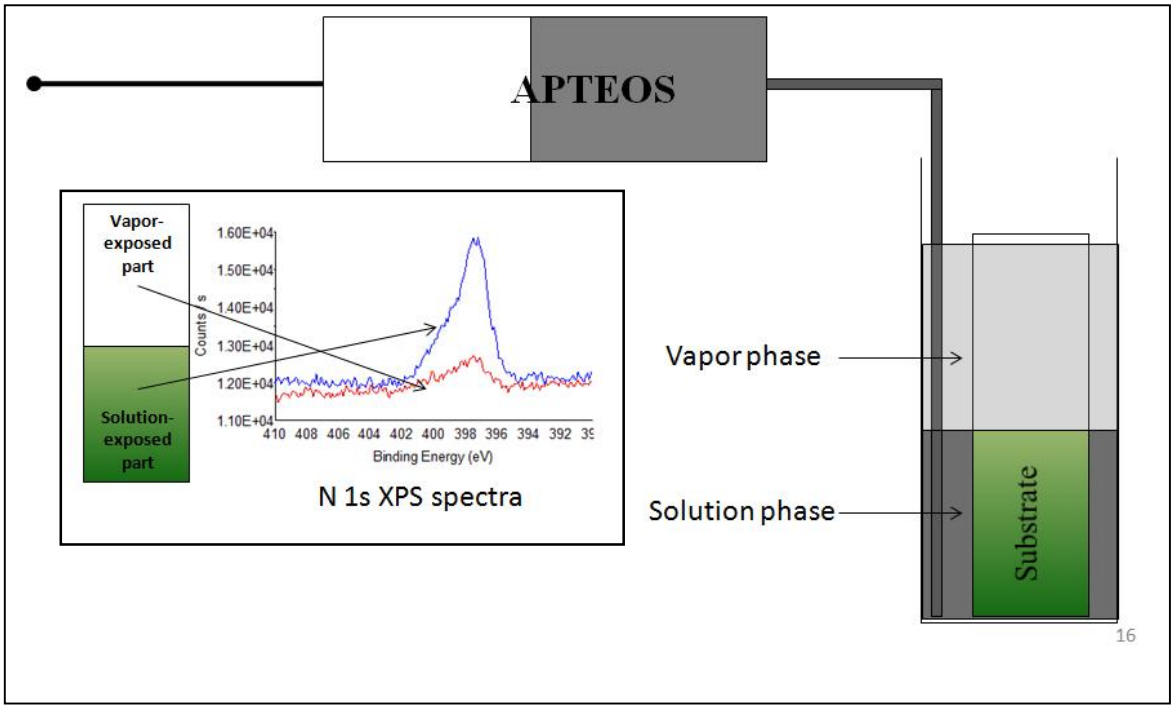

Figure 3.5. Schematic sketch that shows the set-up for vapor-phase reactivity experiments. Inset shows N1s spectra of vapor exposed part and solution exposed part of the sample.

Given these results, it is concluded that much of the nitrogen at distance = 0 likely results from the fast reactivity of APTEOS with surface silanol groups. Previous work has noted that the reaction of APTEOS with silica surfaces occurs on three different time scales.[66] The overall process includes an initial fast reaction, occurring in seconds, and subsequent slower processes occurring over minutes and hours.[66] To evaluate the contributions of the fast process to our system, a base-layer coated slide was place in a fresh APTEOS solution (aged for 5 to 28 min) for a given period of time ranging from two minutes to 25 minutes and then removed and rinsed.

The area under the N1s peak in the XPS spectrum for the sample exposed to APTEOS for 2 minutes was 8600 CPS eV whereas a slide soaked for 25 minutes was 13,600 CPS eV. After taking into account the baseline levels of nitrogen present in the negative control, it is concluded the APTEOS deposited by the fast reaction corresponds to approximately half the total APTEOS deposited at the top of the gradient. While this fast reaction leads to a relatively uniform initial coating on the slide and hence, the nonzero offset at the top of the gradient (near distance = 0), the shape of the gradient is determined predominately from the slow reaction of APTEOS with the surface.

3.4.3 Gradient Profile Control

An important attribute of the controlled-rate infusion method is that it affords the means to change the steepness of the gradient at arbitrary positions along the film. Changes in the gradient profile can be accomplished by simply changing the sol infusion rate in a controlled fashion. To demonstrate the value of this approach, several gradients were prepared in this mode, characterized by XPS, and fit to a simple kinetic model. Although the kinetics of reaction are known to be complex,[66] a simple single-step kinetic model was employed. One nice feature of this simple kinetic model is that it can be used to predict the overall shape of the gradient profile. The kinetics of film growth was assumed to exhibit first order dependences on the silica precursor concentration and the density of reactive sites on the base-layer surface:

$$\frac{dN_s}{dt} = -kC_{sol}N_s \qquad (1)$$

where k is the rate constant for the condensation reaction, C_{sol} the concentration of reactive silica precursors dissolved in the sol and N_s the density of reactive silanol sites on the base-layer surface. Rearranging and integrating Eqn. 1 shows that the density of amine modified sites, N_a,

should exhibit a simple exponential dependence upon the total time each region of the base-layer is exposed to the sol. It is shown by the derivation below.

N_a is related to N_s by eqn 2 below

$$N_a(t) = N_s(0) - N_s(t) \quad (2)$$

Rearranging and integrating equation 1,

$$\ln (N_s(t)/ N_s(0)) = -kC_{sol}t$$

$$N_s(t)/N_s(0) = \exp(-kC_{sol}t)$$

$$N_s(t) = N_s(0) \exp(-kC_{sol}t) \quad (3)$$

Substitute equation 3 in 2

$$N_a(t) = N_s(0) - N_s(0) \exp(-kC_{sol}t)$$

$$N_a(t) = N_s(0) ((1- \exp(-kC_{sol}t)) \quad (4)$$

Not shown in Eq. (4), is the presence of an offset. As noted above, the offset results predominately from adventitious nitrogen contamination and the initial fast reaction of APTEOS with surface silanol groups. When the data are fit, this constant is allowed to float.

The simplest demonstration of gradient profile control, and the dependence on first-order kinetics, is to vary the infusion rate between separate depositions. Figure 3.6 shows the N1s XPS results obtained from gradients prepared at two different infusion rates, differing by a factor of 15. As can be seen, the initial slopes of the two plots (i.e., the gradient steepness) are vastly different. Furthermore, as expected, "saturation" of available surface sites was not observed when the infusion rate was fast. The solid lines appended to Figure 3.6 depict fits of the XPS data to Eqn. 4 in which kC_{sol} was held to 11.8 h^{-1}, while $N_s(0)$ and the offset described above were allowed to float. This rate constant is similar to that reported previously for the

intermediate rate reaction (24.9 h^{-1})[66] in the three-step process whereby APTEOS is believed to react with the silica surface. Because the XPS data cannot be collected at very top of the gradient (presumably d = 0), some differences will undoubtedly be present at the beginning of the gradient. The overall high quality fits to the XPS data, however, demonstrate that deposition ***leading to the gradient profile*** is dominated by a single first-order process.

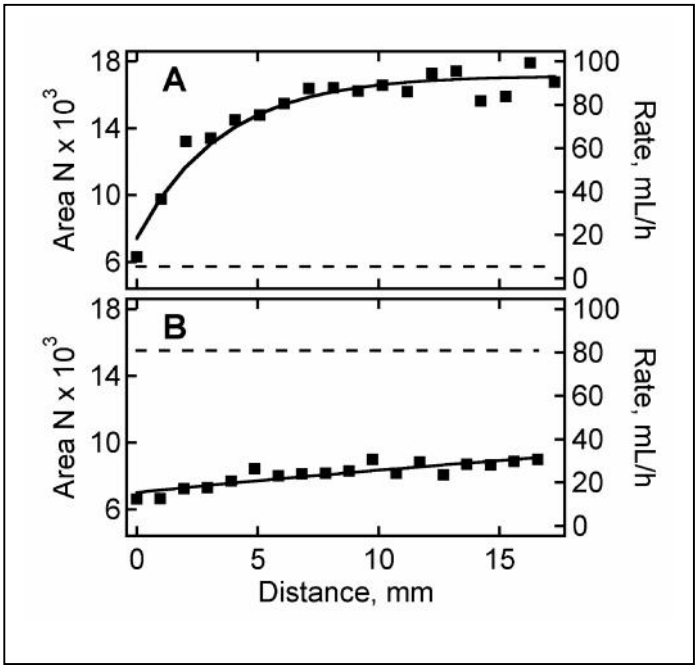

Figure 3.6. Area under the N1s XPS peak (squares) as a function of distance along the length of the substrate for gradients prepared at infusion rates (dashed line) of (**A**) 5.4 mL/h and (**B**) 81 mL/h, using identical sols. The solid lines depict first order kinetic models (Eqn. 4) for the XPS data using kC_{sol} = 11.8 h^{-1}. These results demonstrate that the gradient profile (e.g. steepness) can be controlled by simply changing the infusion rate.

The gradient profile can also be altered at any given position in the gradient by strategically programming the infusion rate. Figure 3.7 depicts the results obtained when the infusion rate was changed at predefined positions along the gradient. Shown are XPS data from gradients

prepared using six-step (A, B), three-step (C), and two-step (D) programmed infusion rates. A distinct break in the profile can be readily seen in the gradient formed using two different infusion rates (Fig. 3.7 D). At about the half-way mark, the steepness of the gradient increases. Likewise, two distinct breaks can be seen in the profile formed when three different infusion rates were employed during the course of gradient formation (Fig. 3.7C). For the 6-step gradient, the breaks are naturally much smaller and harder to discern. The solid lines appended to Figure 3.7 depict fits to Eqn. 4, obtained by holding kC_{sol} constant. The fits mimic the observed data, suggesting that gradient profiles can be predefined and prepared by simply choosing the appropriate infusion program. Differences between the fits and experimental XPS results likely arise from difficulties associated with correlating the "exact" positions at which the XPS data were collected with the "exact" points in time when the infusion rate was changed as well as uncertainties associated with contributions from the fast reaction of APTEOS and surface silanol groups. This is most noticeable at the top of the gradient and near where the rate of infusion is changed. Nevertheless, these results demonstrate that this simple model can be used to predict gradient profiles and that the gradient profile (e.g., steepness) can be altered during deposition by simply changing the infusion rate.

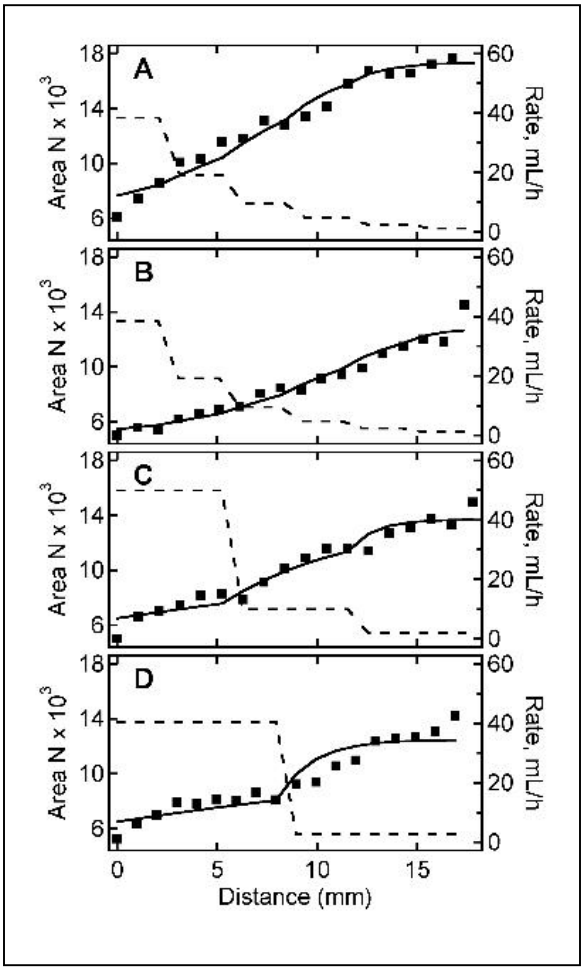

Figure 3.7. Area under the N1s XPS peak (squares) as a function of distance along the length of the substrate for programmed gradients prepared using varied infusion rates. Shown are data from gradients prepared using (**A**) six-step, (**B**) six-step (two-fold diluted solution), (**C**) three-step and (**D**) two-step programmed infusion rates (dashed lines). The solid lines depict first order kinetic models for the XPS data using kC_{sol} = 11.8 h^{-1} for **A**, **C**, and **D** and kC_{sol} = 5.9 h^{-1} for **B**.

3.4.4 Contact angle analysis

Contact angle measurements (sessile drop) were also undertaken to verify the presence of a gradient in NH_2 groups on the film surface. Although the relationship between amine modification and contact angle is not a simple one, contact angle measurements can give valuable information on hydrophobicity differences across the length of the film. The as-prepared positive (uniformly distributed NH_2) and negative (dimethylsilane, silanol, siloxane groups) controls showed contact angles that differed by only a few degrees. Such small changes are likely due to the heterogeneous nature of the silica surface, which contains groups of varying

polarity (unreacted silanol groups, siloxane, amine group and its associated propyl moiety). In an attempt to amplify the differences in the hydrophilicity across the film, the films were exposed to HCl vapor for 30 min as shown in Figure 3.8. The negative control before and after exposure to HCl shows the same contact angle (82°), which would be expected for a methyl/silanol covered surface with few basic sites. The positive control shows a clear dependence on exposure to HCl as expected for a surface that contains amine groups. After protonation, the contact angle decreases to ~ 65° from ~80° measured before protonation. As described in the literature, it is likely that not all the surface amine groups will be protonated as many are H-bonded with neighboring silanol groups.[67] Nevertheless, a significant difference in contact angle is observed. After exposure to HCl vapor, the gradient sample clearly shows a decrease in contact angle from top to bottom, in support of the XPS results. Figure 3.8 shows the water contact angle profile on gradient sample after HCl exposure; the gradual decrease in the contact angle from top (~ 80°) to bottom (~ 60°) is reflected by the changes in droplet shape along the gradient surface.

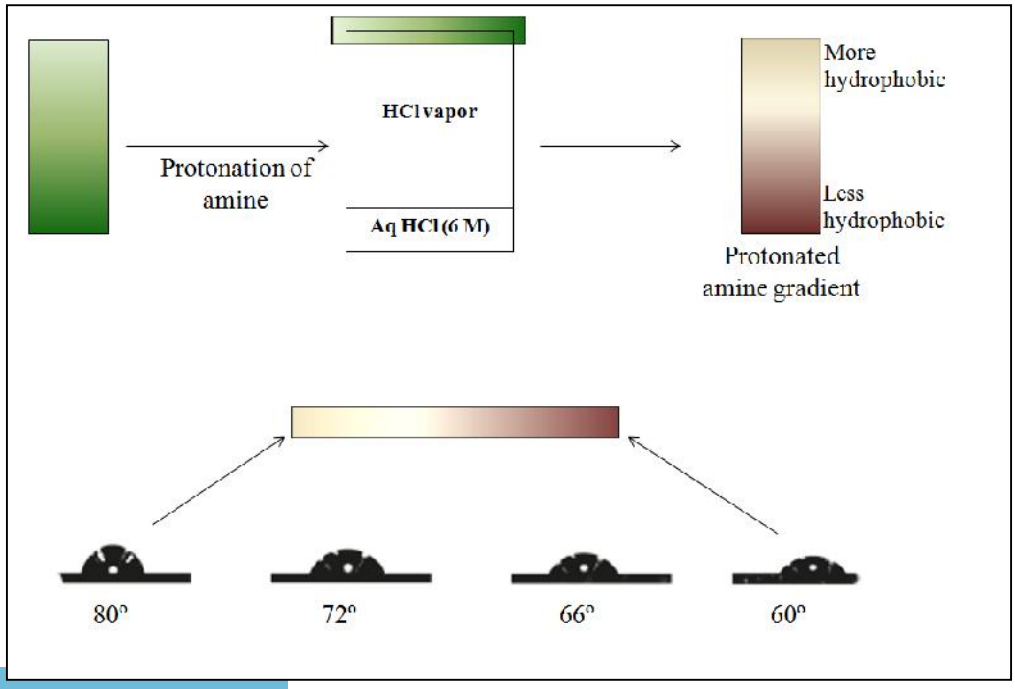

Figure 3.8. Top: Experimental scheme to enhance the difference in hydrophobicity in the amine gradient formed on a base-layer coated silicon wafer. **Bottom:** Water droplets along a 1D surface amine gradient.

3.5 Summary

A straightforward, controlled-rate infusion approach for building surface chemical gradients of strategically-controlled profiles has been described. This method not only allows for preparation of separate gradients exhibiting different profiles, it also affords the means to change the gradient steepness at arbitrary positions within a single gradient. Deterministic changes in gradient steepness are produced by simply adjusting the rate of infusion into the deposition reservoir. By this method, gradients exhibiting a wide variety of profiles can be prepared, including those incorporating spatially distinct regions having steep and gradual variations in chemical functionality. Gradients exhibiting near linear variations in their composition and/or properties can also be prepared. Importantly, in situations where film deposition is governed by simple kinetics, the infusion rates required to produce a particular gradient profile can be determined in advance. Control over the gradient profile is particularly important in applications that rely on mass transport such as haptotaxis where it may be necessary to slow down or speed up the movement of cells on a surface or for applications that require a high degree of spatial control to build more complex surfaces. The ability to tailor the hydrophobicity/hydrophilicity of the base-layer provides additional means to change the surface chemistry and subsequently control transport.

Chapter 4: Aminoalkoxysilane Reactivity in Surface Amine Gradients Prepared by Controlled-Rate Infusion

Adapted from Kannan, B.; Higgins, D. A.; Collinson, M. M., *Langmuir* **2012,** *28* (46), 16091-16098

4.1 Abstract:

The reactivity of a series of substituted aminoalkoxysilanes used for surface amine gradient formation has been studied using the previously described time based silane exposure method termed controlled-rate infusion (CRI). The aminoalkoxysilanes used include those that contain primary, secondary, and tertiary monoamines as well as more than one amine group (diamine and triamine). X-ray photoelectron spectroscopy (XPS) was used to confirm the presence of a gradient in each case, and to acquire detailed information on gradient composition, from which kinetic data was obtained. The total area under the N1s XPS spectra allow for the extent of amine modification to be quantitatively assessed along each gradient. The N1s peaks actually appear as doublets, providing additional data on the level of protonation, and hence, amine basicity on the dry surface. The degree of protonation showed an interesting trend toward smaller values running from top to bottom along gradients incorporating the most basic amines. The gradient profiles, including initial steepness and extent of saturation, were shown to be highly dependent on the aminoalkoxysilane precursor employed. The highest levels of modification were achieved for the diamine and primary monoamine precursors while the more hindered amines produced lower levels of surface modification and took longer for saturation to be achieved. By fitting the gradient data to a simple first order kinetic model, rate constants for the condensation reaction between each aminosilane and accessible surface silanol groups were obtained. The rate constants follow a similar trend as the level of surface modification: triamine ~ diamine > monoamine and primary > secondary > tertiary, indicating kinetic factors play an important role in controlling surface modification. The presence of more than one amine group

on the silane is found to enhance the rate of condensation to the surface silanol groups, while the more hindered secondary and tertiary amines slow condensation. Collectively, the results provide valuable new data on how the number of amine groups, degree of substitution, and steric hindrance influence silane reactivity with silica surfaces, amine surface coverage and basicity along the gradient profile.

4.2 Introduction

The reactivity of the organoalkoxysilane is one of the key factors in controlling the gradient profile in CRI. As discussed previously, in CRI, the time scale of reactivity between the organosilane and the hydroxylated surface must match the rate of infusion, typically 2 – 60 minutes. APTEOS works well because the amine functionality also serves as a catalyst to speed up hydrolysis and condensation. Other aminoalkoxysilanes will react differently, depending on the number of amine groups, degree of substitution, and nature of the alkoxide group. Understanding the nature of these variables will provide the knowledge needed to tailor functionally graded surfaces for chromatography and/or biological applications. Characterization of the gradient profile, on the other hand, can provide a straightforward approach to evaluate the rate of condensation of an aminosilane to a surface, which is of direct importance to the broad field of surface functionalization and modification.

The primary objective of this work was to examine a series of aminoalkoxysilanes having different degrees of substitution (i.e., primary, secondary and tertiary) and different numbers of amine groups (i.e., monoamines, diamines, triamines), Scheme 4.1, to elucidate the most important factors controlling their reactivity with the substrate surface. Gradient surfaces have been prepared from these silanes, characterized with X-ray photoelectron spectroscopy (XPS),

and the results fit to a first-order kinetic model to extract a rate constant for the condensation reaction of the silane with surface OH groups. As shown below, the gradient profile was strongly dependent upon the reactivity of each silane, which was governed by the number of amine groups on the molecule and the degree of amine substitution. Furthermore, a detailed analysis of the N1s XPS spectra revealed an interesting trend in basicity for the more basic amines, with these surfaces exhibiting a decrease in the level of protonation with increasing amine coverage running from top to bottom along the gradient surface.

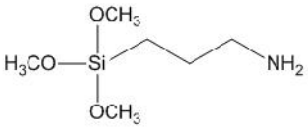

Aminopropyltrimethoxysilane (APTMOS)

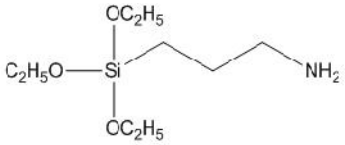

Aminopropyltriethoxysilane (APTEOS)

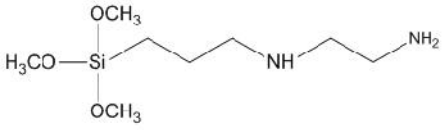

***N*-[3-(Trimethoxysilyl)propyl]ethylenediamine (Diamine)**

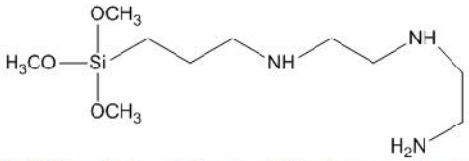

***N*-[3-(Trimethoxysilyl)propyl]diethylenetriamine (Triamine)**

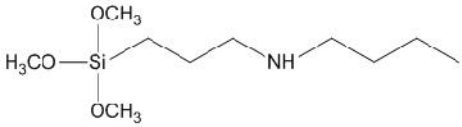

N-butylaminopropyltrimethoxysilane (N-Butyl)

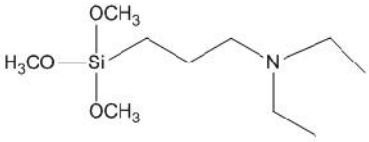

NN-diethylaminopropyltrimethoxysilane (N,N-Diethyl)

Scheme 4.1 Aminoalkoxysilanes used in the study.

4.3 Experimental Section

4.3.1 Sample Preparation

N-[3-(trimethoxysilyl)propyl] ethylenediamine (Diamine, 97%) was purchased from Sigma Aldrich. N-[3-(trimethoxysilyl)propyl] diethylenetriamine (Triamine), n-butylaminopropyltrimethoxysilane (N-Butyl), N,N-diethylaminopropyl trimethoxysilane (N,N-Diethyl) were purchased from Gelest, Inc. Tetraethoxysilane (TEOS, 98%), dimethyldiethoxysilane (DMDEOS, 97%) and 3-aminopropyltriethoxysilane (APTEOS, 99%) were purchased from Acros Organics. 3-Aminopropyltrimethoxysilane (APTMOS, 97%) was purchased from TCI America. All the silanes were used as received. Silicon wafers (University Wafer, B-doped, <111>) were cut to the appropriate size (1 x 2 cm) and then cleaned with fresh conc. H_2SO_4:H_2O_2 (70:30) for 10 minutes at 70° C in a water bath (CAUTION: Piranha solutions are extremely dangerous and react violently with organic materials). As previously described, the silica sol for the base-layer consisted of ethanol, TEOS, DMDEOS, 0.1 M HCl, and water in a 1:0.5:0.15:0.15:0.15 volume ratio and was aged for 24-36 h prior to use.[74] This sol was spin coated on the wafers at 4000 rpm for 30 s and dried in a desiccator overnight. Prior to gradient preparation, the base-layer coated silicon wafer was soaked in ethanol for 10 to 12 h for stabilization.

Surface amine gradients were prepared by slowly infusing a freshly prepared aminosilane solution into a vial containing the above substrate. The rate of infusion was controlled by use of a programmable syringe pump (NewEra, NE-1000). During infusion, the base-layer coated substrate was exposed to the aminosilane solution for different amounts of time along its length, thus producing a gradual variation in the level of amine modification from top to bottom. The

aminosilane solution used for infusion was prepared by mixing ethanol : silane : water in a 5 : 0.25 : 0.05 volume ratio.

4.3.2 XPS characterization

X-ray photoelectron spectroscopy (XPS) analysis was performed with a ThermoFisher ESCAlab 250 imaging X-ray photoelectron spectrometer (Al Kα (1486.68 eV)), 500 μm spot size, 50 eV pass energy, 0.1 eV step size). Samples were placed on top of conducting tape on a 5 cm x 2 cm sample holder. XPS spectra were acquired at constant intervals (typically every 1-2 mm) across the wafer and starting ~ 1 mm from the edge (line scan). The spectra were calibrated by taking the C1s peak as 284.6 eV. XPS curve fitting was performed using commercially available software and a Gaussian-Lorentzian (70:30) function, after smart background subtraction, similar to published work on amine modified surfaces by Unger et al.[137]

4.4 Results and Discussion

4.4.1 Gradient Formation

Similar to the process described in Chapter 3 on gradient formation using APTEOS, the process of gradient deposition begins with the formation of a reactive, homogeneous base-layer, formed by spin coating a sol containing TEOS and DMDEOS on a silicon wafer. This substrate provides a uniform layer of silanols to react with the various aminoethoxysilanes.[74] The aminosilane solution is infused at constant rate into a vial containing the vertically aligned wafer. Because the bottom of the substrate is exposed to the silane for a longer period of time relative to the top, the surface concentration of the amine groups should decrease from bottom to top. The profile (shape) of the gradient will depend on the concentration of silane in the solution, the rate of infusion, and the rate of condensation of the aminosilane with surface silanol groups (k_c). In

this work, the reactivity of a series of aminosilanes was evaluated. All but one (APTEOS) incorporate hydrolysable methoxy groups, but each differs in the substitution (primary, secondary, tertiary amines) and the number (monoamine, diamine, triamine) of amine groups. By keeping the concentrations and infusion rate constant (or nearly constant), the gradient profile will be determined primarily by k_c.

Figure 4.1 shows N1s spectra acquired at defined intervals along the length of gradient surfaces prepared using Diamine, Triamine, N-Butyl, N,N-Diethyl, and APTMOS. Each plot consists of a total of 12 spectra acquired every ~1.5 mm along the length of the film. For comparison, APTEOS XPS data from our previous work[74] are also shown. As expected, on all six surfaces, the intensity of the N1s peak increases from top to bottom, confirming the presence of a gradient in nitrogen content, and hence, the level of amine modification. In contrast, control samples prepared by soaking the base-layer coated substrate in an aminosilane solution showed a uniform concentration of nitrogen across the length of the substrate. The signal intensity was significantly higher for Diamine and Triamine, in part because these precursors have two and three nitrogen atoms, respectively, per molecule. The signal intensity was lowest for the secondary and tertiary amines (N-Butyl and N,N-Diethyl), indicating that a smaller amount of the aminosilane deposited on the surface relative to either APTEOS or APTMOS, which show similar intensities.

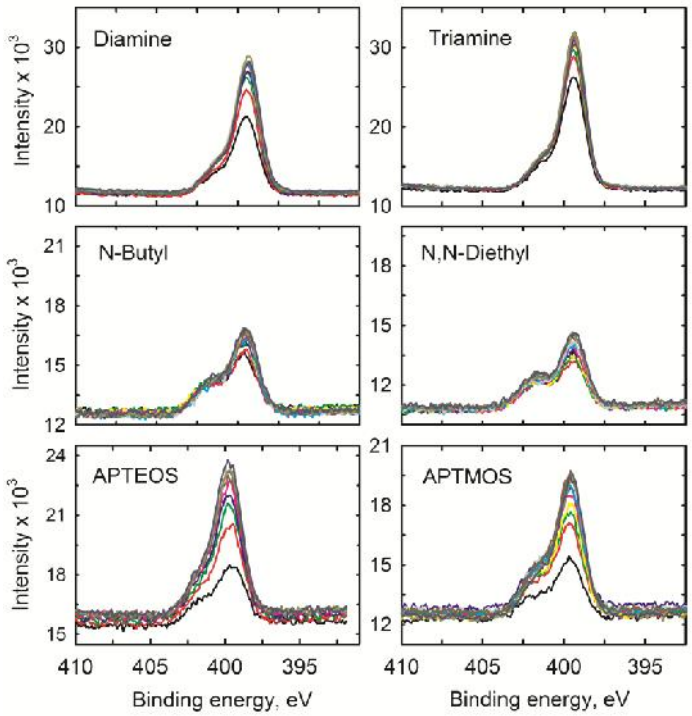

Figure 4.1 N1s spectra acquired along the length of the gradient from top to bottom at ~ 1.5 mm intervals for six amine gradients prepared from Triamine, Diamine, N-Butyl, N,N-Diethyl, APTEOS[14] and APTMOS. Infusion solution: ethanol:silane:water volume ratio: 5:0.25:0.05). Infusion time was ~30 min. The black line corresponds to the spectrum acquired at the very top of the gradient.

The profile (shape) of the different gradients can be best seen by integrating the area under the N1s peak and plotting it as a function of distance, Figure 4.2. In this figure, the area under the N1s peak for Diamine and Triamine was divided by 2 and 3 because these precursors have two and three nitrogen groups per molecule, respectively. The non-zero intercept observed in all the profiles has four possible origins as described in Chapter 3:[74] the position at which the XPS data was acquired does not exactly correspond to the top of the gradient; contamination by adventitious nitrogen; vapor phase reactivity of the aminosilanes; and contributions from an initial fast reaction.[66, 138]

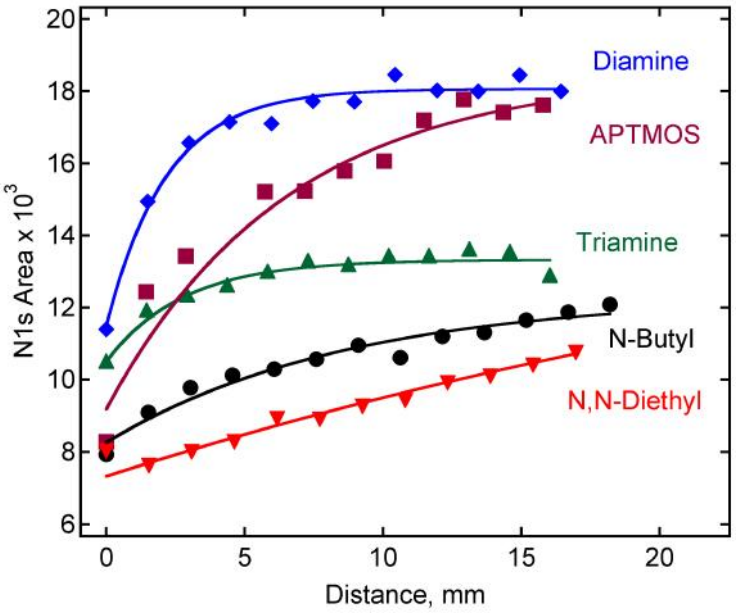

Figure 4.2. N1s XPS area as a function of distance along the length of the gradient from top (distance = 0 mm) to bottom for gradient films prepared from Diamine (diamonds), Triamine (triangles), N-Butyl (circles), N,N-Diethyl (inverted triangles), and APTMOS (squares). The data for Diamine and Triamine were divided by 2 and 3, respectively. Infusion solution: ethanol:silane:water (5:0.25:0.05) by volume. The solid lines represent fits to the kinetic model described below.

The contribution of the first is small relative to the other three, but would obviously be higher for a very steep gradient. An estimate of the contribution of adventitious nitrogen can be obtained from negative control samples, which consist of the base-layer coated silicon wafer. There are some month to month variations, but the N1s peak area typically ranges from 1100-3500 CPS eV. To evaluate vapor phase reactivity, the boiling points of the silanes were compared. All were higher than APTEOS with the exception of APTMOS, which has a boiling

point of 92ºC. To evaluate the importance of vapor phase reactivity for APTMOS, the silane solution was infused until the lower half of the substrate was immersed. During infusion, the upper half was then exposed to silane vapor for 15 min. The sample was subsequently rinsed and the N1s peak area for the vapor-exposed part of the substrate (e.g., upper half) was determined. The area under the N1s peak in this region was determined to be 4100 ± 200 CPS eV (N=3), which is comparable to the negative control N1s area of 3300 ± 200 CPS eV evaluated on that day, confirming that the reaction occurs predominately in the solution phase. Thus, a significant contribution to the nonzero intercept is concluded to result from an initial fast reaction of the aminosilane with surface silanol groups.[74]

The reproducibility of the XPS profile and the uniformity of the gradient across its entire width can be seen in Figure 4.3. In this figure, the N1s line scans were acquired across the width of the N-Butyl and N,N-Diethyl gradients and the area under the N1s peak in each case is plotted. In both the plots, the standard deviation is < 10% of the absolute peak area, except for the first two points in the N-Butyl gradient. This deviation might be due to the small variation in positioning the sample in the sample holder, which could lead to a large variation in the signal, especially at the low amine end.

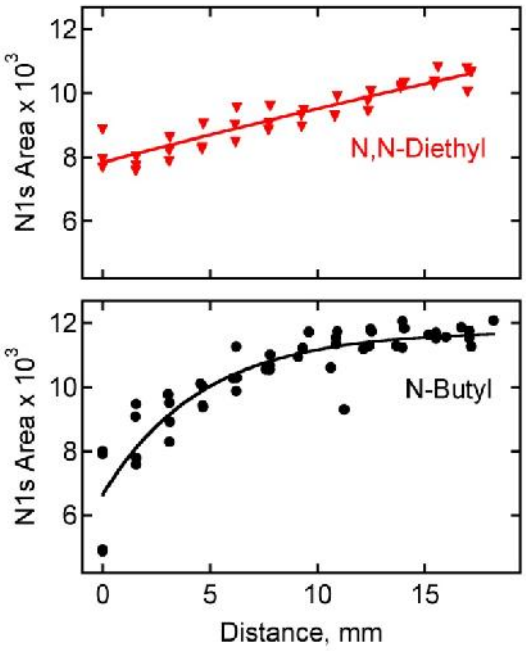

Figure 4.3 N1s XPS area as a function of distance along the length of the gradient from top to bottom for gradient films prepared from N,N-Diethyl and N-Butyl. Infusion solution: ethanol:silane:water (5:0.25:0.05 by volume). The infusion time was ~30 min. The solid lines represent fits to the kinetic model described below.

4.4.2 Gradient Profile

Although the infusion rates, silane concentrations, and timescales for infusion (~30 min) were similar for all the gradients, the profiles obtained are very different for the different aminomethoxysilanes, particularly in the nitrogen density on the surface and the rate at which it increases with distance. The highest levels of modification following a 30 min infusion were achieved using the Diamine and Triamine precursors while the lowest level of surface modification was observed for the tertiary aminoalkoxysilane. To determine if the observed level of modification reflects a different saturation level for each aminosilane (i.e., a different maximum surface coverage), the base-layer coated substrates were soaked in the individual

aminosilane solutions for 4 h, a time significantly longer than the 30 min infusion time. Results from XPS analysis are given in Table 4.1. The average N1s peak area obtained for the APTMOS, Diamine and Triamine samples are within 10% of the values obtained at the end of the gradient after a 30 min infusion time, indicating that saturation or near saturation of the surface has been achieved. The maximum surface coverage for the Triamine precursor, however, is significantly smaller than that observed for APTMOS or Diamine. A lower surface coverage in this case could result from steric hindrance due to size differences in the two silanes.[139, 140] A simple calculation of the cross-sectional area[141] yields a surface concentration of ~7 x 10^{-10} moles/cm^2 for APTMOS, ~5 x 10^{-10} moles/cm^2 and ~4 x 10^{-10} moles/cm^2 for the Diamine and Triamine, respectively. It was calculated b the below equation.

Cross sectional area $CSA = 1.091[M/(N \rho)]^{2/3}$

M – Molecular weight of the surface amine group

N – Avogadro number

ρ – Density of the amine group

Once the cross sectional area was calculated in cm^2/molecule, the surface concentration (SC) of monolayer coverage was calculated by

SC = (1/CSA) (1/N)

SC = (molecule/cm^2) (moles/molecule)

SC = moles/cm^2

The observed reduction in the N1s peak area is consistent with the increase in precursor size. It is also possible that because Triamine hydrolyzes and condenses quickly, oligomers could also be present in solution. The relatively large size of these oligomers would hinder their binding to free silanol groups, leading to lower coverage.[139] In contrast, for N,N-Diethyl and N-Butyl, the

N1s peak area was 25-30% higher after a four hour immersion period, indicating that saturation was not achieved in 30 min.

Silane	N1s area after 4 hr soak	N1s area after 30 min infusion[b]
Diamine[a]	16000 ± 50	18000 ± 200
Triamine[a]	12000 ± 300	13000 ± 400
APTMOS	20000 ± 500	18000 ± 200
N-butyl	16000 ± 3000	12000 ± 300
N,N-diethyl	14000 ± 500	10000 ± 300

[a] Diamine and Triamine divided by 2 and 3, respectively
[b] Average and standard deviation of last three points in Figure 4.3.

Table 4.1. Average N1s area for samples prepared by soaking a base-layer coated substrate in the aminosilane solution (same ethanol, silane & water ratio used for gradients in Figure 4.1) for 4 h. The diamine and triamine areas have been divided by 2 and 3, respectively.

In addition to the level of saturation, the gradient profiles for the different silanes differ greatly in their shapes (Figure 4.2). Gradients prepared under these conditions with Diamine and Triamine have a large positive intercept, are relatively steep at the low amine end and reach saturation within 7 to 8 min. In contrast, the N-Butyl and N,N-Diethyl gradients are shallow and saturation is not observed on the time scale of the experiment (~ 30 min). APTMOS falls somewhere in between. The non-zero intercepts are also different for the different aminoalkoxysilanes. Results obtained from APTMOS are similar to that previously described for APTEOS,[74] indicating the two precursors have similar reactivity.

4.4.3 Reactivity of Aminosilanes and Profile Control

To better understand the origins of the differences in aminosilane reactivity, the kinetics of reactivity with the surface were investigated. Gradients prepared by CRI provide a valuable route to obtain such information, since by design the reaction time increases down the gradient.

By fitting the gradient N1s XPS data to a simple first-order kinetic model which was developed initially for APTEOS (Chapter 3), information on the reaction rates is directly obtained. As described previously, the kinetics of APTEOS deposition are complex, including fast and slow components.[66, 138] The fast component is too fast to be resolved in these experiments and appears as a constant offset in the model.[74] The slower component governs the gradient profile observed (see Figures 4.2 and 4.3). The expression employed in fitting these data is as follows (derivation shown in chapter 3):

$$N_a(t) = N_s(0)[1- \exp(-kC_{sol}t)]$$

where N_s and N_a represent the number of accessible reactive surface silanol sites originally present and the number of amine groups on the surface, respectively, while k is the rate constant for the slow surface condensation reaction and C_{sol} the concentration of reactive silica precursors in the sol. The solid lines in Figures 4.2 and 4.3 depict the individual fits to the above expression. The values of k obtained from the data shown in Figure 4.2 are given in Table 4.2. For comparison, kC_{sol} for APTEOS was found to be 11.8 h^{-1} in our prior work.[74]

Table 4.2: Results from fit to a single-step kinetic model

Gradient	**C_{sol} (mM)**	**k ($mM^{-1}h^{-1}$)**
Diamine	0.22	97±10
Triamine	0.18	91±16
N-butyl	0.19	28±7
N,N-diethyl	0.22	5.5±6.5
APTMOS	0.27	39±9

From Table 4.2, it can be seen that the reactivity of individual aminosilanes with surface silanol groups on the base-layer coated substrate is strongly dependent on the precursor, with the tertiary amine reacting most slowly and the aminosilanes containing multiple N groups reacting significantly faster. On a 30 min time scale, the Diamine and Triamine gradients reach saturation whereas the secondary and tertiary gradients do not. Also, the non-zero intercept is slightly larger for the Diamine and Triamine precursors. The order of reactivity follows the trend: Diamine ~ Triamine > APTMOS > N-Butyl > N,N-Diethyl.

Aminosilanes follow a unique reaction mechanism because of the presence of the basic amine group.[142] In particular, hydrolysis and condensation of aminoalkoxysilanes occur rapidly because of the self-catalyzing ability of the basic amine group.[69, 73, 142-145] Furthermore, the silane and its hydrolysis and condensation products have excellent water solubility.[69, 73, 142-145] The efficiency at which the aminoalkoxysilane reacts with surface silanol groups can be increased by maximizing hydrolysis and limiting self condensation.[143] This efficiency will depend on a number of factors, most notably the number of amine moieties and whether the amine is sterically and electronically hindered.[139, 143, 144, 146]

The rate of condensation of APTEOS with surface silanol groups on silica particles with different porosity was previously studied by Okabayashi.[66, 138] In these studies, kinetic information was obtained for APTEOS via ^{29}Si CP MAS (cross-polarization and magic-angle spinning) NMR, DRIFT (diffuse reflectance infrared Fourier transform), and/or elemental analysis. The results reported ($k \sim 10^{-2}$ to 10^{-3} s^{-1}),[66, 138] are similar to our results, but their experiments were obviously more complex than the ones described herein. To our knowledge, the condensation rates of other substituted aminoalkoxysilanes to silica have not been studied.

Salon and coworkers, however, have qualitatively studied the hydrolysis and self-condensation of substituted aminoalkoxysilanes ***in ethanol/water solutions*** by monitoring the formation of hydrolyzed species and oligomeric species via NMR.[139, 143, 144, 146 147] They noted that in solution, hydrolysis and condensation were fast for all the aminosilanes studied, the rates of which were strongly dependent on the number of amine groups and the presence of substituents on the amine moiety.[139, 144] For those precursors that contained more than one amine group (i.e., Triamine), hydrolysis and self-condensation was greatly enhanced relative to the monoamine.[144] The presence of a bulky substituent on the amine, however, increased hydrolysis times and restricted self-condensation.[144] Likewise in a study on the catalytic effect of substituted amines (primary, secondary, and tertiary) on the hydrolysis and condensation of vinyltrimethoxysilane-grafted ethylene-propylene copolymer, it was reported that the amine with the smallest substituent had the fastest rate of hydrolysis.[72] The degree of cross-linking (condensation) also followed the order: primary > secondary > tertiary amine.[72] As can be seen from the data in Table 4.2, the order of reactivity as evaluated from the gradient profile, follows the same trend: primary > secondary > tertiary amine. It can be concluded that an increase in alkyl substitution on the amine (secondary and tertiary) group leads to a decrease in the rate and efficiency of cross-linking due to steric crowding in the transition state.[72]

Another factor that could potentially influence reactivity is the basicity of the amine. In solution, basicity as defined by pK_b values is typically: primary < secondary > tertiary. For example, the pK_b in solution for n-propylamine, an analogue to APTMOS, is 3.47 while di-n-propylamine and tri-n-propylamine, analogues of N-butyl and N,N-Diethyl, have a pK_b of 3.00 and 3.35, respectively.[148] Thus, the secondary amine is the strongest base, followed by the tertiary and primary amines (secondary > tertiary > primary). While the analogues of APTMOS

and N,N-Diethyl have nearly identical pK_b values (differing only by ~0.1 pK_b unit) and thus, similar basicities, they have very different reactivities, indicating that basicity is not a determining factor. A similar conclusion was reached by Adachi and Hirano upon examining the effect of amine compounds on the hydrolysis and condensation of vinyltrimethoxysilane grafted ethylene-propylene copolymer, which was that the reactivity of the amine compounds did not depend on their base dissociation constants.[72]

4.4.4 Gradient Amine Basicity

In addition to the differences in solution-phase basicity discussed above, the different aminosilanes were also found to yield gradients having different basicities ***in the dry state***. The basicity of the gradient surface and how it changes as a function of position can also be ascertained from the XPS data. The N1s band in the XPS spectra shown in Figure 4.1 appears as a doublet with binding energies near 399 eV and 401 eV. Each spectrum can thus be fitted to two peaks, N_1 and N_2; the lower energy nitrogen peak is from the free amines (N_1) and the higher energy peak is due to protonated and H-bonded amines (N_2).[67, 149] Hydrogen-bonding interactions take place between the amine groups and neighboring surface silanol groups; the nitrogen abstracts a proton from a neighboring silanol, in an acid-base reaction to yield the protonated species.[67, 136, 149-151] Figure 4.4 shows curve fitted N1s spectra obtained near the bottom of the gradient (~12-13 mm from the top of the slide). By comparing the ratio of the two peaks, information can be obtained about the basicity of the surface bound amine groups as a function of surface coverage in a single sample. The area ratio (N_1/N_2) of the high energy (N_1) to low energy (N_2) peak varied for the different aminosilanes as shown in Figure 4.5.

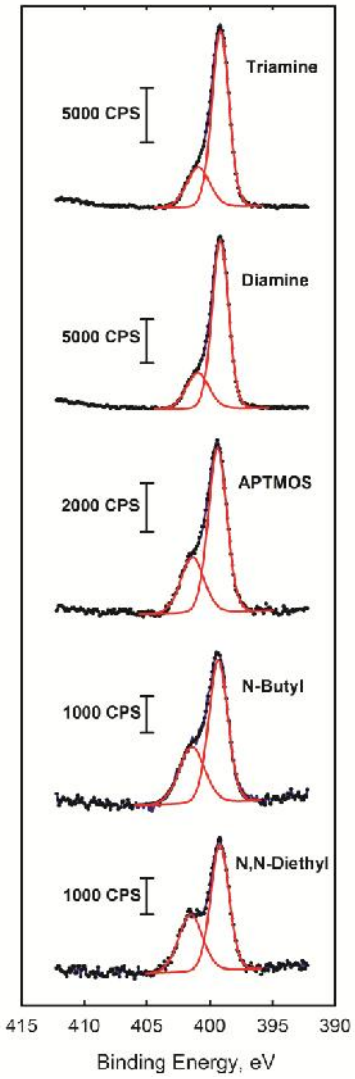

Figure 4.4. N1s high resolution XPS spectra curve fitted to obtain two peaks. Spectra were collected near the bottom of the gradient.

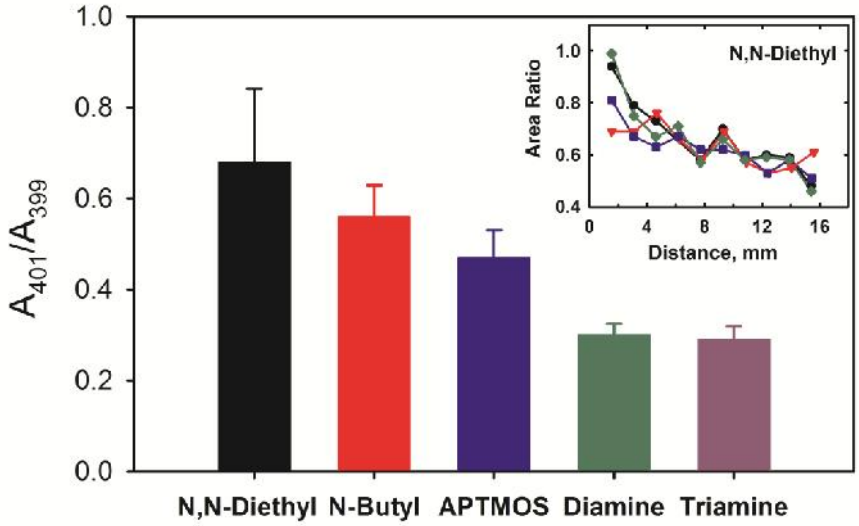

Figure 4.5. Area ratio of the N1s high energy peak (protonated amine) to low energy peak (free amine) for the different aminosilane precursors. Inset: Trend in the area ratio vs distance along the length of the film from top (1 mm) to bottom (16 mm) for four line scans acquired on the gradient film prepared from the N,N-Diethyl precursor.

Based on the N1s area ratios, basicity in the dry state follows the trend: Diamine ~ Triamine < APTMOS < N-Butyl < N,N-Diethyl, consistent with vapor phase basicity that follows the same trend.[152] Choi and coworkers[153] recently examined primary, secondary, and tertiary amines on mesoporous silica and examined at the adsorption of CO_2 and showed that the adsorption amount and bonding affinity increased with basicity in the same order: primary, secondary and tertiary. The area ratio is lower for the gradients deposited with di- and triamines, likely because protonation of consecutive amines in Diamine and Triamine becomes more difficult. XPS results from Metwalli and coworkers on APTEOS, Diamine, and Triamine coated glass support this conclusion.[151]

For most of the films investigated, the peak area ratio, and hence the surface basicity, were found to be relatively invariant with position along the gradient. Clear exceptions were found for

the most basic of the silanes investigated, N,N-Diethyl and the N-Butyl silanes, both show trends to smaller values along the length of the gradient from top to bottom. For the gradient films prepared from the N,N-Diethyl silane, Figure 4.5 inset, the data was very distinct, depicting a clear trend to smaller ratios at the 99.99% confidence level. For N-Butyl, the data demonstrate a similar trend at 94% confidence (Figure 4.6)

.

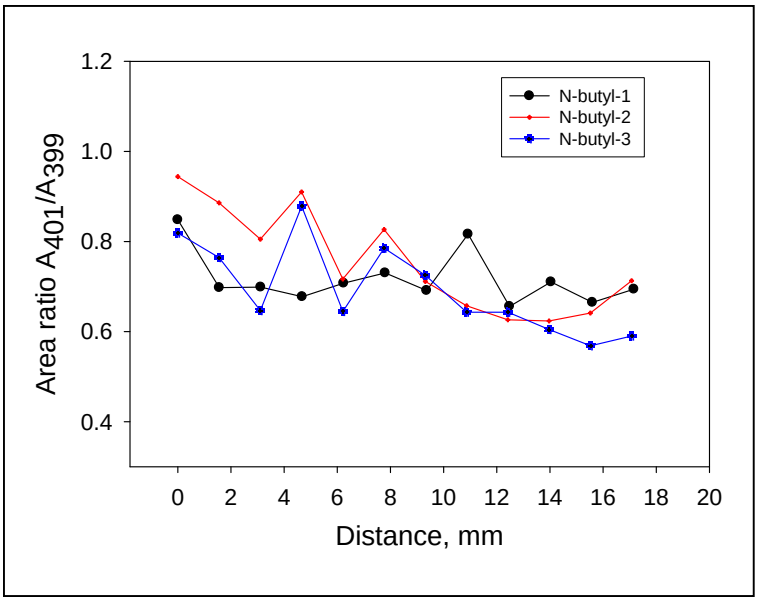

Figure 4.6. Trend in the area ratio vs distance along the length of the film from top (1 mm) to bottom (16 mm) for three line scans acquired on the gradient film prepared from the N-Butyl gradient.

It is interesting that the extent of protonation is smaller at the bottom of the gradient compared to the top. The higher packing density at the bottom of the film may make it difficult for the substituted amines to interact with surface silanol groups, thus decreasing the extent of protonation. Changes in hydrogen bonding interactions along the length of the gradient can alter acid/base dissociation constants. The close proximity of the amine groups at the bottom of the gradient will favor intramolecular interactions, in turn altering pK_b, and the extent of protonation.

Such an effect has been studied before using individual nongradient films in solution prepared by self-assembling carboxylic acid terminated alkanethiols on gold.[154, 155] The pK value for acid groups in a mixed monolayer, for example, were shown to be slightly smaller than in a pure film, which was attributed to changes in hydrogen bonding interactions and solvation.[154, 155] These findings demonstrate an appealing characteristic of gradient surfaces – how one single sample can be used to study surface density effects that would otherwise require several nongradient samples to be made and studied one at a time.

4.5 Summary

The preparation of surface amine gradients with well-defined profiles (shapes) requires a detailed understanding of the reactivity of aminoalkoxysilanes. By understanding factors such as reactivity, basicity, and steric effects, it is possible to engineer surface chemical gradients with carefully controlled properties in order to achieve a desired outcome. From a different perspective, gradient surfaces prepared from controlled-rate infusion provide a relatively simple and unique way to evaluate the rate of condensation of silane precursors with surface silanol groups as well as how the chemical properties (e.g., basicity) change as surface density changes.

In this work, six aminoalkoxysilanes having different levels of substitution and/or differing numbers of amine groups were chosen for study. The reactivity of the aminosilane with surface silanol groups clearly influenced the gradient profile both in terms of its shape and degree of saturation. Those precursors with more than one amine group reacted and reached saturation more quickly than aminosilane precursors with just one amine group. Of the monoamine-based silanes, reactivity followed the trend: primary > secondary > tertiary. Saturation was not attained for the secondary and tertiary amines during the 30 min infusion time

scale at the concentrations used. The results described herein can be explained in terms of steric hindrance resulting from the substitution around the amine group. Apart from the direct applications like cell adhesion studies and chromatographic stationary phases, these amine functionalized surfaces are ideal surfaces to further modify and build more complex platforms. The amine group can be chemically linked to other reagents (proteins, enzymes, dyes) in solution via simple covalent coupling strategies. The Diamine and Triamine gradients can be used to prepare metal ion gradients that make use of the chelating abilities of these functional groups. Chapter 5 will cover such metal chelation gradients on amine modified surfaces.

5. Fabrication and Investigation of Surface Metal-Chelation Density Gradients Prepared by Controlled-Rate Infusion.

5.1 Abstract

Aminosilanes containing chelating ligands such as ethylenediamine and diethylenetriamine have been used in this work to form gradients in metal-amine complexes on a base-layer coated silicon wafer. This was accomplished by preparing surface amine gradients by controlled-rate infusion (CRI) using these chelating aminosilanes and then exposing them to a metal ion solution to form the metal-complex gradients through chelation. CRI is a well-established method for the preparation of chemical gradients of various length scales for a broad range of applications. This approach is based on controlling the extent of reaction on a surface via exposure/contact time of the substrate to the silane solution. In this work, two metal ions, copper (Cu^{2+}) and zinc (Zn^{2+}), were used for metal coordination with surface gradients of ethylenediamine and diethylenetriamine ligands. X-ray photoelectron spectroscopy (XPS) was used to characterize the gradient profiles of the amine as well as the metal complexes. Metal complex formation was investigated along the diamine and triamine gradient surfaces with different gradient profiles prepared using different concentrations of aminosilanes. The profile plot of normalized peak area ratio of N1s to metal 2p peaks showed a variation in metal-amine coordination number along the gradient. XPS results revealed that Cu^{2+} ion formed a gradient in metal-amine complex density whereas Zn^{2+} formed a gradient in metal-amine coordination number along the gradient. Apart from providing a simple approach for varying metal ion concentration on surfaces through chelation, this research can also be helpful to study the effect of metal complexation on surfaces

with strategically varied ligand concentration. Also, a gradient in ligand density on a chromatographic support will be useful in the separation and concentration of metal ions.

5.2 Introduction

Silane coupling agents have been widely used to alter the surface properties of silica and metal oxide surfaces.[156-160] Metal binding on silica surfaces is one such area where the non-hydrolyzable groups on the alkoxysilanes such as amines and thiol groups etc., can act as ligands to form metal ion complexes.[161-163] This is usually achieved in two different ways: (1) Surface modification with the ligand-modified silane followed by treatment with the metal ion and (2) by directly grafting the metal-ligand complex, which is prepared separately.[164] Silica surfaces grafted with amine groups have been widely used to bind metals by forming metal-amine complexes.[165-168] These surface metal-amine complexes were formed with various metals such as nickel and copper, for applications in catalysis,[169-171] separation sciences,[166, 172-175] solid phase extraction[176] etc. Copper immobilization through the amine groups in organosilanes is one of the well-known methods for the preparation of packings for complexation chromatography.[166, 172, 173, 175, 176] Another notable application of ligand immobilization on surfaces such as silica is the separation of metal ions by column[177] and thin layer chromatography.[178-180]

In this work, surface gradients of chelating amine ligands, such as ethylenediamine and triethylenediamine were prepared by controlled-rate infusion (CRI) and subsequently metal-complex gradients were formed by exposing these gradients to metal ions in solution. The CRI approach has been shown to be a very effective and straight-forward method for preparing surface chemical gradients.[74] CRI is a contact-time based approach where the contact time of the precursor solution with the substrate is gradually varied to form continuous chemical gradients.[74]

It is accomplished by infusing a freshly prepared silane solution into a vial containing the substrate. This method has a unique advantage of showing incredible control over the gradient profile by simply changing the concentration of silane solution and infusion rates.[74] In our previous work, gradient profile control was investigated using this approach by varying and programming the infusion rates. It was shown that the CRI approach is capable of forming surface gradients with strategically controlled gradient profiles.[14, 74] Surface chemical gradients were prepared by this approach were applied for chromatographic separations[14, 181] (Chapter 5) and to study the reactivity of precursor solutions (Chapter 4).[182] In this Chapter, diamine and triamine gradients were prepared using different concentration of silane solutions to obtain gradients with different steepness.

Cu^{2+} and Zn^{2+} complexes were formed on ethylenediamine and diethylenetriamine gradients on planar support. X-ray photoelectron spectroscopy (XPS) was used to evaluate the variation in surface densities of the metal ion relative to the ligand along the length of the gradient. In the case of copper, metal complex formation depended on the ligand density for both the diamine and triamine gradients. However, zinc complex formation was almost independent of ligand density along the gradients except at very low concentration of amine density. This approach of metal-complex gradient preparation on silica substrates is not only useful for the chromatographic separation of metal ions but also useful for the high-throughput investigation of metal complexation at different ligand concentrations.

5.3 Experimental Section

5.3.1 Sample Preparation

(3-Trimethoxysilylpropyl)Diethylene triamine (triamine, 97%), was purchased from Gelest, Inc. (N-3-Trimethoxysilylpropyl)ethylene diamine (diamine, 97%), Tetraethoxysilane (TEOS, 98%), dimethyldiethoxysilane (DMDEOS, 97%) and 3-aminopropyltriethoxysilane (APTEOS, 99%) were purchased from Acros Organics. All the silanes were used as received. Silicon wafers (University Wafer, B-doped, <111>) were cut to the appropriate size (1 x 2 cm) and then cleaned with fresh conc. H_2SO_4:H_2O_2 (70:30) for 10 minutes at 70° C in a water bath (CAUTION: Piranha solutions are extremely dangerous and react violently with organic materials). The procedure for the preparation of the dimethyl base-layer coated substrate using a sol containing TEOS and DMDEOS was described in Chapter 3. Once the base-layer coated substrates were prepared and dried for 12 hours under vacuum at room temperature, they were subsequently soaked in ethanol for 10 to 12 hours for stabilization before the gradient preparation.

Surface amine gradients were prepared by simply infusing a freshly prepared aminosilane solution into a vial containing the base-layer coated Si wafer at a controlled rate using a syringe pump (NewEra, NE -1000). During the infusion, the base-layer coated substrate was exposed to the aminosilane solution for a different timescale along the length of the substrate, which produces a gradual variation in amine concentration from top to bottom (see Chapter 1 and Chapter 3). The aminosilane solution for infusion was prepared by mixing ethanol : silane : water in slightly different ratios. To prepare the metal-amine complex (Cu^{2+} and Zn^{2+}) gradient film from the diamine and triamine surface gradients, these amine gradients were soaked in $CuSO_4$/$ZnSO_4$ solution (0.1 M in water) for ~ 3 hrs followed by rinsing with water and blowing dry with nitrogen.

5.3.2 XPS measurements

X-ray photoelectron spectroscopy (XPS) was performed with a ThermoFisher ESCAlab 250 imaging X-ray photoelectron spectrometer (Al Kα (1486.68 eV), 500 μm spot size, 50 eV pass energy, 0.1 eV step size). Samples were usually placed on top of a piece of conducting tape on a 5 x 2 cm sample holder. XPS spectra were acquired in regular fashion (typically every 1-2 mm) across the wafer starting about ~ 1 mm from the edge (line scan). Spectra were calibrated by taking the C1s peak as occurring at 284.6 eV. Details of XPS data processing were described in Chapter 2.

5.4 Results and Discussion

5.4.1 Cu^{2+}-amine complex gradients

The metal-complex gradients were prepared by exposing the di and triamine gradients to the metal-ion solution. The substrate used in this method is the same base-layer described in Chapter 3, which was formed by spin-coating the sol prepared by co-hydrolysis/co-condensation of TEOS and DMDEOS on a silicon wafer. In the case of copper, three different concentrations of aminosilane solution (Diamine, Triamine) were used for infusion to obtain different gradient profiles to study the Cu-amine gradient formation. The aminosilane solutions were prepared by mixing ethanol : silane : water in the volume ratios of 5 : 0.05 : 0.005 (H), 5 : 0.025 : 0.0025 (M), and 5 : 0.01 : 0.001 (L). The copper amine gradient prepared with high (H), medium (M) and low (L) concentration of aminosilanes were termed as Cu-Di-H, Cu-Di-M and Cu-Di-L respectively. Similarly, triamine gradients were named as Cu-Tri-H, Cu-Tri-M and Cu-Tri-L. The silane solutions were taken for infusion immediately after preparation. The infusion rate for the preparation of all the above mentioned gradients was 0.6 mL/min and infusion times were ~ 4 minutes. The total infusion volume in each case was ~2.4 mL for a ~ 2 cm long base-layer coated substrate. Figure 5.1 shows the overlaid N1s spectra and Cu2p spectra of Cu-diamine

gradients G-Di-H, Cu-Di-M and Cu-Di-L. The N1s peak arises because of nitrogen present in the diamine groups and the Cu2p peak forms because of Cu^{2+} binding with the amine groups through chelation. The binding energy for the N1s peak is 399.9 ± 0.1 eV. In the Cu2p spectrum, two major peaks are observed ($Cu2p_{3/2}$ and $Cu2p_{1/2}$) peak with the binding energy values of 933.3 ± 0.2 eV and 953 ± 0.2 eV respectively. A small peak at binding energy 944.2 ± 0.2 eV was observed sometimes, which corresponds to the $Cu2p_{3/2}$ satellite peak. The binding energy values are closely matching with those reported for Cu(II) complexes in powder form by Roe et al.[183]

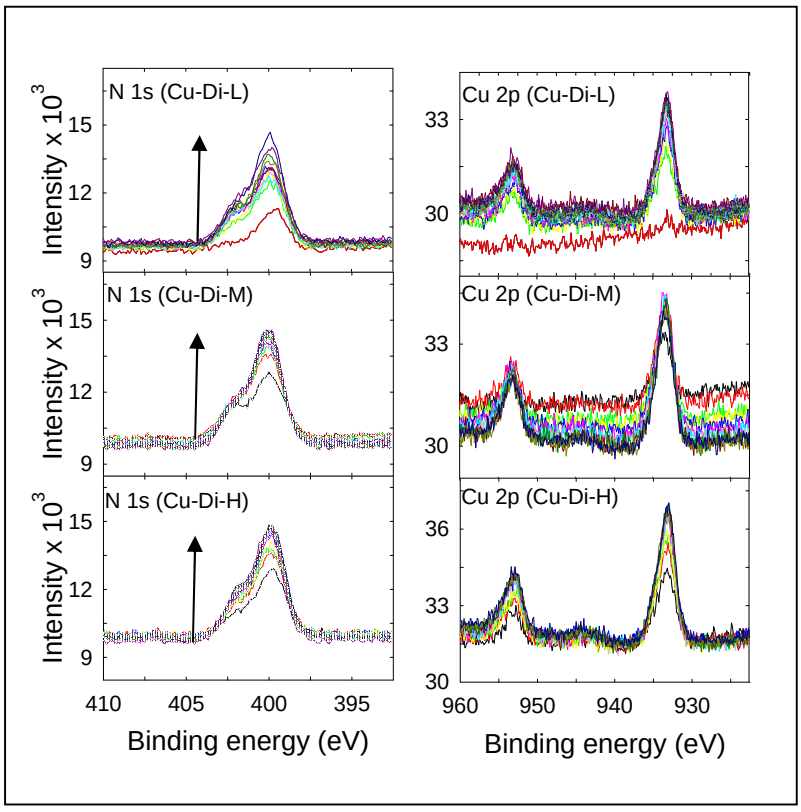

Figure 5.1. N1s and Cu2p spectra of Cu^{2+}-diamine complex for three different gradient profiles. Cu-Di-L, Cu-Di-M and Cu-Di-H. The arrow indicates gradient direction from low amine end to the high amine end.

To more easily see how the intensity of N1s and $Cu2p_{3/2}$ peaks vary along the gradient, profile plots were obtained by integrating the area under the N1s peak for N and the more intense $Cu2p_{3/2}$ peak for Cu. Figure 5.2A is the profile plot of N1s peak area (area versus distance along the gradient) for all three gradients, and Figure 5.2B is the corresponding $Cu2p_{3/2}$ profile plot. The profile plot clearly shows that the variation in peak area for both N and Cu is gradual from the top to the bottom of the substrate. The shape of the N1s gradient for both the diamine and triamine are similar to those noted in Chapter 4 Section 4.4. Both the ligand density and Cu-amine complex density vary in a similar fashion along the length of the gradient. Cu-Di-M and Cu-Di-H showed similar N1s and Cu2p profiles. It might be due to the fact that the magnitude of amine deposition between the two silane concentrations at this short time period (4 min) is not significantly different.

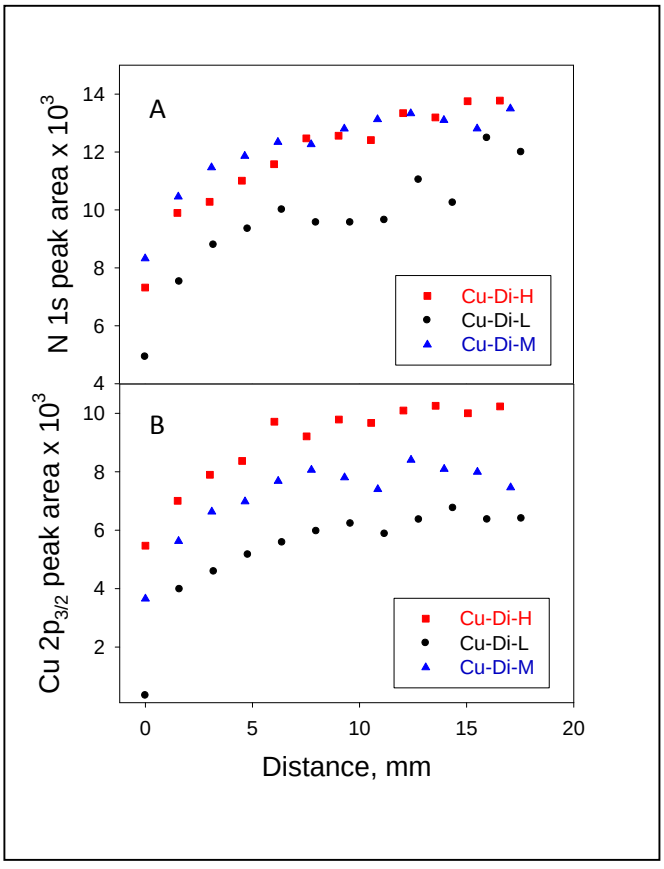

Figure 5.2. Peak area profile of N1s (A) and Cu2p (B) peaks along the Cu^{2+}-diamine complex gradients at three different gradient profiles (Cu-Di-L, Cu-Di-M and Cu-Di-H).

Similar to Cu-diamine, Cu-triamine gradients were also prepared with three different concentrations; Figure 5.3 shows the overlaid N1s spectra and the corresponding $Cu2p_{3/2}$ spectra of Cu-diamine gradients of Cu-Tri-L, Cu-Tri-M and Cu-Tri-H. Again, the N1s peak arises because of nitrogen present in the triamine groups and the Cu2p peak forms because of Cu^{2+} binding on amine through chelation. The binding energy of N1s is 399.9 ± 0.1 eV. In the Cu2p spectrum, two major peaks are observed for $Cu2p_{3/2}$ and $Cu2p_{1/2}$ peak with the binding energy values of 933.3 ± 0.2 eV and 953 ± 0.2 eV. A small peak at binding energy 944.2 ± 0.2 eV was observed in all the Cu2p spectra which correspond to $Cu2p_{3/2}$ satellite peak. The satellite peak intensities are proportional to the Cu2p peak intensities and hence triamine shows relatively more intense satellite peaks.

The N1s area reported in this work is significantly lower than those reported on Chapter 4 which is mainly because of the 5 to 25 fold higher concentration of silane used in the earlier work (Chapter 4). Also, in Chapter 4, the N1s area was normalized by the number of amine groups in the precursor. So, the N1s areas of diamine and triamine were divided by two and three respectively. It was observed that the triamine area were lower than the diamine area after normalization because of steric factors. However, in this work, after dividing the N1s area by two and three for diamine (Cu-Di-M) and triamine (Cu-Tri-M), the values are not significantly different except at position ‘0’cm (Table 5.1). The low concentration of aminosilane used in this work is the reason why the triamine are is not significantly lower than diamine as reported in Chapter 4, Section 4.4.

Figure 5.4A is the profile plot of N1s peak area (area versus distance along the gradient) for all three gradients and Figure 5.4B is the $Cu2p_{3/2}$ profile plot. The N1s profile plot reveals that the gradient profiles depends highly on the concentration of aminosilane in solution. The

steepness of the $Cu2p_{3/2}$ gradient also varied in a similar way when compared to N1s profile, again indicating that the Cu chelation follows a simple binding mechanism with these amines.

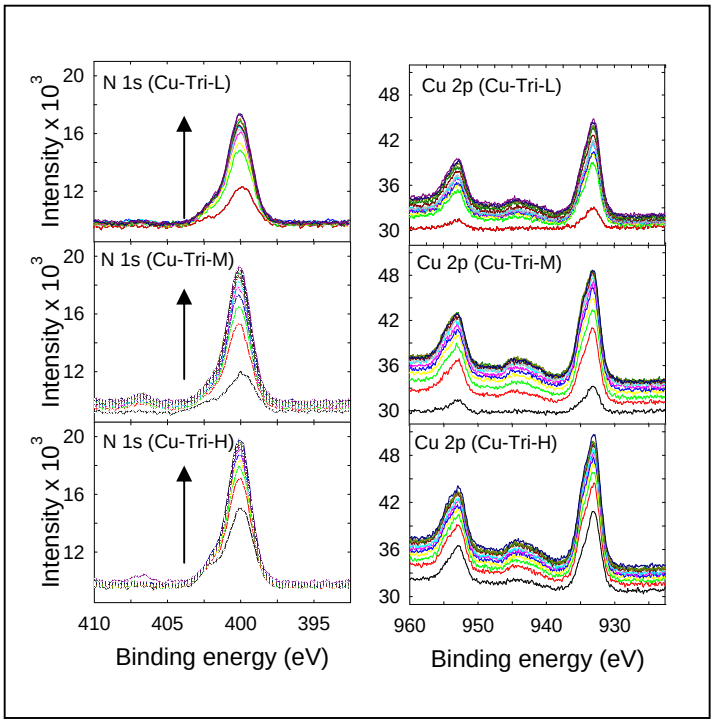

Figure 5.3. N1s and Cu2p spectra of Cu^{2+}-triamine complex for three different gradient (Cu-Tri-L, Cu-Tri-M and Cu-Tri-H). The arrow indicates the direction of the gradient from the low amine end to high amine end.

Table 5.1. N1s area of diamine (Cu-Di-M) and trimaine (Cu-Tri-M)gradients after normalization for the number of amine groups

Distance (cm)	Cu-Di-M N1s area/2	Cu-Tri-M N1s area/3
0.0	4162	2469
1.6	5229	4516
3.2	5732	5237
4.8	5931	5714
6.4	6172	6040
8.0	6132	6194
9.6	6402	6306
11.2	6565	6276
12.8	6666	6428
14.4	6549	6825
16.0	6403	6642
17.6	6750	6670

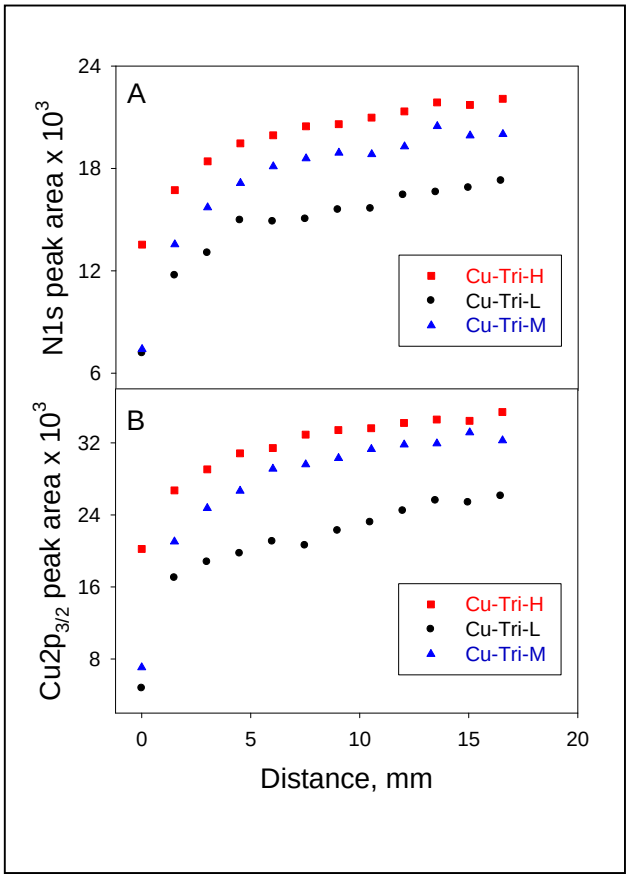

Figure 5.4. Peak area profile of N1s (A) and $Cu2p_{3/2}$ (B) peaks along the Cu^{2+}-triamine complex gradients for three different gradient profiles (Cu-Tri-L, Cu-Tri-M and Cu-Tri-H).

5.4.2 Controls

Control experiments were done to show that the Cu2p peak observed in XPS is only due to treatment of the amine gradient with the Cu^{2+} ion solution. Another control experiment is to show that the Cu binding is only through chelation on this surface. First, to firmly establish that the Cu2p peaks observed in the XPS spectra originated from the solution and not from adventitious impurities in the infusion solution and/or atmosphere, N1s and $Cu2p_{3/2}$ peaks were compared for the negative and positive control. In this case, the negative control (NC) was a uniformly modified diamine surface and the positive control (PC) was Cu^{2+} bound to a uniformly modified- diamine surface through chelation. These materials were formed by first immersing

two base-layer coated substrates in diamine solution (ethanol: silane ratio of 5 : 0.1) for 5 minutes to self-assemble the chelating agent to the surface. This forms two uniformly diamine modified surfaces. One of the two self-assembled samples served as the negative control and the other was soaked in the Cu^{2+} solution to form the positive control. Figure 5.5 shows both the N1s spectra and Cu2p spectra of both the NC and PC. The N1s spectra for both the PC (soaked in Cu^{2+}) and the NC (not soaked in Cu^{2+}) are all of similar intensity yielding profile plots that show little variation in the N peak area vs distance, as expected for an uniformly diamine modified surface. The N1s peak area is slightly smaller for the PC compared to the NC and is attributed to the surface sensitivity of XPS. The presence of metal ions decreases the signal intensity due other elements present on the surface.[184] Cu was only observed on the PC, which was purposely soaked in the Cu^{2+} solution. Again, the area under the $Cu2p_{3/2}$ peak was relatively constant with distance consistent with the uniform layer of Cu^{2+}-diamine complex on the surface.

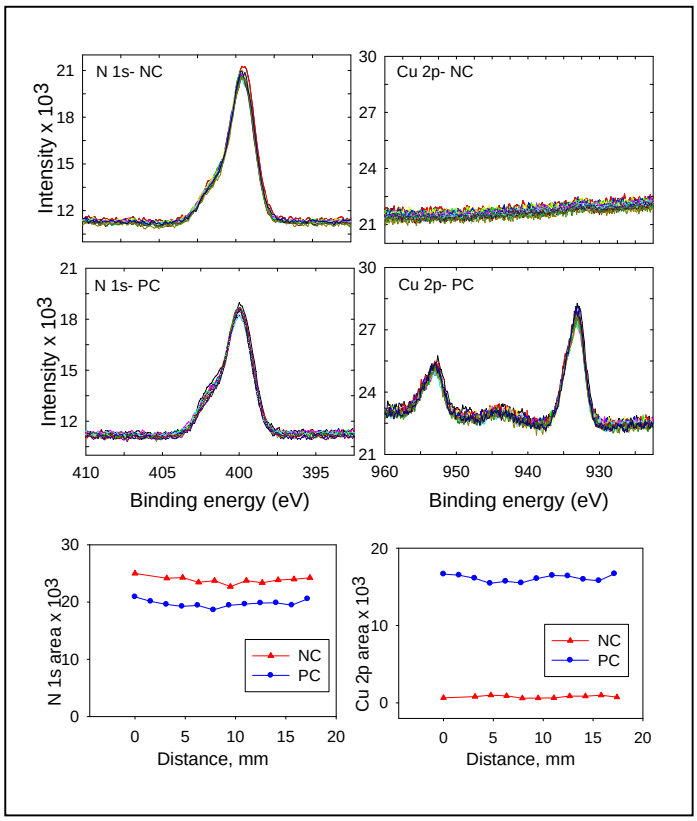

Figure 5.5. N1s and Cu2p spectra and corresponding area under the N1s and Cu ($2p_{3/2}$) peak acquired along the length of the substrate at ~ 1.5 mm intervals for a negative control (NC) sample prepared from diamine but not exposed to Cu^{2+} solution and a positive control (PC) sample exposed to Cu^{2+} solution.

Another control experiment was performed to confirm whether the Cu-amine complex formation would form with an amine group containing only one N. A gradient was prepared with 3-APTEOS (ethanol : silane ratio of 5:0.25) at an infusion rate of 0.1 mL/min (~ 30 minutes) and soaked in diamine solution. Figure 5.6A and B below shows the N1s and Cu2p spectra respectively and their corresponding profile plot is shown in Figure 5.6C and D. It clearly shows that there is no copper binding on base-layer surface that contains monoamine and the Cu-amine complex formation is through chelation.

Cu^{2+} ion binding however, was observed on aminopropyl (monoamine) modified silica gel prepared by mixing tetraethoxysilane and APTEOS, which is contradictory to our result.[185] However, in our work with a thin film of the monoamine silane, the Cu^{2+} , which could have bound weakly, to the monoamine was rinsed off while washing the substrate with water. This indicates Cu^{2+} binding is observed only when the surface contains the chelating ligand. A similar effect where chelation is necessary for metal binding on surface was observed by Moriguchi and coworkers in which ruthenium complex formation occurs on diamine SAM through chelation and not in monoamine.[186]

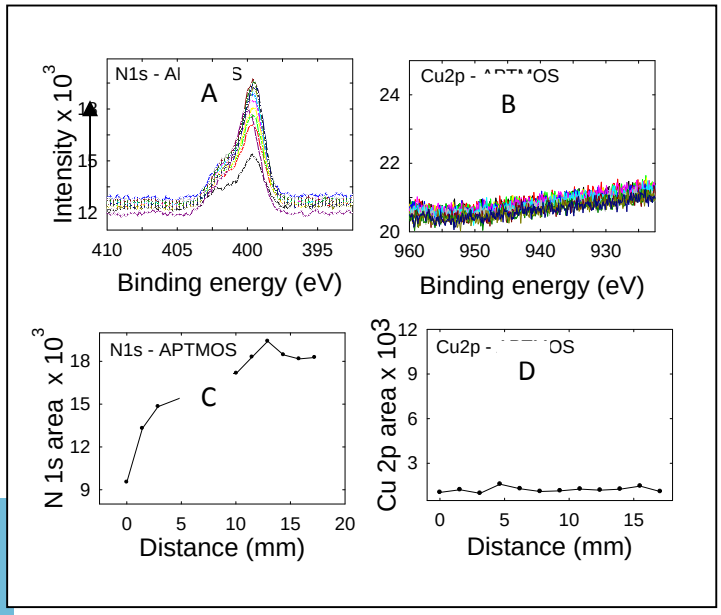

Figure 5.6. N1s (A) and Cu2p (B) spectra along APTMOS gradient soaked in Cu^{2+} (C) and (D) are the profile plots of N1s area and $Cu2p_{3/2}$ area. Arrow indicates the direction of the gradient from low amine end to high amine end.

5.4.3 Metal-amine coordination number along the gradients

Coordination number is the number of ligands bound to the metal ion. Cu^{2+} can form complexes with 1:2 and/or 1:3 metal : ligand ratio with diamine. Hence, it would be interesting to see if and how the relative coordination number of metal-di/triamine complexes varies with ligand density. This was accomplished by determining the ratio of normalized area of N1s to $Cu2p_{3/2}$ peak. The normalized area takes into account the XPS sensitivity factors of N1s and $Cu2p_{3/2}$. The N/Cu ratio cannot be taken as coordination number of metal-amine complexes because of the presence of free amine groups on the surface which are not bound to metal ion. However, if this ratio varies, it suggests that relative coordination number of metal-amine complex also varies. The variation in coordination number of metal-amine complex on ligand density has not been studied extensively so far. Cu^{2+} forms stable bis complex (1:2 metal:ligand) with diamine.[187] Based on this and our highly correlating gradient profiles for N1s and $Cu2p_{3/2}$, the N/Cu ratio is not expected to vary along the gradient. However, it would be different for other metal ion (Zn^{2+}) studied here. The step-by-step procedure for calculating the normalized-area ratio for N1s and $Cu2p_{3/2}$ was described in Chapter 2.

Figure 5.7A and B shows the profile plots of the normalized area ratio (N1s / $Cu2p_{3/2}$) for the three Cu^{2+}-diamine and Cu^{2+}-triamine gradients. The N/Cu ratio for diamine is the range of 9 to 12 and for triamine is 3 to 5. This shows that there are a greater number of free amine groups present in the diamine gradient when compared to triamine. This is also reflected in $Cu2p_{3/2}$ profile plot of diamine and triamine (Figure 5.2B and Figure 5.4B) where the area of $Cu2p_{3/2}$ peak for diamine is about 4 times lower than triamine. The diamine is a bidentate ligand whereas

triamine is a tridentate ligand and the above result indicates that the Cu binding increases with denticity of the ligand. Figure 5.8 A and B shows diamine coordination on the surface structurally and schematically with free diamine on the gradient surface. Figure 5.8 C shows the effect of free amine groups on N/Cu ratio which in our case is relatively high for diamine when compared to triamine.

From this profile, it can be observed that except for the first point (0 mm), the ratio has not changed significantly considering the experimental error. The same result is observed for Cu-triamine gradient where the normalized area ratio of N1s/Cu2p$_{3/2}$ did not vary with distance from the top to the bottom of the substrate (Figure 7B).

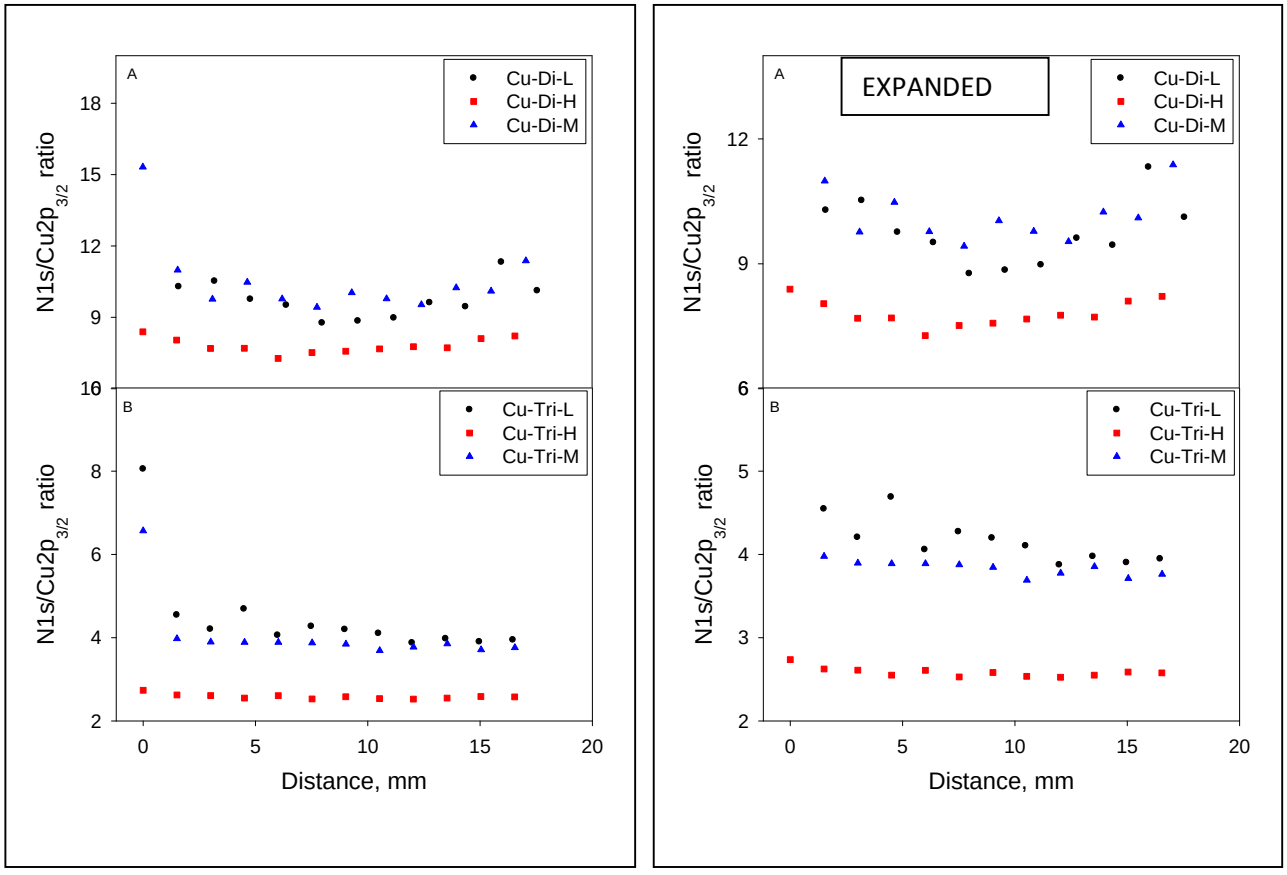

Figure 5.7. Normalized peak area ratio (N1s to Cu2p$_{3/2}$) of Cu^{2+}-diamine gradients (A) and Cu^{2+}-triamine gradients (B) The profiles of the three gradients prepared with different concentrations of amine are indicated in black, blue and red (low, medium and high, respectively).

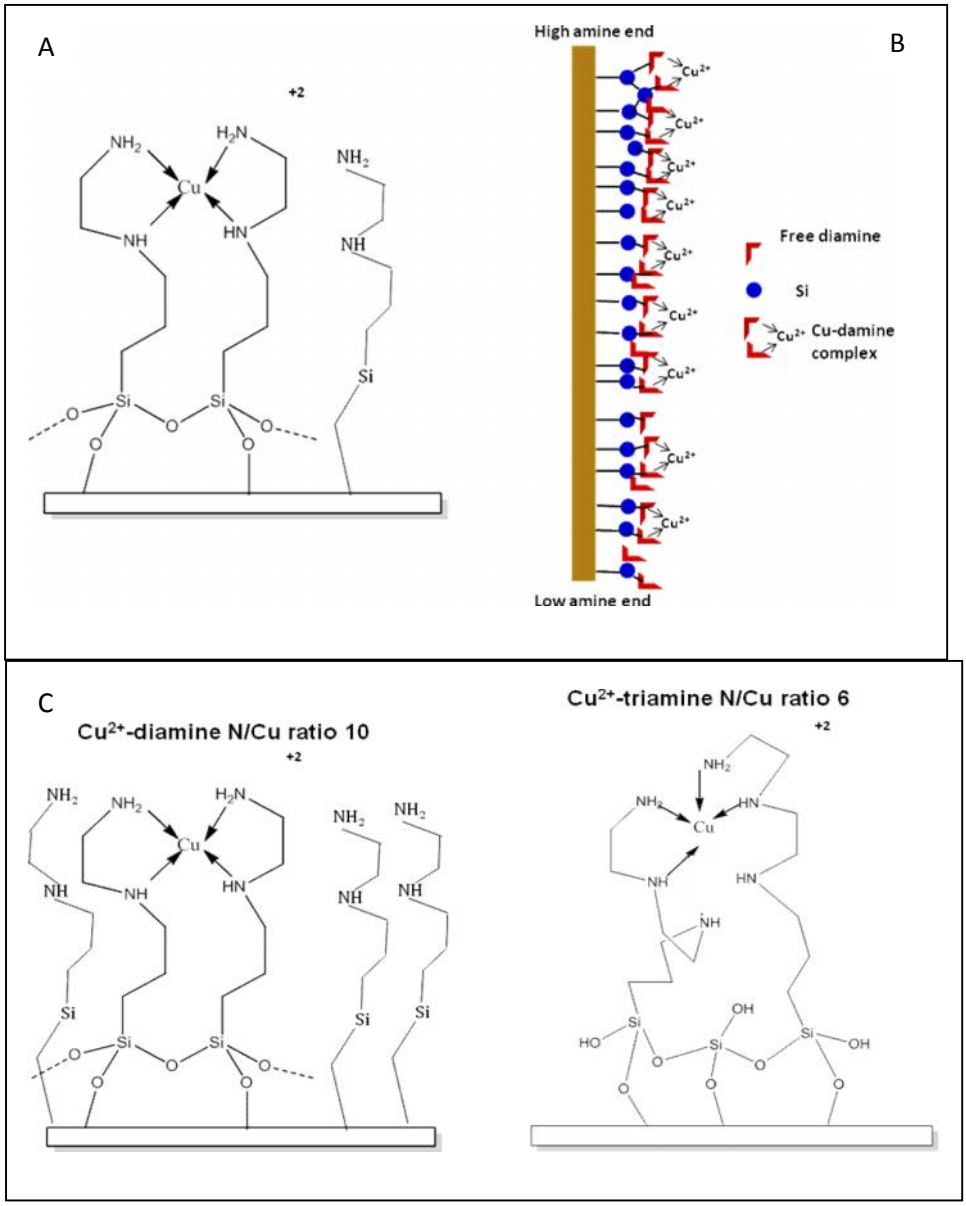

Figure 5.8. Structural (A) and schematic (B) representation of Cu^{2+} diamine complex on gradient surface. (C) Effect of free amine groups on N/Cu ratio.

5.4.4 Zn^{2+} amine gradients

Similar to the Cu-amine complex, Zn-amine complex gradients were also formed from ethylene diamine and diethylenetriamine gradients prepared by the controlled-rate infusion approach. In

the case of Zn-amine gradients, diamine and triamine gradients were prepared from two different concentrations of diamine (Zn-Di-H and Zn-Di-L) and triamine (Zn-Tri-H and Zn-Tri-L) respectively to obtain gradients with different steepness. These gradients were then treated with Zinc Sulphate solution ($ZnSO_4$) before characterization using XPS. As in the case of the Cu-amine gradients in which the $Cu2p_{3/2}$ peak was analyzed, here the $Zn2p_{3/2}$ peak was used.

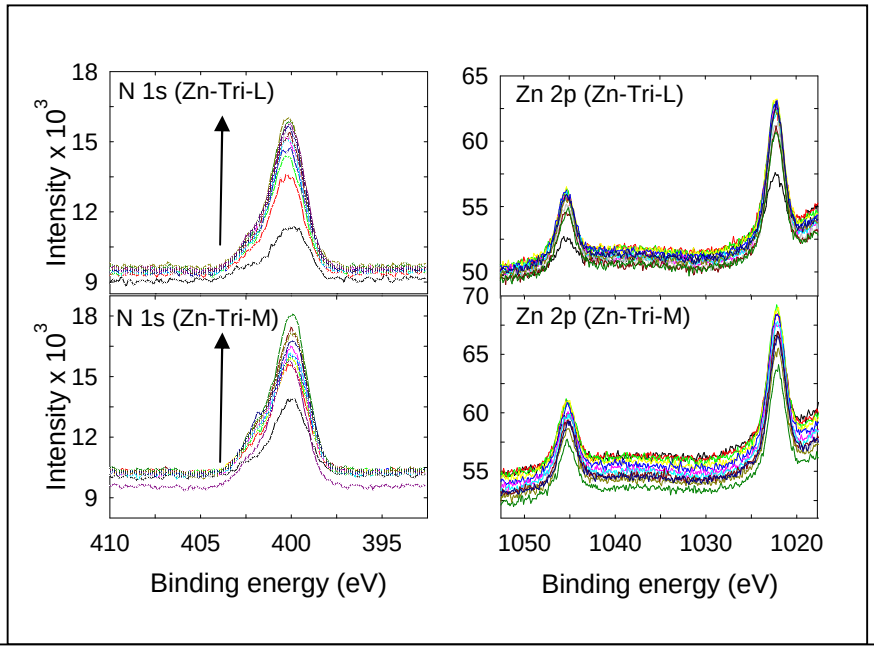

Figure 5.9. N1s and Zn 2p spectra of Zn^{2+}-triamine complex at two different gradient profiles: Zn-Tri-L and Zn-Tri-M. Arrow indicates the direction of the gradient from low amine end to high amine end.

Figure 5.9 shows the N1s and Zn2p overlaid spectra of Zn^{2+}-triamine gradient with two gradient profiles (Zn-Tri-L and Zn-Tri-M). In the Zn2p spectrum the peak at binding energies 1022.3 eV and 1045.5 eV corresponds to $Zn2p_{3/2}$ and $Zn2p_{1/2}$ respectively. The binding energy values are matching with that of Zn2p spectra obtained for Zn^{2+} doped films reported by Mu and coworkers.[188]

Since the intensity of $Zn2p_{3/2}$ peak is significantly higher than $Zn2p_{1/2}$ peak, the peak area of $Zn2p_{3/2}$ peak was evaluated. The variation in the area of the $Zn2p_{3/2}$ peaks along the length of

the gradient is shown in figure 5.9. The profile plot of $Zn2p_{3/2\ peak}$ area of Zn-triamine gradients (figure 5.10B) at two different concentrations reveals that the Zn content increases early in the profile and then saturates unlike $Cu2p_{3/2}$ profile, which is similar to the N1s profile. This shows that the coordination of the metal ions such as Zn^{2+} follows a different trend when compared to Cu^{2+} with chelating triamine ligands.

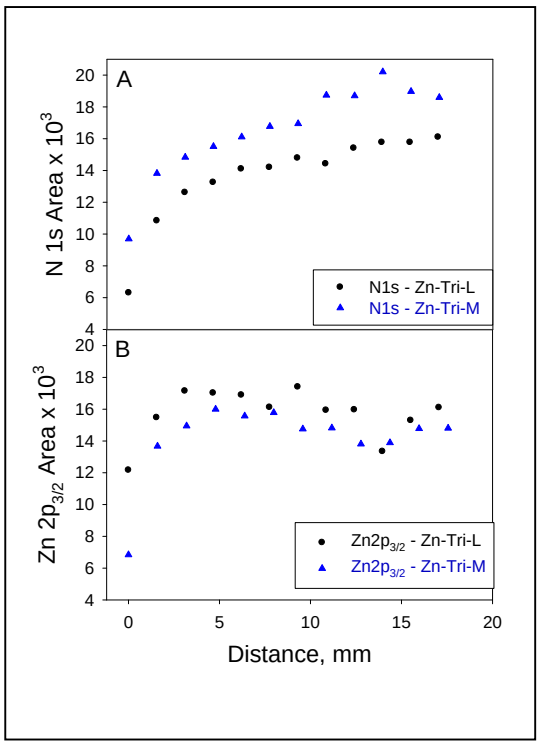

Figure 5.10. Peak area profile of N1s (A) and Zn $2p_{3/2}$ (B) peaks along the Zn^{2+}-triamine complex gradients at two different gradient profiles (Zn-Tri-L and Zn-Tri-M).

Since there was not much trend in the Zn content on the triamine gradient, it is important to verify the trend in relative coordination number of Zn–diamine complex along the gradient. Zinc is known to form coordination complexes with a range of coordination numbers with tetrahedral, square pyramidal, trigonal bipyramidal and octahedral geometries depending on the availability of ligand sites.[27] The coordination was assessed by verifying the profile of the

normalized area of N1s to $Zn2p_{3/2}$ along the length of the gradient. Figure 5.11 shows the profile plot of the normalized area ratio of Zn-triamine gradients at two concentrations, which takes into account the sensitivity factors of Zn and N, which are 4.8 and 0.42. This plot explicitly shows that the ratio gradually increases from the low amine end to the high amine end of the gradient. This is an indication of increasing trend of the coordination number of the Zn-triamine complex. This is the case for Zn^{2+}-triamine; however, Zn^{2+}-diamine complex formation along the gradient is slightly different.

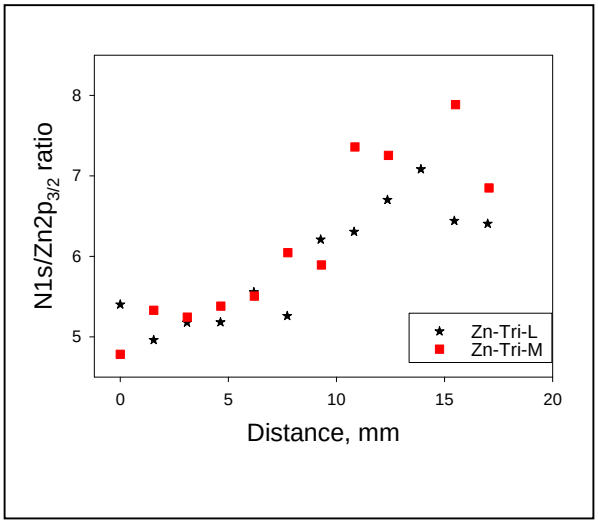

Figure 5.11. Normalized peak area ratio (N1s to Zn $2p_{3/2}$) of the Zn^{2+}-triamine gradients. Two gradients in this case are formed with different profiles and are shown in black and red (low and medium).

As mentioned above, Zn^{2+}-diamine gradient was formed using two different concentrations of aminosilane. Figure 5.12 shows the overlaid N1s spectra and Zn2p spectra along Zn-diamine gradient (Zn-Di-L and Zn-Di-M). Again, the N1s spectra reveal that the diamine concentration varies along the gradient and Zn2p spectra shows only a slight increase.

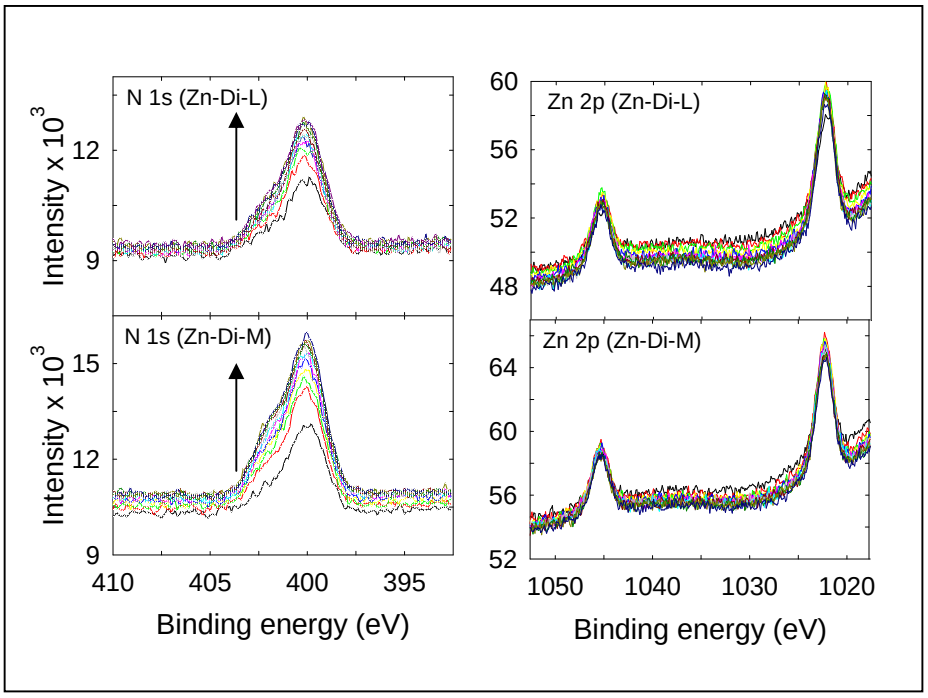

Figure 5.12. N1s and Zn 2p spectra of Zn^{2+}-diamine complex at two different gradient profiles. Zn-Di-L and Zn-Di-M. Arrow indicates the direction of the gradient from low amine end to high amine end.

The profile of the N1s peak area (Figure 5.13A) and the $Zn2p_{3/2}$ peak area (Figure 5.13B) are similar to those obtained for triamine, except at very low diamine concentration (N1s peak area < 8000 CPS eV) where $Zn2p_{3/2}$ peak also shows a low intensity. The Zn^{2+}-diamine complex formation on the diamine gradients shows a slightly increasing trend from the low amine to the high amine end of the gradient before it becomes saturated. This is slightly more pronounced in Zn-Di-L because of the fact that the amine surface density is less for the diamine gradient prepared from such a low concentration of aminosilane (0.2% v/v).

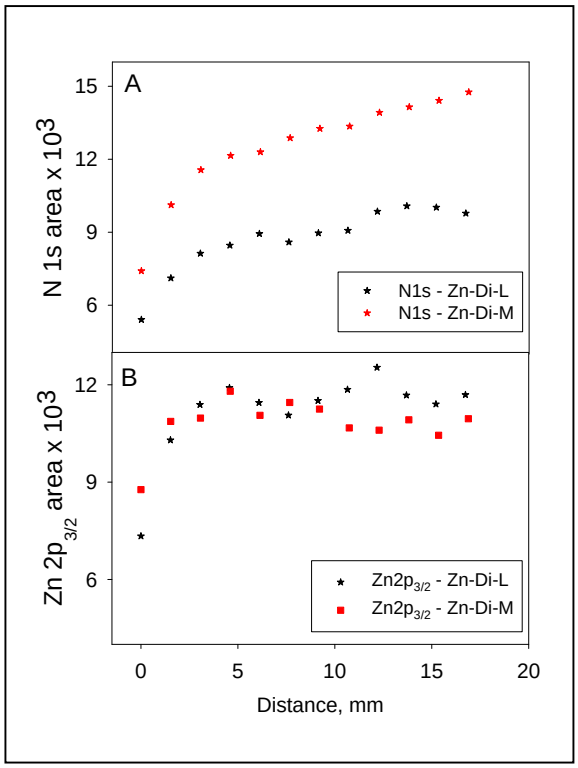

Figure 5.13. Peak area profile of N1s (A) and Zn $2p_{3/2}$ (B) peaks along the Zn^{2+}-diamine complex gradients at two different gradient profiles (Zn-Di-L and Zn-Di-M).

The above mentioned effect of Zn-D-L can also be observed in the normalized area ratio profile as well (Figure 5.14). This clearly shows that Zn-D-L gradient (black symbols), which is prepared with a low concentration of diamine, shows a shallow gradient profile of N1s/Zn2p ratio, in which the ratio just varied by 1 unit across the gradient. This is mainly because the diamine (ligand) density is very low to show a steep variation in Zn^{2+}-diamine coordination number as in the case of Zn^{2+}-triamine gradients.

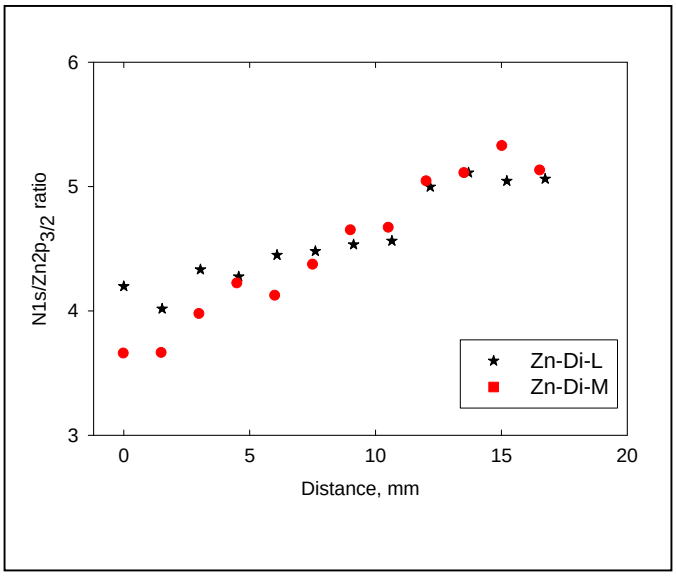

Figure 5.14. Normalized peak area ratio (N1s to Zn $2p_{3/2}$) of Zn^{2+}-diamine gradients. Black symbols correspond to the Zn-Di-L profile and the red is for the Zn-Di-M gradient profile.

Based on the above results, it can be seen that there is an obvious difference in complex formation of Cu^{2+} and Zn^{2+} on the chelating ligand density gradients. Cu^{2+} forms a coordination complex based on the stability of the complex and the geometry did not vary along the gradient, unlike Zn^{2+} which has coordination flexibility[189-191] and can form complexes with coordination number ranging from 4 to 6.[192] Fujita and coworkers have reported the formation of bis (1:2) and tris (1:3) complexes of Zn^{2+}-ethylenediamine in solution by varying the mole ratio of Zn^{2+} ion and the ligand.[193] This suggests that the gradual variation of N/Zn ratio with distance on the ligand density gradient is due to the difference in coordination along the gradient. The relatively low ratio (4 to 5 for diamine and 5 to 7 for triamine) suggests that there may be fewer free amines present. In the case of Cu^{2+}, the N/Cu ratio remains almost the same (except at '0' cm position) along the gradients unlike Zn^{2+} gradients, in which there is a linearly increasing trend

of N/Cu ratio (Table 5.2). Figure 5.15 schematically shows the variation in coordination number of Zn^{2+}-diamine complex on the low and high amine side of the gradient.

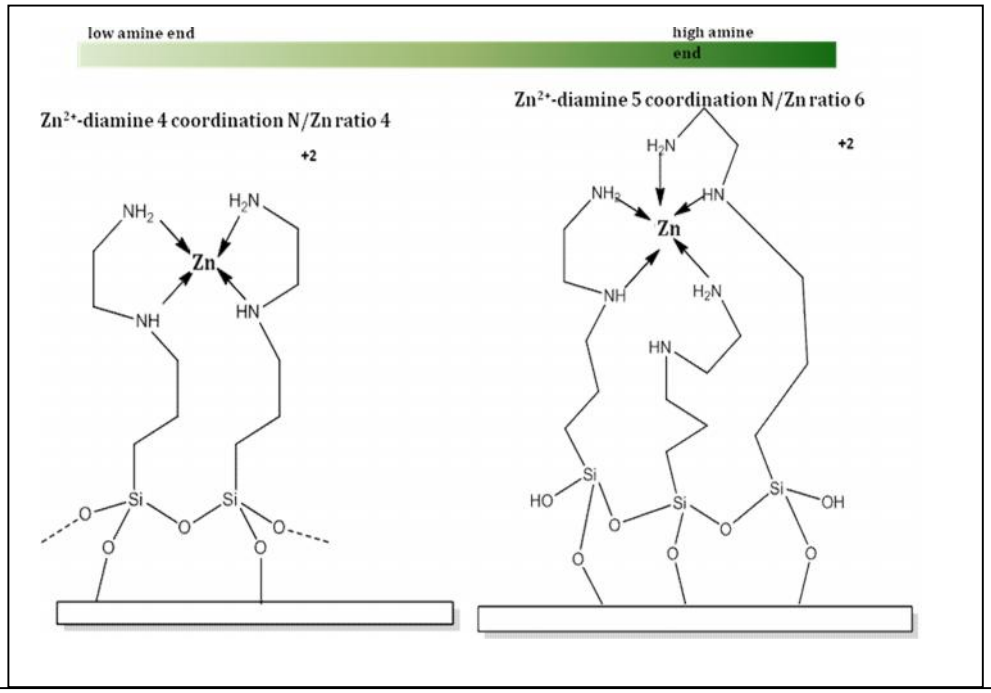

Figure 5.15. Structural representation of Zn^{2+}-diamine complex on the top and bottom of the gradient based on N/Cu ratio.

Table 5.2. N/Metal ratio (normalized area) of Cu^{2+} and Zn^{2+} gradients

Position(cm)	Cu-Di-L	Zn-Di-L	Cu-Di-M	Zn-Di-M	Cu-Tri-L	Zn-Tri-L	Cu-Tri-M	Zn-Tri-M
0.0	81.2	4.2	15.3	3.7	8.1	5.4	6.6	4.8
1.6	10.3	4.0	11.0	3.7	4.5	5.0	4.0	5.3
3.2	10.5	4.3	9.8	4.0	4.2	5.2	3.9	5.2
4.8	9.8	4.3	10.5	4.2	4.7	5.2	3.9	5.4
6.4	9.5	4.4	9.8	4.1	4.1	5.6	3.9	5.5
8.0	8.8	4.5	9.4	4.4	4.3	5.3	3.9	6.0
9.6	8.8	4.5	10.0	4.6	4.2	6.2	3.8	5.9
11.2	9.0	4.6	9.8	4.7	4.1	6.3	3.7	7.4
12.8	9.6	5.0	9.5	5.0	3.9	6.7	3.8	7.3
14.4	9.4	5.1	10.2	5.1	4.0	7.1	3.9	9.0
16.0	11.3	5.0	10.1	5.3	3.9	6.4	3.7	7.9
17.6	10.1	5.1	11.4	5.1	3.9	6.4	3.8	6.9

5.5 Summary

A unique application of the CRI approach was shown previously (Chapter-5) where the gradient formation by CRI method was used to study the reactivity of the precursor silanes. Similarly, another application was shown in this Chapter where the amine groups on the gradients act as chelating ligands. Surface gradients formed with amines containing more than one amine groups such as ethylenediamine and diethylenetriamine were used for metal complexation. Two metal ions with different chelating properties (Cu^{2+} and Zn^{2+}) were allowed to bind with the ligand in the gradients. These two metals showed different trends for the metal-amine complex formation by chelation on the ligand density gradients. Cu^{2+} ion formed gradients in Cu-amine complex on the surface of diamine and triamine gradients with different gradient profiles. On the other hand, Zn^{2+} did not exhibit a gradient in Zn-amine complex density along the surface. However, the relative coordination number of Zn^{2+}-amine complex varied as it moves along the gradient from top to bottom. This research has opened up a simple way for not just preparing gradients in metal concentration on silica surfaces for applications such as metal-chelate affinity chromatography, but shows that this technique is also useful for studying metal-ligand coordination at various surface ligand densities.

Chapter 6. Continuous Stationary Phase Gradients for Planar Chromatographic Media

Adapted from Kannan, B.; Marin, M. A.; Shrestha, K.; Higgins, D. A.; Collinson, M. M., *Journal of Chromatography A* **2011,** *1218* (52), 9406-9413

6.1 Abstract

A simple, elegant method for the formation of a continuous stationary phase gradient for use in chromatographic separations is described. Its applicability to separation science is demonstrated by using thin-layer chromatography as a test case. Gradient stationary phases were formed on activated high performance thin-layer chromatography (HP-TLC) plates using a CRI approach which has been elaborately dealt in previous chapters. The SiOH groups on the activated HP-TLC plates were reacted with 3-aminopropyltriethoxysilane (APTEOS) in a time dependent fashion to control the rate of APTEOS infusion into the deposition reservoir. The shape (profile) of the gradient was controlled by the rate of infusion and imaged by taking advantage of the concentration-dependent color formation reaction between amine groups and ninhydrin. The advantages of such gradients in optimizing the retention and separation of various components in different mixtures was illustrated using mixtures of (1) four weak acids and bases and (2) three widely-used over-the-counter drugs. The separation of the individual components on the gradient stationary phase was clearly improved relative to those on either traditional normal-phase TLC plates or uniformly amine-modified TLC plates. Precise control over component retention and separation was also demonstrated by strategically modifying the steepness of the gradient.

6.2 Introduction

The separation of complex, multicomponent mixtures by liquid chromatography has always been an exciting and challenging area for separation scientists. The difficulties associated with separating mixtures of ever increasing complexity has led to the development of numerous new methods and technologies, including gradient elution methods, hydrophilic interaction chromatography (HILIC),[194] ultra high pressure separation,[195] sol-gel columns,[196, 197] silica and polymer monolithic columns,[198-202] porous polymer monoliths for TLC,[203, 204] hierarchical stationary phases,[205, 206] colloidal crystal packings,[207, 208] and micropillar based columns.[209-212] In gradient elution chromatography, the eluent strength is varied during separation.[213] This method has proven to be very successful for separating mixtures of components having large differences in polarity.[213] As a result, there have been numerous applications of gradient elution in high performance liquid chromatography (HPLC) for the separation and quantitation of a wide range of analytes, from simple compounds to complex biological mixtures and metabolites. A number of gradient separations methods have also been demonstrated for use in thin layer chromatography (TLC).[89] These rely upon temporal variations in solvent content (solvent gradients), the demixing of multicomponent solvents on the TLC plate, exposure to different solvent vapors, and controlled evaporation of mobile phase components during the separation.[77, 89, 214, 215]

An alternative paradigm for changing the mobile phase composition to effect a separation is to change the composition of stationary phase (such as adsorbents, bonded phase etc.,) and use what are termed 'stationary phase gradients'. Such gradients for planar chromatographic separations have been prepared since 1960 for various applications.[89, 91-93, 216] In most of the TLC stationary phase gradients reported so far, either different bonded phases or adsorbents (such as

silica, cellulose etc) were combined together using a specified tool or manually. Recently, silica gel and cellulose adsorbents were combined together to form adsorbent gradient to separate water soluble vitamins.[90] While gradient stationary phases have shown enhanced resolution compared to stationary phases of uniform composition, these methods are not simple to implement, except in few cases where the adsorbents were bound together using a clamp.[90] Moreover, those approaches typically produce discontinuous gradients (i.e., stepwise gradient) and are not easily adapted to form gradient stationary phases on any type of platform including planar supports, capillaries, and microfluidic channels. Clearly, there exists a need to develop efficient strategies for creating and implementing continuous gradient stationary phases as well as evaluating their performance relative to non-gradient stationary phases.

In this work, we report a simple, inexpensive, and relatively rapid approach to prepare continuous stationary phase gradients using TLC as the proof-of-principle separation technique. We demonstrate the utility of these new gradient TLC plates in separations of a simple mixture of four weak acids and bases, and a mixture of three over-the-counter drugs. Our approach to gradient preparation utilizes silane chemistry, specifically the reaction of 3-aminopropyltriethyoxysilane (APTEOS) with surface Si-OH groups on the porous silica comprising the TLC stationary phase. When this chemistry is used in conjunction with "controlled-rate infusion",[74] a gradient in amine functionality can be prepared over the full length of each TLC plate. For analyte mixtures with components that have a wide range of physicochemical properties like hydrophilicity/hydrophobicity, acidity/basicity etc., optimum separation cannot easily be achieved on a single stationary phase such as silica gel or amine modified silica gel. In such cases, a continuous stationary phase gradient would allow the analyte-stationary phase interactions to vary along the bonded stationary phase packing. In this

work, proof of principle demonstrations are obtained by separating four weak acids/bases whose pK_as range from ~4.2 to 9.5. In addition, through gradient profile control, we also show the ease with which three commonly used drugs (acetaminophen, diphenhydramine hydrochloride and doxylamine succinate) can be separated and their retention factors controlled.

Once the gradients containing amine groups was successfully prepared, characterized and applied for a simple separation, CRI was extended to prepare gradients on TLC plates with other bonded phases such as phenyl and cyano, which are widely used in normal and reverse phase separations. Phenyl gradients on TLC plates were prepared by infusing a phenyltrimethoxysilane (PTMOS) sol at a controlled rate into a reaction vial containing an activated silica TLC plate containing a fluorescent dye. The variation in phenyl group density on silica surfaces was visualized under UV light (254 nm). Because the phenyl groups quench the green fluorescence, a phenyl gradient TLC plate will exhibit a gradual variation in fluorescence quenching under UV light (254 nm). In case of the cyano gradient, the infusion procedure is same but the characterization of the gradient was achieved using an FTIR microscope (reflection mode). The intensity of the sharp peak at 2250 cm^{-1} corresponds to the CN stretch variations along the TLC plate for the gradient in cyano group.

6.3. Experimental

6.3.1. Reagents

3-aminopropyltriethoxysilane (APTEOS, 99%), phenyltrimethoxysilane (PTMOS, 97%) and 3-(triethoxysilylpropyl)propionitrile (CNTEOS, 97%) were purchased from Acros Organics. Benzoic acid (BA), 3-Aminobenzoic acid (ABA), 2-aminopyridine (APy) and 4-aminophenol (APh) were purchased from Sigma-Aldrich. Acetaminophen (Ac), diphenhydramine hydrochloride (Dp) and doxylamine succinate (Dx) were purchased from Fisher Chemicals. Drug

tablets (CVS brand) containing acetaminophen (500 mg tablet), diphenhydramine hydrochloride (25 mg tablet) and doxylamine succinate (25 mg tablet) were obtained from CVS pharmacy. One acetaminophen pill, two diphenhydramine hydrochloride and two doxylamine succinate pills were individually crushed using a mortar and pestle. Diphenhydramine hydrochloride and doxylamine succinate were stirred for 1 hour in small vials containing 2 mL of chloroform while acetaminophen was stirred for an hour in 5 mL of ethanol. After stirring, each solution was syringe filtered (0.45 micron), transferred into clean 5 mL vials, and 50 µL aliquots were mixed in a 1 mL vial for spotting on the TLC plates.

6.3.2 Stationary Phase Preparation

HP-TLC plates (Whatman 100 µm thick, 5 µm particle size, 254 nm fluorescence excitation) were cut in the size of 10 x 1.5 cm and were activated by drying in an oven for 20 minutes at ~ 100 °C. After the plates cooled to room temperature, they were soaked in ethanol. The soaking helped remove adsorbed impurities from the plates and also acts as a wetting process to minimize wicking (solvent transport by itself in porous silica plates) during gradient fabrication. Controlled rate infusion for gradient formation was accomplished by placing the TLC plate in a suitable reaction chamber (in this case, a 25 mL graduated cylinder). An APTEOS solution was then infused into the chamber at a rate that ranged from 80 mL/hr to 1000 mL/hr using a syringe pump (New Era, NE-1000). The composition of the APTEOS solution was ethanol:APTEOS:H_2O (100:10:2) v/v. The total time for infusion ranged from ~1.5 min to 17 min, depending on the flow rate. The volume of infusion was 22.5 mL. The TLC plates were immediately removed from the cylinder, thoroughly rinsed with ethanol, and dried. Positive controls (PC) were made by simply soaking the activated TLC plates in APTEOS solution (22.5 mL) for 17 min to uniformly coat the entire silica surface with amine functionalities. Negative

controls (NC) were the as-received silica plates soaked in ethanol and dried. In another experiment, designed to show control over analyte retention, two silica plates (10 cm) were activated and soaked in APTEOS solution, one with half the volume of APTEOS required to cover the entire length and another with one-fourth the volume. This procedure produced modified TLC plates where the aminopropyl bonded phase covered one-half and one-fourth the length of the plate, respectively. Phenyl and cyano gradients on TLC plates were prepared in a manner similar to the amine gradient except for the preparation of silane solution. As described earlier, amine groups in APTEOS self-catalyzes and increases the rate of hydrolysis and condensation. In the case of PTMOS and CNTEOS this was done using a two-step method: acid was first added to hydrolyze the silanes followed by base to increase condensation. Hence, these silane solutions were prepared by first stirring the mixture of ethanol : silane : 0.05 M HCl in the volume ratio 10 : 1 : 0.5 mL for 30 minutes to hydrolyze the silane followed by the addition of 0.75 mL of 0.05 M NaOH and continued stirring for additional 1 hr prior to infusion.

6.3.3. Stationary Phase Characterization

To characterize the profile of amine groups on the surface of the TLC plates, a simple method was developed using ninhydrin as a universal reagent for the identification of amines/amino acids.[113] When treated with ninhydrin, primary amines will react and form a purple-colored dye. The ninhydrin solution was prepared by dissolving 1.5 g of ninhydrin (Sigma Aldrich, ACS reagent) in 25 mL of 1-butanol and 3 mL of acetic acid and then diluting to 100 mL with 1-butanol. This solution was spotted every 6 mm with a ~ 3 mm spot size along the length of the HP-TLC plates (gradient, PC and NC). After spotting, the plate was allowed to dry for ~8 min and then photographed using a digital camera. In each case, the procedure was performed three times to evaluate reproducibility. The digital image was loaded into an

enhanced version of the TLC Analyzer software[114] to obtain a plot of color intensity versus distance.

6.3.4. Separation

Gradient TLC plates were spotted with the mixtures to be separated on either the low amine or high amine end, as indicated in the text. In the first part of this work, the mixture of four weak acids and bases (BA, ABA, APh and APy) was dissolved in methanol and subsequently spotted onto the plates. The concentration of each analyte was 2.0 mg/mL, except for APy, which was 5.0 mg/mL. Separation was performed under both basic (methylene chloride:methanol:triethylamine, 90:10:0.5 v/v) and acidic (methylene chloride:methanol:acetic acid, 90:10:0.5 v/v) mobile phase conditions. The interior of the development chamber was surrounded with saturation pads and allowed to equilibrate prior to the addition of the TLC plate. The solvent front typically traveled ~ 8.5 cm up each TLC plate. The spots on the TLC plates were visualized under 254 nm UV radiation and photographs were taken using a digital camera. The pictures were loaded into the TLC Analyzer software[114] to extract the green-channel data (of the red-green-blue color scale). In the second part of this work, the mixture of the three over-the-counter drugs (Ac, Dp and Dx) was spotted on the gradient plates. Each separation was carried out using a mobile phase consisting of ethyl acetate:methanol:water (7:7:1.5) in a solvent-saturated development chamber. In this case, the elution time was 18 min, during which the solvent front moved ~ 6 cm up the TLC plate. Afterwards, the TLC plates were dried under atmospheric conditions for 5 min before being photographed under UV radiation and processed using the TLC Analyzer software.[114]

6.4. Results and Discussion

6.4.1. Characterization of gradient

In prior work, we described how the method coined 'controlled-rate infusion' could be used to prepare amine gradients on the surfaces of dimethylsilane-modified silicon wafers. In this process, a reactive aminoalkoxysilane is slowly infused using a programmed syringe pump into a glass vial containing an appropriately modified substrate, in the present case, a silica HP-TLC plate. When the volume of solution reaches the top of the TLC plate, the plate is immediately removed and rinsed. The extent of the gradient thus formed depends on the reactivity of the aminoalkoxysilane with surface silanol groups and the rate at which the sol is infused into the reaction vial. The longer a particular plate region is exposed to the reactive precursor, the more aminosilane is deposited, until, the point of saturation is reached. Aminoalkoxysilanes ($NH_2RSi(OR')_3$), which have unhydrolyzable amine groups, tend to self-catalyze and the rate of hydrolysis and condensation with reactive silanol groups is relatively fast.[73] Thus, by taking into consideration the kinetics of reaction between aminosilanes and surface silanol groups, a continuous gradient of controlled profile (i.e., steepness) and running from high to low amine concentration can be formed from the bottom of the TLC plate to the top.

In this work, several different gradient TLC plates were prepared by changing the rate of infusion: some incorporated a very shallow amine gradient, others a steeper gradient that reached saturation. To confirm the presence of a gradient on the TLC plates and evaluate its profile (shape), a new method had to be developed. X-ray Photoelectron Spectroscopy, which was used in our prior work (Chapters 3 and 4), could not be employed because the TLC plates could not be sufficiently outgassed before analysis. Our current method utilizes ninhydrin, a universal color reagent for detection of amines. The reaction between ninhydrin and the amine forms a Schiff base followed by the formation of an intermediate amine which further condenses with another molecule of ninhydrin to give a purple product[217]. Spotting the ninhydrin along the

gradient creates the colored product on the TLC plate, the intensity of which is related to the concentration of the surface amine groups.

Figure 6.1A (inset) shows a digital picture of a ninhydrin-spotted gradient (infusion rate = 80 mL/hr) TLC plate. The spot intensity data were extracted from this image as well as images from the NC and PC using the TLC Analyzer software. Each spot in the digital photographs appears as a peak whose intensity is related to the amine concentration on the plate at that location. Figure 6.1b is the screen shot of DETLC analyzer in which the picture to be analyzed was uploaded. The software scans a line drawn on the photograph to obtain red, green, blue, b/w spectra across the scanned line. In the figure, the scanned line is on the ninhydrin spots across the gradient plate and it can be observed that the black and white (b/w) scans show an increasing trend of peak intensity from the low amine end to the high amine end of the gradient. In most peaks, the peak apex shows a dip because of the concentration of purple color at the outer ring of each spot. Hence, the peak intensity (height) was measured after smoothing the peaks. The smoothing factor was same for all the spots on gradient and control plates. Figure 6.1a also shows a plot of intensity (peak optical density) versus distance along the three samples (NC, PC, Gradient). The absence of color formation on the NC plate reflects the absence of amine groups (flat line with zero intensity). The PC plate showed a near constant amount of amine across the length of the substrate, consistent with a uniform aminopropyl bonded-phase. In the gradient, the color intensity increased from the low amine end to the high amine end and saturation was also observed, in concordance with our previously reported XPS results on Si wafers. This colorimetric method, which is significantly simpler and less costly than XPS, confirms the presence of a gradient in amine groups on the surface of the TLC plate.

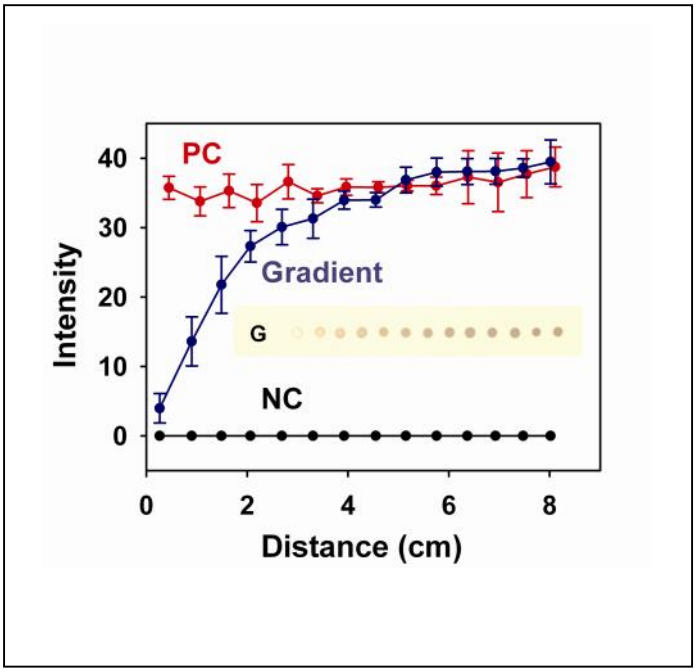

Figure 6.1a Plot of spot intensity after exposure to ninhydrin vs distance along the length of the plate for PC (red), gradient (blue, infusion rate = 80 mL/hr), and NC (black). The error bars signify ±1σ. N=3. Inset: A digital photograph of the gradient TLC plate from which the intensity data were extracted. Chromatographic data for these TLC plates are shown in Figures 6.5 and 6.6.

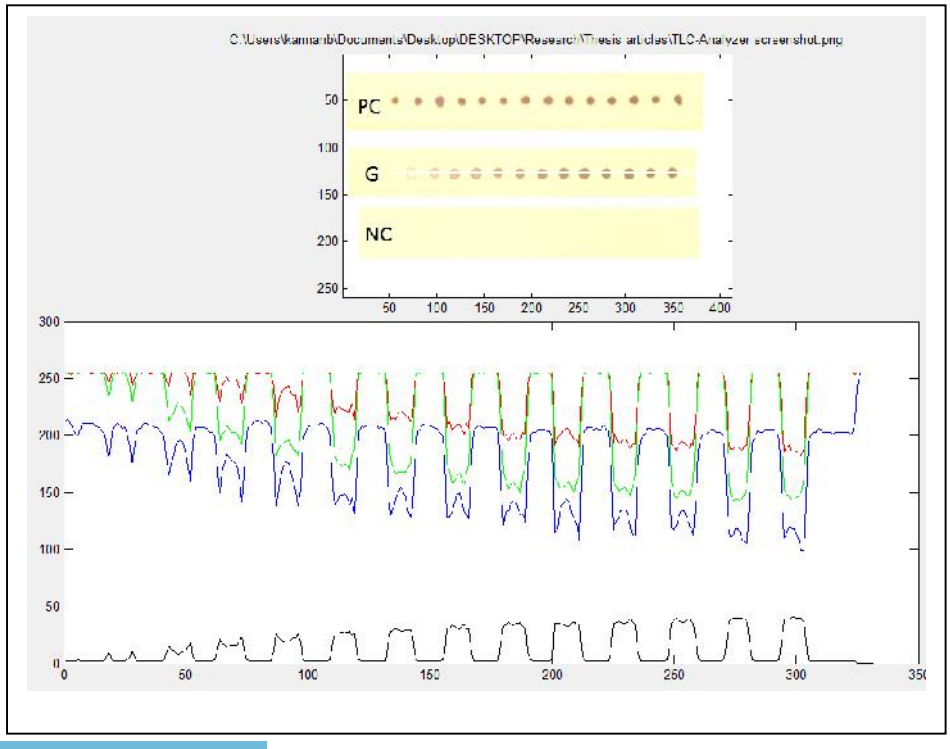

Figure 6.1B Screenshot of DETLC analyzer. The picture from Figure 6a is uploaded and ninhydrin spots across the gradient plate were scanned. Below are the four spectra (red, green, blue and b/w). The b/w spectra were used to make the gradient profile plots.

The shape of the gradient can easily be changed by changing the infusion rate and/or the concentration of the aminoalkoxysilane in the reacting solution. In this work, three different infusion rates were used to create gradient TLC plates having different slopes. Their profiles were confirmed using the ninhydrin method. Figure 6.2 shows spot intensity plots for the three gradient TLC plates, along with a positive and negative control. As the infusion rate increased from 400 mL/hour to 1000 mL/hr, the slope of the gradient profile decreased in the manner expected. In contrast to what was observed in Figure 6.1A, these gradients did not reach saturation. As shown in section 6.4.3 below, the ability to vary the steepness of the gradient becomes valuable when the need exists to optimize retention and improve resolution.

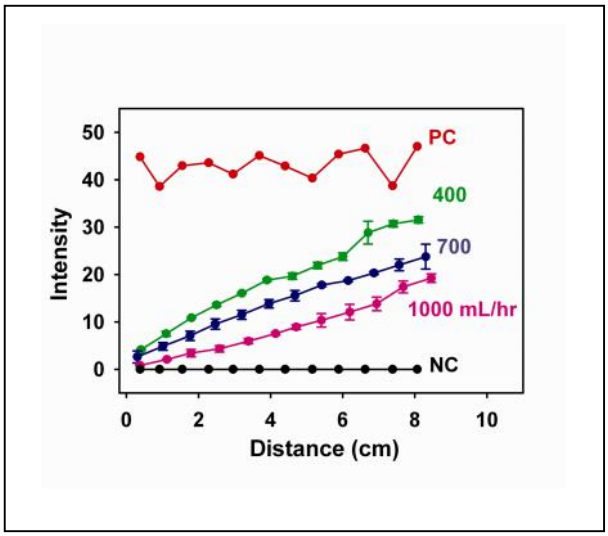

Figure 6.2 Plot of spot intensity after exposure to ninhydrin as a function of distance along the TLC plate for PC (red), NC (black), and gradient TLC plates. Gradient formation was accomplished using an infusion rate of 400 mL/hr (green), 700 mL/hr (blue), and 1000 mL/hr (pink). The error bars signify ±1σ. N = 3.

6.4.2 Separation of Weak Acids and Bases

A mixture containing four weak acids and bases (Benzoic acid (BA), 3-Aminobenzoic acid (ABA), 2-Aminopyridine (APy) and 4-Aminophenol (APh), (Scheme 6.1) was used for initial demonstration of stationary phase gradient separations. This mixture was prepared in methanol and spotted on an amine gradient TLC plate, a NC (regular silica TLC plate) and a PC (fully amine modified TLC plate). The gradient TLC plates were prepared using an 80 mL/hr infusion rate with a total time and volume of infusion of 17 min and 22.5 mL, respectively.

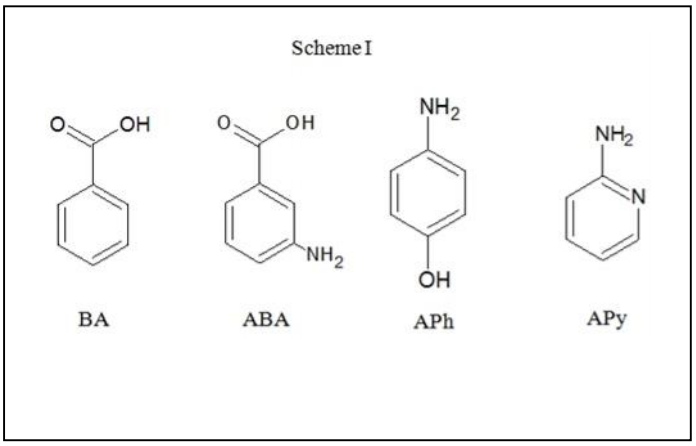

Scheme 6.1. Structures of acidic and basic compounds separated.

Gradient TLC plates were prepared in duplicate; on one plate, the sample was spotted on the low amine end; on the other, the plate was spotted on the high amine end. In the former, the analytes will experience a gradient in which the surface amine concentration gradually increases during the course of separation whereas in the latter, the analytes will encounter a gradient stationary phase where the amine concentration decreases. In case of NC and PC, analyte spotting location does not matter since both NC and PC are uniform across its length (Figure 6.3).

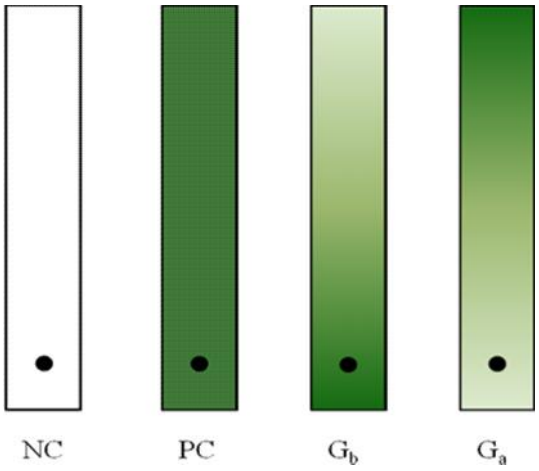

Figure 6.3. Spotting location on gradient and control plates. G_a is gradient where analyte mixture was spotted on low amine end and G_b is gradient in which analyte mixture was spotted on the high amine end.

The mobile phase used for each separation was methylene chloride:methanol:acetic acid (90:10:0.5). On each plate (NC, PC and gradient), the compounds to be separated were spotted in three separate lanes. The mixture of four compounds was spotted in one, while the pure compounds were spotted in pairs (BA and ABA, APy and APh) alongside the mixture in the other two lanes for identification purposes. Once developed, the TLC plate was dried under atmospheric conditions for 5 to 10 min before visualization under UV radiation (254 nm). Digital photographs taken of the TLC plates consisted of dark spots on a bright green background.

The image was scanned using the TLC Analyzer software,[114] which extracts the red, green and blue channels for color images. When plotted from the origin (where the mixture is spotted) to the solvent front, the green channel data provides a TLC chromatogram as all of the analytes quench the green fluorescence from the HP-TLC plates. The image of four plates (NC, PC, Gb

and Ga) under UV light (254 nm) are shown in Figure 6.4a in which the separation was performed in 3 separate lanes; In each of the plates, it can be observed that in the first lane, 2 basic compounds were eluted; the second lane shows the elution of two acidic compounds and third lane is of all four compounds. For clarity, in the remaining part of this chapter, only the chromatogram obtained from the mixture of all four compounds is shown in all cases.

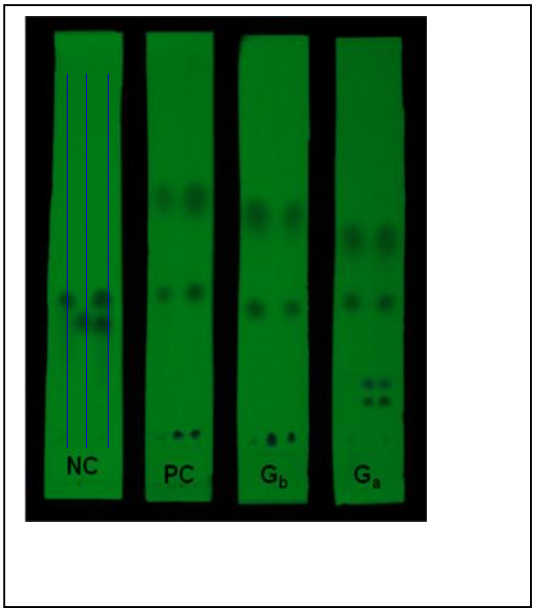

Figure 6.4A Image of four TLC plates (NC, PC, G_b and G_a) where the separation of two basic (lane 1), two acidic (lane 2) and all 4 component (lane 3) separation was performed under acidic mobile phase conditions. The blue lines in the NC plate indicated the three lanes. The picture was taken under UV light (254 nm).

Figure 6.4 B shows the screenshot from DETLC analyzer software when the scanning of gradient TLC plates was performed on the third lane where the mixture of all the four compounds was spotted and separated. The screenshot shows the image and the four chromatograms (red, green, blue and b/w) generated for the scan along the gradient Ga. For the

separation of four components in the gradient TLC plate, four peaks were clearly observed in the green chromatogram.

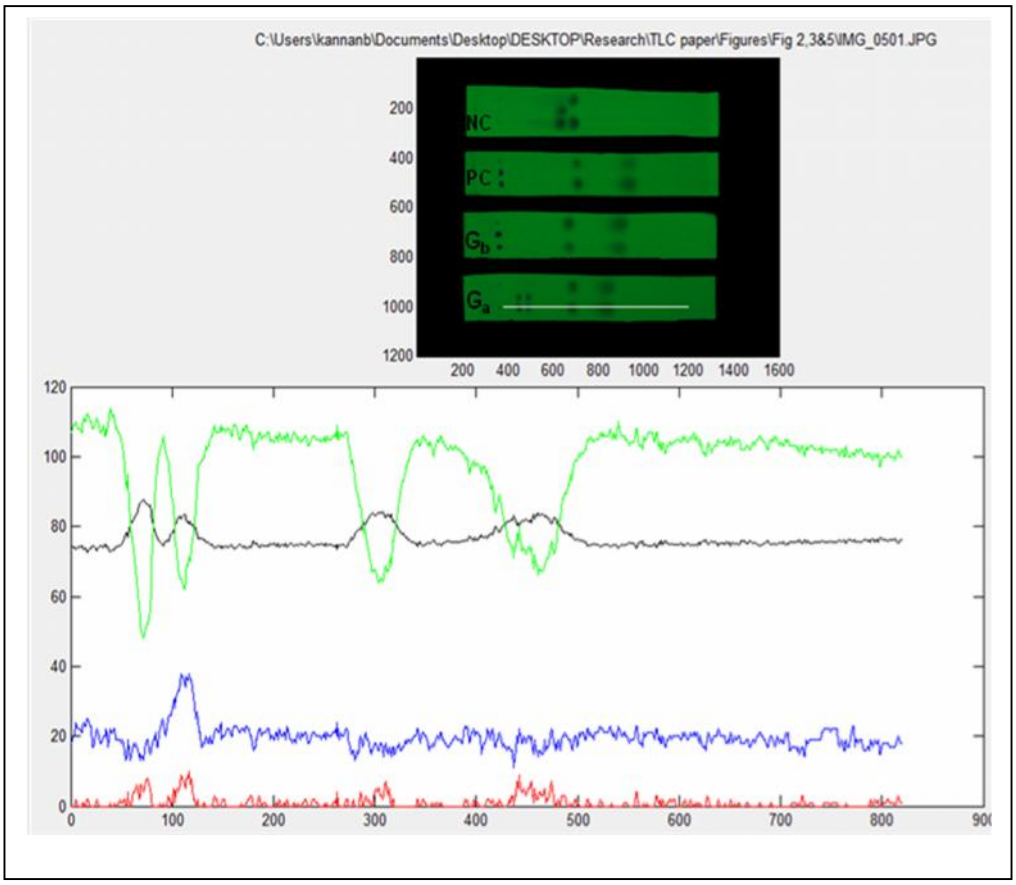

Figure 6.4B Screenshot from DETLC analyzer. The top of the figure is the image of TLC plates (NC, PC, G_b and G_a). Below are the red, blue, green and b/w chromatograms for the corresponding line scan in the Gradient (G_a) image where the separation of four compounds occurred.

Figure 6.5 shows the TLC chromatograms obtained from gradients and control plates; Table 6.1 reports retention factors (R_f) and resolution (R_s) between neighboring peaks. The latter was calculated using Eqn (6.1) where d is the center-to-center distance between spots and W is the base width of the spots measured from the densitometric scan. For the unresolved peaks, the full

width of the base of the overlapped peaks was used as $W_1 + W_2$ in this calculation. Plate counts were not calculated because of the uncertainties associated with the initial spot width.

$$R_s = \frac{d}{(W_1 + W_2)/2} \tag{6.1}$$

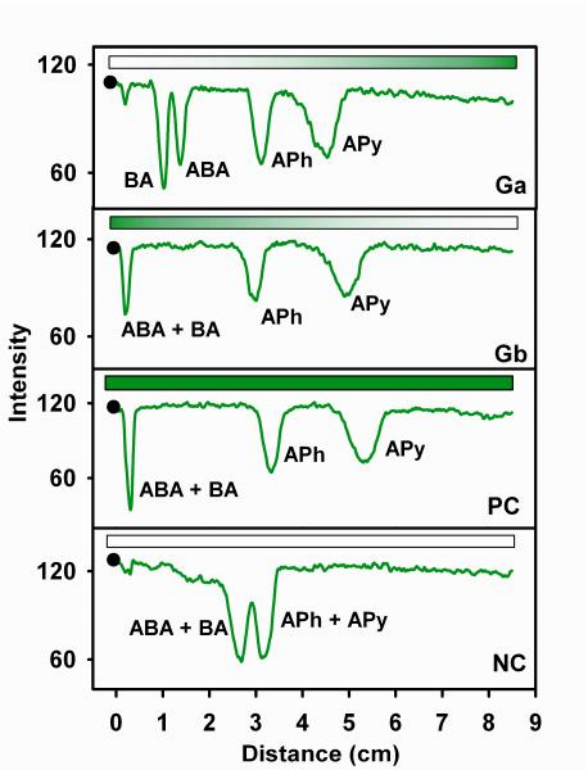

Figure 6.5 TLC chromatograms for the negative control (NC), positive control (PC), and the gradient TLC plates (Ga, Gb) where the mixture (benzoic acid (BA), 3-aminobenzoic acid (ABA), 2-aminopyridine (APy) and 4-aminophenol (APh)) was spotted on the high amine end (Gb) and the low amine end (Ga). The dots in each plot represent the point where the analyte mixture was spotted. Rectangular bars at the top of each plot represent the amine density (dark brown for high amine) along the length of the gradient. Mobile phase: Methylene chloride:methanol:acetic acid (90:10:0.5).

Table 6.1 Chromatographic parameters (retention factor (R_f) and resolution (R_s)) obtained for the TLC plates in Figure 6.5 (Acidic mobile phase). Benzoic acid (BA), 3-aminobenzoic acid (ABA), 2-aminopyridine (APy) and 4-aminophenol (APh) are the analytes.

	BA		ABA		APh		APy	
Stationary phase	R_f	R_s	R_f	R_s	R_f	R_s	R_f	R_s
NC	0.32	0.0	0.32	0.0	0.37	0.0	0.37	0.0
PC	0.04	0.0	0.04	0.0	0.39	2.3	0.62	2.3
Gradient (Gb)	0.02	0.0	0.02	0.0	0.35	2.4	0.58	2.4
Gradient (Ga)	0.16	1.1	0.12	1.1	0.36	1.7	0.53	1.7

Figures 6.5 Ga and Gb are the same gradients except in Figure 6.5 Ga, the analyte mixture was spotted on the low amine end whereas in Figure 6.5 Gb, it was spotted on the high amine end. Figures 6.5 PC and NC depict the separations on positive and negative control plates, respectively. On the NC plate under acidic mobile phase conditions, only two peaks were observed. Compounds with carboxylic acid groups (BA and ABA) moved but remained overlapped, as was also the case for APh and APy. Clearly, the use of an acidic mobile phase and an as-received normal phase TLC plate does not allow for the separation of this mixture with this mobile phase. On the uniformly amine modified TLC plate (Figure 6.5 PC), substances BA and ABA hardly moved from the origin because of the strong interaction between their carboxylic acid functional groups and the amine on the stationary phase. Again complete separation of the mixture of four compounds was not observed; only 3 peaks were observed.

Very different results were obtained on the gradient plates. As expected, the direction of the gradient significantly influenced the separation. When the samples were spotted on the low amine end of the gradient (Figure 6.5 Ga), all four substances moved appropriately ($0 < R_f < 1$)

and were resolved (Rs > 1). These data show that ABA and BA traveled further than they did on the PC because of the interactions with the stationary phase were lessened due to the lower concentration of the amine groups on the surface but less than they did on the NC because some amine was still present. APh was retained in a similar fashion on the different plates while APy was slightly less retained relative to the NC but slightly more relative to the PC. The low amine concentration at the beginning of the plate enables the first two compounds (BA, ABA) to separate (whereas they don't on a fully aminated surface, PC) while the gradually increasing amine allows the other two (APh, APy) to separate (whereas they don't on the silica only surface, NC). When the mixture is spotted on the high amine end, the separation looks similar to that observed on the positive control (Figure 6.5 Gb). ABA and BA, for example, are not resolved and hardly move from the origin (i.e., each has an R_f near 0) due to strong interactions with the stationary phase. The high density of amine groups at the origin obviously limits the distance the more acidic substances can travel and thus be able to be separated.

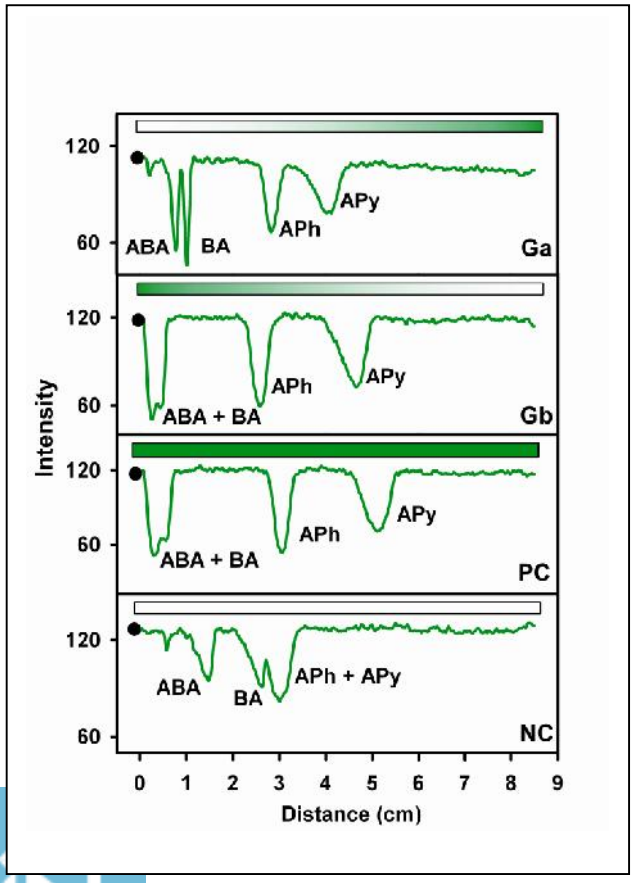

Figure 6.6. TLC chromatograms for the negative control (NC), positive control (PC), and gradient TLC plates (Ga, Gb) where the mixture (benzoic acid (BA), 3-aminobenzoic acid (ABA), 2-aminopyridine (APy) and 4-aminophenol (APh)) was spotted on the high amine end (Gb) and low amine end (Ga). The dots in each plot represent the point where the analyte mixture was spotted. Rectangular bars at the top of each plot represent the amine density (dark brown for high amine) along the length of the gradient. Mobile phase: Methylene chloride:methanol:triethylamine (90:10:0.5).

Table 6.2 Chromatographic parameters (retention factor (R_f) and resolution (R_s)) obtained for the TLC plates in Figure 6.6 (basic mobile phase). Benzoic acid (BA), 3-aminobenzoic acid (ABA), 2-aminopyridine (APy) and 4-aminophenol (APh) are the analytes.

	BA		ABA		APh		APy	
Stationary phase	R_f	R_s	R_f	R_s	R_f	R_s	R_f	R_s
NC	0.31	0.5	0.17	1.7	0.35	0.0	0.35	0.0
PC	0.07	0.6	0.03	0.6	0.36	2.6	0.60	2.6
Gradient (Gb)	0.05	0.5	0.03	0.5	0.30	2.6	0.55	2.6
Gradient (Ga)	0.12	1.0	0.09	1.0	0.33	1.6	0.47	1.6

The separation of a mixture containing weak acids and bases also is expected to depend on the pH of the mobile phase. To evaluate the separation of this mixture on the gradient TLC plates, using a more basic mobile phase, acetic acid was replaced by triethylamine in the mobile phase. Figure 6.6 shows chromatograms obtained for the separation of the same mixture under these new conditions. Table 6.2 provides R_f values for all the spots along with the resolution (R_s) between neighboring peaks. As can be seen, there are slight differences in the separation of the four compounds with a basic mobile phase. Most significantly, on the gradient plate (Ga), the elution order of BA and ABA changed from that observed under the acidic mobile phase. On the as-received silica TLC plate (Figure 6.6 NC), all four substances moved along the plate as

expected, but the weak acids (BA and ABA) were better separated under the basic mobile phase because of stronger interactions, whereas the weak bases (APh and APy) overlapped. On the uniformly modified plate (PC), the more basic substances, APh and APy, moved and separated while the weak acids remained close to the origin. Again, when a gradient stationary phase was employed, the direction of the gradient significantly influenced the separation. Upon spotting the mixture on the low amine end (Ga), all four compounds were well separated. Again, the low density of amine groups at the beginning of the plate enables the first two compounds (BA, ABA) to separate as the interactions between the carboxylic acid group on the analyte and the amine groups on the stationary phase are lessened relative to that taking place on the PC. When spotting on the high amine end (Gb), the separation resembled that observed on the PC with ABA and BA overlapping. Again, the strong interactions between the carboxylic groups on ABA and BA and the initially high density of amine groups at the origin limit their movement. Collectively, these experiments indicate that the gradient TLC plates are less sensitive to mobile phase pH relative to as-received normal phase TLC plates and, most importantly, they demonstrate that by altering the degree of interaction between the analyte and the stationary phase during the course of a separation (as is done using gradient elution) a working separation results.

To verify that gradient formation was the result of controlled-rate infusion and could not be accomplished by the simple wicking of the aminosilane modifier up the TLC plate, an additional control experiment was performed. In this experiment, the TLC plate was placed in the deposition chamber and the aminosilane solution was allowed to wick from bottom to top via capillary action alone (in contrast to infusion). The wicking time was similar to the infusion time (22 min vs 17 min). When the solvent front reached the top, the plate was removed, rinsed with

ethanol and dried. It was then spotted with the mixture described above and separation under the same mobile phase conditions proceeded. When visualized under UV radiation, the locations of the spots were very similar to those obtained on a regular, as-received, silica HP-TLC plate (NC). Indeed, when this control plate was spotted with ninhydrin, amine was only detected on the bottom of the plate where the plate was exposed to APTEOS solution. This result demonstrates that gradient formation in "controlled-rate infusion" relies upon transport of aminosilane to the TLC plate surface from bulk solution. The wicking method likely fails to produce a detectable gradient because the aminosilane is quickly depleted from the thin film transported up the plate by reaction with the silica surface.

6.4.3. Separation of Over-the-Counter Drugs

Applications of chromatographic separations for pharmaceutical preparations are very common and widely reported.[218-220] To demonstrate the usefulness of these gradient TLC plates in such applications, as well as to demonstrate the ability to control retention, over-the-counter tablets of three common drugs were separated: those that contain either acetaminophen (AC), doxylamine succinate (Dx), and diphenhydramine (Dp). Two of the three drugs are structurally similar to each other (Scheme 6.2). The drugs were extracted from tablets, separated on the gradient and control TLC plates and visualized with UV radiation, as described earlier.

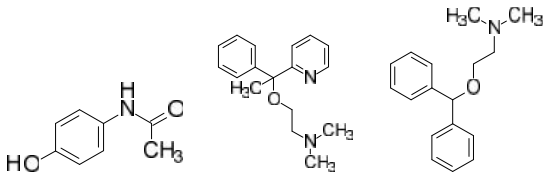

Ac **Dx** **Dp**

Scheme 6.2. Structures of over-the-counter drugs separated.

Once again, individual extract solutions were run alongside the 3-component mixture on the TLC plate. A representative image was shown in Figure 6.7 containing three gradient-TLC plates prepared at three different infusion rates (1000 mL/hr, 700 mL/hr and 400 mL/hr). Though each plate contains 3 different lanes for identification of individual component, only the data for the mixture is shown for clarity.

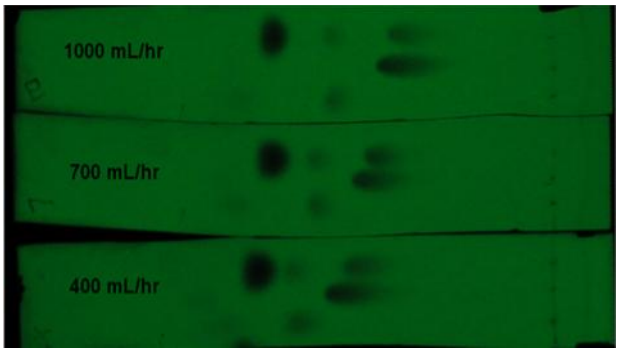

Figure 6.7. Image of gradient-TLC plates under UV light after the separation. Each plate has three lanes in which the two bottom lanes show elution of the individual components (Dx and Dp). Only the top lane on each plate shows the separation of all three drug compounds. Mobile phase: Ethyl acetate: methanol:water (7:7:1.5).

Figure 6.8 shows the TLC image of gradient prepared with three different infusion rates to form different profiles. In each plate, the top lane is the elution of all three components. Figure 6.8 shows the corresponding chromatograms depicting the separation of Dx, Dp and Ac on three gradient TLC plates and two control plates. Table 6.3 provides R_f values for all the spots along with the resolution (R_s) between neighboring peaks. On the as-received TLC plate (NC), Dx hardly moved from the point of spotting due to a strong interaction with the silica gel stationary phase relative to the mobile phase. Dp moves some distance, indicating it has greater affinity for the mobile phase relative to the stationary phase, while Ac, which has the greatest affinity for the mobile phase (on all the plates) and moves the most. While the R_s values are good, the R_f factor

for Dx is smaller than would normally be preferred. While resolution of all compounds is important, achieving proper retention factors is also important.

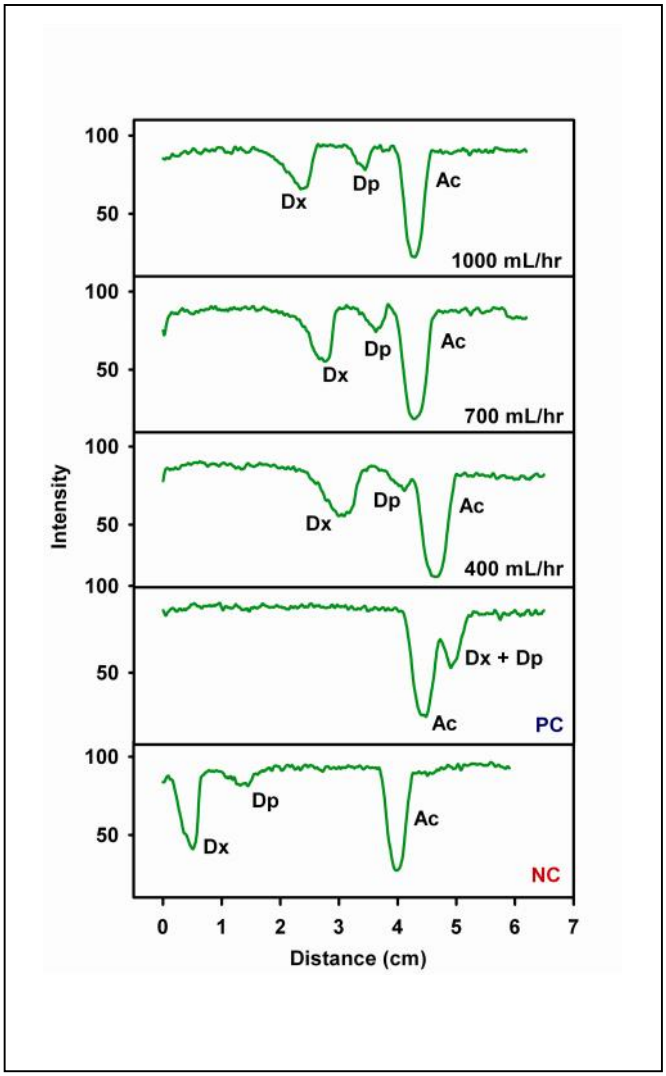

Figure 6.8. TLC chromatograms for the separation of doxylamine succinate (Dx), diphenhydramine hydrochloride (Dp) and acetaminophen (Ac) on a negative control (NC), a positive control (PC) and three gradient TLC plates formed using infusion rates of 1000 mL/hr, 700 mL/hr, and 400 mL/hr. The samples were spotted on the high amine end (at 0). Mobile phase: Ethyl acetate: methanol:water (7:7:1.5).

Satationary phase	Dx		Dp		Ac	
	R_f	R_s	R_f	R_s	R_f	R_s
NC	0.09	1.3	0.25	1.3	0.67	3.5
PC	0.76	0.0	0.76	0.0	0.69	0.7
400 mL/hr	0.46	1.5	0.63	0.9	0.71	0.9
700 mL/hr	0.44	1.4	0.59	1.2	0.69	1.2
1000 mL/hr	0.38	1.6	0.56	1.5	0.69	1.5

Table 6.3 Chromatographic parameters (retention factor (R_f) and resolution (R_s)) obtained for the TLC plates in Figure 6.8 (Drug mixture). Doxylaminesuccinate (Dx), diphenhydramine (Dp), acetaminophen (Ac) are the analytes.

The R_f factor for Dx (and Dp) can be changed via the addition of amine groups to the surface of the stationary phases, while Ac retention remains relatively unaffected. The addition of the amine groups on the stationary phase decreases the degree at which Dx and Dp interact with the SiOH stationary phase. When the TLC plate was uniformly modified with amine groups such that the surface was saturated or nearly-saturated, the R_f factors for Dx and Dp increased significantly and nearly overlapped with Ac (Figure 6.8). In this case, all three compounds are spending too much time in the mobile phase and are not being sufficiently retained on the stationary phase. The key to the separation of this mixture is to have some amine groups in the stationary phase, but not too many. It can be seen in Figure 6.8 (and Table 6.3), that the individual R_f and R_s values for Dx and Dp, in particular, strongly depend on the slope of the gradient profile. The separation of Dx, Dp and Ac improved as the rate of infusion increased from 400 mL/hr (total infusion time = 4 min) to a significantly faster infusion rate of 1000 mL/hr (total infusion time = 1.35 min). The best separation defined in terms of **both** retention factor and resolution for this drug sample was obtained on the TLC plates that incorporated a very

shallow gradient. Thus, the significance of gradient steepness on separation was illustrated by simple over-the-counter drug mixture.

6.4.4. Preparation of other bonded-phase gradients

As mentioned earlier, CRI was also used to prepare gradients in other bonded phases such as phenyl and cyano groups. In Figure 6.9, a phenyl gradient (G), negative (NC) and positive control (PC) plates are shown under UV light (254 nm). The NC plate shows only the green fluorescence, as it does not contain any phenyl groups and the PC plate shows uniform quenching as it is uniformly modified with phenyl groups.

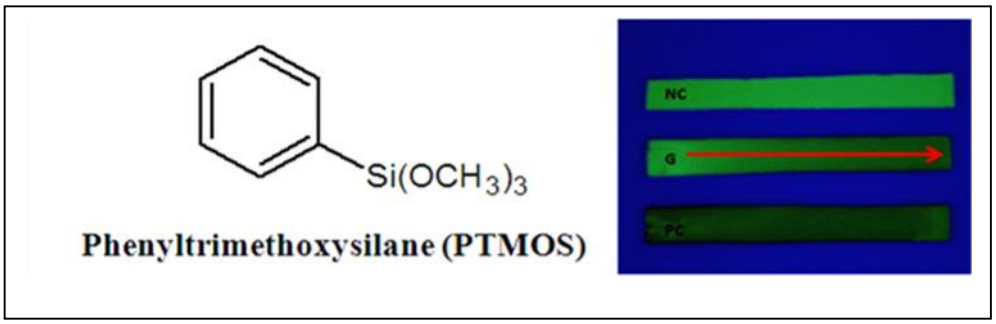

Figure 6.9. Phenyltrimethoxysilane (PTMOS) structure and TLC plates modified with PTMOS. Gradient (G) prepared by CRI using a solution containing PTMOS to form gradient that visualized under UV light (254 nm). Control plates are also shown for comparison (NC & PC). The red arrow on the gradient shows the direction of increasing intensity of quenching due to the presence of phenyl gradient.

In the gradient plate, the quenching gradually increases from low phenyl to high phenyl end, which confirms the presence of a gradient in phenyl group density along the TLC plate. A gradient in CN was also made using a similar procedure and characterized using FTIR microscope (reflectance mode). Figure 6.10 shows a representative FTIR spectra of a CNTEOS modified TLC plate acquired with a 150 µm aperture averaged with 300 scans. In this case, the

background was collected from a regular silica plate. Other than the CN stretch at 2250 cm^{-1} and the CH stretch at 2950 cm^{-1}, no significant peaks can be ascertained from the spectrum. The FT-IR spectra scans were run with automatic atmospheric correction to avoid atmospheric water and CO_2 peaks correction. A magnified view of the CN region of the spectrum along the length of the gradient and a PC can be seen in Figure 6.11.

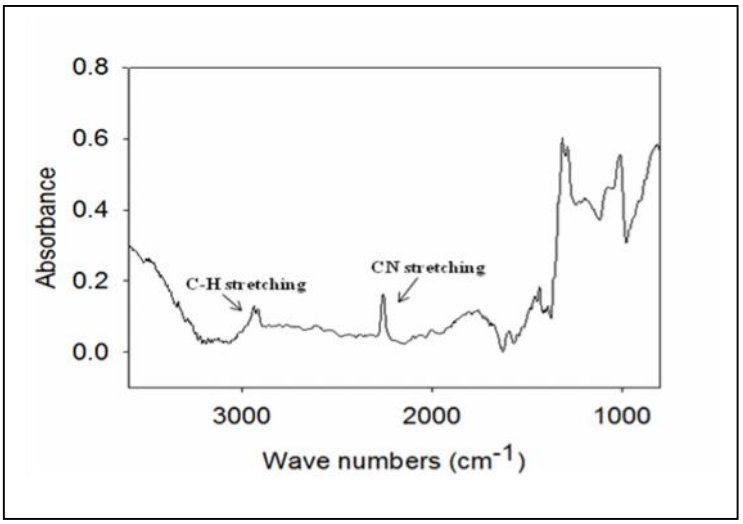

Figure 6.10. Representative FT-IR spectra CN-TEOS modified TLC plates. A regular silica TLC plate was used as the background.

As can be seen in Figure 6.11, the intensity of the 2250 cm^{-1} peak (CN stretch) stays approximately the same along the uniformly modified plate (Figure 6.11) but increases from top to bottom for the gradient plates. The arrow indicates the direction of the gradient from low and high cyano end. To better see the gradient, the area near the CN stretch was magnified.

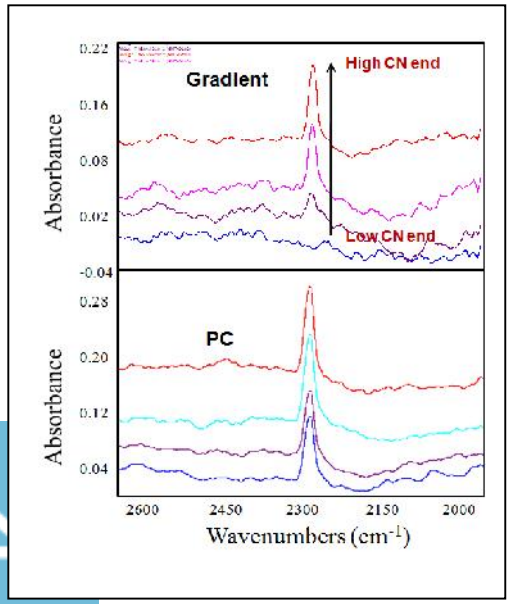

Figure 6.11. FT-IR spectra of gradient (G) and uniformly modified (PC) cyano plates. The CN gradient was prepared by CRI using a solution of CNTEOS. The arrow in the gradient spectra indicates the direction of the gradient from low to high cyano end.

6.5 Summary

A simple, straight-forward, and inexpensive approach for the preparation of continuous stationary-phase gradients for chemical separations has been described and its applicability to the separation of mixtures demonstrated. Controlled-rate infusion was used to prepare amine gradients on HP-TLC plates and the shape of these gradients was established via the use of the color reagent, ninhydrin. The separation of a mixture of four aromatic weak acids and bases was clearly improved on a gradient TLC plate relative to either an as-received, normal phase silica gel plate or a fully-coated amine modified plate. By spotting the mixture on the low amine end of the plate, all four compounds could be resolved, under the solvent system chosen for development. None of the other TLC plates tested resolved all four compounds. To further explore the advantages of this approach, a mixture of three simple over-the-counter drugs was separated on gradient TLC plates made using high infusion rates. Again, for the solvent system chosen, separation was better on the gradient plates compared to control plates. In contrast to the separation of the mixture of acidic/basic aromatic compounds that worked best with a steep gradient, separation of this mixture of drugs proved to be the best on plates with shallow gradients. This gradient preparation approach is not just limited to prepare amine stationary phase gradients. It can also be used to prepare phenyl and cyano bonded phase gradients. These phases were characterized by a direct visualization method and FITR spectroscopic method, respectively.

7. Fabrication of Surface Charge Density Gradients on Open-tubular Capillary and its Characterization by Pulsed Streaming/Zeta Potential Measurements

7.1. Abstract

One of the most important potential applications of capillary gradients is in capillary iso-electric focusing (CIEF) where the separation of proteins is accomplished on a pH gradient in a capillary under the influence of applied potential.[221] From the advent of CIEF, numerous researchers have been working on gradient capillaries for electrophoretic and electrochromatographic separations. Later, applications of such gradient capillaries were widened for the separation of small molecules as well. In this work, a simple and rapid method is reported for the preparation of continuous amine gradients on a silica capillary using controlled-rate infusion (CRI). Since the amine groups exhibit a positive charge on the capillary surface, zeta potential measurements along the gradient surface were used to visualize the gradient profiles. The zeta potential values were obtained via streaming potential measurements on the capillaries using 2 mM NaCl as electrolyte. Also, a change in the gradient steepness was visualized through the zeta potential measurements along the gradient. X-ray photoelectron spectroscopy was used to confirm that the presence of nitrogen groups on the surface. Surface charge density gradients on silica capillaries induced by aminopropyl groups will be highly useful for open-tubular capillary chromatographic separation of mixtures with a range of pI values such as peptides/proteins and also in small molecule separations with a wide range of pKa values.

7.2. Introduction

7.2.1 Types of capillary column

There are two main types of capillary columns for capillary chromatography: packed and open tubular. Packed columns are the capillaries filled with particulate materials typically silica and silica based bonded-phase particles. Open tubular columns are the capillaries in which the inner wall is coated with the stationary phase such as an octadecylsilica (ODS) moiety. Another sub-class of capillary columns is monolith columns. These columns have shown unique advantages over packed columns, such as high permeability and separation efficiency, etc., and are considered as new generation stationary phases.[222-224] There have been tremendous developments in the field of capillary chromatographic stationary phases in the past two decades and few of the prominent developments have been covered in these reviews.[224-226] Both packed and open tubular (OT) columns have been equally applied for the separation of proteins and small molecule separations. However, the preparation of OT columns is simple and straight-forward when compared to packed columns. Thus, this work is based on open tubular column format.

7.2.2 Surface coating on open-tubular capillary column

Surface coatings on open tubular capillaries have been prepared in several different ways.[226, 227] Direct chemical bonding, sol-gel derived coating and molecular imprinted polymer coating are the few notable methods used to prepare stationary phases for capillary electrophoresis and chromatography.[226] Sol-gel derived coatings are promising because of the wide variety of organosilanes that are available. The silanes used for these coatings form stable bonds and

exhibit strong analyte-stationary phase interactions allowing for better separation. Although sol-gel technology for the preparation of capillary stationary phases was introduced in the late 1980s,[228-230] Colon and coworkers in 1995 simplified the sol-gel based coating procedure for OT capillary column.[196] Further development have been made by Malik and other researchers to produce useful bonded phases such as octyl (C_8),[231] tertiary ammonium bonded phase,[232, 233] stearyl,[234] and other bonded phases.[235] Recently, Lu et al[236] prepared chitosan-grafted-(β-cyclodextrin) stationary phases using sol-gel techniques and these columns showed better stability and separation of structural isomers. Similar to sol-gel based techniques, molecular imprinted polymer (MIP) techniques have been widely used for capillary stationary phase fabrication especially for chiral separations.[237-240] Direct chemical bonding on an etched capillary surface was introduced by Jorgenson et al in 1983 and then later developed by other research groups.[241, 242] Recently, chemically bonded reactive silanes such as aminosilanes on fused silica capillaries have been used directly as a stationary phase[243] and as well as derivatized with gold nanoparticles[244] and graphene oxide.[245-247]

In this work, the focus is on the formation of a **continuous gradient stationary phase** on an open tubular capillary using a direct chemical bonding method that takes advantage of the fast reactivity of aminoalkoxysilane on hydroxylated silica surfaces. A surface chemical gradient on an open tubular capillary is prepared for the first time and the length scale of the gradient shown here is about 40 cm and it can be extended up to 100 cm as well. This is the maximum length scale achieved for continuous gradients on a capillary so far.

7.2.3 Gradients on capillary column

There are mainly two different types of capillary gradients that have been reported so far:

i) pH gradients on capillaries.

ii) Polymer/monolith based gradient capillary column.

pH gradients in capillary columns have become very popular for iso-electric focusing where peptides and proteins are separated based on their isoelectric point (pI).[221, 248] A recent review by Koshel et al. discusses the development of capillary iso-electric focusing (CIEF) in detail.[249] These gradients are actually gradients in pH. Yang et al. immobilized carrier ampholytes (CAs) based on their isoelectric point (pI) through gluteraldehyde links on a monolith capillary columns which carries epoxy linkages. Carrier ampholytes are mixture containing various comopounds used to form a gradient in isoelectric point (pI). Proteins with a wide range of pIs are separated using the above pH gradient.[250] Similarly ampholine, one type of carrier ampholyte was immobilized on polyacrylamide based monolith column, as reported by Zhu and coworkers.[251] This column was reported to have high mechanical and chemical stability. Separation of a complex protein mixture from rat lung cancer cells was described using this column.

Other than isoelectric focusing (IEF) of proteins and peptides, gradients on capillary columns have been prepared for small molecules separations as well. Copolymerization of different composition of monomers to form a monolith gradient inside the capillary has been accomplished using thermal and photo polymerization. Thermal polymerization of various compositions of monomers by sequential filling produced a polymer monolith hydrophobicity gradient. The separation of alkylbenzene derivatives was shown to prove the separation efficiency of the gradients.[252] Similarly, photo-initiated polymerization was used by Pucci et al.[253] and Currivan et al.[99] for the preparation of stationary phase gradients on silica capillaries. This was achieved by using a moving shutter and neutral density filter to control the irradiation

time and UV light intensity respectively. Except for the photo-grafting method, all the above methods can only produce only discontinuous gradients. This is mainly because of the fabrication method which involves filling the polymerization reaction mixture of different concentration to a specified length and polymerizing it. Gradients in capillary columns was also reported quite recently by varying the ratio of acidic and basic monomers in a polymerization reaction.[254] In this work, the mixture of monomers with increasing pH values were filled in the previously amine-modified capillary and thermally polymerized to form pH gradient. The separation of egg white proteins was demonstrated on this open-tubular pH gradient. This is also considered to be a discontinuous gradient.

In the present work, CRI was used to form continuous amine gradients on silica capillaries and were visualized using streaming potential measurements. Also, the gradient profile has been strategically varied using this approach. The application of such open tubular capillary gradients is to act as continuous stationary phase gradients for open tubular capillary electrochromatography (OTCEC). Gradients in OTCEC column will open a new dimension to the OTCEC separation because of the following reasons,

i) Gradients in aminopropyl groups can act as a charge density gradient for applications such as protein separation and also act as an effective chromatographic bonded phase for small molecule separation when the analytes interact with the gradient. Separations involving such gradients will trigger new interests in the field of separation.

ii) Since the amine group is reactive, it is always possible to covalently react with it and form various other gradient bonded-phases, such as proteins, and even to attach nanoparticles for separation purposes.

Since this work involves the fabrication of stationary phase supports for OTCEC, the following section provides a brief introduction.

7.2.4. Open tubular capillary electochromatography (OTCEC)

OTCEC is a separation technique using a micro open tubular column that combines the attributes of HPLC and capillary electrophoresis. OTCEC is one of the modes of operation of CE where the solute interacts with the stationary phase based on its electrophoretic mobility.[255] In OTCEC, the mobile phase movement is not pressure-driven but driven by the electroosmotic flow (EOF). The applied electric field produces EOF, which has a flat-plug like flow profile. This flat flow profile rather than a parabolic flow profile (Figure 7.1) lessens the band-broadening and gives highly efficient peak separation.

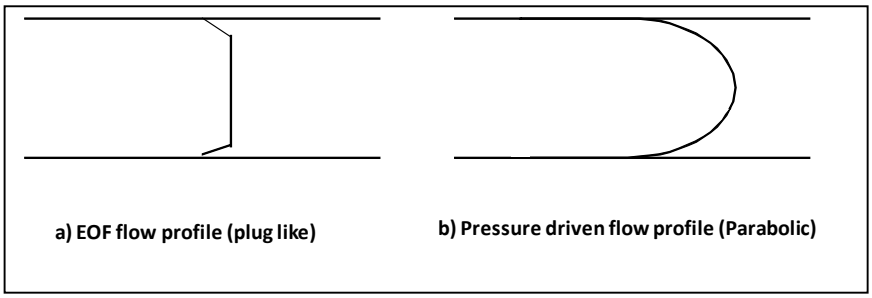

Figure 7.1. a) EOF and b) Pressure driven flow profiles

Other than that, CEC has a few other advantages like rapid analysis times, low sample volumes, low cost etc. For the past decade, OTCEC has found numerous applications in the separation of a wide variety of compounds ranging from simple acidic-basic mixtures[256] to complex protein separations.[226, 255, 257] Immobilized nanoparticles on silica capillaries for OTCEC have also become popular for the separation of a range of compounds from polymeric

hydrocarbons to peptides.[226, 258-260] Preparation of stationary phase is the main step involved in OTCEC for reproducible results. The sol-gel process is one of the simplest and most reproducible preparation methods for OTCEC columns. Colon and coworkers first introduced organosilanes for the preparation procedure. These workers incorporated octadecyl groups in the glass film covalently attached to the inner walls of a silica capillary.[196] Later, the same group and a few other researchers were successful in preparing such organic-inorganic hybrid capillary column for OTCEC.[261-263]

7.2.5. Gradient characterization on capillary column

The characterization of a chemical gradient on the surface of a capillary plays an equally important role in gradient fabrication, especially for open-tubular and packed capillary columns. Scanning electron microscopy is one method that has been to visualize gradient capillaries.[250, 251, 254] Pucci et al used electron probe microanalysis to measure the sulfur content in a gradient monolith along the capillaries to evaluate the gradient in sulfonic acid groups.[253] A unique characterization was reported by Currivan and coworkers called capacitively coupled contactless conductivity detection.[99] The conductivity responses along the gradient capillaries were used to visualize the gradient profiles of capillary columns.

Characterization of gradient capillary columns is quite different than that of uniformly coated capillaries because in gradient columns the whole gradient length needs to be studied whereas representative segments can be visualized in the uniformly coated capillaries. Also, chemical and functional gradients formed on micro-sized cylindrical surfaces are difficult to visualize, unlike those on planar surfaces such as silicon wafers, glass substrates, TLC plates, etc. The amount of silane that is deposited on the surface of the capillaries is relatively low

compared to other types of surface gradients because the capillaries have small internal diameters. The length of the gradient in a capillary is 5 to 10 times larger than on a planar substrate, which is typically 10 cm. The above factors preclude the use of conventional techniques such as X-ray photoelectron spectroscopy (XPS) and contact angle measurements for the characterization of chemical gradients on capillaries.

In this work, the CRI approach was used to prepare a gradient in surface amine density on the surface of a silica capillary that is 40 cm in length. Aminopropyl groups on surfaces will exhibit a positive charge in acidic and neutral environments, and hence zeta potential measurements along the capillary can be used to visualize the gradient profiles. Zeta potential can be measured through one of the electrokinetic effects namely electrophoresis, electroosmosis and streaming potential. Measurement of streaming potential has been used to determine the zeta potential on various surfaces such as microfluidic system,[264] membranes,[265] disk-shaped surface,[266] etc. Alvarez et al. have developed a system for the measurement of pulsed streaming potentials and have used it for the label-free detection of model analytes,[267] to study adsorption kinetics of proteins on polymer surfaces[123] and, more importantly for the determination zeta potential on charged surfaces.[268] We have utilized the same pulsed-streaming potential system for the determination of the zeta potential along the length of the gradient in aminopropyl groups. The theory of streaming zeta potential measurements for the characterization of surface chemical gradients was discussed in Chapter 2.

7.3 Experimental Section

7.3.1 Gradient preparation

Aminopropyltriethoxysilane (APTEOS) was purchased from Acros Organics (99%), ethanol from Pharmaco Aaper (200 proof absolute anhydrous) and potassium hydroxide from Fisher Chemicals (97%). Fused silica capillaries (75 µm ID, 375 µm OD, Polymicro Technologies) were cut to a length of 40 cm and activated by infusing fresh 1 M KOH through them at 5 µL/min for 40 minutes. After that, the capillary end was reversed and the KOH infusion continued for an additional 40 minutes. The capillary was then washed with deionized water using an infusion rate of 30 µL/min from both the ends of the capillary for 1.5 hours each. Once washing was over, the capillary was connected to a GC oven held at 150º C under flowing nitrogen (20 cc/min) for 48 hours. Before gradient preparation, the capillary volume was calculated by $\pi r^2 l$ where r is the radius of the capillary and l is the length. For a 40 cm capillary, the volume is 3.14 x 0.0375^2 mm^2 x 400 mm = 1.77 µL. Then the infusion rate was calculated based on the desired steepness of the gradient. The activated silica capillary was connected through a high pressure union (IDEX P-720) to 5 µL syringe containing the freshly prepared APTEOS solution with a given ratio of ethanol : silane: water. Typically the ratio is 1 : 0.05 : 0.005 and the infusion volume is ~2 µL. After infusion, the capillary was immediately flushed with ethanol for 5 minutes by infusing at 50 µL/min infusion rate from the low amine end before it was dried by pushing air through it. To measure the streaming potential along the length of the gradient, the capillary was cut in such a way that 1.2 cm pieces were obtained at equal interval (4 cm) as shown in figure 7.2

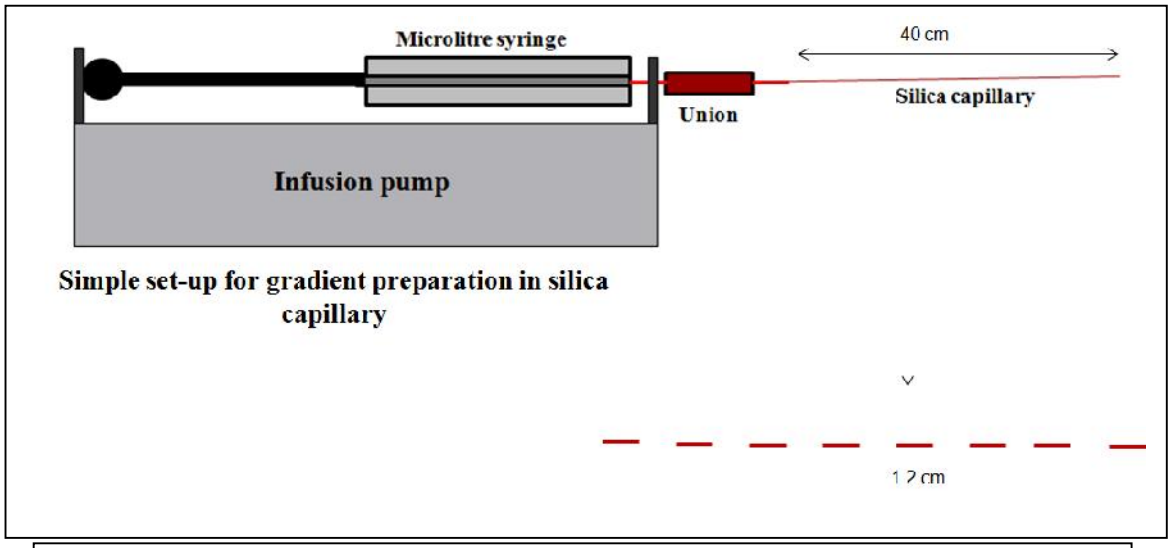

Figure 7.2. Infusion set-up for the gradient preparation on silica capillary by a CRI method. After gradient preparation, the capillary was cut into 1.2 cm segments and characterized via streaming potential measurements.

7.3.2. Measurement of Streaming Potential.

In initial experiments, a micro-channel type fabrication method was first developed to measure the streaming potential of small segments of the 40 cm. In this set-up, the ~1.5 cm capillary segment was sandwiched between two 4 x 2 cm cyclic olefin copolymer (COC) plates (Figure 7.3). Two holes on each polymer plate were drilled as shown in the figure. The streaming potential measurements were performed on the sandwiched plates using phosphate buffers ranging between pH 3 to 10. The amine gradient was supposed to give a gradient in isoelectric point (pI) when it is plotted along the gradient length. However, this set up did not give reproducible results and the pipette tip approach described below was developed as. The failure of the polymer sealed capillary (micro-chip) might be due to partial electrolyte flow outside the capillary. Moreover, fabrication of such chips was laborious when compared to the method that is currently being used (Figure 7.4).

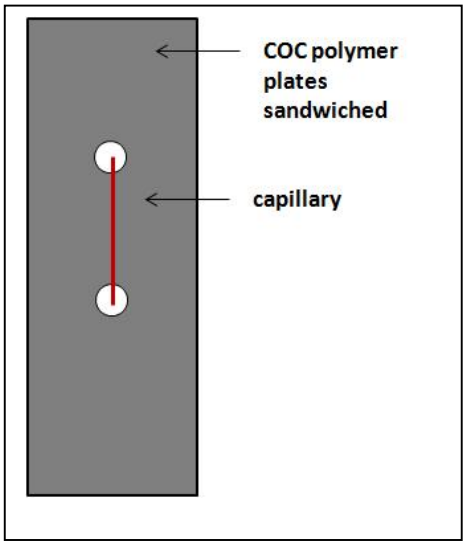

Figure 7.3. Schematic shows the micro-chip made with a 1.5 cm modified silica capillary

To measure the streaming and zeta potentials in a small section of the capillary (~1.2 cm segments were cut using an Agilent capillary cutter); the following procedure was performed immediately after the small section was cut. The capillary was sealed to the narrow end of a microlitre pipette tip (20 – 200 µL, VWR) as shown in Figure 7.4A using a hot-glue gun. Once it was confirmed that there was no leak in the seal, the sealed capillary was used for streaming potential measurements. A schematic of the streaming potential measurement set-up is shown in Figure (Inset in figure 7.4A).

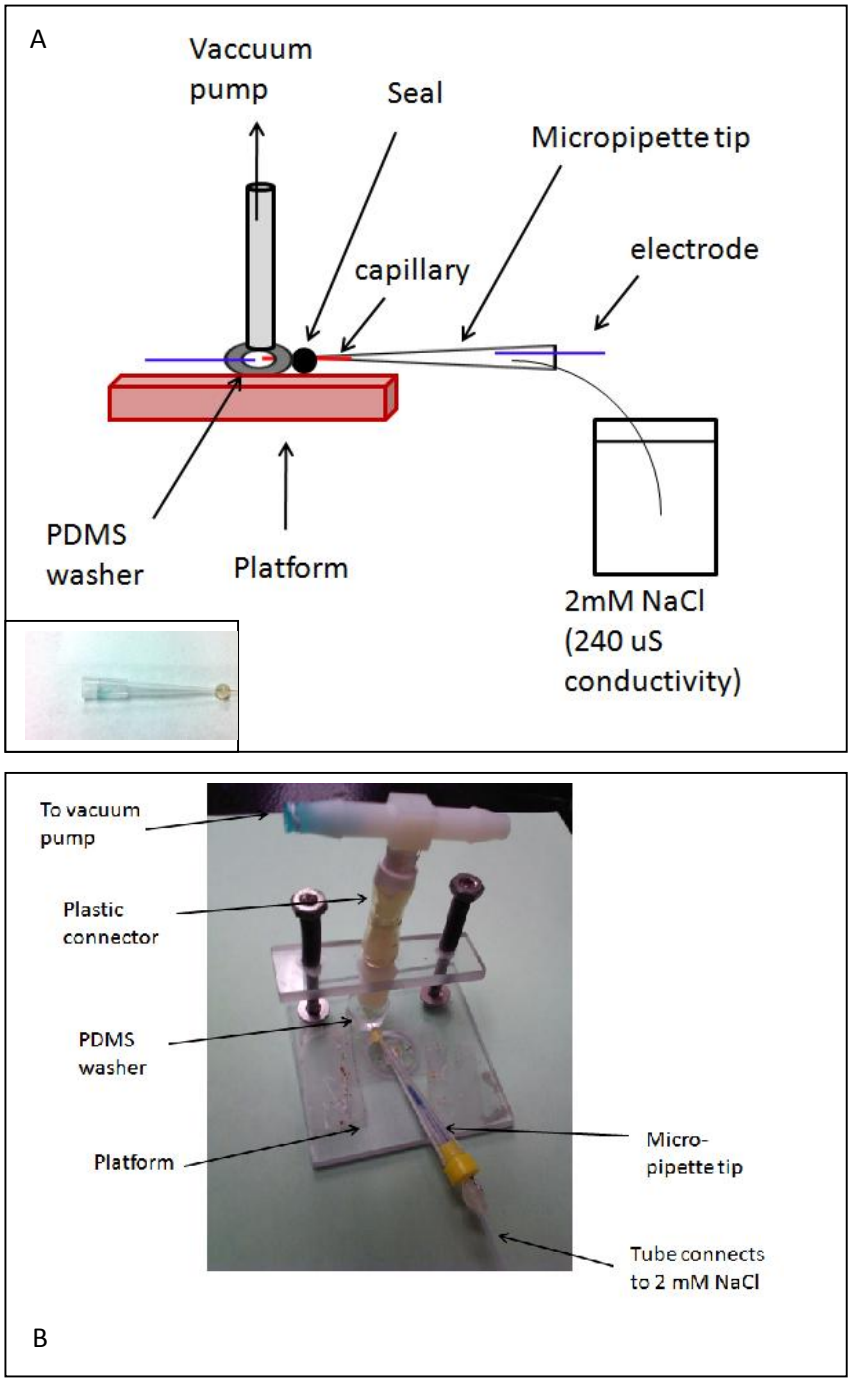

Figure 7.4. (A) Schematic for streaming potential measurements on surface amine gradient on capillary. Inset: Photograph of a capillary sealed to a micropipette tip with glue. **(B)**. Photograph of streaming potential measurement set-up.

The outer end of the capillary from the tip was carefully inserted into a circular (doughnut shaped) PDMS washer (0.5 cm ID, 1.5 cm OD), which was prepared by mixing the PDMS

elastomer and curing agent in the ratio of 10:1 and baked at 100° C for 45 minutes. A thin platinum wire electrode of length 1.5 cm and diameter of 0.5 mm was also inserted into the PDMS washer. On the other end of the micropipette tip (wider end), a platinum wire (electrode) and plastic tubing (1 mm ID, 15 cm length) was connected to withdraw the 2 mM NaCl solution placed in a beaker. The pipette set-up was placed on a platform as shown above, and the hole in PDMS washer was covered tightly with a plastic connector, which was connected to the vacuum pump as shown in the Figure 7.4B. A pulsed pressure (1 sec on and 1 sec off) was created for each cycle using the vacuum pump, and Labview software was used to measure the potential difference during the pulse as described previously.[267] Streaming potential and zeta potential values from each segment of the capillary were obtained from an average of five cycles (about 10 sec) per run using Labview software. The streaming potential value from the five cycles is averaged and converted into zeta potential using the viscosity of the solvent (η), the pressure applied (P), the conductivity of the electrolyte (λ). The detail of this conversion is discussed extensively in Section 2.5.

7.4 Results and Discussion

A surface charge density gradient on a 75 μm id open-tubular silica capillary was fabricated by adopting a previously reported organoalkoxysilane based approach called controlled-rate infusion (CRI). In this method, an aminosilane solution is gradually infused into a capillary at a controlled rate where it reacts with surface bound Si-OH groups in a time-controlled fashion. Gradient formation largely depends on the rate of infusion and the concentration of the aminosilane in solution. The challenges associated with making a gradient on a 75 μm diameter capillary column are (1) the small volumes needed and (2) characterizing and quantifying the

density of amine groups along a 40 cm length, and (3) the uniform generation of surface silanols along 40 to 50 cm capillary length. For example, the capillary volume was calculated for a 40 cm capillary and was found to be < 2 µL. Infusing such a low volume at a controlled rate for a calculated amount of time is challenging. A small leak at any point of infusion will lead to large errors.

The two important breakthroughs in this research are the formation of a continuous gradient in charged groups on the surface of a 75 µm id open-tubular capillary using a straight-forward approach, and the unique characterization method of the gradient profile along the length of the capillary. Although streaming potential and zeta potential measurements have been used for the evaluation of amine functionalities on glass substrates,[151] silica particles[269] and silica capillaries,[122] they have not been explored so far to characterize functionally graded surfaces.

In this work, an amine gradient was first prepared using a solution containing ethanol, APTEOS, and water at a volume ratio of 20: 0.5: 0.005, respectively. Given an infusion rate of 0.1 µL/min, it took about 17 minutes to form the gradient. Once the gradient preparation was complete, the modified capillary was characterized by plotting zeta potential versus distance along the length of the capillary. Along with the gradient, a negative control capillary (NC) and a positive control capillary (PC) were prepared and the zeta potentials were plotted as a function of distance along the length of the 40 cm capillary.

Streaming potential measurements were made using the pulsed method described by the Alavarez group.[267] Figure 7.5 depicts a representative streaming potential plot of five pressure pulses obtained on one segment of an amine modified capillary using 2 mM NaCl as the electrolyte. The upward peak direction (i.e., positive streaming potential) indicates that the surface under investigation contains predominantly positive charges. The height of the peak

measures the streaming potential value. It is converted into zeta potential using the Smoluchowsky equation as explained in Chapter 2 using the following variables i) η is the viscosity of the solution in Pascals- second (Pa-s), ii) λ is the conductivity of the solution in Siemens per meter (S/m), iii) **ε** is the dielectric constant of water,, iv) $\boldsymbol{\varepsilon_0}$ is dielectric permittivity of vacuum, v) ΔE is streaming potential in volts and vi) P is pressure in Pa. Lab view software calculates the average zeta potential of five cycles with the standard deviation.

where $\eta = 0.936 \times 10^{-3}$ Pa.s

$\varepsilon_r = 79$

$\varepsilon_0 = 8.85 \times 10^{-12}$ F/m

$\lambda = 0.024 \pm 0.001$ S/m (exact value was measured each time using conductivity meter)

$P = 65 \times (1.333 \times 10^3)$ Pa

ΔE = Streaming potential in V

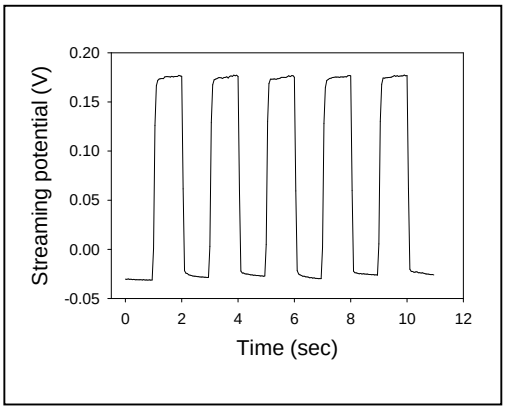

Figure 7.5. Representative streaming potential plot of a single run (five cycles) of a 1.2 cm amine modified capillary section.

Figure 7.6A shows the streaming potential plots for the control (NC and PC) and the gradient capillaries. As mentioned earlier, each run consists of 5 cycles (pressure pulses) and the plot shown here is the overlay of 10 capillary segments along the control capillaries (each 4 cm apart). As can be clearly observed from this figure, the streaming potential values are negative for an activated silica capillary, since it contains mostly deprotonated silanol groups that are responsible for the negative value. The PC exhibits a positive streaming and zeta potential because of the positively charged amine groups. In the gradient capillary, the streaming potential varies from a low to high streaming potential values as a function of distance and the streaming potential values for the control capillaries are almost same (< 10% variation) indicating the capillaries are uniformly modified. For the gradient capillary, however, the positive zeta potential value gradually increases from a lower to higher value for the capillary segments of low amine end to the high amine end (Figure 7.6B). This clearly shows that the gradual variation in positive surface charge density along the capillary as expected for a gradient surface.

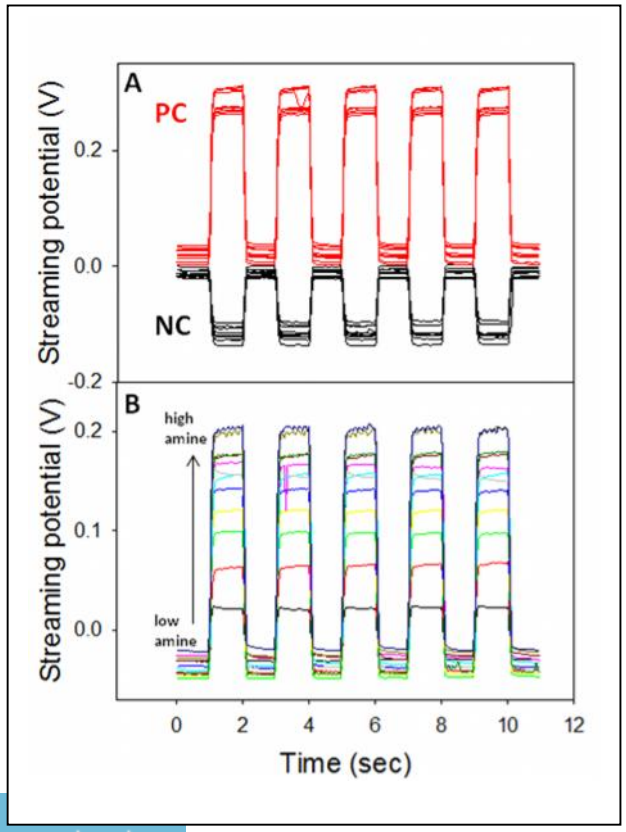

Figure 7.6. Streaming potential plots (five cycles per run) along the control capillaries (A) and a surface charge gradient capillary (B).

Figure 7.7 shows a plot of the average zeta potential vs distance along the length of the capillary for the gradient and control samples (NC and PC) (~ 40 cm). Labview averages the streaming potential from the five pulses. A total of three runs for each 1.2 cm segment of capillary was obtained. The error bars shown at each position in each profile is ± 1 standard deviation of three measurements (N = 3). This zeta potential profile plot on the negative control and positive control samples clearly show that the surface is uniform along the capillary as expected (Figure 7.7A). The negative zeta potential on silica capillary is due to the deprotonated silanol groups while the positive value on uniformly coated amine capillary is due to protonated amine groups. On the other hand, the gradient capillary prepared by CRI approach using ethanol : aminosilane : water ratio of 20 : 1 : 0.1 exhibits a gradual variation of positive zeta potential and positive charge density on the surface (Figure 7.6B). The infusion rate of silane solution for this gradient preparation was 0.1 µL/min and total infusion time was ~ 17 minutes (Gradient 1).

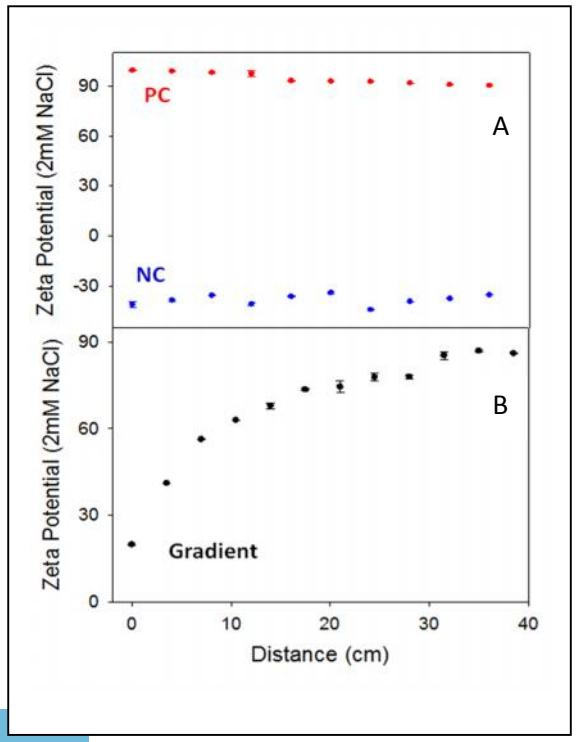

Figure 7.7. Zeta potential profile plot on the negative (NC) and positive (PC) control capillaries (A) and a gradient capillary (B). Error bar at each position is ±1 standard deviation of three measurements (N=3).

The gradient profile on the capillary is similar to the shape of the amine gradient prepared on a TLC plate by the same CRI method.[74] Specifically, the surface amine density steeply increases and then reaches almost saturation at the middle of the gradient profile. The shape or profile of a surface chemical gradient is very important as previously described in Chapters 3, 4 and 6. In fact, one of the important attributes of CRI is the preparation of gradients with strategically controlled gradient steepness by simply changing the rate of infusion or by changing the concentration of aminosilane in the solution.[74] In chromatography, this provides a means to control retention time and selectivity factors.[14] To validate the ability of CRI to prepare gradients with different slopes on a capillary column, amine gradients have been prepared with two other conditions. One with the same aminosilane concentration (Gradient 2) but at double the infusion rate (0.2 µL/min) and another gradient by varying both the concentration and infusion rate (20 : 0.5 ethanol : silane ratio; program infusion rate of 0.1 µL/min for 0.8 µL and 0.4 µL/min for the remaining 0.8 µL. The latter (Gradient 3) is expected to give two gradient profiles with different steepness. Gradient 2 was repeated on a different day and the zeta potential values from the two measurements (Gradient 2A and Gradient 2B) are plotted along the distance (Figure 7.8A). The variation in zeta potential values between the two measurements might be due to the slight variation in capillary position for measuremnts. Also the gradient within the 1.2 cm segments was not taken for consideration and the zeta potential value corresponds to total charge in the 1.2 cm segment. This could also affect the reproducibility of the measurements. Figure 7.8B shows the profile plot (zeta potential versus distance) of the all the above discussed gradients.

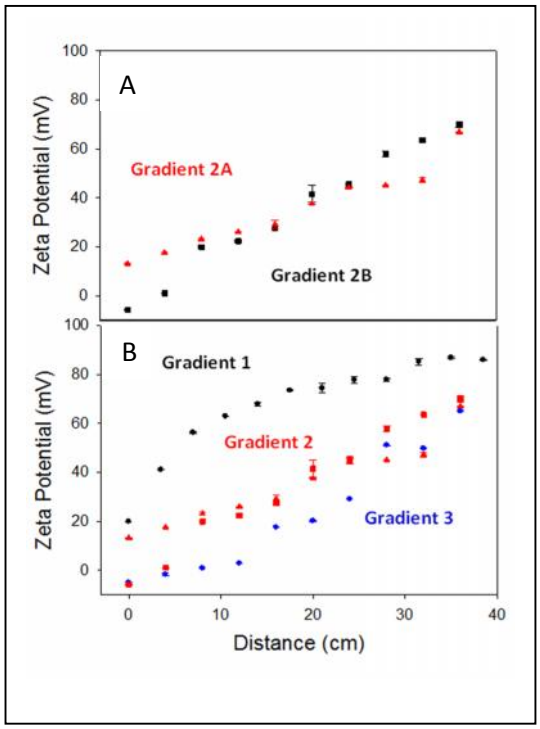

Figure 7.8. (A) Zeta potential profile plot of surface charge density gradients (Gradient 2) prepared on two different days. (B) Zeta potential profile plot of surface charge density gradients prepared under three different conditions (Gradient 1, Gradient 2 and Gradient 3) as described in the text.

As expected, the zeta potential profile of gradient 2 and gradient 3 in Figure 7.8 B shows a shallower slope for the faster infusion rate. In the case of Gradient 3, the slope of the gradient profile changes mid-way down the capillary as a result of the infusion rate increasing by a factor of four from 0.1 µL/min to 0.4 µL/min. For the first 18 cm of the capillary, corresponding to the top of the gradient, the zeta potential profile is very shallow as infusion was complete in ~2 minutes and the aminosilane had little time to react with the surface silanol groups. Near the bottom the gradient, corresponding to the remaining 18 cm, the slope of the gradient is steeper because the aminosilane had more time to react. This result is consistent with our previous work on aminosilane gradients on planar substrates (e.g., a silicon wafer)[74] where a change in the infusion rate changes gradient steepness. In the previous work, XPS was used to characterize the

gradient profile; in this work, it was a new method (zeta potential). This is a good sign that zeta potential measurements properly describe the gradient shape/profile.

To further confirm the presence of nitrogen on the inner surface of the capillary, an XPS experiment was undertaken. In this experiment, a larger (500 µm inner diameter, 700 µm outer diamter) capillary of 10 cm length was taken as the substrate and an amine gradient was formed on the inner capillary walls in a similar fashion with that of 75 µm ID capillary using ethanol : silane : water 20 : 1 : 0.1. After gradient formation, the 10 cm length capillary was then cut in to ~ 1.5 cm pieces. For each segment, the capillary was manually opened in such a way that the inner wall of the capillary was exposed to the X-ray beam for analysis (Figure 7.9). The opened capillaries were placed on the sample holder containing conducting tape and it was loaded into the preparation chamber of XPS instrument for pump down. In the first instance, an X-ray beam size of size of 200 µm was used because of the smaller inner diameter of the capillary. Because N1s signal was not observed, the beam size was changed to 500 µm. Since it was difficult to focus on the inner wall of these opened capillaries, only the low amine end and high amine end was scanned and the N 1s area compared to that obtained on a negative control, activated glass capillary (NC) of the same dimensions.

Figure 7.9. Optical image of a capillary segment which is opened to expose the inner wall of the capillary to the X-ray beam in the XPS spectrometer.

Figure 7.10 shows a comparison of N1s spectra obtained at the top of the capillary, bottom of the capillary and on a negative control. As can be seen, the intensity of the N 1s peak at the high amine end of the gradient was significantly larger than that obtained on the low amine end, which in turn shows a slightly larger N 1s peak than the NC. The N1s peak area of high amine end is 5683 CPS eV and the low amine end is 1620 CPS eV. The small trace of N1s peak on the negative control that does not have an amine coating is due to the adventitious nitrogen as reported in our previous studies.[74, 182] The N 1s peaks shown in the figure consist of two peaks from 399 – 402 eV. The higher binding energy peaks is due to the protonated amine groups and the intensity of the protonated amine peak is largely depend upon the sample treatment such as exposing it to humid or acidic environment. In this case, the protonated is slightly high because the sample has been exposed to atmosphere during sample preparation for XPS analysis. Overall, the presence of surface amine groups on the open-tubular capillary column is evident based on the above results in XPS analysis results.

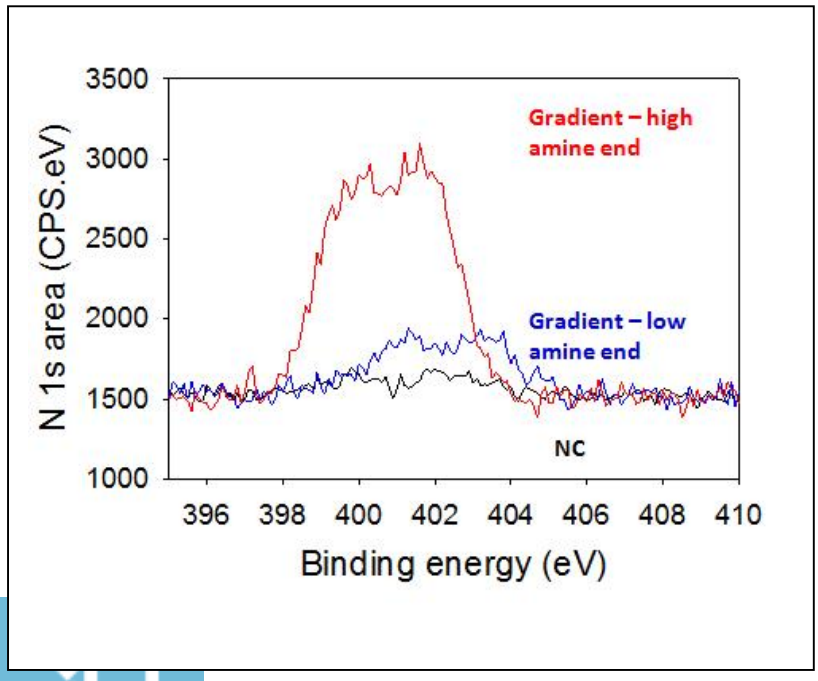

Figure 7.10. N 1s spectra obtained at the top and bottom of the gradient capillary and on a negative control.

7.5 Summary

Continuous gradients on the surface of open-tubular silica capillaries have not been explored extensively as compared to gradients on packed or monolith capillaries. This is probably due to the lack of techniques that are capable of preparing continuous gradient capillary columns with reproducible gradient profiles. The controlled-rate infusion (CRI) approach is well-established for preparing surface chemical gradients on substrates such as modified silicon wafers and planar chromatographic stationary phases. In this work, this approach was extended to prepare continuous surface amine gradients on the inner walls of fused silica capillaries. The main advantage of CRI approach is its straight-forward chemistry and experimental procedure, which allow for gradient fabrication on substrates of various shapes and dimensions. This widens the research areas in which the surface chemical gradients can be applied. Another important attribute of CRI is its control over the gradient profile, which was previously demonstrated on planar substrates. In this work, it is clearly evident that the gradient profile control in CRI is not limited to planar substrates but can be made in capillaries as well. A unique surface charge density gradient characterization method was developed by measuring streaming/zeta potential along the length of the gradient. This method can be modified and used for the characterization of surface charge density gradients on other substrates such as micro-channels and membranes. This research has opened up a simple and rapid way of preparing gradient films for open-tubular capillary chromatographic separation of complex protein/peptide mixtures and also small molecule mixtures that whose components vary in polarity and pKa.

Chapter 8. Conclusion and Future work

8.1 Conclusion.

An elegant and reliable method was developed for the fabrication of surface chemical gradients using organoalkoxysilanes. The controlled-rate infusion (CRI) approach described extensively in this work mainly utilizes the reactivity of these silanes, which can be controlled by the concentration, amount and type of catalyst and the amount of water in the silane solution. Among the various organoalkoxysilanes commercially available, aminoalkoxysilanes have an advantage of self-catalyzing the reaction with surface silanol groups through the basic amine moiety. This research mainly concentrates on surface amine gradients, although the CRI approach is capable of preparing gradients with other chemical functionalities such as nitrile, phenyl and thiol groups. It is mainly because of its relatively fast reactivity and the widespread application of amine modified surfaces to various fields in analytical and inorganic chemistry that we have focused almost exclusively on amine gradients. CRI is extremely straight forward in terms of its experimental design and also the chemistry involved. The CRI approach was first evaluated on homogenous siloxane films spin cast on silicon wafers to form surface amine gradients, and the gradient steepness was systematically varied by controlling the infusion rate and concentration of silane. X-ray photoelectron spectroscopy (XPS) was used to characterize the variation in amine group density along the length of the film by plotting the N1s area as a function of distance from top to bottom of the substrate. Using a simple kinetic model based on the first-order reaction kinetics of aminosilane with surface silanols, theoretical gradient profiles were generated and the results were in concordant with the experimentally obtained profiles. A new dimension to the gradient applications was shown by studying the reactivity of various

substituted aminoalkoxysilanes including secondary, tertiary, and di- and tri-substituted amines. This was accomplished by comparing the slope of the gradient profile since it is related to the precursor's reactivity. Also, the surface amine basicity of all the substituted amines were reported by evaluating the ratio of the protonated and free amine groups on the surface. The application of CRI to evaluate the reactivity of precursors itself is novel.

Fabrication of continuous gradients on stationary phases usually requires a sophisticated set-up and a complex procedure. But CRI is capable of preparing continuous gradient stationary phases for chromatographic separation in a simple one step procedure. As planar chromatographic surfaces are relatively simple and inexpensive to work with, amine gradients were first prepared on silica TLC plates. The gradient plates showed better separation for the chosen acidic/basic component mixture. The significance of gradient steepness in controlling retention was shown using an over-the-counter drug mixture. Metal amine complex formation through chelation was studied on ligand density gradients prepared with ethylenediamine and diethylenetriamine ligands. Such chelation gradients will be useful in separation science and to study the chelation ability of metal ions on gradually varying ligand concentration.

The most remarkable benefit of CRI is that it is not limited to one particular type of substrate such as rectangular planar surface but can be adapted to other geometries. As shown in this work, CRI can be used to form a surface chemical gradient in a fused silica capillary. This type of gradient can be used as a stationary phase for capillary electrophoresis and capillary electrochromatography. Continuous gradients on open tubular capillaries were prepared for the first time on a length scale of about 40 cm, the longest controllable gradient surface reported to

date. The advent of the CRI approach proves the ability of a single method to form gradients on various substrates applied to different fields of science.

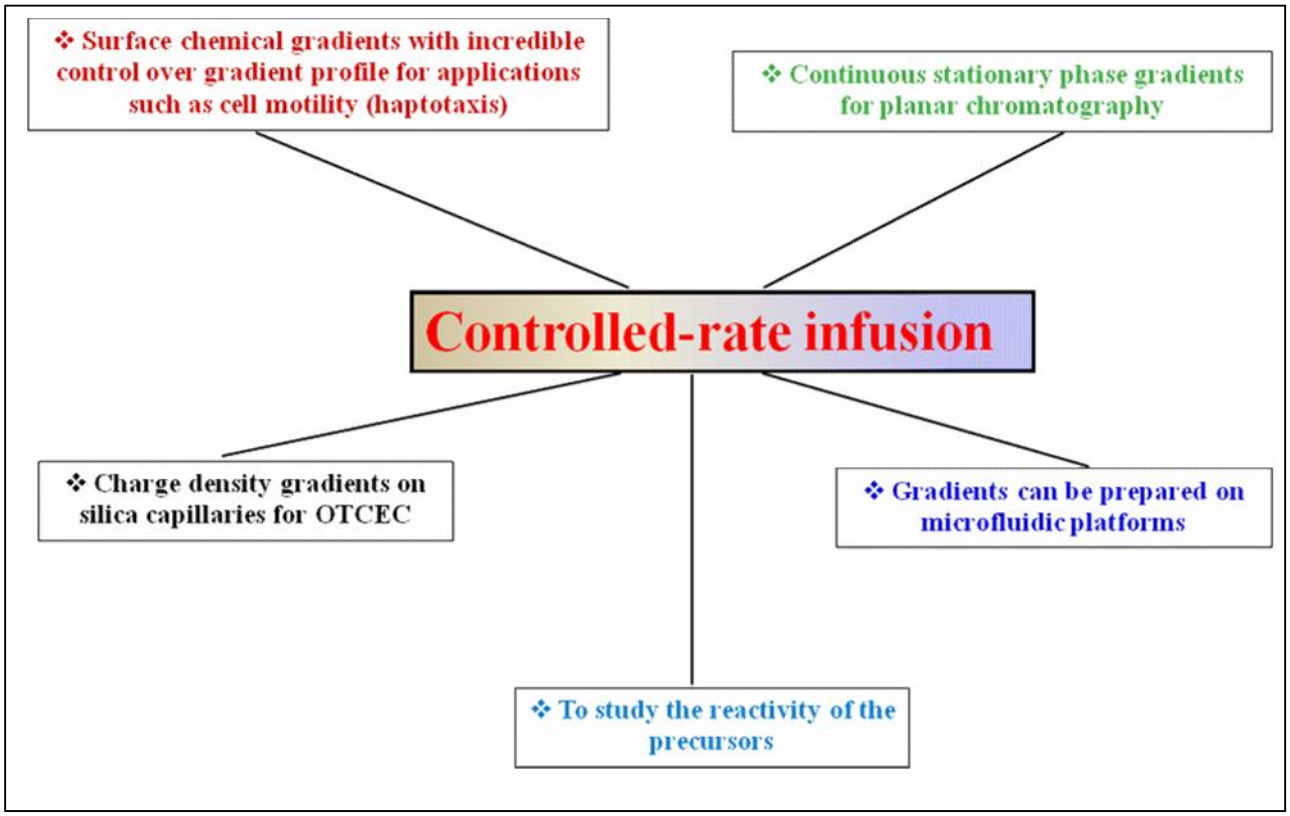

Figure 8.1. Versatility of the controlled-rate infusion (CRI) approach.

8.2 Future work.

8.2.1 Dual bonded-phase gradient stationary phase.

Gradient stationary phase prepared with one silane precursor can be further taken for another infusion with a different precursor to form dual bonded-phase gradients. For example, gradients can be prepared from 3-aminopropyltriethoxysilane (APTEOS) and phenyltrimethoxysilane (PTMOS) to form amine and phenyl gradients together on a single stationary phase support. In

this dual-bonded phase gradient stationary phase, two variations are possible: the amine and phenyl gradients can be in the same direction; the amine and phenyl gradients can be in opposite directions. The presence and shape of the gradients can be characterized via ninhydrin (amine) and the quenching of UV radiation at 254 nm (phenyl). The next step would be to evaluate how the gradient HP-TLC plates are able to separate a mixture of compounds which require both bonded-phase variations. Separation of a mixture of water and fat soluble vitamins using this two -component gradient is currently in progress.

8.2.1 Gradient on high pressure packed column.

Continuous gradient stationary phases on high performance liquid chromatography (HPLC) column can be prepared using this approach. The challenging part would be infusing the silane through a packed column of < 10 μm silica gel particles, which will require a high-pressure pump similar to a HPLC pump. Gradient profile control may also be limited since there is an upper limit for such pumps (~ 400 bars). As a result, preparing a very shallow gradient using fast infusion rates may not be possible. Because of the high surface area of the silica gel powder, a high concentrations of silane would likely be required. Infusion of such a high concentration of silane would then require careful washing as the high-pressure pump can easily get blocked because of solid particles formed from concentrated silane solution. Nevertheless, continuous gradients prepared by this approach will be highly useful for separation of complex mixtures and also in high-throughput method development by determining the choice stationary phase for a particular mixture in one trial.

References

1. Genzer, J., Surface-Bound Gradients for Studies of Soft Materials Behavior. In *Annual Review of Materials Research, Vol 42*, Clarke, D. R., Ed. Annual Reviews: Palo Alto, 2012; Vol. 42, pp 435-468.
2. Genzer, J.; Bhat, R. R., Surface-bound soft matter gradients. *Langmuir* **2008,** *24* (6), 2294-2317.
3. Kunzler, T. P.; Drobek, T.; Schuler, M.; Spencer, N. D., Systematic study of osteoblast and fibroblast response to roughness by means of surface-morphology gradients. *Biomaterials* **2007,** *28* (13), 2175-2182.
4. Kunzler, T. P.; Huwiler, C.; Drobek, T.; Voros, J.; Spencer, N. D., Systematic study of osteoblast response to nanotopography by means of nanoparticle-density gradients. *Biomaterials* **2007,** *28* (33), 5000-5006.
5. Pelham, R. J.; Wang, Y. L., Cell locomotion and focal adhesions are regulated by substrate flexibility (vol 94, pg 13661, 1997). *Proceedings of the National Academy of Sciences. U. S. A.* **1998,** *95* (20), 12070-12070.
6. Morgenthaler, S.; Zink, C.; Spencer, N. D., Surface-chemical and -morphological gradients. *Soft Matter* **2008,** *4* (3), 419-434.
7. Chaudhury, M. K.; Whitesides, G. M., How to make water run uphill. *Science* **1992,** *256* (5063), 1539-1541.
8. Petrie, R. J.; Bailey, T.; Gorman, C. B.; Genzer, J., Fast directed motion of "Fakir" droplets. *Langmuir* **2004,** *20* (23), 9893-9896.
9. Moumen, N.; Subramanian, R. S.; McLaughlin, J. B., Experiments on the motion of drops on a horizontal solid surface due to a wettability gradient. *Langmuir* **2006,** *22* (6), 2682-2690.
10. Shastry, A.; Case, M. J.; Bohringer, K. F., Directing droplets using microstructured surfaces. *Langmuir* **2006,** *22* (14), 6161-6167.
11. Lai, Y. H.; Yang, J. T.; Shieh, D. B., A microchip fabricated with a vapor-diffusion self-assembled-monolayer method to transport droplets across superhydrophobic to hydrophilic surfaces. *Lab on a Chip* **2010,** *10* (4), 499-504.
12. Seidi, A.; Ramalingam, M.; Elloumi-Hannachi, I.; Ostrovidov, S.; Khademhosseini, A., Gradient biomaterials for soft-to-hard interface tissue engineering. *Acta Biomaterialia* **2011,** *7* (4), 1441-1451.
13. Venkataraman, N. V.; Zurcher, S.; Spencer, N. D., Order and composition of methyl-carboxyl and methyl-hydroxyl surface-chemical gradients. *Langmuir* **2006,** *22* (9), 4184-4189.
14. Kannan, B.; Marin, M. A.; Shrestha, K.; Higgins, D. A.; Collinson, M. M., Continuous stationary phase gradients for planar chromatographic media. *Journal of Chromatography A* **2011,** *1218* (52), 9406-9413.
15. Welin-Klintstrom, S.; Lestelius, M.; Liedberg, B.; Tengvall, P., Comparison between wettability gradients made on gold and on Si/SiO2 substrates. *Colloids and Surfaces B-Biointerfaces* **1999,** *15* (1), 81-87.
16. Gunawan, R. C.; Silvestre, J.; Gaskins, H. R.; Kenis, P. J. A.; Leckband, D. E., Cell migration and polarity on microfabricated gradients of extracellular matrix proteins. *Langmuir* **2006,** *22* (9), 4250-4258.
17. Larsson, A.; Liedberg, B., Poly(ethylene glycol) gradient for biochip development. *Langmuir* **2007,** *23* (22), 11319-11325.
18. Park, S. H.; Krull, U., A spatially resolved nucleic acid biochip based on a gradient of density of immobilized probe oligonucleotide. *Analytica Chimica Acta* **2006,** *564* (2), 133-140.
19. DiBenedetto, S. A.; Facchetti, A.; Ratner, M. A.; Marks, T. J., Molecular Self-Assembled Monolayers and Multilayers for Organic and Unconventional Inorganic Thin-Film Transistor Applications. *Advanced Materials* **2009,** *21* (14-15), 1407-1433.

20. Ulman, A., Formation and structure of self-assembled monolayers. *Chemical Reviews* **1996,** *96* (4), 1533-1554.
21. Liedberg, B.; Wirde, M.; Tao, Y. T.; Tengvall, P.; Gelius, U., Molecular gradients of omega-substituted alkanethiols on gold studied by X-ray photoelectron spectroscopy. *Langmuir* **1997,** *13* (20), 5329-5334.
22. Morgenthaler, S.; Lee, S. W.; Zurcher, S.; Spencer, N. D., A simple, reproducible approach to the preparation of surface-chemical gradients. *Langmuir* **2003,** *19* (25), 10459-10462.
23. Morgenthaler, S. M.; Lee, S.; Spencer, N. D., Submicrometer structure of surface-chemical gradients prepared by a two-step immersion method. *Langmuir* **2006,** *22* (6), 2706-2711.
24. Terrill, R. H.; Balss, K. M.; Zhang, Y. M.; Bohn, P. W., Dynamic monolayer gradients: Active spatiotemporal control of alkanethiol coatings on thin gold films. *Journal of the American Chemical Society* **2000,** *122* (5), 988-989.
25. Plummer, S. T.; Bohn, P. W., Spatial dispersion in electrochemically generated surface composition gradients visualized with covalently bound fluorescent nanospheres. *Langmuir* **2002,** *18* (10), 4142-4149.
26. Plummer, S. T.; Wang, Q.; Bohn, P. W.; Stockton, R.; Schwartz, M. A., Electrochemically derived gradients of the extracellular matrix protein fibronectin on gold. *Langmuir* **2003,** *19* (18), 7528-7536.
27. Smith, J. T.; Tomfohr, J. K.; Wells, M. C.; Beebe, T. P.; Kepler, T. B.; Reichert, W. M., Measurement of cell migration on surface-bound fibronectin gradients. *Langmuir* **2004,** *20* (19), 8279-8286.
28. Elwing, H.; Askendal, A.; Lundstrom, I., Desorption of fibrinogen and gamma-globulin from solid-surfaces induced by a nonionic detergent. *Journal of Colloid and Interface Science* **1989,** *128* (1), 296-300.
29. Elwing, H.; Welin, S.; Askendahl, A.; Lundstrom, I., Adsorption of fibrinogen as a measure of the distribution of methyl-groups on silicon surfaces. *Journal of Colloid and Interface Science* **1988,** *123* (1), 306-308.
30. Elwing, H.; Welin, S.; Askendal, A.; Nilsson, U.; Lundstrom, I., A wettability gradient-method for studies of macromolecular interactions at the liquid solid interface. *Journal of Colloid and Interface Science* **1987,** *119* (1), 203-210.
31. Hlady, V.; Ho, C. H., Human low density lipoprotein (LDL) and human serum albumin (HSA) co-adsorption onto the C18-silica gradient surface. *Materialwissenschaft Und Werkstofftechnik* **2001,** *32* (2), 185-192.
32. Genzer, J.; Fischer, D. A.; Efimenko, K., Fabricating two-dimensional molecular gradients via asymmetric deformation of uniformly-coated elastomer sheets. *Advanced Materials* **2003,** *15* (18), 1545-+.
33. Choi, S. H.; Newby, B. M. Z., Micrometer-scaled gradient surfaces generated using contact printing of octadecyltrichlorosilane. *Langmuir* **2003,** *19* (18), 7427-7435.
34. Ye, F. M.; Cui, C. C.; Kirkeminde, A.; Dong, D.; Collinson, M. M.; Higgins, D. A., Fluorescence Spectroscopy Studies of Silica Film Polarity Gradients Prepared by Infusion-Withdrawal Dip-Coating. *Chemistry of Materials* **2010,** *22* (9), 2970-2977.
35. Cui, C. C.; Kirkeminde, A.; Kannan, B.; Collinson, M. M.; Higgins, D. A., Spatiotemporal Evolution of Fixed and Mobile Dopant Populations in Silica Thin-Film Gradients as Revealed by Single Molecule Tracking. *Journal of Physical Chemistry C* **2011,** *115* (3), 728-735.
36. Luzinov, I.; Minko, S.; Tsukruk, V. V., Responsive brush layers: from tailored gradients to reversibly assembled nanoparticles. *Soft Matter* **2008,** *4* (4), 714-725.
37. Lin, X. K.; He, Q.; Li, J. B., Complex polymer brush gradients based on nanolithography and surface-initiated polymerization. *Chemical Society Reviews* **2012,** *41* (9), 3584-3593.

38. Jeong, B. J.; Lee, J. H.; Lee, H. B., Preparation and characterization of comb-like PEO gradient surfaces. *Journal of Colloid and Interface Science* **1996,** *178* (2), 757-763.
39. Bhat, R. R.; Tomlinson, M. R.; Genzer, J., Orthogonal surface-grafted polymer gradients: A versatile combinatorial platform. *Journal of Polymer Science Part B-Polymer Physics* **2005,** *43* (23), 3384-3394.
40. Wu, T.; Efimenko, K.; Genzer, J., Combinatorial study of the mushroom-to-brush crossover in surface anchored polyacrylamide. *Journal of the American Chemical Society* **2002,** *124* (32), 9394-9395.
41. Tomlinson, M. R.; Genzer, J., Formation of grafted macromolecular assemblies with a gradual variation of molecular weight on solid substrates. *Macromolecules* **2003,** *36* (10), 3449-3451.
42. Ionov, L.; Houbenov, N.; Sidorenko, A.; Stamm, M.; Luzinov, I.; Minko, S., Inverse and reversible switching gradient surfaces from mixed polyelectrolyte brushes. *Langmuir* **2004,** *20* (23), 9916-9919.
43. Ionov, L.; Zdyrko, B.; Sidorenko, A.; Minko, S.; Klep, V.; Luzinov, I.; Stamm, M., Gradient polymer layers by "grafting to" approach. *Macromolecular Rapid Communications* **2004,** *25* (1), 360-365.
44. Ionov, L.; Stamm, M.; Diez, S., Size sorting of protein assemblies using polymeric gradient surfaces. *Nano Letters* **2005,** *5* (10), 1910-1914.
45. Harris, B. P.; Metters, A. T., Generation and characterization of photopolymerized polymer brush gradients. *Macromolecules* **2006,** *39* (8), 2764-2772.
46. Caelen, I.; Gao, H.; Sigrist, H., Protein density gradients on surfaces. *Langmuir* **2002,** *18* (7), 2463-2467.
47. Hypolite, C. L.; McLernon, T. L.; Adams, D. N.; Chapman, K. E.; Herbert, C. B.; Huang, C. C.; Distefano, M. D.; Hu, W. S., Formation of microscale gradients of protein using heterobifunctional photolinkers. *Bioconjugate Chemistry* **1997,** *8* (5), 658-663.
48. Mei, Y.; Wu, T.; Xu, C.; Langenbach, K. J.; Elliott, J. T.; Vogt, B. D.; Beers, K. L.; Amis, E. J.; Washburn, N. R., Tuning cell adhesion on gradient poly(2-hydroxyethyl methacrylate)-grafted surfaces. *Langmuir* **2005,** *21* (26), 12309-12314.
49. Morgenthaler, S.; Zink, C.; Stadler, B.; Voros, J.; Lee, S.; Spencer, N. D.; Tosatti, S. G. P., Poly(L-lysine)-grafted-poly(ethylene glycol)-based surface-chemical gradients. Preparation, characterization, and first applications. *Biointerphases* **2006,** *1* (4), 156-165.
50. Kramer, S.; Xie, H.; Gaff, J.; Williamson, J. R.; Tkachenko, A. G.; Nouri, N.; Feldheim, D. A.; Feldheim, D. L., Preparation of protein gradients through the controlled deposition of protein-nanoparticle conjugates onto functionalized surfaces. *Journal of the American Chemical Society* **2004,** *126* (17), 5388-5395.
51. Ruardy, T. G.; Schakenraad, J. M.; vanderMei, H. C.; Busscher, H. J., Preparation and characterization of chemical gradient surfaces and their application for the study of cellular interaction phenomena. *Surface Science Reports* **1997,** *29* (1), 3-30.
52. Wang, Q.; Jakubowski, J. A.; Sweedler, J. V.; Bohn, P. W., Quantitative submonolayer spatial mapping of Arg-Gly-Asp-containing peptide organomercaptan gradients on gold with matrix-assisted laser desorption/ionization mass spectrometry. *Analytical Chemistry* **2004,** *76* (1), 1-8.
53. Klauser, R.; Chen, C. H.; Huang, M. L.; Wang, S. C.; Chuang, T. J.; Zharnikov, M., Patterning and imaging of self-assembled monolayers with a focused soft X-ray beam. *Journal of Electron Spectroscopy and Related Phenomena* **2005,** *144*, 393-396.
54. Lee, J. H.; Kim, H. G.; Khang, G. S.; Lee, H. B.; Jhon, M. S., Characterization of wettability gradient surfaces prepared by corona discharge treatment. *Journal of Colloid and Interface Science* **1992,** *151* (2), 563-570.
55. Pitt, W. G., Fabrication of a continuous wettability gradient by radio-frequency plasma discharge. *Journal of Colloid and Interface Science* **1989,** *133* (1), 223-227.

56. Spijker, H. T.; Bos, R.; van Oeveren, W.; de Vries, J.; Busscher, H. J., Protein adsorption on gradient surfaces on polyethylene prepared in a shielded gas plasma. *Colloids and Surfaces B-Biointerfaces* **1999,** *15* (1), 89-97.
57. Uedayukoshi, T.; Matsuda, T., Cellular-responses on a wettability gradient surface with continuous variations in surface compositions of carbonate and hydroxyl-groups. *Langmuir* **1995,** *11* (10), 4135-4140.
58. Walcarius, A.; Collinson, M. M., Analytical Chemistry with Silica Sol-Gels: Traditional Routes to New Materials for Chemical Analysis. In *Annual Review of Analytical Chemistry*, 2009; Vol. 2, pp 121-143.
59. Thames, S. F.; Panjnani, K. G., Organosilane polymer chemistry: A review. *Journal of Inorganic and Organometallic Polymers* **1996,** *6* (2), 59-94.
60. Brinker, C. J. S., G.W., *Sol-Gel Science: The Physics and Chemistry of Sol-Gel Processing*. 1990; Vol. 1.
61. Arkles, B.; Pan, Y. L.; Kim, Y. M., The Role of Polarity in the Structure of Silanes Employed in Surface Modification. *Silanes and Other Coupling Agents* 2009; p 51-64.
62. Carre, A. B., W.; Lacarriere, V., Glass substrates modified with organosilanes for DNA immobilization *Silanes and Other Coupling Agents* **2007,** *4*, 1-14.
63. Jung, D. H.; Jung, M. S.; Ko, Y. K.; Seo, S. J.; Jung, H. T., Carbon nanotube conducting arrays by consecutive amidation reactions. *Chemical Communications* **2004,** (5), 526-527.
64. Antonucci, J. M.; Dickens, S. H.; Fowler, B. O.; Xu, H. H. K.; McDonough, W. G., Chemistry of silanes: Interfaces in dental polymers and composites. *Journal of Research of the National Institute of Standards and Technology* **2005,** *110* (5), 541-558.
65. Arkles, B.; Steinmetz, J. R.; Zazyczny, J.; Mehta, P., Factors contributing to the stability of alkoxysilanes in aqueous-solution. *Journal of Adhesion Science and Technology* **1992,** *6* (1), 193-206.
66. Shimizu, I.; Yoshino, A.; Okabayashi, H.; Nishio, E.; Oconnor, C. J., Kinetics of interaction of 3-amimopropyltriethoxysilane on a silica gel surface using elemental analysis and diffuse reflectance infrared Fourier transform spectra. *Journal of the Chemical Society-Faraday Transactions* **1997,** *93* (10), 1971-1979.
67. Moses, P. R.; Wier, L. M.; Lennox, J. C.; Finklea, H. O.; Lenhard, J. R.; Murray, R. W., Chemically modified electrodes .9. x-ray photoelectron-spectroscopy of alkylamine-silanes bound to metal-oxide electrodes. *Analytical Chemistry* **1978,** *50* (4), 576-585.
68. Chiang, C. H.; Ishida, H.; Koenig, J. L., The structure of gamma-aminopropyltriethoxysilane on glass surfaces. *Journal of Colloid and Interface Science* **1980,** *74* (2), 396-404.
69. Pena-Alonso, R.; Rubio, F.; Rubio, J.; Oteo, J. L., Study of the hydrolysis and condensation of gamma-aminopropyltriethoxysilane by FT-IR spectroscopy. *Journal of Materials Science* **2007,** *42* (2), 595-603.
70. Chaudhury, M. P., A.V.;, *Adhesion Science and Engineering*. 2002; Vol. 2.
71. Vrancken, K. C.; Possemiers, K.; Vandervoort, P.; Vansant, E. F., Surface modification of silica-gels with aminoorganosilanes. *Colloids and Surfaces a-Physicochemical and Engineering Aspects* **1995,** *98* (3), 235-241.
72. Adachi, K.; Hirano, T., Controllable silane water-cross-linking kinetics and curability of ethylene-propylene copolymer by amine compounds. *Industrial & Engineering Chemistry Research* **2008,** *47* (6), 1812-1819.
73. Vandenberg, E. T.; Bertilsson, L.; Liedberg, B.; Uvdal, K.; Erlandsson, R.; Elwing, H.; Lundstrom, I., Structure of 3-aminopropyl triethoxy silane on silicon-oxide. *Journal of Colloid and Interface Science* **1991,** *147* (1), 103-118.
74. Kannan, B.; Dong, D.; Higgins, D. A.; Collinson, M. M., Profile Control in Surface Amine Gradients Prepared by Controlled-Rate Infusion. *Langmuir* **2011,** *27* (5), 1867-1873.

75. Freiling, E. C., Gradient Elution Theory. *The Journal of Physical Chemistry* **1957,** *61* (5), 543-548.
76. Thanawiroon, C.; Linhardt, R. J., Separation of a complex mixture of heparin-derived oligosaccharides using reversed-phase high-performance liquid chromatography. *Journal of Chromatography A* **2003,** *1014* (1-2), 215-223.
77. Matysik, G.; Giryn, H., Gradient thin-layer chromatography and densitometry determination of Alternaria mycotoxins. *Chromatographia* **1996,** *42* (9-10), 555-558.
78. Bozek, P.; Hutta, M.; Hrivnakova, B., Rapid analysis of porphyrins at low ng/l and mu g/l levels in human urine by a gradient liquid chromatography method using octadecylsilica monolithic columns. *Journal of Chromatography A* **2005,** *1084* (1-2), 24-32.
79. Eggink, M.; Romero, W.; Vreuls, R. J.; Lingeman, H.; Niessen, W. M. A.; Irth, H., Development and optimization of a system for comprehensive two-dimensional liquid chromatography with UV and mass spectrometric detection for the separation of complex samples by multi-step gradient elution. *Journal of Chromatography A* **2008,** *1188* (2), 216-226.
80. Zhao, J. H.; Carr, P. W., An approach to the concept of resolution optimization through changes in the effective chromatographic selectivity. *Analytical Chemistry* **1999,** *71* (14), 2623-2632.
81. Stadalius, M. A.; Quarry, M. A.; Snyder, L. R., Optimization model for the gradient elution separation of peptide mixtures by reversed-phase high-performance liquid-chromatography - application to method development and the choice of column configuration. *Journal of Chromatography* **1985,** *327* (JUN), 93-113.
82. Neue, U. D.; Mazzeo, J. R., A theoretical study of the optimization of gradients at elevated temperature. *Journal of Separation Science* **2001,** *24* (12), 921-929.
83. Dolan, J. W., How much is enough? *LCGC* **2003,** *21* (10).
84. Steuer, W.; Schindler, M.; Erni, F., Gradient elution with normal phases on silica - a comparison between high-performance liquid and supercritical fluid chromatography. *Journal of Chromatography* **1988,** *454*, 253-259.
85. Engelhardt, H. E., H., Problems in the application of gradient elution to high-pressure ljquld chromatography *Jounal of Chromatography* **1975,** *112*, 415-423.
86. Williams, S., Ghost peaks in reversed-phase gradient HPLC: a review and update. *Journal of Chromatography A* **2004,** *1052* (1-2), 1-11.
87. Berry, V. V., Sequential isocratic step liquid-chromatography - a high-throughput, problem-solving approach with sensitive, near-universal detection for wide polarity mixtures. *Journal of Chromatography* **1980,** *199* (OCT), 219-238.
88. Boelens, H. F. M.; Dijkstra, R. J.; Eilers, P. H. C.; Fitzpatrick, F.; Westerhuis, J. A., New background correction method for liquid chromatography with diode array detection, infrared spectroscopic detection and Raman spectroscopic detection. *Journal of Chromatography A* **2004,** *1057* (1-2), 21-30.
89. Niederwiese, A., Some Recent Advances in Thin Layer Chromatography III. Gradient Thin LayerChromatography *Chromatographia* **1969,** *2*, 23-28.
90. Cimpoiu, C.; Hosu, A.; Puscas, A., Thin-layer chromatography with stationary phase gradient as a method for separation of water-soluble vitamins. *Journal of Chromatography A* **2012,** *1223*, 142-146.
91. Stahl, E., Gradient- und transfertechniken in der chromatographie. *Zeitschrift Fur Chemie* **1967,** *7* (2), 75-&.
92. Stahl, E.; Muller, J., New spreader for the preparation of gradient layers in thin-layer chromatography. *Journal of Chromatography* **1980,** *189* (3), 293-297.
93. Warren, B., A gradient spreader for thin-layer chromatography. *Journal of Chromatography* **1965,** *20* (3), 603-606.
94. Mater, H. J. K., O.C.;, Rediction of separation and specifications of chromatographic columns. *Journal of chromatography* **1961,** *8*, 308-318.

95. Chen, K.; Lynen, F.; De Beer, M.; Hitzel, L.; Ferguson, P.; Hanna-Brown, M.; Sandra, P., Selectivity optimization in green chromatography by gradient stationary phase optimized selectivity liquid chromatography. *Journal of Chromatography A* **2010,** *1217* (46), 7222-7230.
96. Lukulay, P. H.; McGuffin, V. L., Solvent modulation in liquid-chromatography - extension to serially coupled columns. *Journal of Chromatography A* **1995,** *691* (1-2), 171-185.
97. De Beer, M.; Lynen, F.; Chen, K.; Ferguson, P.; Hanna-Brown, M.; Sandra, P., Stationary-Phase Optimized Selectivity Liquid Chromatography: Development of a Linear Gradient Prediction Algorithm. *Analytical Chemistry* **2010,** *82* (5), 1733-1743.
98. Nyiredy, S.; Szucs, Z.; Szepesy, L., Stationary phase optimized selectivity liquid chromatography: Basic possibilities of serially connected columns using the "PRISMA' principle. *Journal of Chromatography A* **2007,** *1157* (1-2), 122-130.
99. Currivan, S.; Connolly, D.; Gillespie, E.; Paull, B., Fabrication and characterisation of capillary polymeric monoliths incorporating continuous stationary phase gradients. *Journal of Separation Science* **2010,** *33* (4-5), 484-492.
100. Monaci, L.; Aresta, A.; Palmisano, F.; Visconti, A.; Zambonin, C. G., Amino-bonded silica as stationary phase for liquid chromatographic determination of cyclopiazonic acid in fungal extracts. *Journal of Chromatography A* **2002,** *955* (1), 79-86.
101. Olsen, B. A., Hydrophilic interaction chromatography using amino and silica columns for the determination of polar pharmaceuticals and impurities. *Journal of Chromatography A* **2001,** *913* (1-2), 113-122.
102. Schwarzenbach, R., Separation of some polyhydric alcohols by high-performance liquid-chromatography. *Journal of Chromatography* **1977,** *140* (3), 304-309.
103. Verzele, M.; Simoens, G.; Vandamme, F., A critical-review of some liquid-chromatography systems for the separation of sugars. *Chromatographia* **1987,** *23* (4), 292-300.
104. Valette, J. C.; Demesmay, C.; Rocca, J. L.; Verdon, E., Separation of tetracycline antibiotics by hydrophilic interaction chromatography using an amino-propyl stationary phase. *Chromatographia* **2004,** *59* (1-2), 55-60.
105. Guo, Y.; Huang, A. H., A HILIC method for the analysis of tromethamine as the counter ion in an investigational pharmaceutical salt. *Journal of Pharmaceutical and Biomedical Analysis* **2003,** *31* (6), 1191-1201.
106. Vickerman , J. C. G., I.S., *Surface Analysis. The Principle Techniques*. 2009.
107. Bogart, K. H. A.; Donnelly, V. M., On the constant composition and thickness of the chlorinated silicon surface layer subjected to increasing etching product concentrations during chlorine plasma etching. *Journal of Applied Physics* **1999,** *86* (4), 1822-1833.
108. Biino, G. G.; Groning, P., X-Ray Photoelectron Spectroscopy (XPS) used as a structural and chemical surface probe on aluminosilicate minerals. *European Journal of Mineralogy* **1998,** *10* (3), 423-437.
109. Tougaard, S.; Ignatiev, A., Concentration depth profiles by xps - a new approach. *Surface Science* **1983,** *129* (2-3), 355-365.
110. Cumpson, P. J., Angle-resolved XPS depth-profiling strategies. *Applied Surface Science* **1999,** *144-45*, 16-20.
111. Sherwood, P. M. A., Data Analysis in X-ray Photoelectron Spectroscopy. In *Surface Characterization of Advanced Polymers*, Sabbatini, L. Z., P.G, Ed. VCH Weinheim: pp 257-298.
112. Yuan, Y. L., T.R., Contact Angle and Wetting Properties. In *Surface Science Techniques*, Bracco, G. H., B., Ed. pp 3-33.

113. Friedman, M., Applications of the ninhydrin reaction for analysis of amino acids, peptides, and proteins to agricultural and biomedical sciences. *Journal of Agricultural and Food Chemistry* **2004,** *52* (3), 385-406.
114. Hess, A. V. I., Digitally enhanced thin-layer chromatography: An inexpensive, new technique for qualitative and quantitative analysis. *Journal of Chemical Education* **2007,** *84* (5), 842-847.
115. Sherma, J., Planar chromatography. *Analytical Chemistry* **2006,** *78* (12), 3841-3852.
116. Sherma, J. F., B., *Handbook of Thin-layer Chromatography*. Taylor & Francis Group, LLC: 1999.
117. Stanley, J. S., The Effect of Paraffin Chain Salts on the Charge on Textile Fibers. *The Journal of Physical Chemistry* **1954,** *58* (7), 533-536.
118. Schellman, J. A.; Stigter, D., Electrical double layer, zeta potential, and electrophoretic charge of double-stranded DNA. *Biopolymers* **1977,** *16* (7), 1415-1434.
119. Zhang, Y.; Yang, M.; Portney, N. G.; Cui, D. X.; Budak, G.; Ozbay, E.; Ozkan, M.; Ozkan, C. S., Zeta potential: a surface electrical characteristic to probe the interaction of nanoparticles with normal and cancer human breast epithelial cells. *Biomedical Microdevices* **2008,** *10* (2), 321-328.
120. Sze, A.; Erickson, D.; Ren, L. Q.; Li, D. Q., Zeta-potential measurement using the Smoluchowski equation and the slope of the current-time relationship in electroosmotic flow. *Journal of Colloid and Interface Science* **2003,** *261* (2), 402-410.
121. Scales, P. J.; Grieser, F.; Healy, T. W.; White, L. R.; Chan, D. Y. C., Electrokinetics of the silica solution interface - a flat-plate streaming potential study. *Langmuir* **1992,** *8* (3), 965-974.
122. Gusev, I.; Horvath, C., Streaming potential in open and packed fused-silica capillaries. *Journal of Chromatography A* **2002,** *948* (1-2), 203-223.
123. Luna-Vera, F.; Alvarez, J. C., Adsorption kinetics of proteins in plastic microfluidic channels: Real-time monitoring of lysozyme adsorption by pulsed streaming potentials. *Biosensors & Bioelectronics* **2010,** *25* (6), 1539-1543.
124. Genzer, J., Templating surfaces with gradient assemblies. *Journal of Adhesion* **2005,** *81* (3-4), 417-435.
125. Zhang, J.; Han, Y., Active and responsive polymer surfaces. *Chemical Society Reviews* **2010,** *39* (2), 676-693.
126. Kim, M. S.; Khang, G.; Lee, H. B., Gradient polymer surfaces for biomedical applications. *Progress in Polymer Science* **2008,** *33* (1), 138-164.
127. Bhat, R. R.; Fischer, D. A.; Genzer, J., Fabricating planar nanoparticle assemblies with number density gradients. *Langmuir* **2002,** *18* (15), 5640-5643.
128. Efimenko, K.; Genzer, J., How to prepare tunable planar molecular chemical gradients. *Advanced Materials* **2001,** *13* (20), 1560-1565.
129. Bhat, R. R.; Genzer, J., Tuning the number density of nanoparticles by multivariant tailoring of attachment points on flat substrates. *Nanotechnology* **2007,** *18* (2).
130. Usrey, M. L.; Strano, M. S., Adsorption of Single Walled Carbon Nanotubes onto Silicon Oxide Surface Gradients of 3-Aminopropyltri(ethoxysilane) Described by Polymer Adsorption Theory. *Langmuir* **2009,** *25* (17), 9922-9930.
131. Liu, H.; Xu, J.; Li, Y.; Li, B.; Ma, J.; Zhang, X., Fabrication and characterization of an organic-inorganic gradient surface made by polymethylsilsesquioxane (PMSQ). *Macromolecular Rapid Communications* **2006,** *27* (18), 1603-1607.
132. Roberson, S. V.; Fahey, A. J.; Sehgal, A.; Karim, A., Multifunctional ToF-SIMS: combinatorial mapping of gradient energy substrates. *Applied Surface Science* **2002,** *200* (1-4), 150-164.
133. Loos, K.; Kennedy, S. B.; Eidelman, N.; Tai, Y.; Zharnikov, M.; Amis, E. J.; Ulman, A.; Gross, R. A., Combinatorial approach to study enzyme/surface interactions. *Langmuir* **2005,** *21* (12), 5237-5241.

134. Schubert, U.; Husing, N.; Lorenz, A., Hybrid inorganic-organic materials by sol-gel processing of organofunctional metal alkoxides. *Chemistry of Materials* **1995,** *7* (11), 2010-2027.
135. Culler, S. R.; Ishida, H.; Koenig, J. L., STRUCTURE OF SILANE COUPLING AGENTS ADSORBED ON SILICON POWDER. *Journal of Colloid and Interface Science* **1985,** *106* (2), 334-346.
136. Horner, M. R.; Boerio, F. J.; Clearfield, H. M., AN XPS INVESTIGATION OF THE ADSORPTION OF AMINOSILANES ONTO METAL SUBSTRATES. *Journal of Adhesion Science and Technology* **1992,** *6* (1), 1-22.
137. Graf, N.; Yegen, E.; Gross, T.; Lippitz, A.; Weigel, W.; Krakert, S.; Terfort, A.; Unger, W. E. S., XPS and NEXAFS studies of aliphatic and aromatic amine species on functionalized surfaces. *Surface Sceince.* **2009,** *603* (18), 2849-2860.
138. Yoshino, A.; Okabayashi, H.; Shimizu, I.; Oconnor, C. J., Kinetics of interaction of 3-aminopropyltriethoxysilane with silica gel using elemental analysis and Si-29 NMR spectra. *Colloid and Polymer Science* **1997,** *275* (7), 672-680.
139. Salon, M. C. B.; Abdelmouleh, M.; Boufi, S.; Belgacem, M. N.; Gandini, A., Silane adsorption onto cellulose fibers: Hydrolysis and condensation reactions. *Journal of Colloid and Interface Science* **2005,** *289* (1), 249-261.
140. Vasiliev, A. N.; Golovko, L. V.; Trachevsky, V. V.; Hall, G. S.; Khinast, J. G., Adsorption of heavy metal cations by organic ligands grafted on porous materials. *Microporous and Mesoporous Materials* **2009,** *118* (1-3), 251-257.
141. Livingston, H. K., The cross-sectional areas of molecules adsorbed on solid surfaces. *Journal of Colloid Science* **1949,** *4* (5), 447-458.
142. Beari, F.; Brand, M.; Jenkner, P.; Lehnert, R.; Metternich, H. J.; Monkiewicz, J.; Siesler, H. W., Organofunctional alkoxysilanes in dilute aqueous solution: new accounts on the dynamic structural mutability. *Journal of Organometallic Chemistry* **2001,** *625* (2), 208-216.
143. Paquet, O.; Salon, M.-C. B.; Zeno, E.; Belgacem, M. N., Hydrolysis-condensation kinetics of 3-(2-amino-ethylamino)propyl-trimethoxysilane. *Materials Science & Engineering Materials for Biological Applications* **2012,** *32* (3), 487-493.
144. Brochier Salon, M.-C.; Bardet, M.; Belgacem, M., Solvolysis–hydrolysis of N-bearing alkoxysilanes: Reactions studied with 29Si NMR. *Silicon Chemistry* **2008,** *3* (6), 335-350.
145. Asenath-Smith, E.; Chen, W., How To Prevent the Loss of Surface Functionality Derived from Aminosilanes. *Langmuir* **2008,** *24* (21), 12405-12409.
146. Salon, M.-C. B.; Belgacem, M. N., Competition between hydrolysis and condensation reactions of trialkoxysilanes, as a function of the amount of water and the nature of the organic group. *Colloids and Surfaces a-Physicochemical and Engineering Aspects* **2010,** *366* (1-3), 147-154.
147. Frei, R.; Blitz, J. P.; Gun'ko, V. M.; Frost, B. E.; Sergeev, V. S., Kinetics and Computational Studies of an Aminosilane Reaction with a Silsesquioxane Silanol. *Journal of Physical Chemistry A* **2009,** *113* (24), 6612-6619.
148. Hall , H. K., Correlation of the base strengths of amines. *Journal of the American Chemical Society* **1957,** *79* (20), 5411-5444.
149. Kallury, K. M. R.; Krull, U. J.; Thompson, M., X-ray photoelectron-spectroscopy of silica surfaces treated with polyfunctional silanes. *Analytical Chemistry* **1988,** *60* (2), 169-172.
150. Ishida, H.; Chiang, C. H.; Koenig, J. L., The structure of aminofunctional silane coupling agents .1. gamma-aminopropyltriethoxysilane and its analogs. *Polymer* **1982,** *23* (2), 251-257.
151. Metwalli, E.; Haines, D.; Becker, O.; Conzone, S.; Pantano, C. G., Surface characterizations of mono-, di-, and tri-aminosilane treated glass substrates. *Journal of Colloid and Interface Science* **2006,** *298* (2), 825-831.

152. Brauman, J. I.; Riveros, J. M.; Blair, L. K., Gas-phase basicities of amines. *Journal of the American Chemical Society* **1971,** *93* (16), 3914-&.
153. Ko, Y. G.; Shin, S. S.; Choi, U. S., Primary, secondary, and tertiary amines for CO2 capture: Designing for mesoporous CO2 adsorbents. *Journal of Colloid and Interface Science* **2011,** *361* (2), 594-602.
154. Kim, K.; Kwak, J., Faradaic impedance titration of pure 3-mercaptopropionic acid and ethanethiol mixed monolayers on gold. *Journal of Electroanalytical Chemistry* **2001,** *512* (1-2), 83-91.
155. Quang, D. V.; Kim, J. K.; Sarawade, P. B.; Tuan, D. H.; Kim, H. T., Preparation of amino-functionalized silica for copper removal from an aqueous solution. *Journal of Industrial and Engineering Chemistry* **2012,** *18* (1), 83-87.
156. Iijima, M.; Sato, N.; Lenggoro, I. W.; Kamiya, H., Surface modification of BaTiO3 particles by silane coupling agents in different solvents and their effect on dielectric properties of BaTiO3/epoxy composites. *Colloids and Surfaces a-Physicochemical and Engineering Aspects* **2009,** *352* (1-3), 88-93.
157. Jesionowski, T.; Krysztafkiewicz, A., Influence of silane coupling agents on surface properties of precipitated silicas. *Applied Surface Science* **2001,** *172* (1-2), 18-32.
158. Markowitz, M. A.; Deng, G.; Burleigh, M. C.; Wong, E. M.; Gaber, B. P., Influence of quaternary amine organosilane structure on the formation and adsorption properties of surface-imprinted silicates. *Langmuir* **2001,** *17* (22), 7085-7092.
159. Park, S. J.; Jin, J. S.; Lee, J. R., Influence of silane coupling agents on the surface energetics of glass fibers and mechanical interfacial properties of glass fiber-reinforced composites. *Journal of Adhesion Science and Technology* **2000,** *14* (13), 1677-1689.
160. Sawada, H.; Ikematsu, Y.; Kawase, T.; Hayakawa, Y., Synthesis and surface properties of novel fluoroalkylated flip-flop-type silane coupling agents. *Langmuir* **1996,** *12* (15), 3529-3530.
161. Arakaki, L. N. H.; Airoldi, C., Ethylenimine in the synthetic routes of a new silylating agent: chelating ability of nitrogen and sulfur donor atoms after anchoring onto the surface of silica gel. *Polyhedron* **2000,** *19* (4), 367-373.
162. Prado, A. G. S.; Airoldi, C., Adsorption, preconcentration and separation of cations on silica gel chemically modified with the herbicide 2,4-dichlorophenoxyacetic acid. *Analytica Chimica Acta* **2001,** *432* (2), 201-211.
163. Price, P. M.; Clark, J. H.; Macquarrie, D. J., Modified silicas for clean technology. *Journal of the Chemical Society-Dalton Transactions* **2000,** (2), 101-110.
164. Gemeay, A. H., Catalytic activity of silica gel surface modified by transition metal-aminosilane complexes in the decomposition of hydrogen peroxide. *Colloids and Surfaces a-Physicochemical and Engineering Aspects* **1996,** *116* (3), 277-284.
165. Rykowska, I.; Wasiak, W., Polyamine complexes of copper (II) and chromium (III) for the analysis of nucleophilic compounds by complexation gas chromatography. *Chromatographia* **2000,** *51* (9-10), 623-629.
166. Silva, C. R.; Jardim, I.; Airoldi, C., New stationary phase prepared by immobilization of a copper-amine complex on silica and its use for high performance liquid chromatography. *Hrc-Journal of High Resolution Chromatography* **1999,** *22* (2), 103-108.
167. Wang, L.; Yan, X.; Fu, Z.; Dai, Y.; Shi, Y., Immobilized copper catalyst for atom transfer radical addition and polymerization. *Applied Organometallic Chemistry* **2011,** *25* (3), 190-197.
168. Yang, J. J.; ElNahhal, I. M.; Chuang, I. S.; Maciel, G. E., Synthesis and solid-state NMR structural characterization of polysiloxane-immobilized amine ligands and their metal complexes. *Journal of Non-Crystalline Solids* **1997,** *209* (1-2), 19-39.
169. Barrientos-Ramirez, S.; Montes de Oca-Ramirez, G.; Ramos-Fernandez, E. V.; Sepulveda-Escribano, A.; Pastor-Blas, M. M.; Gonzalez-Montiel, A., Surface modification of natural halloysite clay

nanotubes with aminosilanes. Application as catalyst supports in the atom transfer radical polymerization of methyl methacrylate. *Applied Catalysis a-General* **2011,** *406* (1-2), 22-33.
170. Clark, J. H.; Macquarrie, D. J., Catalysis of liquid phase organic reactions using chemically modified mesoporous inorganic solids. *Chemical Communications* **1998,** (8), 853-860.
171. Krocher, O.; Koppel, R. A.; Baiker, A., Sol-gel derived hybrid materials as heterogeneous catalysts for the synthesis of N,N-dimethylformamide from supercritical carbon dioxide. *Chemical Communications* **1996,** (13), 1497-1498.
172. Rykowska, I.; Smyka, S.; Urbaniak, W.; Wasiak, W., Chemically bonded chelates as selective complexing sorbents for gas chromatography - VII. N- 3-(trimethoxysilyl)propyl diethylenetriamine complexes with CuCl2 and CrCl3. *Journal of Chromatography A* **1999,** *844* (1-2), 239-248.
173. Rykowska, I.; Wasiak, W., Gas chromatography silica packings with chemically bonded complexes of Cu(II) and Cr(III). *Analytica Chimica Acta* **2002,** *451* (2), 271-278.
174. Tishchenko, G.; Hodrova, B.; Simunek, J.; Bleha, M., Nickel and copper complexes of a chelating methacrylate sorbent in the purification of chitinases and specific immunoglobulin G(1) by immobilized metal ion affinity chromatography. *Journal of Chromatography A* **2003,** *983* (1-2), 125-132.
175. Wasiak, W.; Urbaniak, W., Chemically bonded chelates as selective complexing sorbents for gas chromatography .5. Silica chemically modified by Cu(II) complexes via amino groups. *Journal of Chromatography A* **1997,** *757* (1-2), 137-143.
176. El-Nahhal, I. M.; El-Ashgar, N. M.; Chehimi, M. M.; Bargiela, P.; Maquet, J.; Babonneau, F.; Livage, J., Metal uptake by porous iminobis(N-2-aminoethylacetamide)-modified polysiloxane ligand system. *Microporous and Mesoporous Materials* **2003,** *65* (2-3), 299-310.
177. El-Ashgar, N. M.; El-Nahhal, I. M.; Chehimi, M. M.; Babonneau, F.; Livage, J., A new route synthesis of immobilized-polysiloxane iminodiacetic acid ligand system, its characterization and applications. *Materials Letters* **2007,** *61* (23-24), 4553-4558.
178. Chawla, H. M. G., N. K.; Chibber, S. S., TLC Separation and Identification of Some Transition Metal Ions *Journal of HRCC and CC* **1981,** *4*, 657-658.
179. Mohammad, A.; Agrawal, V., Use of cationic micellar mobile phases in normal-phase TLC for enhanced selectivity in the separation of transition metal ions: Simultaneous separation of mixtures of zinc, nickel, mercury, and cadmium or manganese cations. *Acta Chromatographica* **2002,** *12*, 177-188.
180. Yadav, S. K.; Singh, O. V.; Tandon, S. N., Reversed-phase tlc and column chromatographic separations of 3d transition-metal ions using mono(2-ethylhexyl) acid phosphate as impregnant. *Journal of Planar Chromatography-Modern TLC* **1994,** *7* (1), 75-77.
181. Kannan, B.; Nokura, K.; Alvarez, J. C.; Higgins, D. A.; Collinson, M. M., Fabrication of surface charge density gradients in open-tubular capillaries and their characterization by spatially-resolved pulsed streaming potential measurements ***Manuscript under preparation***.
182. Kannan, B.; Higgins, D. A.; Collinson, M. M., Aminoalkoxysilane Reactivity in Surface Amine Gradients Prepared by Controlled-Rate Infusion. *Langmuir* **2012,** *28* (46), 16091-16098.
183. Roe, S. P.; Hill, J. O.; Liesegang, J., An x-ray photoelectron spectroscopic study of some bis(diamine) copper(ii) complexes. *Journal of Electron Spectroscopy and Related Phenomena* **1988,** *46* (4), 315-324.
184. Wagner, A. J.; Wolfe, G. M.; Fairbrother, D. H., Reactivity of vapor-deposited metal atoms with nitrogen-containing polymers and organic surfaces studied by in situ XPS. *Applied Surface Science* **2003,** *219* (3-4), 317-328.
185. El-Ashgar, N.; El-Nahhal, I., Preconcentration and separation of copper(II) by 3-aminopropylpolysiloxane immobilized ligand system. *Journal of Sol-Gel Science and Technology* **2005,** *34* (2), 165-172.

186. Moriguchi, T.; Murase, K.; Sugimura, H., Ruthenium-amine complexation for constructing self-assembled molecular films. *Colloids and Surfaces a-Physicochemical and Engineering Aspects* **2008,** *321* (1-3), 94-98.
187. Burggraf, L. W.; Kendall, D. S.; Leyden, D. E.; Pern, F. J., Photoacoustic studies of complexation of copper(ii) with an ethylenediamine analog immobilized on silica-gel. *Analytica Chimica Acta* **1981,** *129* (AUG), 19-27.
188. Mu, S.; Wu, D.; Qi, S.; Wu, Z., Preparation of Polyimide/Zinc Oxide Nanocomposite Films via an Ion-Exchange Technique and Their Photoluminescence Properties. *Journal of Nanomaterials* **2011**.
189. Crichton, R. R., *Zinc: Lewis Acid and Gene Regulator*. I ed.; Oxford: 2008.
190. Hanas, J. S.; Larabee, J. L.; Hocker, J. R., *Zinc finger interactions with metals and other small molecules*. **2005**; p 39-46.
191. Zhang, J.; Yang, W.; Piquemal, J.-P.; Ren, P., Modeling Structural Coordination and Ligand Binding in Zinc Proteins with a Polarizable Potential. *Journal of Chemical Theory and Computation* **2012,** *8* (4), 1314-1324.
192. Jena, H. S.; Manivannan, V., Molecular structures of dinuclear zinc(II) complexes of chiral tridentate imine and amine ligands: Effect of ligand geometry on diastereoselectivity. *Inorganica Chimica Acta* **2013,** *394*, 210-219.
193. Fujita, T.; Yamaguchi, T.; Ohtaki, H., An x-ray-diffraction study on the structures of bis- and tris-(ethylenediamine)zinc(ii) complexes in solution. *Bulletin of the Chemical Society of Japan* **1979,** *52* (12), 3539-3544.
194. Hemstrom, P.; Irgum, K., Hydrophilic interaction chromatography. *Journal of Separation Science* **2006,** *29* (12), 1784-1821.
195. Jorgenson, J. W., Capillary Liquid Chromatography at Ultrahigh Pressures. In *Annual Review of Analytical Chemistry, Vol 3*, Yeung, E. S.; Zare, R. N., Eds. 2010; Vol. 3, pp 129-150.
196. Guo, Y.; Colon, L. A., A stationary-phase for open-tubular liquid-chromatography and electrochromatography using sol-gel technology. *Analytical Chemistry* **1995,** *67* (15), 2511-2516.
197. Wang, D. X.; Chong, S. L.; Malik, A., Sol-gel column technology for single-step deactivation, coating, and stationary-phase immobilization in high-resolution capillary gas chromatography. *Analytical Chemistry* **1997,** *69* (22), 4566-4576.
198. Guiochon, G., Monolithic columns in high-performance liquid chromatography. *Journal of Chromatography A* **2007,** *1168* (1-2), 101-168.
199. Siouffi, A. M., Silica gel-based monoliths prepared by the sol-gel method: facts and figures. *Journal of Chromatography A* **2003,** *1000* (1-2), 801-818.
200. Svec, F., Recent developments in the field of monolithic stationary phases for capillary electrochromatography. *Journal of Separation Science* **2005,** *28* (8), 729-745.
201. Svec, F.; Huber, C. G., Monolithic materials - Promises, challenges, achievements. *Analytical Chemistry* **2006,** *78* (7), 2100-2107.
202. Wu, R. a.; Hu, L.; Wang, F.; Ye, M.; Zou, H., Recent development of monolithic stationary phases with emphasis on microscale chromatographic separation. *Journal of Chromatography A* **2008,** *1184* (1-2), 369-392.
203. Bakry, R.; Bonn, G. K.; Mair, D.; Svec, F., Monolithic porous polymer layer for the separation of peptides and proteins using thin-layer chromatography coupled with MALDI-TOF-MS. *Analytical Chemistry* **2007,** *79* (2), 486-493.
204. Frolova, A. M.; Konovalova, O. Y.; Loginova, L. P.; Bulgakova, A. V.; Boichenko, A. P., Thin-layer chromatographic plates with monolithic layer of silica: Production, physical-chemical characteristics, separation capabilities. *Journal of Separation Science* **2011,** *34* (16-17), 2352-2361.

205. Hodgson, R. J.; Chen, Y.; Zhang, Z.; Tleugabulova, D.; Long, H.; Zhao, X. M.; Organ, M.; Brook, M. A.; Brennan, J. D., Protein-doped monolithic silica columns for capillary liquid chromatography prepared by the sol-gel method: Applications to frontal affinity chromatography. *Analytical Chemistry* **2004,** *76* (10), 2780-2790.
206. Nakanishi, K.; Tanaka, N., Sol-gel with phase separation. Hierarchically porous materials optimized for high-performance liquid chromatography separations. *Accounts of Chemical Research* **2007,** *40* (9), 863-873.
207. Malkin, D. S.; Wei, B.; Fogiel, A. J.; Staats, S. L.; Wirth, M. J., Submicrometer Plate Heights for Capillaries Packed with Silica Colloidal Crystals. *Analytical Chemistry* **2010,** *82* (6), 2175-2177.
208. Zheng, S.; Ross, E.; Legg, M. A.; Wirth, M. J., High-speed electroseparations inside silica colloidal crystals. *Journal of the American Chemical Society* **2006,** *128* (28), 9016-9017.
209. Eghbali, H.; Verdoold, V.; Vankeerberghen, L.; Gardeniers, H.; Desmet, G., Experimental Investigation of the Band Broadening Arising from Short-Range Interchannel Heterogeneities in Chromatographic Beds under the Condition of Identical External Porosity. *Analytical Chemistry* **2009,** *81* (2), 705-715.
210. Gzil, P.; Vervoort, N.; Baron, G. V.; Desmet, G., Advantages of perfectly ordered 2-D porous pillar arrays over packed bed columns for LC separations: A theoretical analysis. *Analytical Chemistry* **2003,** *75* (22), 6244-6250.
211. He, B.; Tait, N.; Regnier, F., Fabrication of nanocolumns for liquid chromatography. *Analytical Chemistry* **1998,** *70* (18), 3790-3797.
212. Lavrik, N. V.; Taylor, L. C.; Sepaniak, M. J., Enclosed pillar arrays integrated on a fluidic platform for on-chip separations and analysis. *Lab on a Chip* **2010,** *10* (8), 1086-1094.
213. Harris , D. C., *Quantitative Chemical Analysis,*. W.H. Freeman Co., New York: 2007.
214. Glowniak, K.; Matysik, G.; Bieganowska, M.; Soczewinski, E., Gradient thin-layer chromatography of coumarins and furocoumarins. *Chromatographia* **1986,** *22* (7-12), 307-310.
215. Soczewinski, E.; Matsik, G., A simple device for gradient elution in equilibrium sandwich chambers for continuous thin-layer chromatography. *Journal of Liquid Chromatography* **1985,** *8* (7), 1225-1238.
216. Aures, D.; Fleming, R.; Hakanson, R., Separation and detection of biogenic amines by thin-layer chromatography - micro-analysis of tissue amines and of enzymes involved in their metabolism. *Journal of Chromatography* **1968,** *33* (3-4), 480-&.
217. Bottom, C. B. H., S.S.; Siehr, D.J., Mechanism of the ninhydrin reaction. B*iochemical education* **1978,** *6*, 1.
218. Bonicamp, J. M., Separation and identification of commonly used drugs - a thin-layer chromatography experiment for freshman chemistry. *Journal of Chemical Education* **1985,** *62* (2), 160-161.
219. Carroll, M. A.; White, E. R.; Zarembo, J. E., Over-the-counter drug analyses with hplc. *Analytical Chemistry* **1981,** *53* (9), 1111-&.
220. Jenkins, A. L.; Hedgepeth, W. A., Analysis of chiral pharmaceuticals using HPLC with CD detection. *Chirality* **2005,** *17*, S24-S29.
221. Wehr, T.; Zhu, M.; RodriguezDiaz, R., Capillary isoelectric focusing. *High Resolution Separation and Analysis of Biological Macromolecules, Pt A* **1996,** *270*, 358-374.
222. Legido-Quigley, C.; Marlin, N. D.; Melin, V.; Manz, A.; Smith, N. W., Advances in capillary electrochromatography and micro-high performance liquid chromatography monolithic columns for separation science. *Electrophoresis* **2003,** *24* (6), 917-944.
223. Svec, F., Organic polymer monoliths as stationary phases for capillary HPLC. *Journal of Separation Science* **2004,** *27* (17-18), 1419-1430.

224. Ou, J.; Lin, H.; Zhang, Z.; Huang, G.; Dong, J.; Zou, H., Recent advances in preparation and application of hybrid organic-silica monolithic capillary columns. *Electrophoresis* **2013,** *34* (1), 126-140.
225. Qu, Q. S.; Wang, S.; Mangelings, D.; Wang, C. Y.; Yang, G. J.; Hu, X. Y.; Yan, C., Monolithic silica xerogel capillary column for separations in capillary LC and pressurized CEC. *Electrophoresis* **2009,** *30* (6), 1071-1076.
226. Guihen, E.; Glennon, J. D., Recent highlights in stationary phase design for open-tubular capillary electrochromatography. *Journal of Chromatography A* **2004,** *1044* (1-2), 67-81.
227. Liu, C. Y., Stationary phases for capillary electrophoresis and capillary electrochromatography. *Electrophoresis* **2001,** *22* (4), 612-628.
228. Tock, P. P. H.; Boshoven, C.; Poppe, H.; Kraak, J. C.; Unger, K. K., Performance of porous silica layers in open-tubular columns for liquid-chromatography. *Journal of Chromatography* **1989,** *477* (1), 95-106.
229. Crego, A. L.; Diezmasa, J. C.; Dabrio, M. V., Preparation of open-tubular columns for reversed-phase high-performance liquid-chromatography. *Analytical Chemistry* **1993,** *65* (11), 1615-1621.
230. Cortes, H. J.; Pfeiffer, C. D.; Richter, B. E.; Stevens, T. S., Porous ceramic bed supports for fused-silica packed capillary columns used in liquid-chromatography. *Journal of High Resolution Chromatography & Chromatography Communications* **1987,** *10* (8), 446-448.
231. Constantin, S.; Freitag, R., Preparation of stationary phases for open-tubular capillary electrochromatography using the sol-gel method. *Journal of Chromatography A* **2000,** *887* (1-2), 253-263.
232. Hayes, J. D.; Malik, A., Sol-gel monolithic columns with reversed electroosmotic flow for capillary electrochromatography. *Analytical Chemistry* **2000,** *72* (17), 4090-4099.
233. Hayes, J. D.; Malik, A., Sol-gel open tubular ODS columns with reversed eleotroosmotic flow for capillary electrochromatography. *Analytical Chemistry* **2001,** *73* (5), 987-996.
234. Zhao, Y. X.; Zhao, R.; Shangguan, D. H.; Liu, G. Q., A new type of capillary column for open-tubular electrochromatography. *Electrophoresis* **2002,** *23* (17), 2990-2995.
235. Hoegger, D.; Freitag, R., Investigation of mixed-mode monolithic stationary phases for the analysis of charged amino acids and peptides by capillary electrochromatography. *Journal of Chromatography A* **2003,** *1004* (1-2), 195-208.
236. Lü, H.; Li, Q.; Yu, X.; Yi, J.; Xie, Z., Preparation of chitosan-graft-(β-cyclodextrin) based sol-gel stationary phase for open-tubular capillary electrochromatography. *Electrophoresis* **2013**, n/a-n/a.
237. Tan, Z. X. J.; Remcho, V. T., Molecular imprint polymers as highly selective stationary phases for open tubular liquid chromatography and capillary electrochromatography. *Electrophoresis* **1998,** *19* (12), 2055-2060.
238. Zaidi, S. A.; Han, K. M.; Hwang, D. G.; Cheong, W. J., Preparation of open tubular molecule imprinted polymer capillary columns with various templates by a generalized procedure and their chiral and non-chiral separation performance in CEC. *Electrophoresis* **2010,** *31* (6), 1019-1028.
239. Zaidi, S. A.; Cheong, W. J., Long open tubular molecule imprinted polymer capillary columns with excellent separation efficiencies in chiral and non-chiral separation by capillary electrochromatography. *Electrophoresis* **2009,** *30* (9), 1603-1607.
240. Zaidi, S. A.; Han, K. M.; Kim, S. S.; Hwang, D. G.; Cheong, W. J., Open tubular layer of S-ofloxacin imprinted polymer fabricated in silica capillary for chiral CEC separation. *Journal of Separation Science* **2009,** *32* (7), 996-1001.
241. Jorgenson, J. W.; Guthrie, E. J., Liquid-chromatography in open-tubular columns - theory of column optimization with limited pressure and analysis time, and fabrication of chemically bonded reversed-phase columns on etched borosilicate glass-capillaries. *Journal of Chromatography* **1983,** *255* (JAN), 335-348.

242. Pesek, J. J.; Matyska, M. T., Electrochromatography in chemically modified etched fused-silica capillaries. *Journal of Chromatography A* **1996,** *736* (1-2), 255-264.
243. Zhang, X.; Lin, X.; Chen, Z.; Wang, X.; Wu, X.; Xie, Z., Triamine-bonded stationary phase for open tubular capillary electrochromatography. *Journal of Separation Science* **2010,** *33* (20), 3184-3193.
244. Liu, F. K.; Hsu, Y. T.; Wu, C. H., Open tubular capillary electrochromatography using capillaries coated with films of alkanethiol-self-assembled gold nanoparticle layers. *Journal of Chromatography A* **2005,** *1083* (1-2), 205-214.
245. Xu, Y.-y.; Niu, X.-y.; Dong, Y.-l.; Zhang, H.-g.; Li, X.; Chen, H.-l.; Chen, X.-g., Preparation and characterization of open-tubular capillary column modified with graphene oxide nanosheets for the separation of small organic molecules. *Journal of Chromatography A* **2013,** *1284*, 180-187.
246. Qu, Q.; Gu, C.; Hu, X., Capillary Coated with Graphene and Graphene Oxide Sheets as Stationary Phase for Capillary Electrochromatography and Capillary Liquid Chromatography. *Analytical Chemistry* **2012,** *84* (20), 8880-8890.
247. Wang, C.; de Rooy, S.; Lu, C.-F.; Fernand, V.; Moore, L., Jr.; Berton, P.; Warner, I. M., An immobilized graphene oxide stationary phase for open-tubular capillary electrochromatography. *Electrophoresis* **2013,** *34* (8), 1197-1202.
248. Hjerten, S.; Zhu, M. D., Adaptation of the equipment for high-performance electrophoresis to isoelectric-focusing. *Journal of Chromatography* **1985,** *346* (OCT), 265-270.
249. Koshel, B. M.; Wirth, M. J., Trajectory of isoelectric focusing from gels to capillaries to immobilized gradients in capillaries. *Proteomics* **2012,** *12* (19-20), 2918-2926.
250. Yang, C.; Zhu, G. J.; Zhang, L. H.; Zhang, W. B.; Zhang, Y. K., Repeatedly usable immobilized pH gradient in a monolithic capillary column. *Electrophoresis* **2004,** *25* (12), 1729-1734.
251. Zhu, G.; Yuan, H.; Zhaol, P.; Zhang, L.; Liang, Z.; Zhang, W.; Zhang, Y., Macroporous polyacrylamide-based monolithic column with immobilized pH gradient for protein analysis. *Electrophoresis* **2006,** *27* (18), 3578-3583.
252. Maruska, A.; Rocco, A.; Kornysova, O.; Fanali, S., Synthesis and evaluation of polymeric continuous bed (monolithic) reversed-phase gradient stationary phases for capillary liquid chromatography and capillary electrochromatography. *Journal of Biochemical and Biophysical Methods* **2007,** *70* (1), 47-55.
253. Pucci, V.; Raggi, M. A.; Svec, F.; Frechet, J. M. J., Monolithic columns with a gradient of functionalities prepared via photoinitiated grafting for separations using capillary electrochromatography. *Journal of Separation Science* **2004,** *27* (10-11), 779-788.
254. Yang, C.; Wang, S.; Chang, C.; Wang, Y.; Hu, X., Capillary Isoelectric Focusing with an Open Tubular Immobilized pH Gradient. *Analytical Chemistry* **2010,** *82* (5), 1580-1583.
255. Kapnissi-Christodoulou, C. P.; Zhu, X. F.; Warner, I. M., Analytical separations in open-tubular capillary electrochromatography. *Electrophoresis* **2003,** *24* (22-23), 3917-3934.
256. Dube, S.; Smith, R. M., Application of open tubular electrochromatography for acidic and basic analytes. *Chromatographia* **2003,** *57* (7-8), 485-492.
257. Kasicka, V., Recent developments in CE and CEC of peptides (2009-2011). *Electrophoresis* **2012,** *33* (1), 48-73.
258. Nilsson, C.; Nilsson, S., Nanoparticle-based pseudostationary phases in capillary electrochromatography. *Electrophoresis* **2006,** *27* (1), 76-83.
259. Liu, Z.-S.; Zheng, C.; Yan, C.; Ga, R.-Y., Molecularly imprinted polymers as a tool for separation in CEC. *Electrophoresis* **2007,** *28* (1-2), 127-136.
260. Rezanka, P.; Ehala, S.; Koktan, J.; Sykora, D.; Zvatora, P.; Vosmanska, M.; Kral, V.; Miksik, I.; Cerovsky, V.; Kasicka, V., Application of bare gold nanoparticles in open-tubular CEC separations of polyaromatic hydrocarbons and peptides. *Journal of Separation Science* **2012,** *35* (1), 73-78.

261. Yan, L. J.; Zhang, Q. H.; Zhang, W. B.; Feng, Y. Q.; Zhang, L. H.; Li, T.; Zhang, Y. K., Hybrid organic-inorganic phenyl monolithic column for capillary electrochromatography. *Electrophoresis* **2005,** *26* (15), 2935-2941.
262. Deng, N.; Liang, Z.; Liang, Y.; Sui, Z.; Zhang, L.; Wu, Q.; Yang, K.; Zhang, L.; Zhang, Y., Aptamer Modified Organic-Inorganic Hybrid Silica Monolithic Capillary Columns for Highly Selective Recognition of Thrombin. *Analytical Chemistry* **2012,** *84* (23), 10186-10190.
263. Yan, L. J.; Zhang, Q. H.; Zhang, H.; Zhang, L. Y.; Li, T.; Feng, Y. Q.; Zhang, L. H.; Zhang, W. B.; Zhang, Y. K., Hybrid organic-inorganic monolithic stationary phase for acidic compounds separation by capillary electrochromatography. *Journal of Chromatography A* **2004,** *1046* (1-2), 255-261.
264. Renaud, L.; Kleimann, P.; Morin, P., Zeta potential determination by streaming current modelization and measurement in electrophoretic microfluidic systems. *Electrophoresis* **2004,** *25* (1), 123-127.
265. Xie, H.; Saito, T.; Hickner, M. A., Zeta Potential of Ion-Conductive Membranes by Streaming Current Measurements. *Langmuir* **2011,** *27* (8), 4721-4727.
266. Hoggard, J. D.; Sides, P. J.; Prieve, D. C., Measurement of the streaming potential and streaming current near a rotating disk to determine its zeta potential. *Langmuir* **2005,** *21* (16), 7433-7438.
267. Pu, Q.; Elazazy, M. S.; Alvarez, J. C., Label-free detection of heparin, streptavidin, and other probes by pulsed streaming potentials in plastic microfluidic channels. *Analytical Chemistry* **2008,** *80* (17), 6532-6536.
268. Gupta, M. L.; Brunson, K.; Chakravorty, A.; Kurt, P.; Alvarez, J. C.; Luna-Vera, F.; Wynne, K. J., Quantifying Surface-Accessible Quaternary Charge for Surface Modified Coatings via Streaming Potential Measurements. *Langmuir* **2010,** *26* (11), 9032-9039.
269. Hayes, R. A.; Bohmer, M. R.; Fokkink, L. G. J., A study of silica nanoparticle adsorption using optical reflectometry and streaming potential techniques. *Langmuir* **1999,** *15* (8), 2865-2870.

Vitae

BALAMURALI KANNAN

EDUCATION:

Doctor of Philosophy in Chemistry (Analytical), GPA- 3.9 July 2013.

Virginia Commonwealth University, Richmond, VA

Master of Science in Analytical Chemistry, GPA – 5.3/6.0 June 2003.

University of Madras, Chennai, India

Bachelor of Science in Chemistry, Aggregate 81% May 2001.

University of Madras, Chennai, India

PUBLICATIONS

1. Kannan, B.; Higgins, A. D.; Collinson, M. M. Aminoalkoxysilane reactivity in surface amine gradients prepared by controlled-rate infusion. *Langmuir* **2012**, *28(46)*, 16091-16098.
2. Kannan, B.; Marin, A. M.; Shrestha, A.; Higgins, A. D.; Collinson, M. M. Continuous Stationary Phase Gradients for Chemical Separations. *Journal Of Chromatography A*, 1218, **2011**, 9406-9413.
3. Kannan, B.; Dong, D.; Higgins, A. D.; Collinson, M. M. Profile Control in Surface Amine Gradients Prepared by Controlled-Rate Infusion. *Langmuir* **2011**, *27(5)*, 1867-1873.
4. Cui, C.; Kirkeminde, A.; Kannan, B.; Collinson, M. M.; Higgins, A. D. Spatiotemporal Evolution of Fixed and Mobile Dopant Populations in Silica Thin-Film Gradients as Revealed by Single Molecule Tracking. *J. Phys. Chem. C* **2011**, *115*, 728-735.
5. Kannan, B.; Nokura, K.; Alvarez, J.C.; Higgins, A. D.; Collinson, M. M. Fabrication of surface charge density gradients in open-tubular capillaries and their characterization by spatially resolved pulsed streaming potential measurements (Manuscript under preparation).

CONFERENCES & PRESENTATIONS

***Pittconn 2011*,** Atlanta, GA, Oral presentation

Title : One- and two-dimensional surface amine gradients by controlled-rate infusion

Authors : **Balamurali Kannan**, Dong Dong, Daniel A. Higgins, Maryanne M. Collinson

***SERMACS 2011*,** Richmond, VA. Oral presentation

Title : Continuous stationary phase gradients for chemical separation.

Authors : **Balamurali Kannan**, Maryanne M. Collinson

Virginia Commonwealth University, Richmond, VA

***Pittconn 2013*,** Philadelphia, PA, Oral presentation

Title : Amine-Phenyl dual gradient stationary phase for the separation of water-fat soluble vitamins

Authors : Veeren Dewoolkar, **Balamurali Kannan**, Maryanne M. Collinson

Department of Chemistry, Virginia Commonwealth University 2010, Richmond, VA, Oral presentation.

Title : "Smart" gold nanoparticles for photothermal therapy

Authors : **Balamurali Kannan**

AWARDS AND FELLOWSHIPS:

- David F. Ingraham scholarship award, 2012-2013, **The Richmond Chromatography Group,** Richmond, VA
- Billy-Stump Ray-Ottenbrite scholarship, 2011-2012, **Virginia Commonwealth University**. VA
- Altria fellowship for fall 2011 & spring 2012, **Virginia Commonwealth University**, VA
- Altria fellowship for summer, 2010, **Virginia Commonwealth University**, VA
- Class topper in Master's and Bachelor's degree, 2001 & 2003, **University of Madras**, India

TEACHING EXPERIENCE

Graduate Teaching Assistant

Virginia Commonwealth University, Richmond

- Taught general chemistry and organic chemistry concepts for freshmen, sophomore and junior undergraduate students.
- Assisted in setting up general chemistry and organic chemistry lab experiments and helped students in handling instruments such as FT-IR, UV and NMR.
- Evaluated and graded lab reports and quizzes and conducted class tests.